University of California
Santa Barbara

At the Junction of Organic Solar Cells: Charge Generation and Recombination at Donor/Acceptor Interfaces

A dissertation submitted in partial satisfaction
of the requirements for the degree

Doctor of Philosophy
in
Materials Chemistry

by

Niva Alina Ran

Committee in charge:

Professor Thuc-Quyen Nguyen, Chair
Professor Guillermo C. Bazan
Professor Michael L. Chabinyc
Professor Luke Theogarajan

March 2017

The Dissertation of Niva Alina Ran is approved.

Professor Guillermo C. Bazan

Professor Michael L. Chabinyc

Professor Luke Theogarajan

Professor Thuc-Quyen Nguyen, Committee Chair

December 2016

At the Junction of Organic Solar Cells: Charge Generation and Recombination at Donor/Acceptor Interfaces

Niva Alina Ran

Somewhere, something incredible is waiting to be known.

– Carl Sagan

Acknowledgements

I have been fantasizing about this part of my thesis dissertation for years. I feel that there are so many people I have to thank, and am full of gratitude when I think back at my path to this point. I have long held the view that despite the emphasis on the achievements of the PhD candidate, the road to a PhD is far from solitary, and is in fact the accomplishments of the 'village.' As such, although I have made a point of trying to be conscientious and make note of all those who inspired me, supported me, pushed me to achieve higher, taught me, and laughed with me, it is highly likely that I have missed some people - if this is the case I sincerely apologize, and ask that you let me know. Below I will attempt to acknowledge and thank all those who gave me support and inspiration, and took part in my growth into a PhD. I'll warn you, that I also have a tendency to become sentimental, so read on at your own volition.

I am grateful to all my committee members, who despite their busy schedules and other demands have made the time to meet with me, and were flexible with their plans and schedules, importantly for my thesis defense.

First and foremost I want to thank Prof. Thuc-Quyen Nguyen, my advisor for the last 5.5 years. Quyen has given me support, encouragement, the push when I needed it, an open and empathic ear to listen to my experience and the care to respond to my experience. From a professional standpoint, Quyen encouraged me to work on projects of high caliber, set me up with opportunities to collaborate with some of the leading researchers in our field, and provided me the freedom to grow independent and strong. I appreciate that she has been very open and straighforward with us, from her experiences as a professor, travel stories, and feedback she received or heard about our and other's work - all of which provides us, the students, a window into the life of a successful professor. It is also notable that Quyen has made a point of creating a nurturing, hard

working, and well equipped lab: this includes the people she accepted into the group, and the technical tools we have in our group or the network that Quyen has built to allow us to collaborate with those who have complementary expertise. But perhaps what was most remarkable and outstanding in my experience as a graduate student in Quyen's group, is that she has been very receptive to hearing feedback, and even when we had misunderstandings or tensions, she was very caring and appreciative of my perspective, which always meant a lot. I am also grateful to Prof. Guillermo Bazan. Although Gui was not my official advisor, I worked closely with him on a number projects, and used materials synthesized in his lab in all of my projects. I really enjoyed working on manuscripts with Gui, where his skill and creativity in writing dramatically improved the quality and elegance of the papers, in addition to his keen and sharp attention which has a number of times pointed at details I missed. Especially towards my later grad-student years, when I was able to generate useful and interesting data, Gui was very encouraging of me and ready to listen to what I had to say (even if most of the time we argued, in good spirits). When I needed support, Gui stepped up to help.

My committee members, Prof. Michael Chabinyc and Prof. Luke Theogarajan, have also been very good to me, and I wish I had interacted with them more. Michael is an incredible source of knowledge and wisdom; he taught the 200 series of Materials classes in my first two years, which gave me a broad and extensive introduction to information that was important for me to get started on my own research. (In fact, having looked back a few times at the class notes later in my studies, I realize he taugt us also many things which answered questions that came later). Michael has been very sharp and on-point with his opinions and advice: a few times he has offered a question or perspective, the depth and accuracy of which I often understood only upon further contemplation. In addition to Michael's knowledgeable perspective, however, Michael has been very available and quick to respond to me, even in instances when I asked

him for a recommendation letter for fellowship applications, close to the deadline for the applications. I appreciate the time Michael had dedicated to me both for his technical perspective and advice (even when I still had plenty to learn), and for his perspective on larger questions pertaining to career decisions. Luke agreed to be on my committee, despite the fact that his expertise and research lie in a different field. Because of this, Luke brought a fresh perspective to our discussions and really challenged me to understand things to a deeper level. When I was preparing for the third year Chemistry proposal exam, Luke met with me to talk about my proposal and push it to a deeper level.

Especially during my younger graduate-student years, I have had a number of mentors, to whom I am indebted for the pushes, the support, and for teaching me how to think. Dr. ir. Martijn Kuik played a major role in my developing into an independent researcher during my second year as a PhD student. When I needed guidance Martijn took me by the hand, when I needed encouragement he told me I could do this easily, and when I needed to be pushed into the water he was there to do that, too. Dr. Oleksandr (Alex) Mikhnenko is a very sharp thinker with a unique way of thinking. I really cherished talking to him and getting glimpses of his perspective, which often profoundly opened my eyes and gave me new tools with which to see. Alex is also an incredibly creative thinker, and only seeing him develop his project was inspiring. Dr. John (Jack) Love, who was merely a year ahead of me in his PhD studies, was also an inspiring researcher to work with and talk to, with strong, logical thinking and an interesting point of view. Jack was an insightful, kind teacher and co-worker, who also helped me push the quality and depth of the work I was doing. Dr. Peter Zalar was the first to show me the ropes around the lab, and even though our research diverged, he has remained a very encouraging friend even after he left UCSB. Dr. Koen Vandewal, whom I have only met a few times, played a significant role in my development as a researcher. First, Koen was influential when I was first starting to do research of the charge transfer (CT) state

(see more below ;)): Koen is the researcher who has most popularized the role of the CT state in organic solar cells, and was very generous in helping me get started with my research by sharing small details and tips that were necessary to do the measurements and data processing. Furthermore, Koen has been very frank and open with me about his experience and professional path, which was very useful for me in demystifying the path to become a PhD scientist myself. I appreciate the frank conversations and the the generosity especially because I was a student starting out as a researcher, not even affiliated with Koen, yet he dedicated time and thought to help me out. Finally, I also want to thank Dr. Alexander Mikhailovsky, who runs the Optical Characterization Facility at UCSB. Alexander trained me on using equipment in his facility, and then shared the facility and his time with me for the last 5 years. He was very kind in sharing his space and time with me, even when my experiments ran over time and he had to change his schedule. It has been a privilege to have Alexander work so close to us: he has helped us fix various equipment in the lab, built new pieces of equipment, written software for us to run the equipment, and often has an interesting and critical point of view.

All the work I did as a PhD student was only possible thanks to materials that were synthesized by chemists at UCSB: Dr. Chunki Kim, Dr. Thomas van der Poll, Dr. Ikuhiro Nagao, Dr. Ming Wang, Dr. Xiaofeng Liu, and Dr. Jianyu Yuan. Most of these researchers worked in Gui's group when they synthesized these materials, and many of the materials were inspired by previous generations of semiconductors. Most of these chemists were the first to synthesize the semiconductors, but Xiaofeng (who is himself a great chemist and has made many original molecules) who actually made another batch of a semiconductor which was integral for much of my work - H1, or p-SIDT(FBTTh$_2$)$_2$. In order to elucidate the physics behind how organic photovoltaics work, it is imperative first to have good, clean semiconductor materials. On a similar contribution, when our thermal evaporator broke down and we had trouble fabricating good inverted solar cells,

Dr. Hengbin Wang was so kind as to agree to make devices for us to complete our study of PIPCP (which Ming had synthesized). Since then, Hengbin had generously made batches of devices with sometimes varying requirements (different thicknesses, different additives). I am so appreciative of Hengbin's willingness to fabricate these devices, even though this does not directly benefit him. Thank you to all the chemists who gave me the foundation to do the work described in this dissertation.

I have had the fortune of being involved in a number of collaborations with researchers working around the world: Dr. Steffen Roland and Prof. Dieter Neher (Potsdam University); Victoria Savikhin, Dr. Stefan Oosterhout, and Dr. Mike Toney (Stanford University, SSRL); Dr. Aditya Sadhanala and Sir. Richard Friend (Cambridge University); Dr. Veaceslav Coropceanu, Dr. Yao-Tsung Fu, Dr. Hong Li, and Prof. Jean-Luc Brédas (Georgia Tech); Xuechen Jiao and Prof. Harald Ade (North Carolina State); Dr. Julien Gorenflot and Prof. Frédéric Laquai (Max Planc and now KAUST); Steve Brown, Ryan DeCrescent, and Prof. Jon Schuller (UCSB). It has been stimulating and exciting to work with so many intelligent researchers both at UCSB and around the world, with different expertise, with whom we were able to put together interesting, comprehensive stories (as elaborated on in the rest of this document). I've enjoyed many of these collaborations and getting to know the collaborators through the work. Due to the nature of my work, I was also deeply involved with the Center for Advanced Organic Photovoltaics (CAOP) Multi University Research Initiative (MURI), where I interfaced with many leading researchers who provided their feedback and opinions on the ideas and research I presented. I want to extend my gratitude to this group of scientists: the faculty, researchers, and students alike, who took interest and engaged with me through this forum.

I want to thank all of the past and present Nguyen and Bazan group members with whom I've shared and maintained a lab for the past 5 years: Reila Amarel, Justin Beavers, Eline Begemann, Dr. Viktor Brus, Dr. Mark Burgers, David Cao, Sam Collins,

Dr. Chelsea Catania, Dr. Jessica Coughlin, Dr. Xuan-Dung Dang, Dr. Jenny Du, Dr. Binh Duong, Michael Ford, Dr. Michele Guide, Dr. Mike Heiber, Dr. Yuanyuan Hu, Dr. Ye (Jessica) Huang, Jianfei Huang, Michael Hughes, Dr. Seiichiro Izawa, Aldo Jordan, Akchheta Karki, Dr. Nate Kirchhofer, Dr. Seojin Ko, Dr. ir. Martijn Kuik, Dr. Hui Li, Kenny Liao, Alex Lill, Dr. Jason Lin, Dr. Jianhua Lin, Dr. Jack Love, Ben Luginbuhl, Caitlin McDowell, Dr. Oleksandr Mikhnenko, Prof. Takashi Okubo, Dr. Hung Phan, Tyler Postle, Dr. Chris Proctor, Dr. Lijiao Ren, Zachary Rengert, Katie Rosenthal, Martin Seifrid, Dr. Alex Sharenko, Dr. Jes Sherman, Dr. Chris Takacs, Dr. Cristiano Woellner, Dr. Jianyu Yuan, Brett Yurash, Dr. Peter Zalar, and Dr. Yuan Zhang. Most of these people have taken active part in cleaning, maintaining, stocking, and fixing the lab. The lab continues to run because everyone working there takes an active part in lab maintenance.

I want to thank my officemates, Sam Collins, Yuanyuan Hu, Michael Hughes, Martijn Kuik, Jack Love, Alex Mikhnenko, Zach Rengert, and Cristiano Woellner, with whom I have shared daily joys and frustrations, and who often brightened my day with insight or shenanigans. My classmates, Hung Phan, Sam Collins, Chelsea Catania, Jessi Coughlin, and Mark Burgers with whom I went through the stages of the PhD, and figured out the necessary details and steps. The post-docs that have enlightened and challenged me: Viktor Brus, Xuan-Dung Dang, Jenny Du, Binh Duong, Mike Heiber, Yuanyuan Hu, Jessica Huang, Martijn Kuik, Hui Li, Jianhua Liu, Alex Mikhnenko, Lijiao Ren, Cristiano Woellner, Yuan Zhang . The older graduate students who trained me, answered my questions, and took part in my development: Michele Guide, Jason Lin, Jack Love, Chris Proctor, Alex Sharenko, Jes Sherman, Chris Takacs, and Peter Zalar. The younger students with whom I had the chance to work with directly: Reila Amarel, Justin Beavers, Michael Hughes, Akchheta Karki, Ben Luginbuhl, Caitlin McDowell, Katie Rosenthal, and Brett Yurash. And the younger students with whom I discussed our research: Eline

Begemann, David Cao, Jianfei Huang, Kenny Liao, Alex Lill, Tyler Postle, and Zach Rengert. Many of these people are very special to me: they have made my experience in grad-school fun and supportive both personally nad professionaly. I hope you know who you are.

Although this is not directly pertaining to the dissertation document, I also want to put in writing that I am grateful to my colleagues and friends who have been so supportive of me during the time that I was preparing for my defense and writing this document. I was especially touched when Akchheta Karki, Ben Luginbuhl, Katie Rosenthal, and David Cao took it upon themselves to prepare amazing home-made food for snacks at my defense, presented with a most professional arrangement. At the same time, Michael Hughes, Dr. Seojin Ko, David Cao, and Michael Ford, were very kind to me in offering jokes, chocolates, little good-luck and 'bear-up' gifts, and by taking responsibilities off my hands before the defense. In a similar line, I want to thank those of you who helped me prepare for my defense talk by listening to it once before the defense itself, and providing me with comments, questions, criticism and compliments: Brett Yurahs, Ben Luginbuhl, Katie Rosenthal, Michael Hughes, Dr. Seojin Ko, and Sam Collins. You are all wonderful, sweet people.

Finally, I am so thankful for the love, encouragement, teaching and advice I have received from my family, friends, and significant others. In particular, my immediate family: my parents and my siblings. You are incredible, and I love you all dearly.

I am filled with love and appreciation for many of the people I encountered on this path. Thank you all.

This dissertation was supported by the National Science Foundation (NSF) Graduate Research Fellowship Program (GRFP), John H. Tokuyama Memorial Fellowship, and De-

partment of the Navy, Office of Naval Research Award No. N00014-14-1-0580. Through my graduate studies I was awarded two travel fellowships from the Dow Materials Institute and the Materials Research Laboratory, and a UCSB Doctoral Student Travel Grant.

Curriculum Vitæ

Niva Alina Ran

Education

2017 Doctor of Philosophy in Chemistry (Materials Chemistry), University of California, Santa Barbara, CA 93106 USA.

2011 Bachelor of Science in Chemical Engineering conc. in Biochemical Engineering, University of Massachusetts, Amherst, Amherst, MA .

First Author Publications

2016 *Charge generation and recombination in a system with a low E_{loss}*, N. A. Ran, M. P. Hughes, M. C. Heiber, J. A. Love, X. Jiao, A. Karki, H. Wang, M. Wang, V. V. Brus, B. Kippelen, D. Neher, H. Ade, G. C. Bazan, and T.-Q. Nguyen. Submitted (2016).

2016 *Impact of Interfacial Molecular Orientation on Radiative Recombination and Charge Generation Efficiencies*, N. A. Ran, S. Roland, J. A. Love, V. Savikhin, C. J. Takacs, Y.-T. Fu, H. Li, V. Coropceanu, X. Liu, J.-L. Brédas, G. C. Bazan, M. F. Toney, D. Neher, and T.-Q. Nguyen. Under Review (2016).

2016 *Small is Powerful: Recent Progress in Solution-Processed Small Molecule Solar Cells*, S. D. Collins,* N. A. Ran,* M. C. Heiber,* and T.-Q. Nguyen. *Adv. Energy Mater.* Accepted (2015). *Authors contributed equally

2015 *Harvesting the Full Potential of Photons with Organic Solar Cells*, N. A. Ran, J. A. Love, C. J. Takacs, A. Sadhanala, J. K. Beavers, S. D. Collins, Y. Huang, M. Wang, R. H. Friend, G. C. Bazan, T.-Q. Nguyen. *Adv. Mater.* **28**, 1482 (2015). [DOI]

2014 *Understanding the Charge Transfer State and Singlet Exciton Emission from Solution Processed Small Molecule Organic Solar Cells*, N. A. Ran, M. Kuik, J. A. Love, C. M. Proctor, I. Nagao, G. C. Bazan, and T.-Q. Nguyen. *Adv. Mater.* **26**, 7405 (2014). [DOI]

Co-author Publications

2016 *Limits for Recombination in a Low Energy Loss Organic Heterojunction*, S. M. Menke, A. Sadhanala, M. Nikolka, N. A. Ran, M. K. Ravva, S. Abdel-Azeim, H. L. Stern, H. Sirringhaus, T.-Q. Nguyen, J.-L. Brédas, G. C. Bazan, and R. H. Friend. *ACS Nano* Article ASAP (2016). [DOI]

2016 *Capacitance Spectroscopy for Quantifying Recombination Losses in Nonfullerene SmallMolecule Bulk Heterojunction Solar Cells*, V. V. Brus, C. M. Proctor, N. A. Ran, and T.-Q. Nguyen. *Adv. Energy Mater.* **6**, 1502250 (2016). [DOI]

2015 *Understanding Open-Circuit Voltage Loss through the Density of States in Organic Bulk Heterojunction Solar Cells*, S. D. Collins, C. M. Proctor, N. A. Ran, and T.-Q. Nguyen. *Adv. Energy Mater.* **6**, 1501721 (2015). [DOI]

2014 *Effects of Processing Conditions on the Recombination Reduction in Small Molecule Bulk Heterojunction Solar Cells*, P. Zalar, M. Kuik, N. A. Ran, and T.-Q. Nguyen. *Adv. Energy Mater.* **4**, 1400438 (2014). [DOI]

Presentations

2016 *Effects of Molecular Orientation in Organic Solar Cells*, Poster Presentation. N. A. Ran, S. Roland, J. A. Love, V. Savikhin, C. J. Takacs, X. Liu, G. C. Bazan, M. F. Toney, D. Neher, T.-Q. Nguyen. **Gordon Research Conference: Electronic Processes in Organic Materials 2016**. Lucca (Barga), Italy.

2016 *Energetic Offsets and Photovoltaic Performance: A high open circuit voltage system plagued with a low fill factor*, Oral Paper. N. A. Ran, J. A. Love, M. Heiber, M. Hughes, J. Beavers, H. Wang, V. Brus, C. Takacs, S. Collins, M. Wang, G. C. Bazan, T.-Q. Nguyen. **CPOS (Center for Polymers and Organic Solids) meeting, 2016**. Santa Barbara, CA.

2016 *Painting a Potential Landscape: the Effects of Molecular Orientation on the Open Circuit Voltage in Organic Solar Cells*, Oral Paper. N. A. Ran, S. Roland, J. A. Love, V. Savikhin, C. J. Takacs, X. Liu, G. C. Bazan, M. F. Toney, D. Neher, T.-Q. Nguyen. **UCSB-Chalmers Symposium 2016**. Santa Barbara, CA.

2015 *Painting the Energetic Landscape: the Importance of Molecular Orientation*, Oral Paper. N. A. Ran, J. A. Love, S. Roland, V. V. Brus, C. J. Takacs, D. Neher, G. C. Bazan, and T.-Q. Nguyen. **Chemical Sciences Student Seminar 2015**. Santa Barbara, CA.

2015 *Painting the Energetic Landscape: the Effects of Molecular Orientation in Organic Solar Cells*, Oral Paper. N. A. Ran, J. A. Love, S. Roland, V. Savikhin, S. D. Collins, C. J. Takacs, M. F. Toney, D. Neher, G. C. Bazan, and T.-Q. Nguyen. **Fπ12 (12th International Symposium on Functional π-Electron Systems) 2015**. Seattle, WA.

2015 *Molecular orientation at the donor-acceptor interface*, Oral Paper. N. A. Ran, S. Roland, J. A. Love, S. Collins, O. Mikhnenko, V. Brus, V. Savikhin, V. Coropceanu, H. Li, Y.-T. Fu, X. Liu, J.-L. Brédas, M. F. Toney, G. C. Bazan, D. Neher, and T.-Q. Nguyen. **CPOS (Center for Polymers and Organic Solids) meeting, 2015**. Santa Barbara, CA.

2015 *The Morphology-Dependent Emission from High-Performing Small-Molecule Solar-Cells*, Oral Paper. N. A. Ran, M. Kuik, J. A. Love, C. M. Proctor, A. Sharenko, and T.-Q. Nguyen. **Spring MRS (Materials Research Society) 2015**. San Francisco, CA.

2014 *On the surprising emission from high-performing small molecule OPVs*, Oral Paper. N. A. Ran, M. Kuik, J. A. Love, A. Sharenko, C. M. Proctor, and T.-Q. Nguyen. **CPOS (Center for Polymers and Organic Solids) meeting, 2014**. Santa Barbara, CA.

2014 *On the "Metallic-Like" Conductivity of Biofilms*, Oral Paper. N. A. Ran and T.-Q. Nguyen. **UCSB Bioelectronics Workshop 2015**. Santa Barbara, CA.

2013 *Probing the Charge Transfer State to Understand Carrier Recombination in Small Molecule Solar Cells*, Oral Paper. N. A. Ran, M. Kuik, J. A. Love, and T.-Q. Nguyen. **Fπ11 (11th International Symposium on Functional π-Electron Systems) 2013**. Arcachon, France.

2013 *Probing the Charge Transfer State to Understand Carrier Recombination in Small Molecule Solar Cells*, Oral Paper. N. A. Ran, M. Kuik, J. A. Love, and T.-Q. Nguyen. **CPOS (Center for Polymers and Organic Solids) meeting, 2013**. Santa Barbara, CA.

Selected Honors

2016 1^{st} Place, Talk Award in the Chemical Sciences Student Seminars, University of California, Santa Barbara

2015 John H. Tokuyama Memorial Fellowship, University of California, Santa Barbara

2015 Outstanding Service to the Department of Chemistry and Biochemistry, University of California, Santa Barbara

2014 1st place, International Womens Hackathon, University of California, Santa Barbara

2012 Phi Lambda Upsilon Award, University of California, Santa Barbara

2012 National Science foundation (NSF) Graduate Research Fellowship Program (GRFP)

Abstract

At the Junction of Organic Solar Cells: Charge Generation and Recombination at Donor/Acceptor Interfaces

by

Niva Alina Ran

Heterojunction, what's your function?

In organic electronic devices composed of donor and acceptor semiconductors, the donor/acceptor interface is most typically the site with all the action: *i.e.* charge-carrier generation and recombination. Developing an understanding of the optimal geometry and energetics at this interface is necessary to optimize the active material and device architecture for their desired application. In this dissertation, we explore the role of morphology and energetics at the donor/acceptor interfaces on photovoltaic performance, but the results can be applied to any device with donor/acceptor heterojunctions.

We begin our investigation by characterizing emission from small-molecule blends. We find a correlation between the emergence of phase separation and crystallinity, electroluminescence from the donor singlet-state, and good photovoltaic performance. Next, upon demonstrating control over the molecular orientation, we then uncover the genuine effects of molecular geometry at the donor/acceptor interface on charge generation and recombination: (i) Face-on devices have a higher open-circuit voltage, due to greater charge transfer state energy and radiative efficiency. (ii) Edge-on devices are more efficient at charge generation, which is attributed to a smaller electronic coupling and a lower activation energy for charge generation.

From the perspective of energetics, we focus on a polymer-fullerene blend system

with small energetic offsets. This system has very low potential losses: it achieves a high open circuit voltage relative to the energy of the absorbed photons. We characterize the energetic landscape in this blend and conclude that the blend has very high energetic order, and that potential losses associated with charge transfer have been minimized. Unfortunately, the blend is also characterized by exceptionally fast bimolecular recombination, most likely resulting from a highly-mixed blend morphology and charge-trapping effects. Nonetheless, these results are promising as they suggest that given an optimized morphology, organic solar cells (and other organic electronic devices) have more potential than we had previously believed.

Contents

List of Figures

List of Tables

Chapter 1

'Cause We Are Living in an Electronic World: An Introduction

Electricity is often called wonderful, beautiful; but it is so only in common with the other forces of nature. The beauty of electricity or of any other force is not that the power is mysterious, and unexpected, touching every sense at unawares in turn, but that it is under law, and that the taught intellect can even govern it largely.

– Michael Farady

We are living in an electronic world. From the evolution of our species, or even preceding our species, efforts have been dedicated to improving and easing our lives. Today, every aspect of our lives is dependent on electronic advancements, and everything requires energy: satisfying almost every aspect of our basic needs has become far more efficient and easy with energy-consuming advancements (providing food and protection from environmental conditions, etc.), our health care, sanitation and waste disposal (which have played a major role in improving our health), and our leisure activities (which would not be possible or relevant without freeing up our time from providing for our basic needs). Indeed, humans have lived and survived without the luxuries afforded by these energy-

centric advancements, but I for one, certainly would not want to unwind and live under conditions that require me to produce all essentials for life from scratch, with no time left for reflection on the self and the world around, the very thing that makes life so enjoyable.

In April of 2016, the 81% of the energy consumed in the U.S. was supplied by fossil fuels: petroleum (36%), natural gas (29%), and coal (16%).[1]. As indicated by the name, these sources of energy require long period of time to form, and are therefore a limited resource, and if human kind continues to burn them for energy the will eventually run out. However, there is an even more grave side effect to the burning of fossil fuels, and that is the introduction of massive amounts of carbon dioxide to the earth's atmosphere. Carbon dioxide is identified by the Environmental Protection Agency to constitute about 80% of total greenhouse gases, which have the effect of global warming.[2] There is unambiguous evidence that human activities, such as the burning of these fossil fuels, plays a role in changing the ecology of our earth, thereby producing unrepairable harm.[3] It is thus of paramount importance that we develop renewable ways to produce energy, so we can continue our exploration of the self and the universe, and with that continue improving the lives of human kind. There are a number of research directions aimed at solving this issue, focusing on different technologies to produce energy, among them wind energy, biofuels, geothermal energy, biomass energy, hydropower, and solar energy. In this dissertation we will focus on harvesting solar power.

1.1 The photovoltaic active layer

Most commonly recognized and commercially used, are solar panels where the material that absorbs light and converts it to power is a layer of silicon. Silicon solar cells are shown for example in Figure 1.1, a picture taken at the Santa Cruz islands directly across

Figure 1.1: Silicon solar cell panels on Santa Cruz Island across from UCSB.

from the University of California, Santa Barbara. Silicon solar cells, while cheaply and efficiently converting solar radiance to useful power, are limited in their applications. Silicon solar cells require processing at harsh conditions, generally under high temperatures and pressures, and the final silicon layer is brittle - this limits the substrates onto which silicon can be grown. In order to absorb enough light, the active layer of silicon must be relatively thick, and the resulting solar cells are heavy and require significant structural support. For these reasons, silicon-based solar cells may be helpful and useful when used in solar-farms, or on top of well-supported structures. However, their application versatility is limited.

Luckily, the active layer of solar cells does not have to be silicon, and among the alternatives are organic semiconductors. Organic semiconductors are molecules with conjugated backbones, primarily comprised of carbon. The conjugation is achieved by

alternating single and double bonds, which allows for electron delocalization along π-orbitals of the molecules. The properties of organic semiconductors can be tailored for the desired application by means of molecular design, opening a vast array of possibilities.[4] Among these tunable properties are the semiconductor bandgap (which will dictate the wavelengths absorbed and emitted), solubility (allow for solution processing out of the preferred solvents), and self-assembly (dictate the morphology of the semiconductor in the solid state, which has profound effects on the properties of the semiconductor - this will be discussed in detail in this dissertation), to name a few. In fact, in 1977 Heeger, MacDiarmid and Shirakawa demonstrated that an organic polymer, polyacetylene, can attain metallic conductivity by doping with iodine.[5] This work eventually lead to the Nobel Prize in Chemistry, awarded to Heeger, MacDiarmid, and Shirakawa in 2000.[6] Figure 1.2 shows a range of semiconductors that were found in the drawers of our lab, dissolved in solution. Using ultraviolet light excitation, the image shows the varying colors of the semiconductors, achieved by modifying the bandgap of the semiconductors. In addition to this great tunability by molecular design, organic semiconductors are far better absorbers than silicon, which will enable fabricating devices that can absorb all incident photons using much thinner active layer thicknesses. Further more, solar cell devices made of organic semiconductors are able to maintain their photovoltaic performance under a wider range of incident angles and light intensities, while silicon solar cells have a larger percent drop in performance under these conditions when compared to direct, high intensity illumination.

These characteristics and advantages of organic semiconductors make them a promising active material for any electronic material. Advances in organic chemistry allows for vast control over the electronic properties of organic semiconductors, and thanks to efforts of many research labs around the word, the field is achieving higher and better performance. Adding solubalizing chains to the organic semiconductors can enable

solution processing, which can be done at ambient temperatures and pressures. This opens the door for fast, large scale, roll-to-roll processing, which can provide for high through-put and cheap manufacturing of devices. While it has been accepted that organic semiconductors will not be able to out-compete silicon in photovoltaic efficiency, even when normalized for price, with single-junction silicon solar cells achieving 26% in the lab, and 17% commercially, and their cost steadily decreasing due to large scale manufacturing and technological improvements (data taken from a report published in November, 2016, but the Fraunhofer Institute for Solar Energy Systems).[7] However, organic semiconductors are particularly well suited for a range of niche applications which require light-weight, flexible, and tunable solar cells. One such example includes efforts by the start-up NEXT Energy Technologies Inc., based in Santa Barbara, and developed from research done at UCSB. NEXT develops photovoltaic window coatings with up to 10% efficiency that can be inserted between dual-pain windows, with varying degrees of transparency and aesthetic choice of colors. These photovoltaic coatings are transparent to most of the visible light, yet they assist in temperature control of the building while generating power. This would not be possible with traditional inorganic solar cells.

However, since this is the introduction to my PhD dissertation, it should come without surprise that organic solar cells are still an active area of research, with many scientists around the world passionately developing new organic semiconductors, device fabrication methods, and studying the physics of charge generation, recombination, and extraction. There exists a vibrant community that is focused on developing a better understanding of the working principles behind solution-processed solar cells, and thereby pushing them to higher efficiencies. Figure 1.3 shows an example of a lab-scale solar cell device fabricated in our lab by spin coating an active layer (from a solution of semiconductors, not unlike the ones shown in Figure 1.2) on a glass substrate sputtered with a transparent electrode (ITO). Metal contacts are evaporated on the active layer to complete the device. The

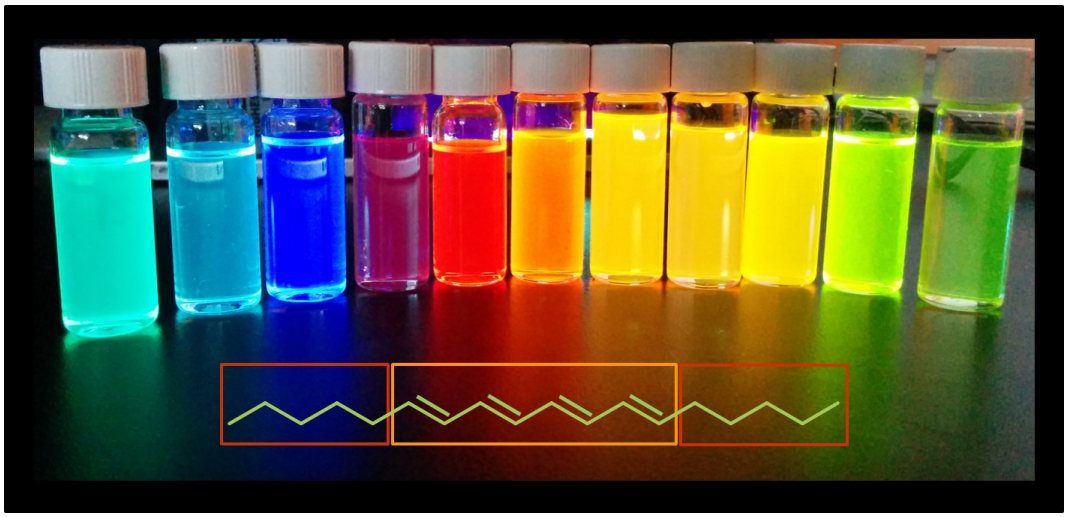

Figure 1.2: Organic semiconductors dissolved in solution and excited by a UV lamp.

device in Figure 1.3 is in a probe station, which can be used to study charge transport in the active layer. Finally, as can be inferred, the underlying aim of the topic of my dissertation is to understand the working principles of organic solar cells.

Befofe we can talk about my research, we need to arrive at a common understanding about a few basics regarding the photovoltaic effect, organic (excitonic) semiconductors, donor/acceptor solar cells, the charge transfer state, and solar cell characterization parameters.

1.2 The photovoltaic effect

Photogeneration is only possible in semiconductor materials, defined, as the name would suggest, as a material with conductivity between a metal and an insulator. Semiconductors have a bandgap which separates the energetic level where electrons reside (often referred to as the ground-state, valence band, highest-occupied molecular orbital (HOMO), or the ionization potential (IP)), and the next available electronic level (re-

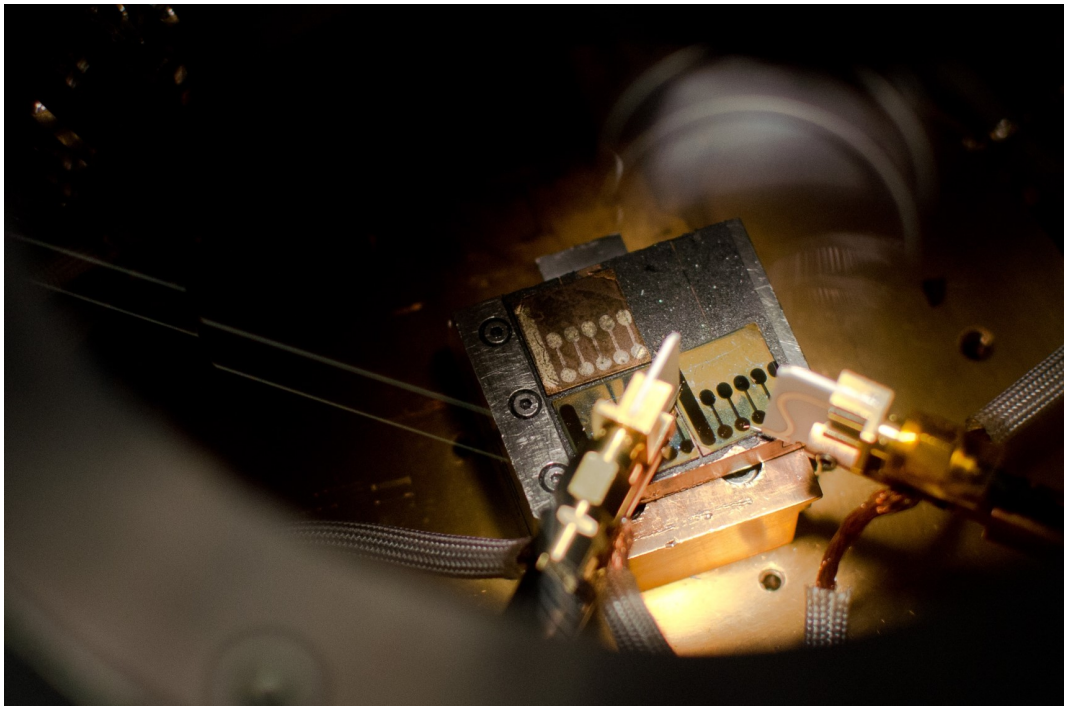

Figure 1.3: A thin film diode devices made in our lab, in a probe station. Picture taken by Oleksandr Mikhnenko.

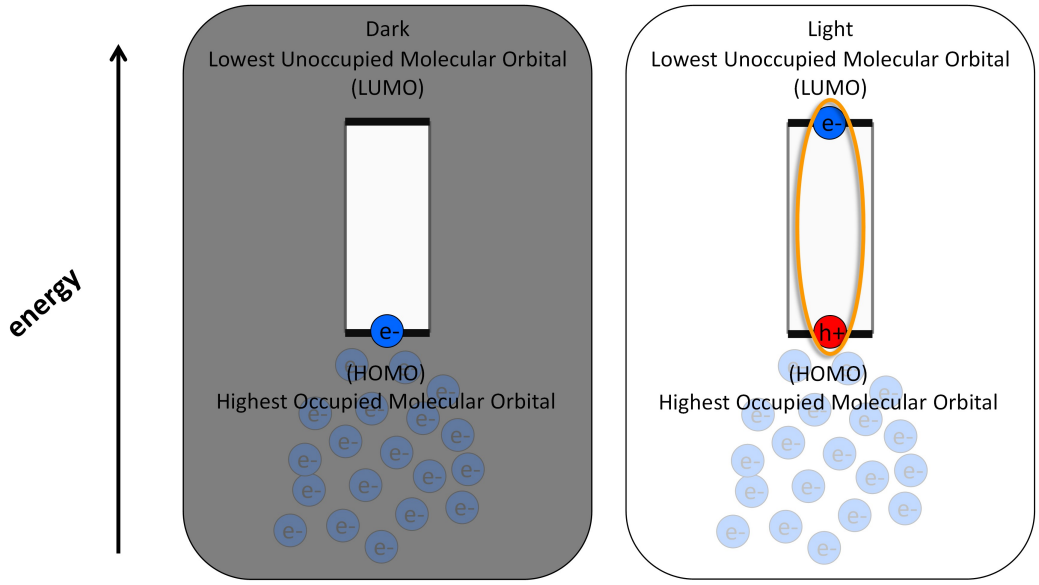

Figure 1.4: An illustration of photoexcitation in an organic semiconductor. On the left, the semiconductor is in the dark, and all electrons are in the HOMO or deeper in energy. On the right, the semiconductor is in the light and an electron has been photoexcited and promoted to the LUMO, leaving a hole in the HOMO.

ferred to as the excited state, conduction band, lowest unoccupied molecular orbital (LUMO), or the electron affinity (EA)). Given the right amount of energy, electrons can be promoted from the HOMO to the LUMO, leaving behind an empty state, referred to as a hole. Electrons are transported through LUMO overlap and holes by HOMO overlap. Photons with energy equivalent to the bandgap, or larger, can supply the necessary excitation to promote the electron, as is schematically represented in Figure 1.4. In Figure 1.4, the HOMO and LUMO levels are represented on an energy scale where vacuum defines energy = 0 eV. HOMO and LUMO levels have negative eV values: the deeper the energy level, the more stable the material, and more energy is required to remove an electron. Besides the HOMO and LUMO levels, there are many electronic levels present, but because we are primarily interested in the HOMO and LUMO, the rest of the electronic levels are not depicted. The bandgap of the semiconductor in Figure 1.4 is represented as a rectangle.

1.3 Organic excitonic semiconductors

Unfortunately, the story for photogeneration in organic semiconductors is more complicated than simply exciting an electron from the HOMO to the LUMO, and creating free carriers (which is true in inorganic solar cells). Organic semiconductors are characterized as excitonic semiconductors. Unlike the case of inorganic semiconductors, such as silicon, when an electron is promoted to the LUMO, it remains bound to the hole that is left in the HOMO, forming a Coulombically bound and localized hole-electron pair, called a Frenkel exciton. The Coulombic binding energy in organic semiconductors is typically between 0.5-1 eV.[8] In Figure 1.4, the exciton is depicted as the orange oval binding the hole and the electron. Excitons can diffuse around from molecule to molecule, and are characterized by certain diffusion lengths and lifetimes. This topic has been the center for a number of PhD dissertations, such as the dissertation of Dr. Jason Lin from our group, and we will not go into depth on this topic. What is necessary to understand for the purpose of this dissertation, is that excitons are characterized by a large binding energy, and require some driving force for charge separation. Without this driving force for charge separation, the electron in the exciton will relax back to the ground state, recombining with the hole, thus losing the potential energy that could be harvested from the photoexcitation.

In organic photovoltaics, the recombination of excitons was overcome by introducing a second semiconductor which has energy levels (HOMO and LUMO) that are both either lower or higher in energy. This provides a thermodynamic driving force for the electron and hole to separate and generate free charge carriers. Electrons always strive to be lower in energy, and holes higher in energy. The semiconductor that has deeper energy levels is thus referred to as the electron acceptor, and the other semiconductor is the electron donor. If the exciton is formed on the donor, it can be transferred to the acceptor, but

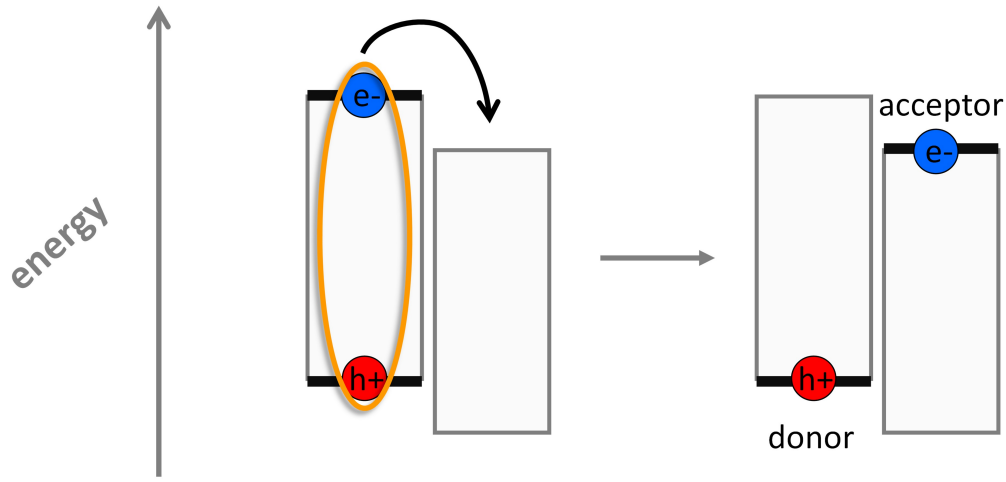

Figure 1.5: A cartoon depiction of the energetic cascade at a donor acceptor interface. The exciton, generated on the donor, has a thermodynamic driving force to split by charge transfer of the electron to the lower-energy LUMO of the acceptor.

the hole will stay on the donor. The process of charge transfer from donor to acceptor is depicted pictorially in Figure 1.5.

1.4 Donor/acceptor solar cells

The research that the organic cell community is conducting is all based on the donor/acceptor charge transfer scheme, and is thus all based on the work of Ching W. Tang. While working at Eastman Kodak Company, in 1986 Tang reported the first heterojunction solar cell, which was made of a donor layer and an acceptor layer, similar to what is shown in panel (a) of Figure 1.6.[9]. It is notable that around the same time Tang was also the first to report on the first organic light emitting diode (LED), the basis of the LED screens used in some Samsung smart-phones today. For the concept of the donor/acceptor driving force to work, excitons generated on a neat material (either in the donor or acceptor layers) must diffuse to a donor/acceptor interface where charge transfer can occur. As noted above, however, excitons have a short diffusion length, on

the order of 10-15 nm.[10] This means, that in order to harvest the energy in the exciton, the donor and acceptor layers cannot be thicker than 15 nm each, which would set such a limitation on the device thickness that the solar cell would hardly absorb any photons. Researchers in the field of organic solar cells have attempted to design the best morphology of the donor and acceptor phases to optimize exciton quenching (by charge transfer at the donor/acceptor interface) and charge transport to the electrodes. Panel (b) in Figure 1.6 shows an example of an interdigitated donor/acceptor morphology, which was offered as a solution to the balance between the exciton diffusion length and absorption strength. However, it has proven significantly challenging to fabricate such a morphology, particularly if the overarching goal is produce low-cost, high-throughput solar cells. The solution to this predicament was finally offered by Yu, Gao, Hummelen, Wudl, and Heeger, in a seminal reserach paper published in *Science*, introducing the concept of a bulk heterojunction (BHJ) solar cell,[11] shown schematically in panel (c) of Figure 1.6.

To fabricate a BHJ solar cell, the donor and acceptor materials are dissolved in the same solution, from which a film is cast. The donor and acceptor then form a "network of internal donor-acceptor heterojunctions" by spontaneously phase separating from each other during the casting process. However, it turns out that BHJ final morphology plays a huge role in the final solar cell performance of the device, and relying on the donor and acceptor materials to phase separate is not sufficient. Panel (d) of Figure 1.6 shows a BHJ morphology where the donor and acceptor are intimately mixed, which is an example of a morphology that time and time again has been shown to lead to very poor solar cell performance.[12] How to spontaneously form a BHJ with optimal morphology is an unanswered question, that will have a tremendous impact on the field of organic solar cells. To date, most research groups use certain techniques to change the film morphology, iteratively trying different conditions to arrive at the optimal solar cell performance. Among these techniques are options such as thermal or solvent vapor

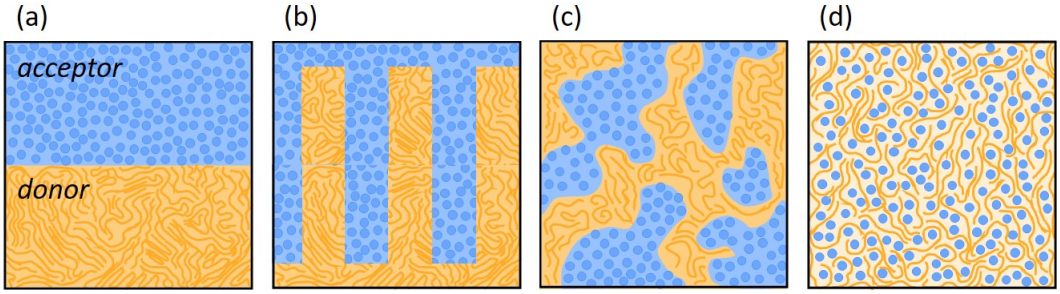

Figure 1.6: Evolution of the architecture for a donor/acceptor heterojunction. (a) bialyer, (b) interdigitated pillars, (c) bulk heterojunction with well separated phases, (d) bulk heterojunction with intimate mixing between donor and acceptor.

annealing (or a combination of both), use of small-molecule solvent additives, use of insulating polymer additives, and ideally control of final morphology by molecular design. Although some examples of high performance BHJ blends that spontaneously form the optimal film morphology,[13, 14, 15] these developments were achieved more by way of accident than by rational design. There are also recent examples of donor polymers which are only soluble in the solution at elevated temperatures, and as the solution cools during the casting process they crash out and form separated phases.[16] While this second example is very clever and allows for blending the same donor with many acceptor but maintaining a good performance, it can be difficult to control and implement effectively. Development of semiconductor blends that can achieve optimal morphology without the need for optimization and additional processing steps can have a very large impact on the performance and viability of organic semiconductors as commercial solar cell materials. Here it is in place to mention that even the concept of the optimal morphology is not well defined to date. What has been established is that it is necessary to have separate, interconnected and bicontinuous donor and acceptor phases with high domain purity (little driving force for mixing between donor and acceptor).

1.5 The charge transfer state

Morphological considerations aside, the development of the donor/acceptor heterojunction introduced more complications into the operation of organic solar cells. Wavefunction overlap, which allows the delocalization of the electrons along the π-orbitals of the semiconductors, can also occur between two different molecules. Ground state wavefunction overlap between the donor and acceptor semiconductors creates a new electronic state in organic solar cells: the charge transfer (CT) state.[17] The CT state became widely accepted and characterized thanks to the seminal work of Koen Vandewal, establishing the relationship between the CT state and the open circuit voltage (V_{OC}, more on this parameter later).[18, 19] The CT state is a state that is formed due to wavefunction overlap between the LUMO of the acceptor and the HOMO of the donor. As it turns out, even after charge transfer from donor to acceptor, the hole and electron are still Coulombically bound.[17] Exactly why charge generation can proceed nearly 100% efficiently in some systems is still unclear, with many researchers quoting various factors that account for charge generation. The underlying reasons for charge generation remain a disputed topic in the literature, and is among the research directions I would have pursued if I were to stay in the field.

The CT state is, by definition, only present in samples composed of donor and acceptor semiconductors. For this reason, the CT state is most often detected by optical measurements: absorption or emission. The CT state is detected as signal at photon energies that are lower than photons absorbed or emitted by the neat blend components. Since the CT state is a state between molecules, it has a very low oscillator strength, which implies it is a very poor absorber and emitter. In fact, regular absorption techniques cannot detect it. Therefore other, more sensitive techniques, must be employed to study the CT state absorption. Such techniques include photothermal de-

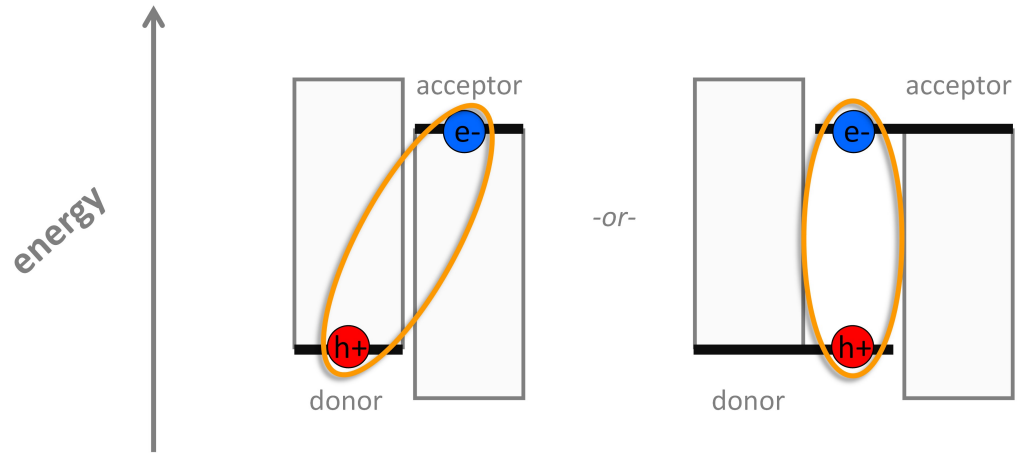

Figure 1.7: Overlap between the donor HOMO and acceptor LUMO creates a new species that is only present in the blend of the two materials, with a bandgap that is lower than either neat component.

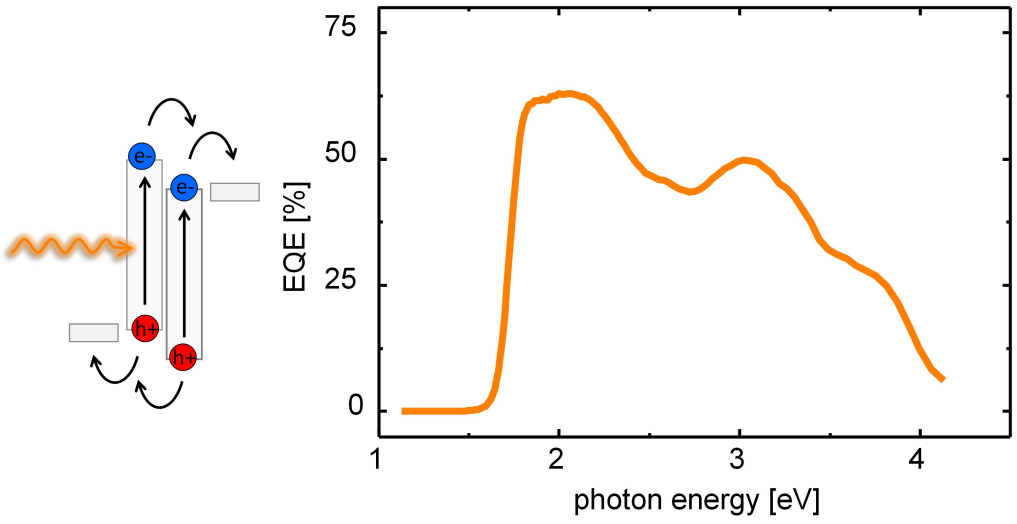

Figure 1.8: The CT state can be probed by means of absorption, such as the External Quantum Efficiency

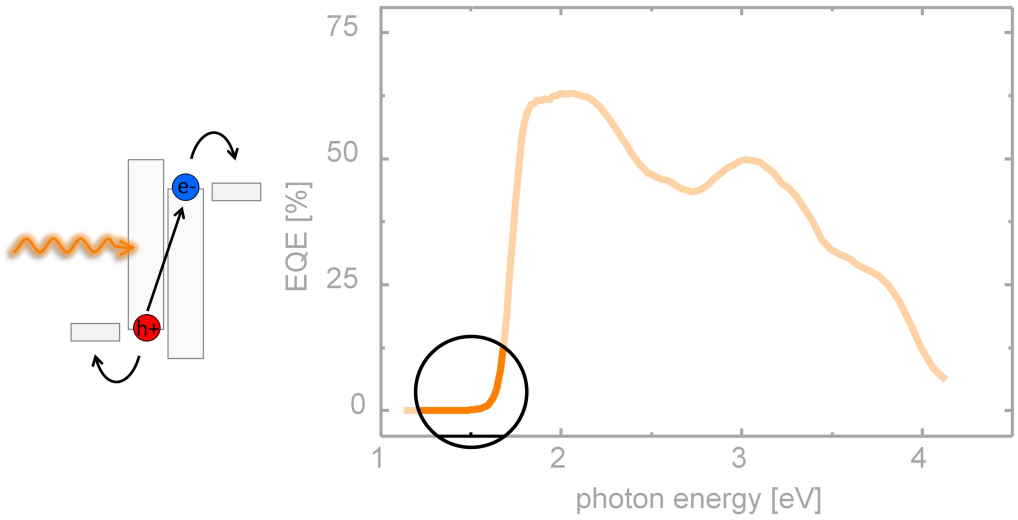

Figure 1.9: The CT state can be probed by means of absorption, such as the External Quantum Efficiency

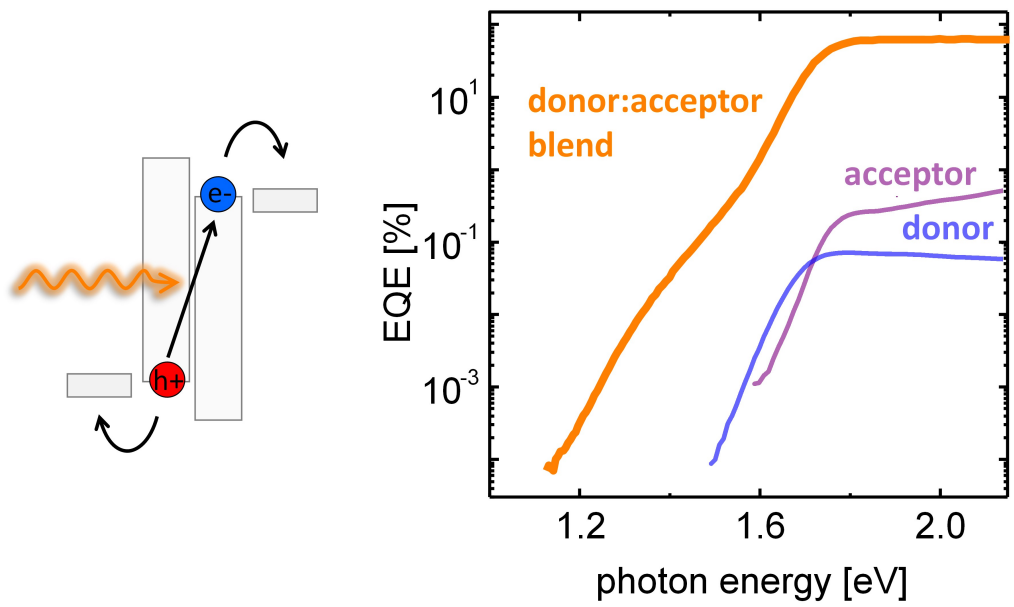

Figure 1.10: The CT state can be seen in the EQE only in the log-lin scale, as current generated from energies lower than where either donor or acceptor can generate current (absorb).

flection spectroscopy,[20] Fourier-transform photocurrent spectroscopy,[21] and external quantum efficiency (EQE) spectroscopy.[22] In the work that will be discussed in this dissertation we used EQE spectroscopy as the method to detect CTS absorption.

An example EQE spectrum is shown in Figure 1.8. The EQE spectrum shown in the figure is a typical spectrum that shows the contribution of photons of different energies to the overall photocurrent. The EQE is therefore not a direct measure of the absorption, but rather a measure of current generation as a consequence of absorption, and should be proportional to the absorption strength. However, as is noted in the cartoon to the left in the figure, most of the signal (and indeed, most of the photocurrent) in the EQE spectrum, is from absorption events in the neat donor and acceptor materials. As noted, the oscillator strength of the CTS is very low, and therefore the signature of the CT state is burried within the low-energy tail of the EQE, as is highlighted in Figure 1.9. In order to see the CT state, the EQE spectrum has be be viewed in a log-lin scale, highlighting the weak absorption events. Figure 1.10 shows the same EQE spectrum as in Figures 1.8 and 1.9, but on a log-lin scale, and focused on low photon-energies. To truly distinguish the CT state signature in the EQE, it is necessary to compare the blend spectrum with the shape of the EQE spectrum of the neat blend components, as is done in Figure 1.10. The blend EQE spectrum follows the spectra of the neat donor and acceptor materials, begins to decrease exponentially at the band-edge of the lower band-gap material, and then it begins to deviate to lower photon energies, creating a shoulder to the neat donor EQE. This shoulder is the characteristic CT state signature seen in the various absorption techniques used to identify it.

lternatively, it is possible to detect the CT state by emission spectroscopy, as well. This can be done either by photoexcitation (photoluminescence, PL)[23] or by electrical excitation (electroluminescence, EL).[24] In photoluminescence the emission spectrum can sometimes be overwhelmed by emission from the donor or acceptor singlet states,

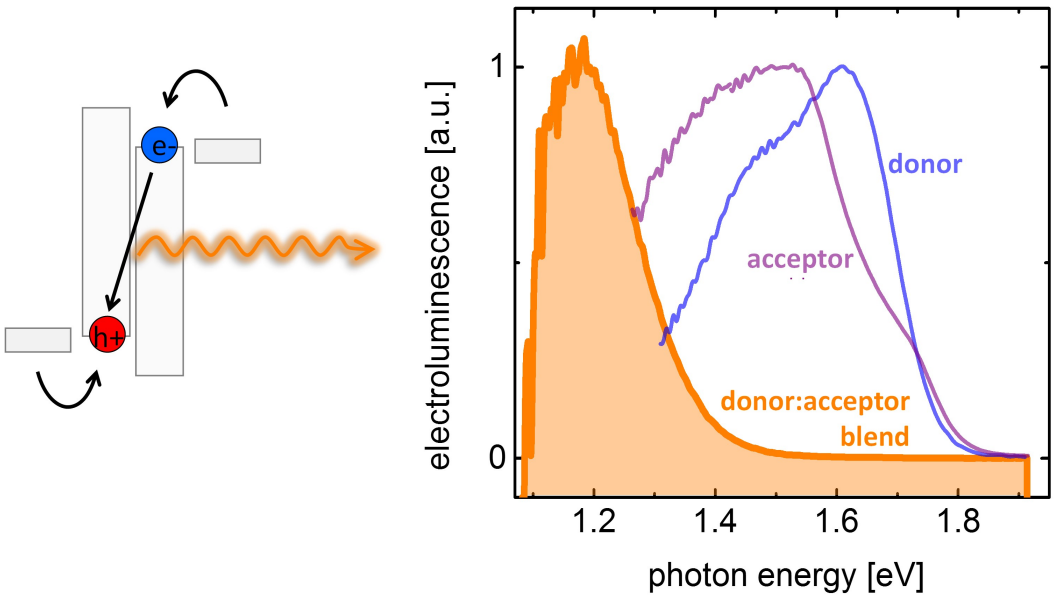

Figure 1.11: The CT state can detected in EL spectra, as emission from the solar cell at low energies (not belonging to either donor or acceptor), and having a broad, featureless emission spectrum.

hiding signal from the CT state. In EL, however, charges are injected from the electrodes due to an applied forward bias, which diffuse through the film until they meet each other and recombine radiatively. It is expected that the charge-carriers will always relax to the lowest available energetic state, through which they will recombine: in the case of most BHJ blends, it is the CT state. EL can therefore be a more sensitive emission probe to the CT state. Similarly to what was described for detecting the CT state in EQE spectra, in EL the spectrum of the blend must be compared to the spectra of donor and acceptor emission. In EL, the CT state is characterized by low-energy, featureless and broad emission spectra. Figure 1.11 shows the EL spectra of the same donor, acceptor, and blend, that were used to generate the data in Figures 1.8-1.10. When collecting the EL spectra of CT states, it is important to understand the voltage-dependence of the EL spectra, and collect the spectra at the lowest possible applied bias. This may require long exposure times or averaging of many spectra. Higher voltages may shift the emission

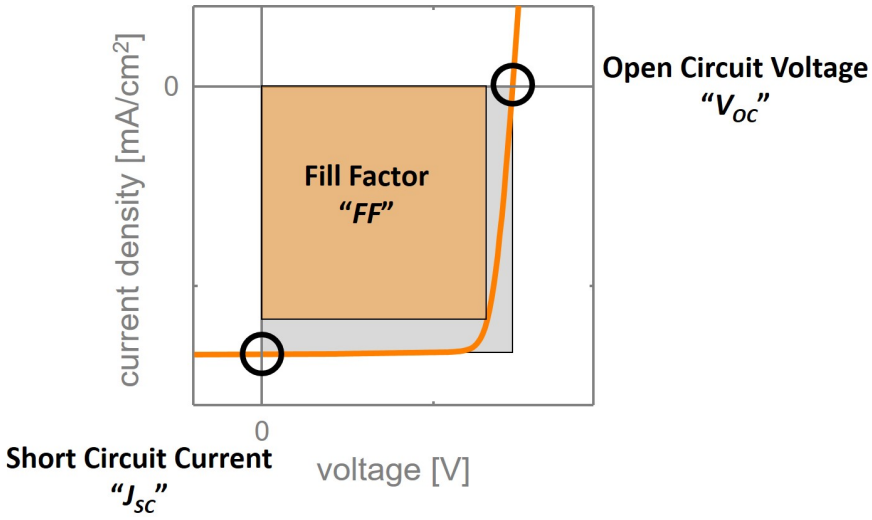

Figure 1.12: Typical J-V characteristics of a solar cell, focused on the power-generting quadrant. The parameters which determine the solar cell efficiency are highlighted in the figure.

spectrum to higher energies, or even populate the singlet state of the donor or acceptor.

1.6 Solar cell characterization parameters

Now, having established the above landscape of OPVs, we finally discuss characterization of a photovoltaic device. The characterize a photovoltaic device, the device is illuminated with white light with a filter that simulates the emission spectrum of the sun. Under illumination, a range of voltages is applied to the solar cell, and the resulting current recorded as a current-voltage (J-V) curve. From this curve, we are interested in a few points: the short-circuit current (J_{SC}), the current generated by the solar cell when the potential between the cathode and the anode is 0 V; the open-circuit voltage (V_{OC}), the voltage under which current generation and recombination in the solar cell are equal, and no current passes through the circuit; and the fill factor (FF), which is a parameter that describes the ratio between the maximum power in the J-V curve (maximum of

$P_{max} = J \times V$) *vs.* the ideal maximum power, $P_{ideal} = J_{SC} \times V_{OC}$ as $FF = \frac{P_{max}}{P_{idea}}$.These three parameters multiplied together determine the power conversion efficiency (PCE) of the solar cells: $PCE = V_{OC} \times J_{SC} \times FF$. An example J-V curve is shown in Figure 1.12, with the V_{OC}, J_{SC}, and FF illustrated on the curve. This is the basis for all solar cell characterization.

1.6.1 Energy levels in a working solar cell

As described above, organic semiconductors are characterized by HOMO and LUMO levels, where the HOMO is the hole transporting level, and the LUMO is the electron transporting level. To complete the solar cell devices, electrodes are necessary to collected the photogenerated charges. However, the electrodes have to be chosen such that they are ohmic to the hole and electron transport levels. This means that one electrode must have a work function that align well with the HOMO of the donor, and the other electrode must have a work function that aligns with the LUMO of hte acceptor. The different work function electrodes create an internal electric field in the devices that can help in charge separation and collection by giving a driving force for the appropriate charges to diffuse to the electrodes. A cartoon that has been very helpful for me in thinking about the physical processes in solar cells is based on band diagrams. While this is not an accurate depiction of the energetics in organic solar cells, since these materials are characterized by a disordered, broad density of states (DOS) which results in hopping transport as opposed to the well-defined bands in inorganic semiconductors, I include in this introduction as a tool to help develop a picture of the physics in organic solar cells. Figure 1.13 shows the evolution of the band diagram for a hypothetical solar cell under varying applied voltages, corresponding to the J-V curve in Figure 1.12.

For simplicity, we can start at J_{SC} condition, where the electrodes are at the same

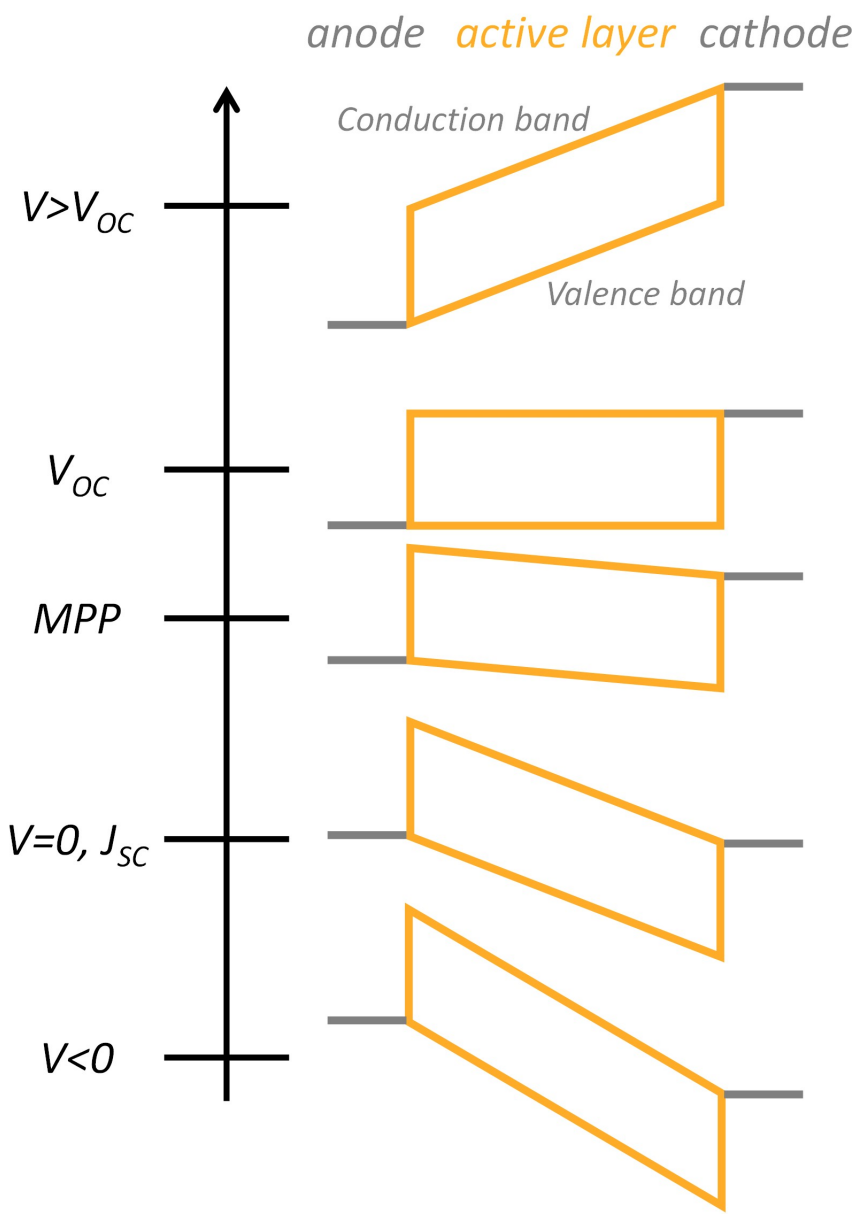

Figure 1.13: Schematic band-diagrams for the varying applied voltages, related to the current-voltage curve of the solar cell (Figure 1.12).

potential (with no applied bias). The orange box denotes the bandgap of the active layer, where the bottom of the rectangle denotes the valence band (or HOMO) and the top denotes the conduction band (or LUMO). At J_{SC} conditions, if an electron is promoted to the conduction band, it has a driving force to diffuse to the cathode (electrons always strive to lower energies) and the hole to the anode (holes want to go uphill in energy). Although there is no applied voltage, there is an internal field that assists in charge separation and charge extraction. If the energy of the cathode is deeper than the anode, this increases the electric across the device and enhances extraction. If the cathode is brought closer to vacuum, the field across the device reduces more, until the conduction and valence bands are in flat-band conditions. Under this condition, there is no driving force to extract charges, and all generated charge-carriers recombine. The voltage necessary to reach this conditions is the V_{OC}. As the cathode is brought even closer to vacuum, charges are injected into the device and recombine in the active layer. This is how EL accomplished.

Here, I would also like to discuss a topic that has sometimes been confused in literature and oral presentations: relating the HOMO and LUMO to electronic states and ionization potential (IP) and electron affinity (EA), respectively. The HOMO and LUMO energies describe one-electron molecular orbitals, which do not include effects such as electron-electron interactions (Coulomb binding energy, spin states), and cannot be thought of as descriptions of electronic states (such as the ground state, singlet excited state, or triplet excited state, etc.). HOMO and LUMO energies are described with respect to vacuum (defined as 0 eV), and since all electrons are bound to the nuclei the HOMO and LUMO are described as negative energies from vacuum (*i.e.* energy input is required to remove electrons from these orbitals). Electronic states, such as the S_1 or T_1 states (singlet and triplet states), while having the same electronic configuration (with one electron in the HOMO and the other electron promoted to the LUMO), have different energies with

respect to the ground state. To think about electronic states, it is necessary to construct a Jablonsky diagram where the ground state, S_0, has energy 0 eV. All other electronic states thus have a positive energy above the ground state. A state diagram would take into account factors such as the spin of the excited state (distinguishing between T_1 and S_1) and the Coulomb binding energy of the hole and electron forming the excited state, which change the energy of the excited state. The IP is the energy required to remove an electron from a neural molecule with many electrons, while the EA is the energy required to add an electron to a neutral molecule with all of the lower electronic levels filled. IP and EA can be experimentally estimated using techniques such as ultraviolet photoelectron spectroscopy (UPS) and cyclic voltametry (CV), both often used in OPV research. While the HOMO and LUMO are related to the IP and EA, respectively, the two can only be rough approximations of each other.

The HOMO to LUMO transition is the relevant process for excitation, but it does not describe the excited state in organic semiconductors. An organic semiconductor molecule in the ground state has a certain configuration in the ground state, which upon excitation changes to account for the excited state. The excited state therefore creates a deformation of the molecule, and may do so for the surrounding molecules, as well – this is called a polaron exciton, an excited state and the resulting deformation of the molecular lattice. Therefore the excited state is described by electronic states (S_1, for example). After charge transfer at the donor/acceptor interface, the donor and acceptor are in the relevant state as described by the product in IP and EA experiments, where the donor is missing an electron and the acceptor has an additional electron. In these cases, the ionized states of the molecules are also called polarons – where the molecules again deform to account for the additional charge (be it positive or negative).

For additional reading on the discussion above and the electronic structure of organic semiconductors, I recommend browsing through the text book written by Anna Köhler

and Heinz Bässler, reference [25], and articles written by Jean-Luc Bredas[26] and Antoine Kahn.[27]

1.6.2 The charge transfer state and the V_{OC}

We have already touched upon the notion that the energy levels in organic semiconductors, the HOMO and LUMO levels, are not discrete bands. Instead, they are characterized by a density of states (DOS) with tail states in the bandgap of the active material. While there is some discussion regarding the most relevant shape of the DOS, it has been established that some distribution of states exists, and that this distribution of states has strong effects on charge transport and the V_{OC}.[28] Given a picture of the DOS, it is thus important to define the CT state energy (E_{CT}) in a more specific manner than just what is shown in a cartoon manner in Figure 1.7 where the HOMO and LUMO are depicted as lines. Figure 1.14 shows a Gaussian DOS distribution for the HOMO of the donor and the LUMO of the acceptor on the same energy scale. The E_{CT} is defined as the difference between the maxima of the two DOS distributions.

It has been shown time and time again that the E_{CT} establishes a reliable relationship to the V_{OC}, according to: $V_{OC} = E_{CT} - 0.6 \pm 0.1eV$.[19] In fact, it has been demonstrated that the E_{CT} sets the upper limit to the V_{OC}.[29, 30] Here it is in place to bring up the Fermi level, defined as the chemical potential of electrons, and the concept of quasi-Fermi levels. upon photoexcitation, electrons are promoted to the LUMO (or EA), and they leave behind holes in the HOMO (or the IP). In this non-equilibrium state, there now exist a quasi-Fermi level for electrons in the LUMO, and a quas-Fermi level for holes in the HOMO, which define a quasi-Fermi level splitting. The quasi-Fermi level splitting is what ultimately dictates the V_{OC}, and will depend on factors such as temperature, carrier density, and DOS.[28] It therefore follows that factors that will reduce the quasi-

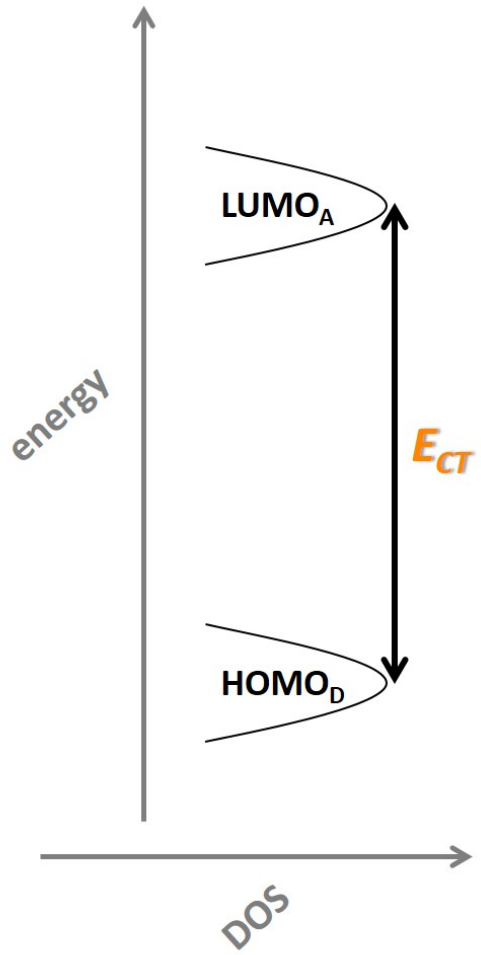

Figure 1.14: Schematic representation of the meaning of the CT state for materials with broadened HOMO and LUMO DOS. Ect is the energy of the CT state.

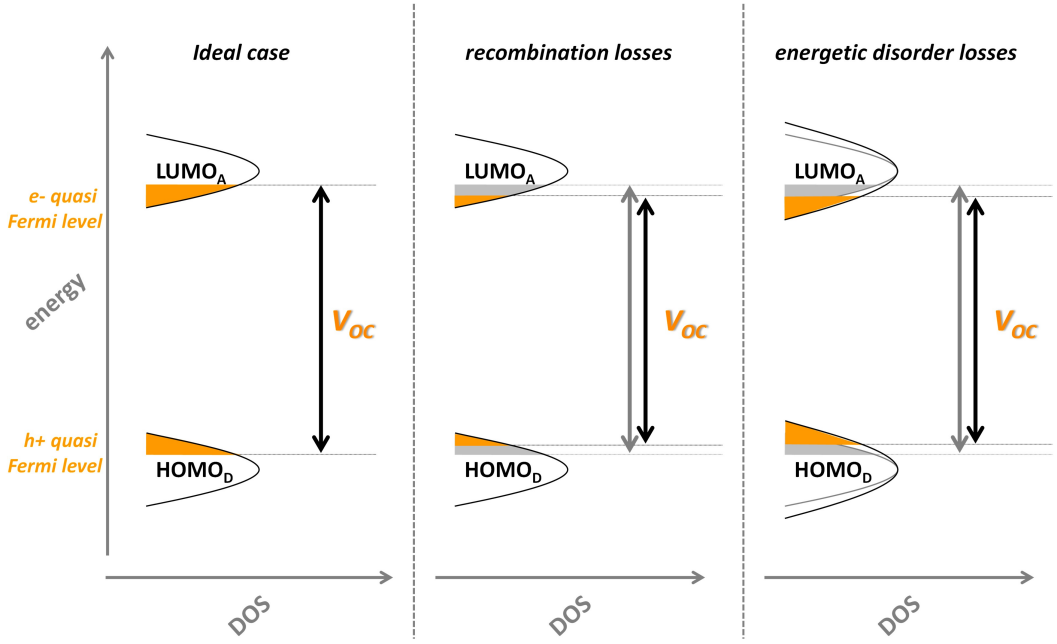

Figure 1.15: Schematic representation of recombination and energetic disorder losses and their effect on the V_{OC}.

Fermi level splitting, will also reduce the V_{OC}. For example, Figure 1.15 shows the effects of recombination losses (changing the carrier density) and energetic disorder (changing the broadening of the DOS) on the V_{OC}. Recombination losses will shift the quasi-Fermi levels deeper in the the tail states of the DOS, while energetic disorder- with the same carrier density- will bring the carriers deeper into the gap and thereby reduce the quasi-Fermi level splitting.

1.6.3 Non-radiative recombination

To detect emission from the CT state, as was done in Figure 1.11, one must first form an excited state. As noted, this can be done by means of photoexcitation or by injection of charges into the active material by a forward bias applied to the electrodes. Relaxation of an excited state can occur radiatively or non-radiatively (Figure 1.16), depending on

a few factors. First, if the active material has some electronic states that are within the bandgap, these states can act as electron or hole traps, where charges get stuck and recombine with a free, oppositely charged carrier. Trap assisted recombination is believed to be non-radiative.[31, 32] Trap assisted recombination is as likely to occur in PL as in EL. Another reason for non-radiative recombination can be due to spin correlation. In the ground state, electron pairs have opposite spins, and are referred to as a singlet ground state. Upon photoexcitation, one of those electrons is promoted to the LUMO, where it retains its spin, forming an excited singlet state. The excited electron can reverse its spin, in a process called intersystem crossing, and form a triplet state: an excited state where the electrons in the ground state and the excited state have the same spin. However, this process is more likely in molecules with heavy atoms such as iodine or bromine, and therefore does not often occur in organic semiconductors. In EL, however, charge-carriers are injected into the active layer, with uncorrelated spins. Due to spin statistics (*i.e.* math), when free charge-carriers (with uncorrelated spins) meet each other they have a 75% chance to form a triplet state. Decay from triplet states is much slower than the decay of singlet states, because triplet states must go through some forbidden transitions to relax to the ground state. In some cases, mostly in molecules that include some metal atoms, triplet decay can be phosphorescent. However, organic semiconductors used in solar cell research are rarely phosphorescent. Triplet decay is therefore considered among the explanations for for non-radiative recombination.[33] When charge-carriers decay non-radiatively, they release their energy by heat, or vibrational relaxation.

The issue of non-radiative recombination has been a topic of much discussion in the OPV community in recent years, with many researchers identifying non-radiative recombination as among the primary reasons that the V_{OC} in organic solar cells is significantly lower than the energy of photons absorbed.[34, 29] This is an open problem in OPV, and I expect that advances in molecular design (especially in acceptor materials) will

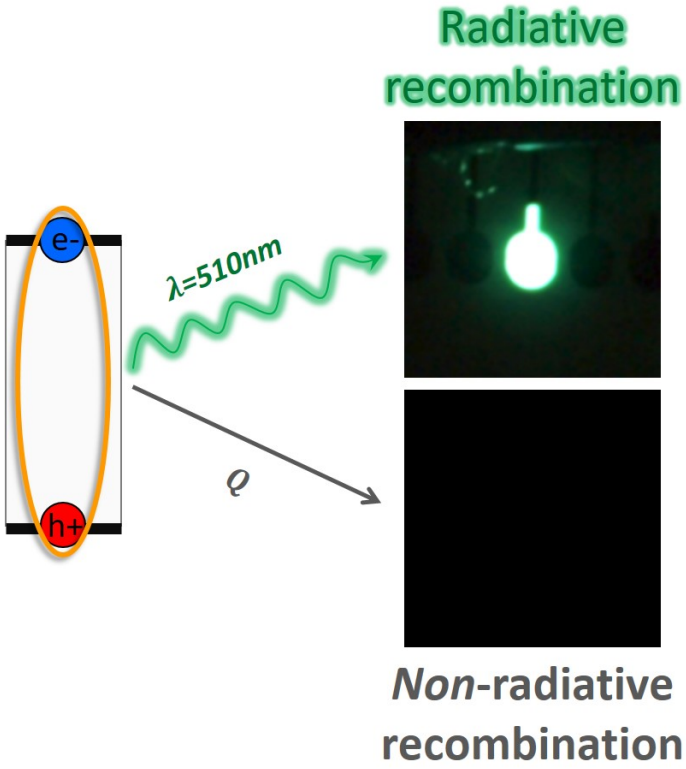

Figure 1.16: Relaxation of an excited species can occur either radiatively, releasing the energy *via* a photon with energy equivalent to the excited species' bandgap, or non-radiatively, releasing the energy *via* thermal vibrations.

lead to improvements in this domain. However, the nature of non-radiative recombination losses in OPV is not fully understood, and there may be other loss pathways (other than triplet decay and trap-assisted recombination) that lead to non-radiative recombination. In fact, some researchers have suggested that non-radiative decay is inherent to carbon-based materials due to vibrations of the carbon-carbon bonds.

1.7 Outline

This thesis dissertation is a compilation of the research I conducted during my time in the research group of Prof. Thuc-Quyen Nguyen. All studies were initiated by questions regarding the structural and electronic properties of the donor/acceptor heterojunction in organic solar cells.

Everything began with comparing the relationship between the EL intensity and applied voltage for optimized solar cells and as-cast solar cells made of small-molecule blends. The EL/applied bias relationship of the optimized solar cells indicated of trap-assisted recombination; this was surprising because these are the best performing devices and because other measurements that confirm the presence of traps did not indicate of trapping. As it turns out, the optimized solar cells did not emit only from the CT state, but also from the donor singlet state, at very low applied voltages. Chapter 2 describes the results pertaining to this, where it turns out that singlet emission is strongly correlated with donor crystallinity and phase separation. One of the molecules that was used in the study about emission from the BHJ blends turned out to be very interesting for other reasons, as well. This molecule, p-SIDT(FBTTh$_2$)$_2$, will completely change its orientation with respect to the substrate, depending on the choice of solvents. This provided us with the foundation to pursue a fundamental question in the field of organic solar cells: what significance does the molecular orientation of the donor (or acceptor)

at the donor/acceptor interface have on solar cell performance? Chapter 3 is the result of our exploration of this question. Gaining an understanding of the effects of molecular orientation on solar cell performance can help direct the rational design of solar cell materials: if donor/acceptor interactions of one orientation are preferred over another, it may be possible to design molecules that will allow for donor/acceptor interactions only along one orientation and inhibit the electronic coupling along another orientation. Furthermore, Chapter 3 also ties in to the results in Chapter 2, which I feel are still incomplete in answering why we see singlet emission in these solar cells.

In Chapters 4 and 5 we shifted directions a little bit, and focused on a polymer donor, PIPCP. When PIPCP is blended with the acceptor $PC_{61}BM$, the resulting BHJ solar cells achieve a very high V_{OC}, despite the low bandgap of PIPCP. First, we wanted to understand how BHJ solar cells based on PIPCP are able to achieve such a high V_{OC}, and which potential losses have been reduced in this system. Chapter 4 describes the studies aimed at answering this question, where we describe that in PIPCP:$PC_{61}BM$ E_g and E_{CT} are very close in energy, thereby minimizing energy losses associated with charge transfer. It is very encouraging to find a BHJ system that performs as well as PIPCP:$PC_{61}BM$ does, as past examples showed large reductions in J_{SC} and FF as E_g and E_{CT} approached in value. Unfortunately, while PIPCP BHJ solar cells are able to achieve really high V_{OC} values, the FF of these blends has remained perpetually limited. We therefore extended our study of this system to understand if the low FF is a direct result of the proximity between E_g and E_{CT}. We conducted a very thorough study on the possible losses and limitations in PIPCP:$PC_{61}BM$, through which we found that PIPCP:$PC_{61}BM$ has a very highly mixed morphology (akin to what is shown in Figure 1.6d), and very fast bimolecular charge-carrier recombination, which out-competes charge-carrier extraction in the absence of the internal field (*i.e.* as the applied voltage approaches V_{OC}). Although not entirely conclusive, these results suggest that the low

energetic offset may not be limiting factor for solar cell performance in PIPCP:$PC_{61}BM$ – if we were able to fabricated a BHJ blend with much improved phase separation and purity.

Each chapter begins with what I have termed the 'Preface' of that project. It seems to me that the process of obtaining a PhD is mystical to those looking from outside. In an attempt to demystify the process, I describe the context for the study: what were we doing in the lab at the time? Why did we start studying this question? How did I get involved? And similar questions. Furthermore, and more importantly, I try to highlight, to the best of my memory, all the people that were part of these studies. I strongly believe that obtaining a PhD is not a solitary endeavor, and really try to emphasize all the wonderful people that I had the pleasure of learning from and working with. While I accept that to some people the PhD is a much more solitary road, the road that I followed and the growth that I did are the result of a collective effort of the 'village.' I am deeply grateful to everyone who has been part of this 'village,' and really want to make this point clear for any younger student who may come across this dissertation- you will have mentors, friends, and partners in lab through the path to obtaining a PhD (and anything else you do in life, I'd like to believe), and this will make your PhD much more successful, influential, and enjoyable. And it is okay, and should be encouraged (well, I cannot encourage it enough) not to be a 'lone genius', but instead to gain from those around you and be generous yourself. I also strongly believe that because this point is not emphasized enough, we do not pay enough attention to the contributions of those around us. I think that we should all be particularly conscientious of where our ideas come from, the inspiration, who first mentioned this to us, and very importantly who did this work for us. And we should celebrate this and declare this without feeling that our own intellectual image is compromised. I would have had a very different PhD without all of my mentors, friends, and colleagues. I am indebted and grateful to them all.

1.8 Permissions and Attributions

1. The contents of Chapter 2 have previously appeared in Advanced Materials, **26**, 7405-7412 (2014) [22]. It is reproduced here with the permission of Wiley-VCH.

    - `http://onlinelibrary.wiley.com/doi/10.1002/adma.201402423/abstract`

2. The contents of Chapter 4 have previously appeared in Advanced Materials, **28**, 1482-1488 (2016) [35]. It is reproduced here with the permission of Wiley-VCH.

    - `http://onlinelibrary.wiley.com/doi/10.1002/adma.201504417/abstract`

Chapter 2

The Surprising Emission from High-Performing Small Molecule Solar Cells

There is a crack in everything, that's how the light gets in.

– Leonard Cohen

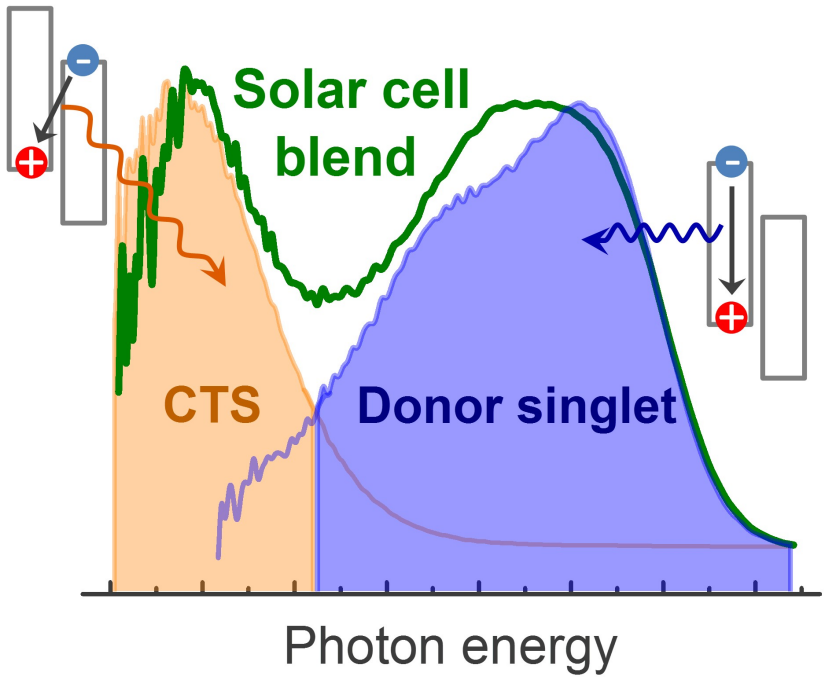

2.1 Preface

This study was the inception of my thesis work, following unsuccessful attempts at depositing negatively charged proteins (I was working with heparin) to act as interlayers in light-emitting diodes. In the process I built an electro-spray setup in our lab, using refurbished parts of a mass-spectrometer, but the results were not very promising. A talk by Prof. Olle Ingans, who was at UCSB for a sabbatical, inspired Prof. Thuc-Quyen Nguyen to ask that I start looking into the charge transfer (CT) state in small-molecule solar cells. At first, there was no specific question we wanted to answer, and the first task was to simply detect the CT state in the small-molecule solar cells which our group and the Bazan group have been developing and optimizing. Of course, just 'observing' the CT state was not so simple, as the observations did not match what was commonly reported in the literature at the time. The following chapter is the exploration that ensued from the unexpected observation.

The work that is described in this chapter marks some of the biggest learning steps in my path towards a doctorate, and a few people played a large role in helping me bridge some necessary gaps. Most notable was Dr. ir. Martijn Kuik, who had come to our group to do a post-doc, after completing his PhD studies in Groningen with Prof. Paul Blom. Martijn was really a great mentor for me at a time that I needed to be encouraged, pushed, and to be taught how to think like a scientist. I think the time when Martijn joined our group and started working with me was among the most difficult in my doctorate career. Martijn had just published a study with his former colleague, and friend, Gert Jan Wetzelaer, that used the relationship between electroluminescence intensity and voltage to identify the presence of charge-carrier traps. So while there was no specific research question in mind, we began by trying to replicate Martijn and Gert-Jan's previous study using our small-molecule solar cells. The article that we ended up

publishing on this work was an offshoot off the initial studies that Martijn and I tried to do.

Dr. John (Jack) A. Love, did a tremendous amount of work on the writing of the manuscript. The story presented herein did not have a very clear structure or message when I started writing it (which accounts largely for the reason it was so difficult to write it). Jack tore the first draft apart, and really helped me get it to a state of a journal article worthy of publishing. Jack was also kind during the process of experiments while I was still learning the art of making high-efficiency solar cells- after I struggled to make very good quality, high efficiency solar cells, Jack volunteered to make some devices for me or give me his devices when he is done, so I could get my measurements done.

Dr. Oleksandr (Alex) Mikhnenko is a phenomenal co-worker. As noted in the acknowledgments, I feel that I've learned so much from Alex about directed focus and critical thinking, both by talking to him about my research and asking him many stupid questions, but also by observing him at work, innovate and understand his project. In this particular study, although it may seem trivial, Alex opened my mind with regard to aesthetic representation of data, and the creative ways to do so clearly and effectively. Dr. Christopher M. Proctor, is an extremely well-read scientist, and not afraid to try new things in the lab. It was with Chris' help that I started measuring the CT state using EQE in our lab, something that had not been done before.

Dr. Alexander Mikhailovsky, trained me on all optical tools that were necessary for this study (and all studies to follow, as was mentioned already). Alexander is a wealth of knowledge and creativity with respect to the science and the equipment we use in the lab, and I really think we would not be able to operate at this level without his help. After training me, Alexander was always very kind in sharing his lab and time with me, even when my measurements would last longer than I had originally anticipated, and he would have to shift his schedule around.

Dr. Alexander Sharenko,. Alex's work, which was unrelated to this study, provided a very helpful building block for making the final correlation between singlet emission and crystallinity as is described below. Furthermore, although Alex was not particularly involved in this study as it was developing, later when I went to give a talk about it for our 'Big Group Meetings' and at the spring Materials Research Society in San Francisco, Alex happened to have GIWAXS data on blends that corresponded to devices I had tested. His GIWAXS data was yet another piece of data supporting the overall conclusions of the correlation.

As our lab was only starting to study the CT state, Quyen arranged that Koen Vandewal, who has established the form of thinking about the CT state in the field, would come to UCSB to lecture and meet with us. Koen was very down to earth, clever and nice to talk to, and very generous- he shared with me his way of dealing with the EQE data, and some other details he had to figure out himself along the way. I really appreciate his generosity and openness to talking about the science, without ever getting the feeling that he is secretive or not telling the full story. It's been an honor to have met and chatted with Koen, who I think is a great scientist and will change things in the field and in our understanding, again (since he's already done that).

Prof. Paul M. Blom visited our campus for two days, during which students from our group were given the chance to meet with him to hear his thoughts about their data. At this point the draft for this paper was mostly written, but Paul provided me with the picture with which to view the temperature-dependent data, according to which we concluded it is best to compare spectra at different temperatures, but at the same driving voltage.

2.2 Introduction

The development of organic semiconductors has opened the field of electronics to the possibilities of solution-processed fabrication and custom-tuning properties such as bandgap, energy levels, solid-state packing, etc., to fit the desired application by means of rational molecular design.[4, 36] In the application of photovoltaics, organic semiconductors continue to improve in performance and have already achieved respectable power conversion efficiencies (PCEs) above 10%.[37] High PCEs are achieved with organic semiconductors by the use of bulk heterojunctions (BHJ)[38] which pull the exciton apart by employing energy differences between two semiconductors highest occupied molecular orbitals (HOMO) and lowest unoccupied molecular orbitals (LUMO). Driven by this energetic offset, electrons are transferred from the donor to the acceptor. Prior to charge separation, however, the electron and hole are still bound across the interface residing on both donor and acceptor molecules in what is often referred to as the charge transfer (CT) state.[20] The CT state is formed by overlapping donor HOMO and acceptor LUMO wavefunctions, and only exists at the interface of the donor and acceptor phases.

In recent years the organic photovoltaic literature has seen a surge of interest in the CT state.[17, 39, 40] Because the CT state is the interfacial state in heterojunctions, it is thought of as a site for charge generation,[20, 41] but also as a site for both geminate and bimolecular recombination.[42, 43] The CT state is most often studied by means of optical transitions with techniques such as photoluminescence (PL),[23] electroluminescence (EL),[24] external quantum efficiency (EQE),[44] transient absorption,[45] among other optical techniques.[46] A clear trend has been established correlating the energy of the CT state (E_{CT}) to the open circuit voltage (V_{OC}) of the BHJ blend.[18, 19, 30, 47] Both the V_{OC} and E_{CT} are known to change with blend ratio and morphology, explained by changes in dielectric constant and crystallinity.[24, 48] The role of excess energy and

delocalization of the CT state have also stirred up discussion in the literature. Some reports suggest that the lowest-energy CT state acts as a trap state, and that excess energy is needed for charge delocalization and separation.[49, 50, 51] Other reports have demonstrated that excess excitation energy has no effect on photoconversion efficiency, and that factors such as the nanostructure at the interface that allow delocalization and field-independent generation are of more critical importance.[52, 53]

There have been many reports on CT state luminescence and absorption in polymer:fullerene BHJ solar cells, but considerably fewer on small-molecule:fullerene solar cells.[30, 54, 55, 56, 57] Here we focus on using EL to gain insight into the CT state at the donor/acceptor interface of molecular BHJ solar cells. In EL measurements charges injected from the contacts by an applied bias are expected to recombine through the lowest lying energy states; in BHJ blends recombination is expected to occur through the CT state.[24] A few studies have shown a correlation between poor photovoltaic performance with observed singlet emission from conjugated polymer:fullerene BHJ blends. Indeed, when the energetic offset between the donor and acceptor materials is small, back electron transfer can compete with charge separation and radiative recombinatinon through the singlet states may occur.[58, 59] However, contrary to this correlation, we exclusively observe singlet EL from high performing molecular BHJ solar cells, and only CT state emission from poor-performing solar cells.

2.3 Charge transfer state in small-molecule BHJ solar cells

This study is centered on three well-studied BHJ systems employing molecular donors: DPP-OT-3,6-bis(5-(benzofuran-2-yl)thiophen-2-yl)-2,5-bis(2-ethylhexyl)pyrrolo[3,4-c]-

pyrrole-1,4-dione (DPP(TBFu)$_2$), 7,7-(4,4-bis(2-ethylhexyl)-4H-silolo[3,2-b:4,5-b]-dithiophene-2,6-diyl)bis(6-fluoro-4-(5-hexyl-[2,2-bithiophene]-5-yl)benzo[c][1,2,5]-thiadiazole) (p-DTS(FBTTh$_2$)$_2$), and benzo[1,2-b:4,5-b]bis(4,4-dihexyl-4H-silolo[3,2-b]-thiophene-2,2-diyl)-bis(6-fluoro-4-(5'-hexyl-[2,2'-bithiophen]-5-yl)-benzo[c]-[1,2,5]-thiadiazole (p-SIDT(FBTTh$_2$)$_2$) (structures shown in Figure 2.1)). When first introduced in 2009, DPP(TBFu)$_2$ was among the pioneering molecular donors to perform comparably to polymer donors blended with fullerene derivatives in solution-processed organic photovoltaics.[33] The HOMO-LUMO levels of DPP(TBFu)$_2$ are 5.2 and 3.4 eV, respectively, measured by ultraviolet photoelectron spectroscopy (UPS) and absorption onset.[60] p-DTS(FBTTh$_2$)$_2$ and p-SIDT(FBTTh$_2$)$_2$ are more recent developments in molecular donors, both belonging to the D^1−A-D^2-A-D^1 molecular architecture (D1,2 being electron rich moieties and A an electron deficient moiety). p-DTS(FBTTh$_2$)$_2$, designed to improve compatibility of a precursor donor with the hole transporting layer poly(3,4-ethylenedioxythiophene):poly(styrenesulfonicacid) (PEDOT:PSS),[61] and was the highest performing small-molecule donor at the time of publishing. The HOMO-LUMO levels for p-DTS(FBTTh$_2$)$_2$ are 5.1 and 3.3 eV, respectively, as measured by cyclic voltammetry (CV). p-SIDT(FBTTh$_2$)$_2$ was designed to lower the HOMO of p-DTS(FBTTh$_2$)$_2$ to increase the V_{OC}.[62] The HOMO-LUMO levels for p-SIDT(FBTTh$_2$)$_2$ are 5.2 and 3.4 eV, respectively, as measured by CV.

Each of the three blend systems requires specific processing conditions to achieve optimal performance. When blended with the commonly used molecular acceptor PC$_{71}$BM ([6,6]-phenyl-C71-butyric acid methyl ester) and cast from pure solvents, all three systems have poor photovoltaic performance. However, altering the solvent or post processing procedures leads to vastly improved fill factors (FF) and short circuit currents (J_{SC}) (Figure 2.2). Of note is that in each system optimized performance is accompanied by a small decrease in V_{OC} in compared to the poor-performing as-cast films (Table

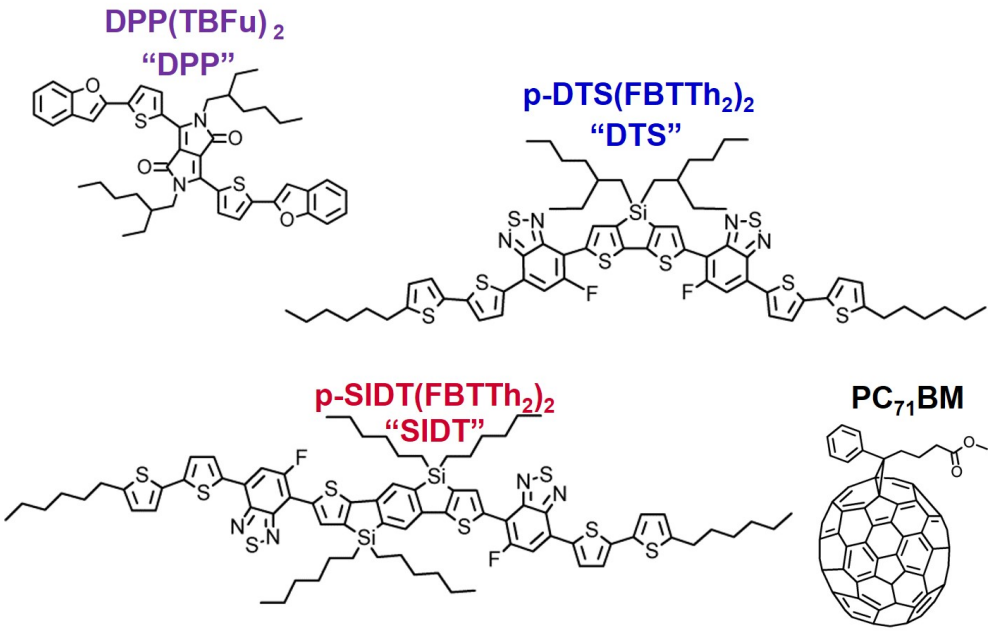

Figure 2.1: Chemical structures of DPP(TBFu)$_2$, p-DTS(FBTTh$_2$)$_2$, and p-SIDT(FBTTh$_2$)$_2$.

tab:ELenergies). Due to the established correlation between E_{CT} and V_{OC},[29, 18, 19, 30] it is reasonable to expect that the CT states in the systems studied here also decrease in energy upon optimization.

The improved PCE for the blends studied here has been attributed in each case to a change in morphology with processing conditions, with each system following the same morphological trend. Specifically, as-cast films result in an intimate mixture with negligible order or phase separation. Thermal annealing of DPP(TBFu)$_2$:PC$_{71}$BM[63] films or the use of the solvent additive diiodooctane (DIO) in p-DTS(FBTTh$_2$)$_2$:PC$_{71}$BM[12] and p-SIDT(FBTTh$_2$)$_2$:PC$_{71}$BM[62] solutions subsequently induce crystallinity and phase separation in the films. The morphology of the three blends in this report has been studied extensively in previous publications. Atomic force microscopy and transmission electron microscopy images of the three blends in this report are presented in Figure 2.3 and Figure 2.4 for convenience; however, we strongly recommend referring to the compre-

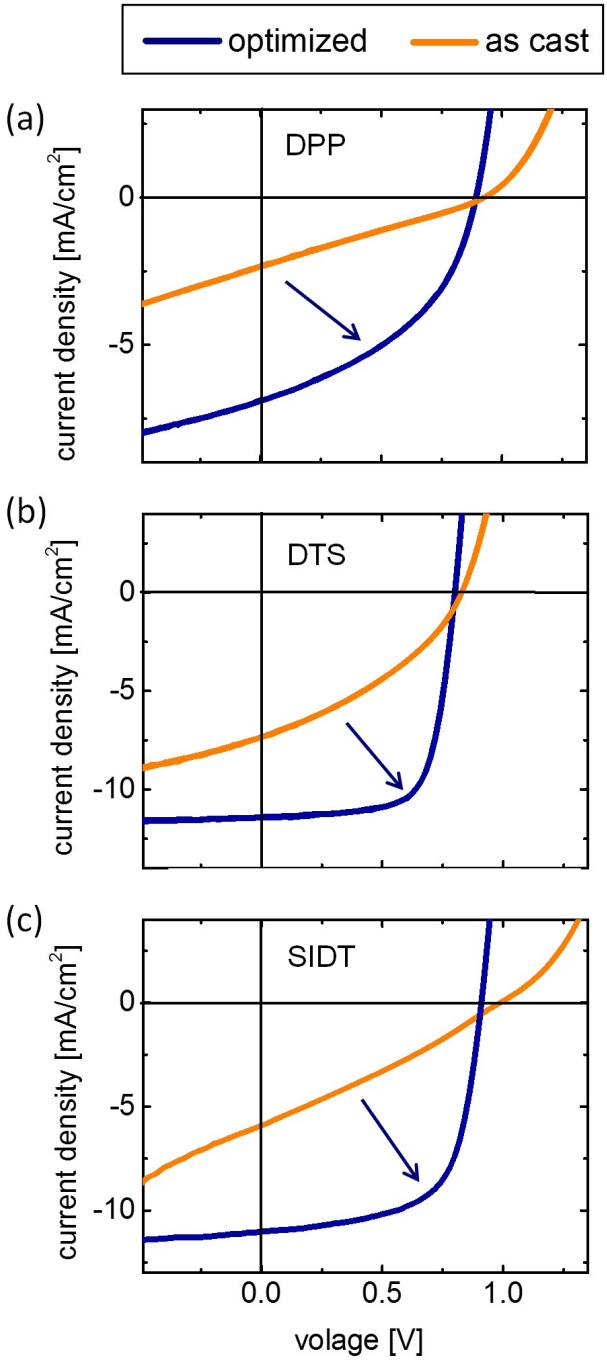

Figure 2.2: Solar cell J-V curves of optimized and as-cast blends under 1 sun illumination for (a) DPP(TBFu)$_2$:PC$_{71}$BM, (b) p-DTS(FBTTh$_2$)$_2$:PC$_{71}$BM, and (c) p-SIDT(FBTTh$_2$)$_2$:PC$_{71}$BM.

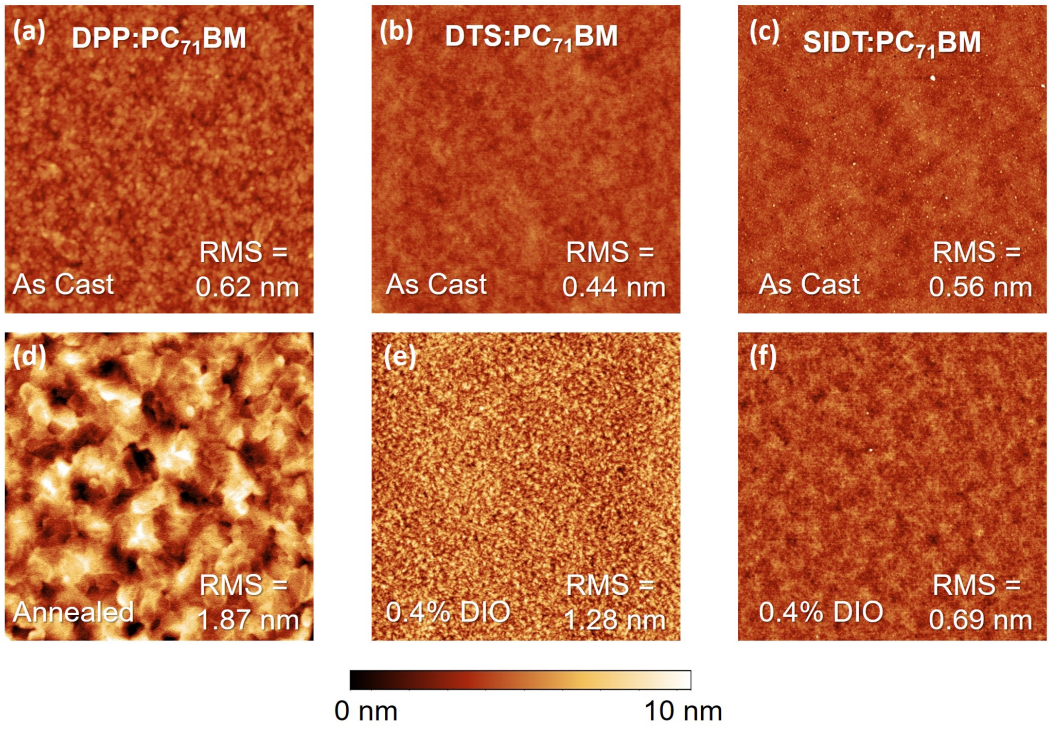

Figure 2.3: AFM of as-cast (a,b,c) and optimized (d,e,f) blend devices for (a,d) DPP(TBFu)$_2$:PC$_{71}$BM, (b,e) p-DTS(FBTTh$_2$)$_2$:PC$_{71}$BM, and (c,f) p-SIDT(FBTTh$_2$)$_2$:PC$_{71}$BM.

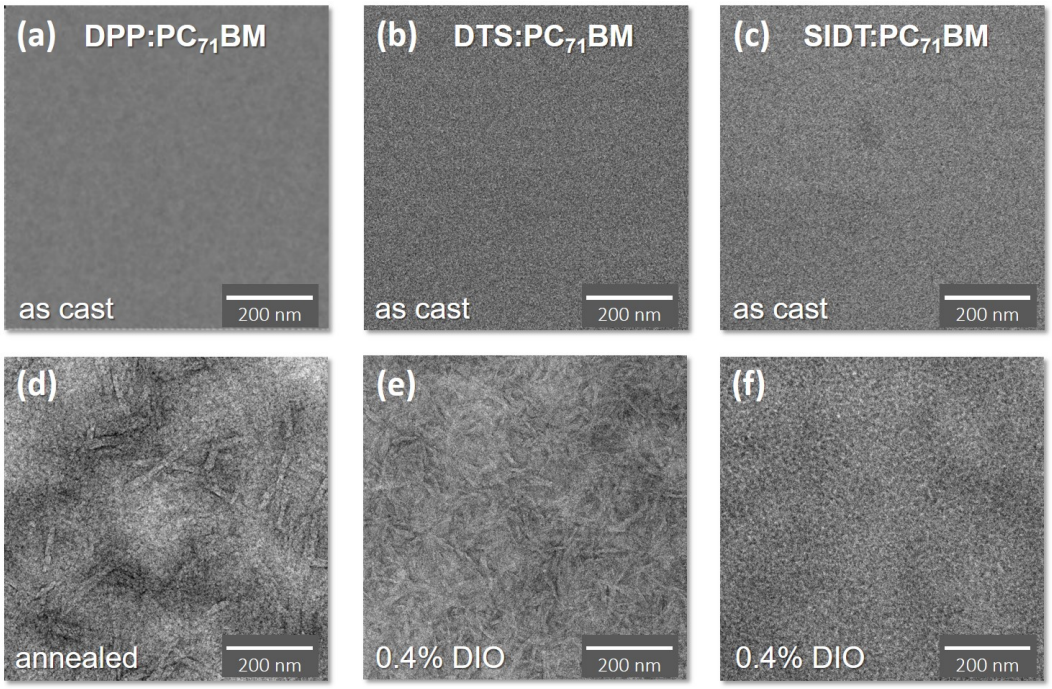

Figure 2.4: TEM of as-cast (a,b,c) and optimized (d,e,f) blend devices for (a,d) DPP(TBFu)$_2$:PC$_{71}$BM, (b,e) p-DTS(FBTTh$_2$)$_2$:PC$_{71}$BM, and (c,f) p-SIDT(FBTTh$_2$)$_2$:PC$_{71}$BM.

hensive morphological reports on these systems. The effect of increased crystallinity and aggregation on polymer:fullerene emission has been reported in a number of systems to be a small red-shift in emission,[46, 24, 64] again suggesting the optimized films studied here will have a lower E_{CT} compared to the CT state of the as-cast films.

2.4 Electornic states determined by EL

To examine the CT state by EL, a blend film is sandwiched between high and low work function electrodes (ITO/PEDOT:PSS and Ca/Al, respectively), identical to the solar cell architecture. Oppositely charged carriers are directly injected into the films by an applied bias. Due to the choice of electrodes, it is expected that electrons are injected into the acceptor and holes into the donor, thus allowing for bimolecular recombination at the donor/acceptor interface once the charges meet. If the CT state emission is radiative, the E_{CT} can be estimated by the energy of the peak emission intensity.[31]

The left-hand side of Figure 2.5 shows EL spectra of the three molecular blend systems as-cast, and their respective pure components at room temperature (RT). The as-cast blends in all three cases show EL that is characteristic of CT state emission: the emission is featureless and lower in energy than EL observed from either pure component of the BHJ.[24] The E_{CT} values of the as-cast devices are 0.34-0.4 eV higher than the corresponding eV_{OC} values (Table tab:ELenergies), in fair agreement with the correlation seen for polymer:fullerene photovoltaics.[24, 18, 19, 47]

Given the slight decrease in V_{OC} and the increased crystallinity in the optimized blends, we expect the EL spectra of the optimized devices to show a red-shifted peak compared to the as-cast devices. However, as is shown on the right-hand side of Figure 2.5, upon photovoltaic optimization, the EL specrum of all blend films shows an additional high-energy emission peak. EL of annealed DPP(TBFu)$_2$:PC$_{71}$BM has a new

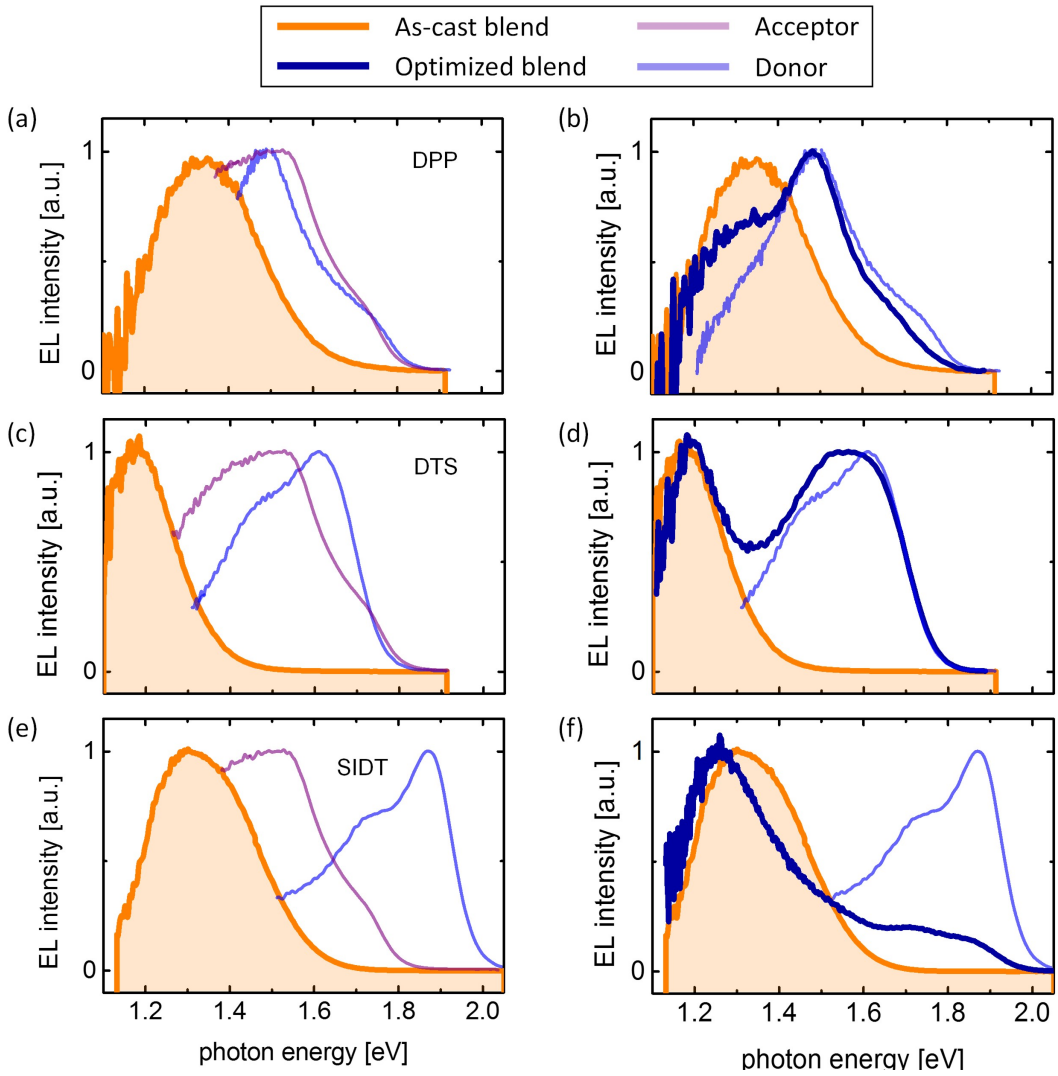

Figure 2.5: EL of as-cast (a,c,e) and optimized (b,d,f) blend devices with the EL of pristine blend components at room temperature for (a,b) DPP(TBFu)$_2$:PC$_{71}$BM, (c,d) p-DTS(FBTTh$_2$)$_2$:PC$_{71}$BM, and (e,f) p-SIDT(FBTTh$_2$)$_2$:PC$_{71}$BM.

Table 2.1: Energies at peak electroluminescence itensity for singlet and CT state emission for the three blend systems. E_{CT} by EL is compared to the corresponding V_{OC} values.

	$PC_{71}BM$	Donor	Pristine		Optimized	
	[eV]	[eV]	E_{CT} [eV]	V_{OC} [V]	E_{CT} [eV]	V_{OC} [V]
DPP	1.55	1.49	1.33	0.93	–	0.89
DTS	1.55	1.62	1.18	0.83	1.19	0.80
SIDT	1.55	1.88	1.32	0.98	1.26	0.91

dominant spectral peak at 1.49 eV, corresponding well with the peak emission from pristine DPP$(TBFu)_2$. Below 1.39 eV the annealed blend emission has a shoulder in the EL spectrum which we attribute to CT state emission. Because the CT state emission peak is burried within neat DPP9TBFu$)_2$ emission, we cannot assign the appropriate CT emission peak for this device. Showing a similar trend, EL of DIO-processed p-DTS$(FBTTh_2)_2$ blends largely follows emission of pristine p-DTS$(FBTTh_2)_2$ at energies greater than 1.37 eV, below which the spectrum resembles the corresponding CT state emission as seen from as-cast devices. The E_{CT} of p-DTS$(FBTTh_2)_2$ blends does not appear to change significantly with the addition of DIO, though we note that peak CT state emission in this system is at energies near detector sensitivity limit and is thus noisier and more difficult to discern. The dominant emission from optimized p-SIDT$(FBTTh_2)_2$:$PC_{71}BM$ films remains CT state emission, but with the emergence of spectral features at energies corresponding to p-SIDT$(FBTTh_2)_2$ singlet emission. The CT state EL spectra of the p-SIDT$(FBTTh_2)_2$ blend shifts to slightly lower energies from roughly 1.31 eV to 1.27 eV with the addition of DIO, consistent with increased order in the film and decrease in V_{OC} as discussed above.

The emergence of singlet emission in optimized solar-cell blends was also observed by Scharber et al., who studied the effect of the solvent additive octanedithiol (ODT) on the

narrow-bandgap polymer PCPDTBT (poly[2,6-(4,4-bis-(2-ethylhexyl)-4H-cyclopenta[2,1-b;3,4-b]-dithiophene)-alt-4,7-(2,1,3-benzothiadiazole)]) blended with $PC_{61}BM$.[65] The addition of ODT and increase in phase separation is speculated to delocalize the CT state thus reducing radiative emission through the CT state. However, the authors focus on the decrease in CT state emission and do not discuss the phenomenon of singlet emission by EL.

2.5 Identifying CT states in external quantum efficiency spectra

While EL measurements probe the CT state from the excited state, it is also accessible from the ground state and can be probed by absorption.[40] We examine EQE spectra of the films to understand if singlet emission can be explained by significant modifications to the CT state. In EQE measurements photovoltaic devices are irradiated with incrementally changing monochromatic light under short circuite conditions, and the subsequent photocurrent is recorded. Because the CT state is lower in energy than the donor and acceptor bandgaps, its contribution to the EQE can be distinguished at energies below absorption of donor and acceptor.[18, 29] However, due to the low absorption of the CT state, its direct contribution to the EQE is so small it can only be seen on a logarithmic scale by a spectral shoulder continued beyond the exponential decay of the pristine materials absorption profile.

The CT state signature in the EQE is observed in all six blend films, irrespective of processing conditions (Figure 2.6). Note that because E_{CT} in these systems is close to the energy of the donor and acceptor bandgaps much of the CT state EQE spectrum is lost within the absorption of the pristine materials. It is therefore challenging to extract

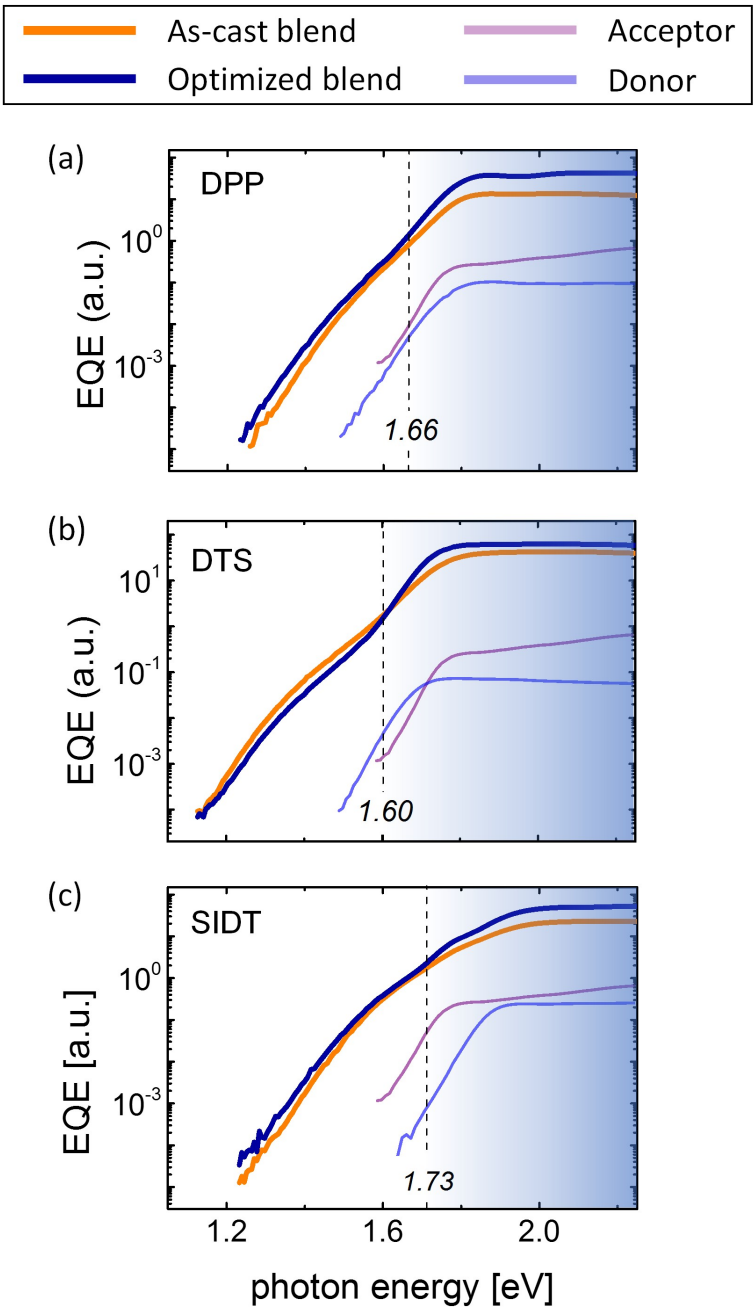

Figure 2.6: EQE spectra of as-cast and optimized blend devices along with EQE spectra of pristine blend components for (a) DPP(TBFu)$_2$:PC$_{71}$BM, (b) p-DTS(FBTTh$_2$)$_2$:PC$_{71}$BM, and (c) p-SIDT(FBTTh$_2$)$_2$:PC$_{71}$BM. A dashed line represents the energy below which photocurrent generation is attributed to the CT state for each blend, marked in italics on the plots.

reliable values for E_{CT} by Gaussian fits as has been demonstrated for a number of other systems.[29, 66] Nevertheless, by comparing the spectral shapes of as-cast blends with optimized blends, the data qualitatively suggests that the solid state packing has minimal effects on the ground CT state in these blends. As is expected by the respective J_{SC} values, all optimized films show significantly higher EQE values than as-cast films, but only at energies that correspond to the absorption of the donor and $PC_{71}BM$. It is therefore apparent that the relative contribution of CT state absorption to the photocurrent is reduced upon optimization, which is consistent with a reduced interfacial area upon phase separation. Otherwise, the EQE spectra do not provide an unequivocal explanation to the reason optimized devices emit from the singlet state at low voltages.

Given these results, it is now of note that the observed singlet emission described here differs from previous reports which correlate poor device performance and singlet luminescence.[58] Detection of singlet EL, in these poor performing systems, is due to an energetic offset between donor and acceptor that is so small that the CT state and singlet state are in resonance. In this scenario singlet emission indicates insufficient driving force for charge separation.[58, 59] In such systems, by EQE there should be no evidence of a CT state shoulder.[59] In the blends studied here, however, the CT state is still detectable in the EQE irrespective of processing conditions. Here singlet emission is observed from optimized blends, correlating with improved PCEs compared to blends that show only CT state emission. It is thus apparent that in devices which show singlet emission there remains a sufficient energy level offset and driving force for charge separation.

2.6 Identifying charge injection by EL turn-on voltage

From a morphological standpoint, as-cast films are intimately mixed while the optimized films have clear phase separation.[62, 63, 12] EL from the donor singlet state may arise if both charge-carriers are directly injected into a donor phase. To test for this possibility we compare the turn-on bias (V_{ON}) from a pristine donor with the V_{ON} of the BHJ blends. The V_{ON} is expected to be proportional to the bandgap of the material into which charges are injected.[24] If singlet emission from the blend is due to direct injection into the donor phase, the V_{ON} where we observe singlet emission should be comparable between an optimized blend device and a pristine donor device with equivalent electrodes. In the same vein, it is expected that the V_{ON} of as-cast devices, which show only CT state emission, be lower than the V_{ON} of optimized devices. This rational assumes that injection from the contact into the donor phases is not significantly altered by the presence of $PC_{71}BM$.

EL intensity vs. applied bias is compared between blend and pristine donor films for DPP$(TBFu)_2$:$PC_{71}BM$ and p-DTS$(FBTTh_2)_2$:$PC_{71}BM$ blends (Figure 2.7). It is clear that significantly larger voltages are necessary to produce luminescence from a pristine donor film than from a blend film, regardless of annealing or processing with DIO. Pristine DPP$(TBFu)_2$ has a V_{ON} of roughly 1.6 V, while emission from DPP$(TBFu)_2$:$PC_{71}BM$ blends turns on around 0.9 V. Similarly, pristine p-DTS$(FBTTh_2)_2$ emission turns on at 1.3 V, and p-DTS$(FBTTh_2)_2$:$PC_{71}BM$ blends have a V_{ON} of 0.7 V. In both molecular blends, the difference between the V_{ON} of pristine donor and blend devices is more than 0.5 V, whereas the potential necessary for emission from blends is very comparable regardless of processing conditions or the resulting emission spectra. We interpret this to that direct injection of both charge carriers into the donor phases is not the cause of the

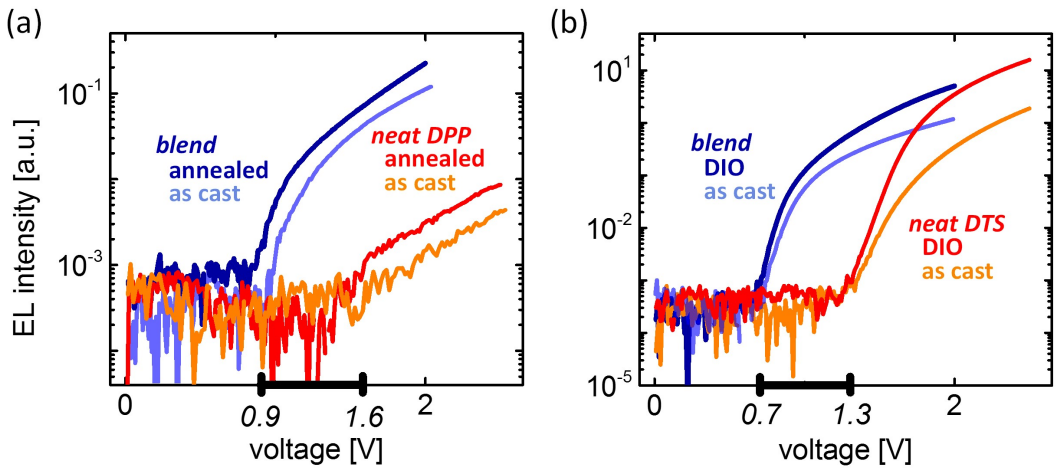

Figure 2.7: EL intensity *vs.* voltage characteristics of as-cast and optimized, blend and neat donor devices (a) DPP(TBFu)$_2$:PC$_{71}$BM and (b) p-DTS(FBTTh$_2$)$_2$:PC$_{71}$BM. Log-linear plot is used to emphasize voltage at which emission is first detected. The difference between the turn-on voltage of the blend and neat donor devices is emphasized on the x-axis by a bold line.

observed singlet emission in the optimized blends. It is notable that the blend EL spectra in Figure 2.5 were collected at biases below the V_{ON} of pristine donor devices. While the EL spectra of the optimized blends indeed changes with applied bias, singlet emission is visible at all voltages well below the V_{ON} of the pristine donor devices. Singlet emission of both DPP(TBFu)$_2$:PC$_{71}$BM and p-DTS(FBTTh$_2$)$_2$:PC$_{71}$BM has a larger dependence on applied bias, and is thus intensified relative to CT state emission as voltage is increased. A more detailed examination of the spectral evolution with applied bias can be found in Figure S3.

2.7 Thermal activation in EL spectra

Previous studies on several polymer:polymer systems have suggested that recombination through CT state compared to singlet states can be temperature dependent.[67, 68, 69, 70, 71, 72, 73] The EL spectra of the three blends collected at 200 K are shown

in Figure 2.8. However, it should be noted that at low temperatures larger potentials are necessary to observe EL. Because recombination through singlet excitons follows a different dependence on applied bias than recombination through the CT state we cannot directly compare the spectra collected at RT (Figure 2.5) and 200 K (Figure 2.8). Instead, the spectra at 200 K must be compared to RT spectra collected at equivalent applied voltages, traced for reference in the low temperature plots.

At 200 K and low applied voltages, EL from annealed DPP(TBFu)$_2$:PC$_{71}$BM predominantly resembles CT state emission, showing a strong temperature dependence (Figure 2.8). Singlet emission is still present as a secondary peak at 1.62 eV, but majority of radiative recombination goes through the CT state. This is in contrast to RT measurement at comparable voltages. Upon decreasing the temperatures further (Figure S4), EL of the annealed blend follows emission of the as-cast blend, showing no singlet features unless high voltages are applied. This is analogous to reports on planar heterojunction polymer light emitting diodes (LEDs) that show singlet emission decreases with reduced temperature compared to emission from the CT state.[68] The strong inhibition of singlet emission at low temperatures may indicate that at RT charges at the interface reach the DPP(TBFu)$_2$ singlet state by thermal excitation. Similarly, also the EL spectra of optimized p-SIDT(FBTTh$_2$)$_2$:PC$_{71}$BM shows temperature dependence (Figure 2.8c). At RT, when the voltage is increased from 1.0 V to 1.4 V, there is a significant increase in the emission at energies of singlet EL from pristine p-SIDT(FBTTh$_2$)$_2$. However, the RT spectrum at 1.4 V shows significantly more singlet emission than the spectrum taken at 200 K when compared to maximum of CT state emission.

In contrast to DPP(TBFu)$_2$ and p-SIDT(FBTTh$_2$)$_2$, the EL spectra from p-DTS(FBTTh$_2$)$_2$:PC$_{71}$BM does not change significantly with temperature (Figure 2.8b). At lower temperatures optimized p-DTS(FBTTh$_2$)$_2$ blends show peak splitting at the energies corresponding to donor emission, which is not uncommon for disordered materials[74]

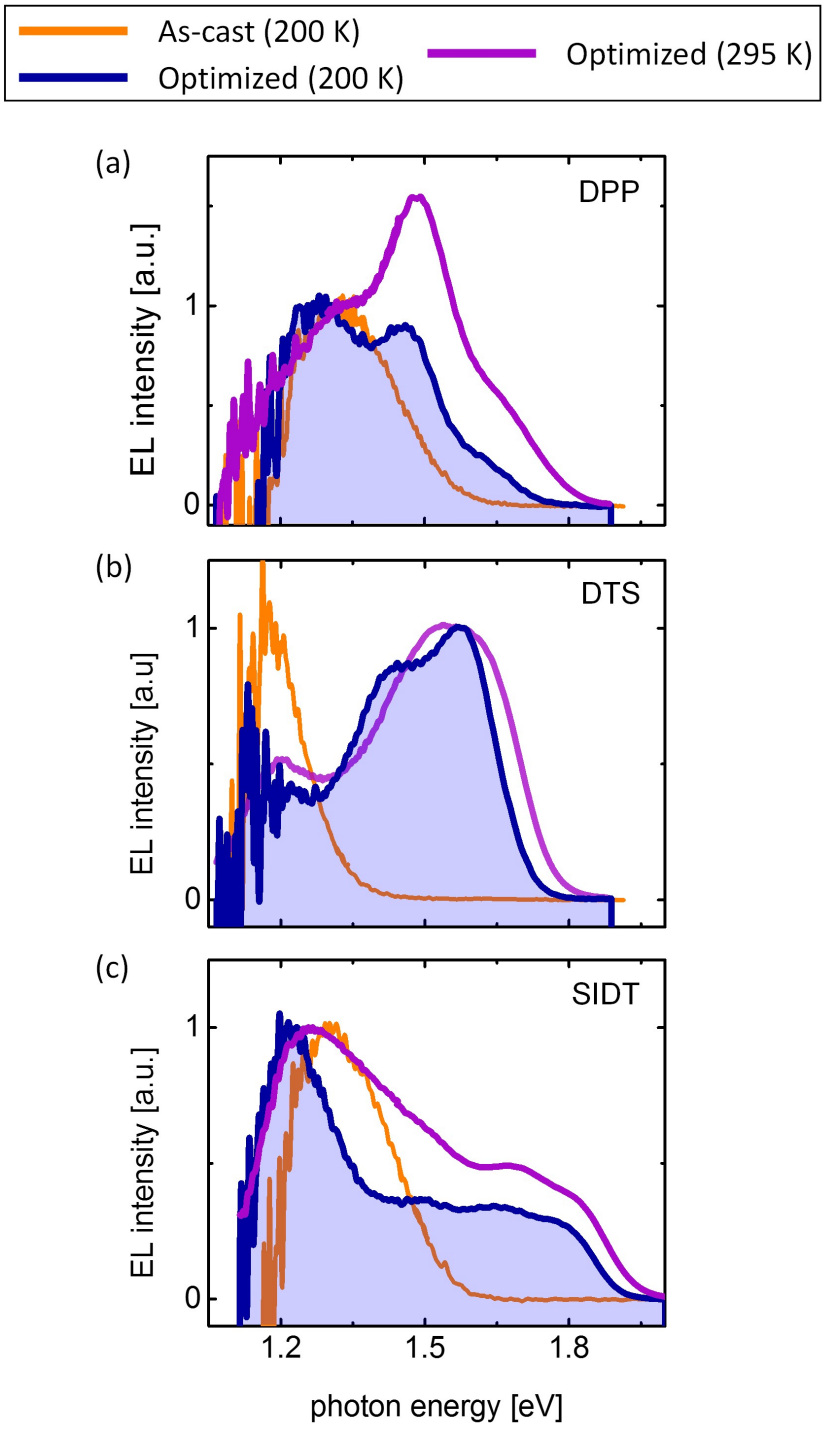

Figure 2.8: Normalized EL of as-cast and optimized blend devices at 200 K, compared to EL of respective optimized device at 295 K for (a) DPP(TBFu)$_2$:PC$_{71}$BM, (b) p-DTS(FBTTh$_2$)$_2$:PC$_{71}$BM, and (c) p-SIDT(FBTTh$_2$)$_2$:PC$_{71}$BM.

and can also be seen in the emission of pristine p-DTS($FBTTh_2$)$_2$ (Figure S5). The agreement between the spectra of optimized p-DTS($FBTTh_2$)$_2$:$PC_{71}BM$ at the same bias but at different temperatures indicates that recombination through the CT state and the donor singlet has a similar temperature-dependence. Therefore, singlet emission from this blend at RT cannot be attributed to temperature activation. The as-cast films of all blends show no spectral evolution with decreased temperature.

The three molecular donors, DPP($TBFu$)$_2$, p-DTS($FBTTh_2$)$_2$, and p-SIDT($FBTTh_2$)$_2$, were designed towards high PCEs, and thus offer high V_{OC} values when blended with $PC_{71}BM$. To achieve high V_{OC} values with narrow bandgap donors, E_{CT} will inevitably approach the donor singlet energy. However, the different EL spectra from as-cast and optimized films of the same blend suggest that small energetic offsets are not enough to explain singlet emission here. Figure 4 suggests that thermal activation may contribute to the observed singlet emission from optimized DPP($TBFu$)$_2$ and p-SIDT($FBTTh_2$)$_2$ blend films, as both show decreased singlet emission at low temperatures. However, thermal activation does not explain the EL spectra of optimized p-DTS($FBTTh_2$)$_2$ blends.

2.8 Crystallinity, phase separation, and singlet EL

We return now to the morphological differences between the as-cast and optimized films. As noted, the donor and fullerene are intimately mixed in as-cast films, while optimized films have phase separation and significant crystallinity.[60, 62, 12] Sharenko et al. have recently shown that phase separation in DPP($TBFu$)$_2$:$PC_{71}BM$ films is driven by donor crystallization. By performing in-situ thermal annealing x-ray scattering, they identify the annealing temperature at which the films become crystalline and phase-separated, and demonstrate that development of phase separation and donor crystallinity coincide.[63] To verify the relationship between crystallinity and phase sepa-

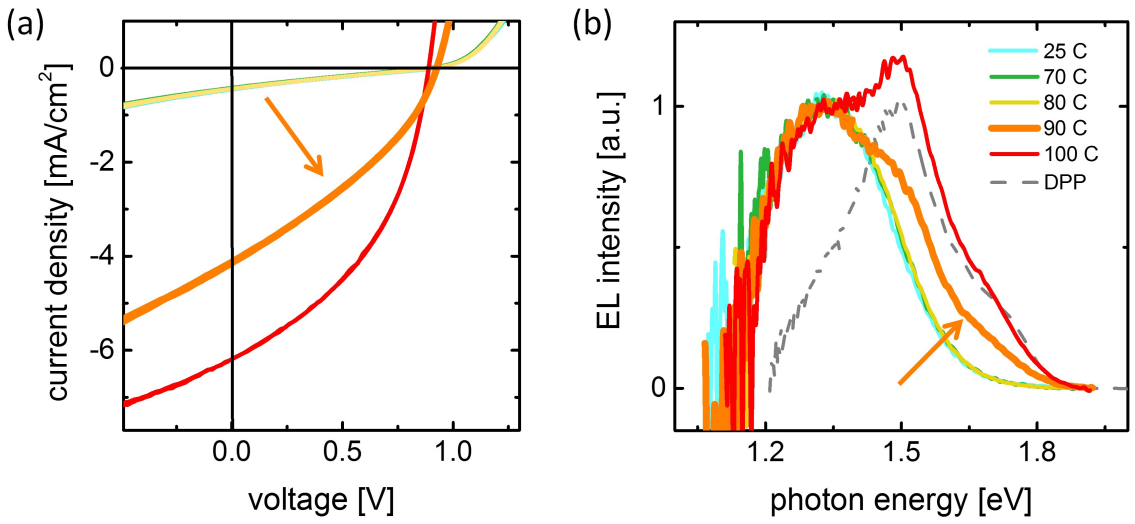

Figure 2.9: Evolution of (a) solar cell performance and (b)EL spectra of 70:30 w/w DPP(TBFu)$_2$:PC$_{71}$BM films with annealing temperature. EL of blends was collected at 1.5 V. Films were annealed for two minutes following procedure by Sharenko et al.[63] EL spectra of pristine DPP(TBFu)$_2$ is included for reference.

ration and singlet emission from the optimized blend, we replicate the conditions used by Sharenko et al. and record the respective EL. Figure 5 shows the EL spectra of 70:30 w/w DPP(TBFu)$_2$:PC$_{71}$BM blend films annealed for two minutes at a range of temperatures. Sharenko et al. found that films of this blend ratio began forming separate phases when annealed for two minutes at 80 C. Singlet emission onset occurs in films annealed at 90 C, corresponding with the point of increased J_{SC}, FF, and electron mobility as noted by Shareko et al.[63] It should be noted here that the x-ray measurements were done at the elevated temperatures, while the EL measurements are done at room temperature. Singlet emission is thus observed once films develop phase separation and crystallinity, and not before.

From a similar point of view, we investigate the effect of blend ratio on film morphology, solar cell peformance, and electroluminescence of p-DTS(FBTTh$_2$)$_2$:PC$_{71}$BM blends processed with 0.4% DIO. Figure 2.10 shows J-V curves under 1-sun illumi-

nation and electroluminescence for devices made with blend ratios ranging from 10:90 donor:acceptor w/w, to 50:50 donor:acceptor w/w. At low donor loadings of 10-20%, the solar cell performance is poor, with low FF and J_{SC} values. The corresponding EL spectra of these blends has great resemblance to the EL spectrum of the as-cast p-DTS($FBTTh_2$)$_2$:$PC_{71}BM$ device, with only a CTS peak, true for all applied voltages. At a donor:acceptor ratio of 30:70, however, the J_{SC} and particularly the FF increase greatly, and the EL spectrum of the device shows the emergence of emission at high photon energies, corresponding to p-DTS($FBTTh_2$)$_2$ singlet emission. Grazing incidence wide-angle X-ray spectroscopy (GIWAXS) of the 20:80 and 30:70 donor:acceptor w/w blend ratio films are also shown in Figure 2.10. GIWAXS can be used to characterize crystallinity in blends, identified by anisotropic diffraction peaks in the images. The images in Figure 2.10 show that at a blend ratio of 20:80, the only discernible signal is an isotropic ring associated with $PC_{71}BM$ diffraction, but no evidence of p-DTS($FBTTh_2$)$_2$. At a blend ratio of 30:70, however, clear diffraction peaks emerge, labeled on the image. The pi-pi diffraction peak, specifically, connotes that p-DTS($FBTTh_2$)$_2$ molecules are stacking along the pi-direction, which is considered favorable for charge transport and delocalization. The emergence of singlet emission, improvements in FF and J_{SC}, are clearly correlated with the onset of donor crystallization.

Enhanced order has long been associated with superior charge transport, and is also believed to decrease the bandgap and increase charge and exciton delocalization. Particular attention has been dedicated to CT state delocalization at the interface,[52, 57, 75, 76, 77, 78] most often correlated with aggregation in the fullerene phase.[75, 76, 57] The small-molecule blends we studied show donor crystallization upon photovoltaic optimization. Hole and electron mobilities in DPP($TBFu$)$_2$:$PC_{71}BM$ and p-DTS($FBTTh_2$)$_2$:$PC_{71}BM$ increase upon annealing and processing with DIO,[79] and in p-SIDT($FBTTh_2$)$_2$:$PC_{71}BM$ the hole mobility increases with DIO.[62] Interestingly, we have also demonstrated less

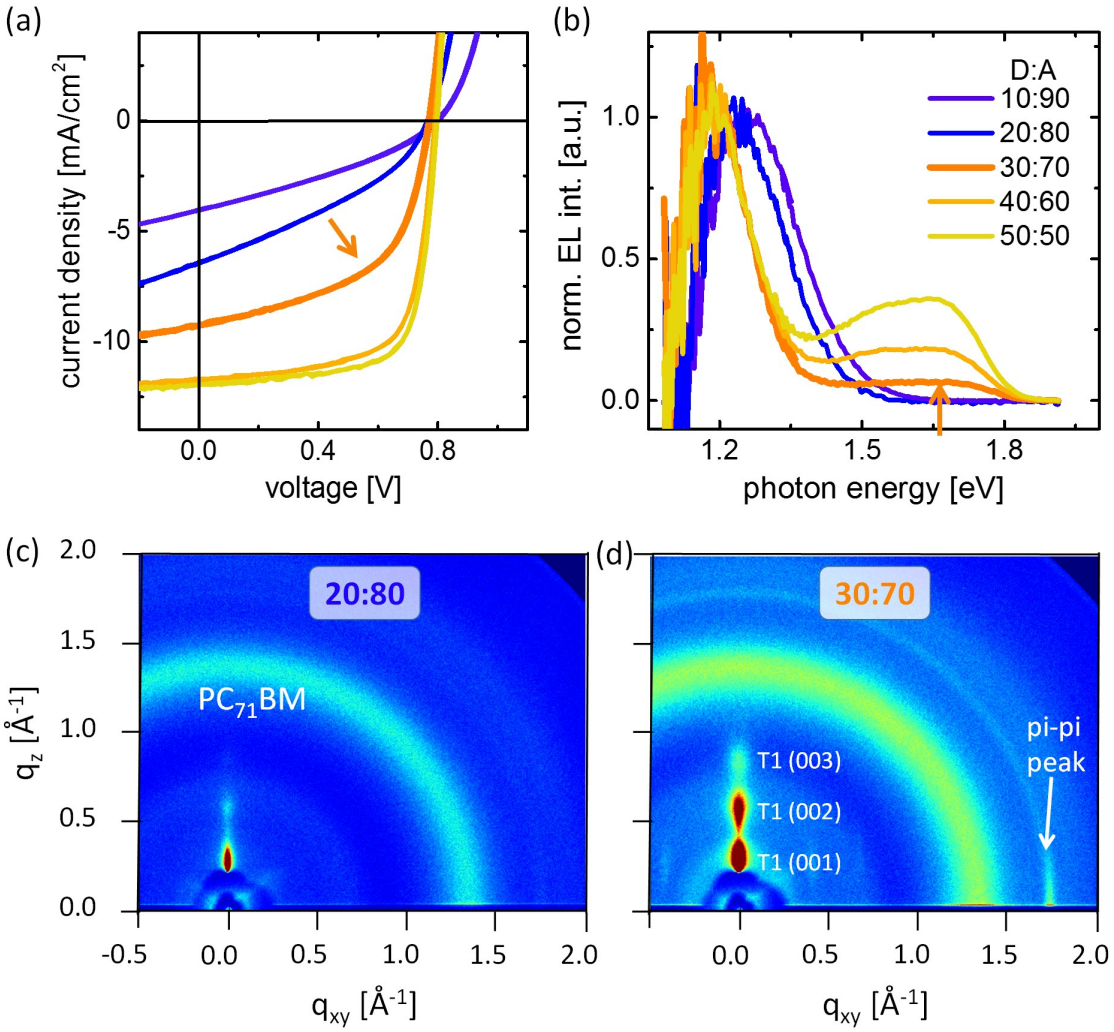

Figure 2.10: Evolution of (a) solar cell performance, (b) EL spectra, and donor crystallinity of DTS(FBTTh$_2$)$_2$:PC$_{71}$BM films with donor:acceptor ratios ranging from 10:90 to 50:50 w/w. GIWAXS images are shown for blend ratios of (c) 20:80 and (d) 30:70 donor:acceptor w/w.

field-dependence of generation in DIO-processed p-DTS($FBTTh_2$)$_2$:$PC_{71}BM$[80] and p-SIDT($FBTTh_2$)$_2$:$PC_{71}BM$[62] films than in their as-cast counterparts. This suggests that the CT states are less localized in these optimized devices. Thus it appears that the same conditions that allow for improved transport and weaker field-dependence also decrease the barrier for electrons to reach the donor phase of the solar cell blends studied in this report, yet this does not impede on achieving IQEs as high as 90%-100%.[62, 12]

It is worth noting that larger phase domains may play a significant role in delocalization and singlet emission, as well. By structural analysis we have shown that the as-cast films have a very mixed morphology, such that donor and acceptor phases can hardly be distinguished.[62, 12, 60] In such a morphological landscape, even if charges or excitons at the interface of as-cast films were able to escape or undergo back transfer, there is a high probability they will find a nearby CT states due to the high interfacial area and small phases. A similar correlation of singlet EL to domain size was also shown for all-polymer LED heterojunctions.[71, 81]

2.9 Bias- and temperature-dependent PL

Emission can be achieved by electrical excitation, when charges are injected into the film *via* contacts and a forward applied bias (EL, as was done above), or by photoexcitation, when excited states are formed by a laser pulse, which proceed to recombine and emit light (photoluminescence, PL). As part of our initial investigation of the luminescence from the small-molecule blends we have discussed in the study above, we also investigated the PL characteristics of the blends. First, we compared the PL and EL from the same films: neat DTS($FBTTh_2$)$_2$ (as-cast, annealed, and with DIO) shown in Figure 2.11, and blend DTS($FBTTh_2$)$_2$:$PC_{71}BM$ (as-cast, annealed, and with DIO) shown in Figure 2.12. DTS($FBTTh_2$)$_2$ LED devices were fabricated with the device structure

of: ITO/PEDOT (45 nm)/DTS($FBTTh_2$)$_2$ (70 nm)/Ca (10 nm)/Al (100 nm), and then encapsulated using a two-part epoxy and a glass microscope slide. Blend devices were fabricated as described in the 'Experimental' section, and also encapsulated. For PL, the active layer was excited with a HeNe laser (633 nm excitation) at an incident angle of 90° from the detector. EL was achieved on the same devices by applying a forward bias that is above the turn-on voltage, as described in the 'Experimental' section.

EL and PL from neat DTS($FBTTh_2$)$_2$ devices show the same emission spectra (Figure 2.11) for all processing conditions. The emission spectra do change, however, between processing conditions: films processed with DIO have the sharpest emission spectra that are most blue-shifted, the annealed film emission spectra are red-shifted by about 50 meV, and the emission from the as-cast films have an additional shoulder to the emission at low energies.

In the blend devices, EL and PL spectra are more different (Figure 2.12). The DIO-processed and annealed films have similar EL and PL spectra, though in both cases the EL spectra are more blue-shifted. From the work above, we now know that this emission is at energies that correspond to emission from the T1 singlet state. The PL emission may originate from singlet excitons that were not successfully quenched by a donor/acceptor interface. As we do not fully understand the process by which we observe EL emission from singlet states in the blend films, other than a relationship to phase separation and crystallinity, it is not unreasonable to suggest that the DTS($FBTTh_2$)$_2$ singlet PL observed is the result of a more complicated process than excitons decaying before reaching an interface. For example, there may be an equilibrium between the CT state and S1 singlet states. Since the quantum efficiency of singlet exciton states is expected to be much higher than of the CT state, it is likely that the number of recombination events that go through S1 singlet states is much lower than the number of recombination events through the CT states. However, the as-cast films show a PL that is

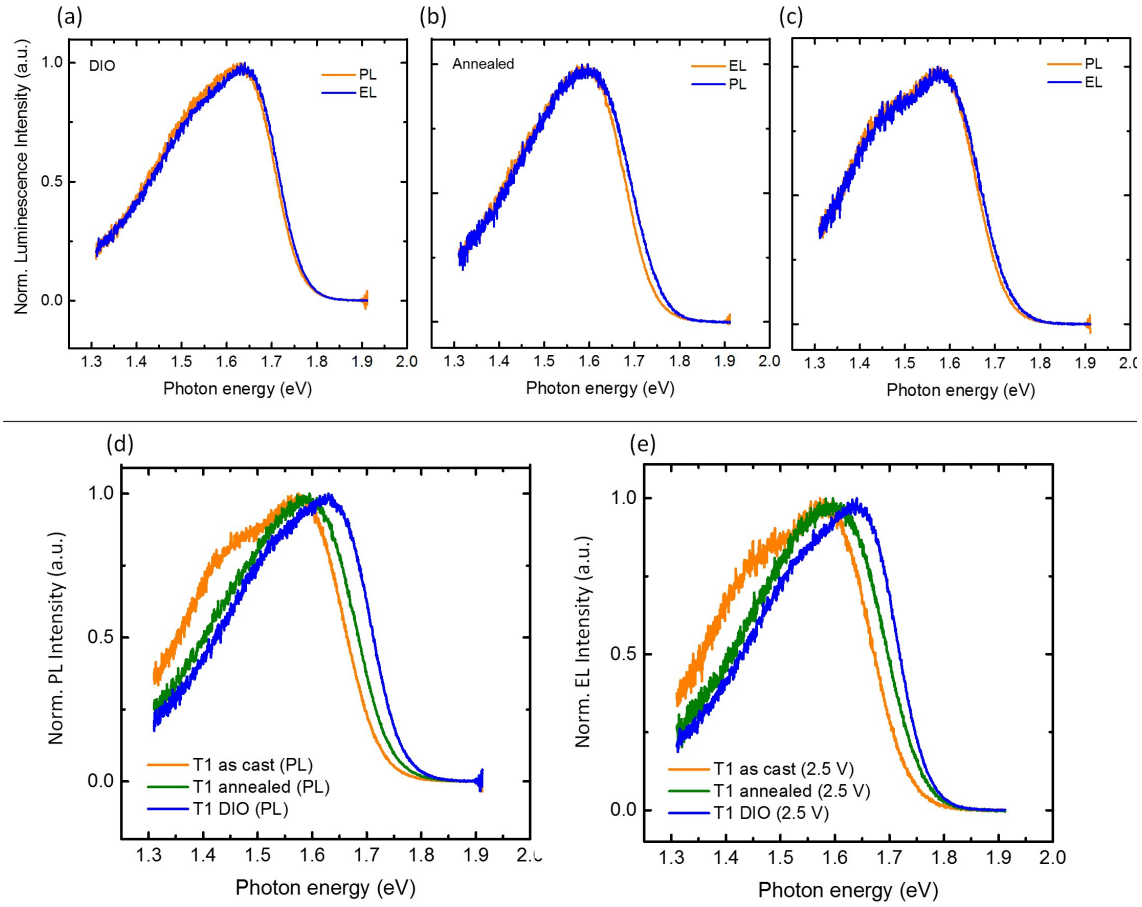

Figure 2.11: Comparison between emission achieved by EL and PL from neat DTS(FBTTh$_2$)$_2$ films fabricated as-cast (a), annealed (b), and with DIO (c). (d) and (e) compare of PL and EL spectra, respectively, from films fabricated with the three different processing conditions.

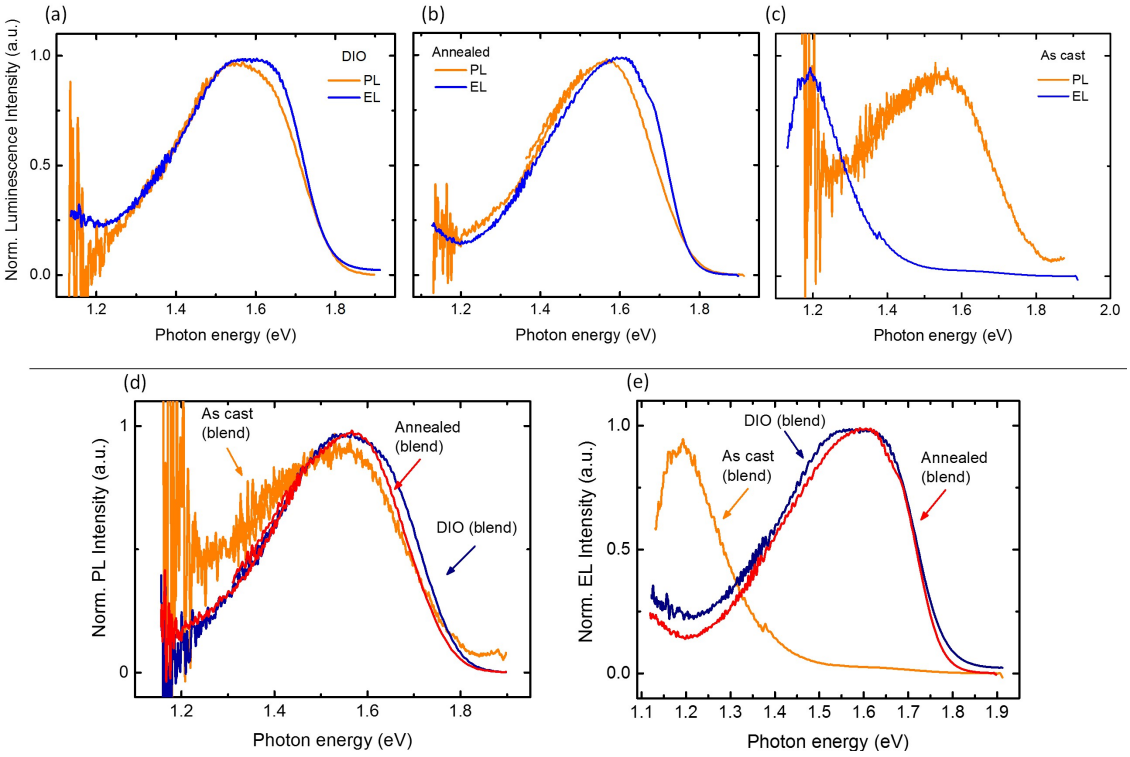

Figure 2.12: Comparison between emission achieved by EL and PL from DTS(FBTTh$_2$)$_2$:PC$_{71}$BM films fabricated as-cast (a), annealed (b), and with DIO (c). (d) and (e) compare of PL and EL spectra, respectively, from films fabricated with the three different processing conditions.

significantly different from the EL: the EL is red-shifted to low energies, already identified as the CT state, while the PL remains at similarly high energies which correspond to the emission of DTS($FBTTh_2$)$_2$ S1 singlet emission. The PL signal from the as-cast film is much weaker, and therefore much noisier than the PL from the other films.

Excitons are generally considered to be neutral particles, which would not be affected by low electric fields (although there exist examples which demonstrated that large electric fields can split excitons[82, 83]). However, if excitons split into free charge carriers, an applied electric field would have an influence on the direction of charge drift within the film: a forward bias would induce further charge recombination, and a reverse bias would induce charge collection and inhibit charge recombination. This is illustrated by the effect of bias on the band diagram shown in the Introduction (Figure 1.13). In addition, the CT state may also be subject to field-dependent splitting (more commonly known as field-dependent generation). Field-dependent generation has been shown to reduce the performance of as-cast small-molecule solar cells,[84, 80] as was shown specifically on p-DTS($FBTTh_2$)$_2$:$PC_{71}BM$ blend devices.[80, 85]If blend films are excited by a laser pulse while an electric field is applied, this may provide us with additional information on the formation of the emissive species. A similar analysis was done on polymer:fullerene solar cells by Tvingstedt *et al.*, see reference [23].

Bias-dependent PL spectra for as-cast p-DTS($FBTTh_2$)$_2$:$PC_{71}BM$ and DPP($TBFu$)$_2$:$PC_{71}BM$ blend films are shown in Figure 2.13a,b. As the extraction field across the films increases (*i.e.* the applied bias is more negative), the PL emission spectrum of the as-cast films changes in both material systems. In DPP($TBFu$)$_2$:$PC_{71}BM$, where the PL emission spectrum largely resembles the EL spectrum of the same device, the entire PL spectrum decreases in intensity. The close spectral overlap and the bias-dependence imply that the PL spectra of as-cast DPP($TBFu$)$_2$:$PC_{71}BM$ films originates from the CT state between DPP($TBFu$)$_2$ and $PC_{71}BM$. The bias dependence, further

suggests that under solar cell operation there are charge carriers that are lost to recombination through the CT state. As noted from Figure 2.12, the PL from as-cast p-DTS($FBTTh_2$)$_2$:$PC_{71}BM$ is significantly different in shape from the EL, with emission at energies that correspond to S1 singlet p-DTS($FBTTh_2$)$_2$ emission. However, there is also significant emission at lower photon energies, implying that recombination is occurring from a range of states. As extraction field is increased, the PL of as-cast p-DTS($FBTTh_2$)$_2$:$PC_{71}BM$ changes in shape with low-energy emission reducing in intensity (Figure 2.13). At the strongest reverse bias, -10 V, the PL from the blend device is close to the PL emission from neat p-DTS($FBTTh_2$)$_2$.This means that as reverse bias is increased, emission from CT states of varying energies is quenched, while emission from singlet p-DTS($FBTTh_2$)$_2$ states is unchanged by the applied field. As was the case with DPP($TBFu$)$_2$:$PC_{71}BM$, this indicates of field-dependent recombination. The data at hand, however, does not specify is this is recombination due to CT states that were not able to separate (geminate recombination), or if free charge carriers met again at a donor/acceptor interface and recombined *via* the CT state (bimolecular recombination). Previous studies on this system which employed temporal resolution suggest that as-cast p-DTS($FBTTh_2$)$_2$:$PC_{71}BM$ devices suffer from field-dependent geminate recombination.

In contrast to the as-cast films, the optimized films (DIO for p-DTS($FBTTh_2$)$_2$:$PC_{71}BM$, and thermal annealing for DPP($TBFu$)$_2$:$PC_{71}BM$), show very little change to the PL spectra with applied reverse bias (Figure 2.13c,d). For both blend systems, PL from the optimized films is largely at energies overlapping with S1 singlet emission of each donor. The spectral shape of the optimized blend PL also agrees well with the PL form the neat donor films. In these films, this data suggests that there is little to no field-dependent generation. Interestingly, devices made with DPP($TBFu$)$_2$:$PC_{71}BM$) have a low *FF* even under the optimized processing conditions, which means the blend system suffers from field-dependent generation. However, the

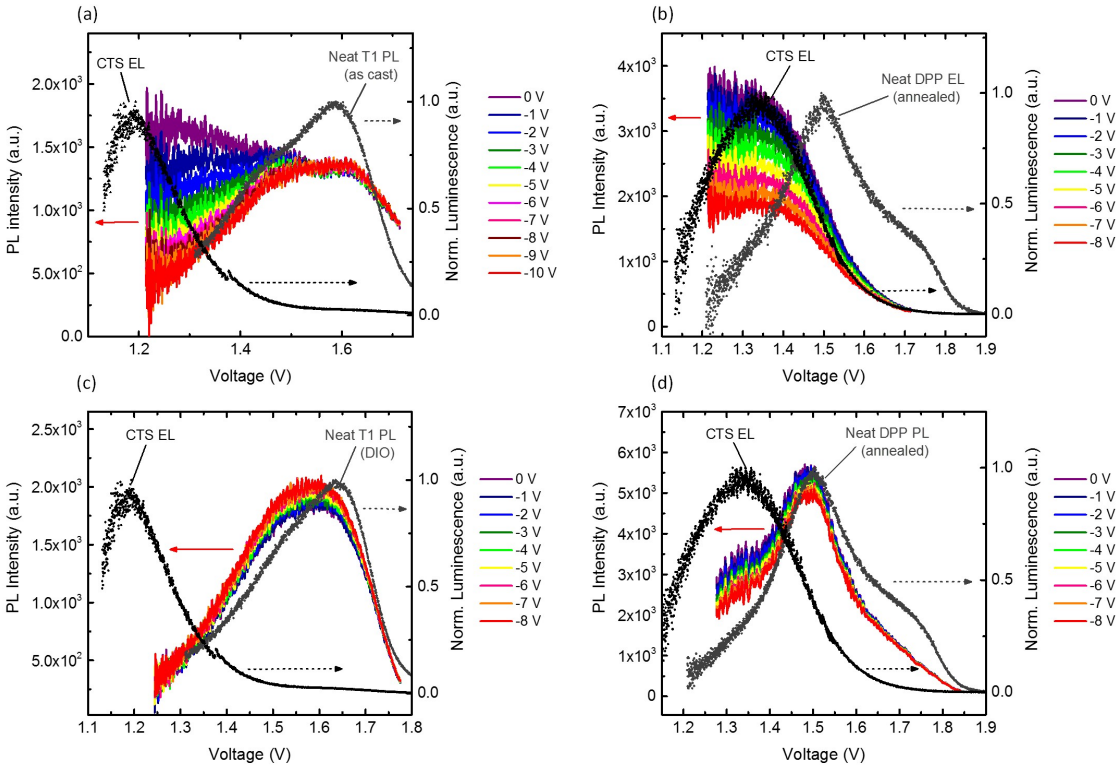

Figure 2.13: Bias-dependent PL from as-cast (a) p-DTS(FBTTh$_2$)$_2$:PC$_{71}$BM and (b) DPP(TBFu)$_2$:PC$_{71}$BM, (c) DIO-processed p-DTS(FBTTh$_2$)$_2$:PC$_{71}$BM, and (d) annealed DPP(TBFu)$_2$:PC$_{71}$BM. All bais-dependent graphs include an overlayed EL spectra of the CT state emission from the as-cast blend films and PL form the neat donor, for comparison. Note that DTS(FBTTh$_2$)$_2$ and DPP refer to p-DTS(FBTTh$_2$)$_2$ and DPP(TBFu)$_2$

lack of a field-dependence in PL suggests that the field-dependent generation takes place primarily *via* non-radiative recombination pathways.

Next, we focused on the PL of as-cast p-DTS(FBTTh$_2$)$_2$:PC$_{71}$BM, but now studying the luminescence under varying temperatures. Figure 2.14 shows the bias- and temperature-dependent PL of as-cast p-DTS(FBTTh$_2$)$_2$:PC$_{71}$BM films as well as neat p-DTS(FBTTh$_2$)$_2$ films. At all temperatures studied, it is evident that the as-cast p-DTS(FBTTh$_2$)$_2$:PC$_{71}$BM PL is bias-dependent, but only at energies that are lower than the S1 p-DTS(FBTTh$_2$)$_2$ singlet state (Figure 2.14a,c,d). At sufficiently high reverse

bias, the PL from the blend films resembles the PL of neat p-DTS($FBTTh_2$)$_2$. In contrast, the PL from neat p-DTS($FBTTh_2$)$_2$ is not vias dependent under any temperature (Figure 2.14b,d,e).

If we compare the emission of ether the as-cast p-DTS($FBTTh_2$)$_2$:$PC_{71}BM$ or p-DTS($FBTTh_2$)$_2$ at different temperatures, a few more details become evident. First, the PL spectrum of neat p-DTS($FBTTh_2$)$_2$ evolves into two well-resolved peaks, and increases in intensity to a small degree (Figure 2.15a). The emergence of these two distinct peaks was studied in more depth in reference [86]. In contrast, the PL from the as-cast p-DTS($FBTTh_2$)$_2$:$PC_{71}BM$ blend films significantly increases with decreasing temperature (Figure 2.15b). Recombination in organic solar cells is known to be temperature dependent, as will be explored in more detail in Chapter 3. In fact, from the perspective of the V_{OC}, at a temperature of 0 K the V_{OC} can reach its maximum value because recombination has been eliminated. Assuming that film can absorb the same amount of photons at the temperatures probed here, the increase in PL with decreasing temperatures implies that not as many charges are decaying through non-radiative pathways. As temperature is decreased, charge separation may also be decreased, if charge generation is temperature dependent.[87] Therefore, this data suggests that non-radiative recombination increases with temperature (and is temperature-dependent), and that non-radiative recombination is more likely as charges are more likely to separate and recombine bimolecularly. This may point at charge-carrier losses due to recombination *via* triplet states, the formation of which would be more favorable compared to singlet states if recombination is bimolecular. Furthermore, if the spectra in Figure 2.15b are normalized to a point at energies corresponding to S1 p-DTS($FBTTh_2$)$_2$ singlet emission, it is evident that the shapes of the PL spectra are temperature-dependent. As temperature is decreased, there is relatively less S1 p-DTS($FBTTh_2$)$_2$ singlet emission compared to CT state emission from the blend devices. This suggests that the singlet PL from this blend is not simply due

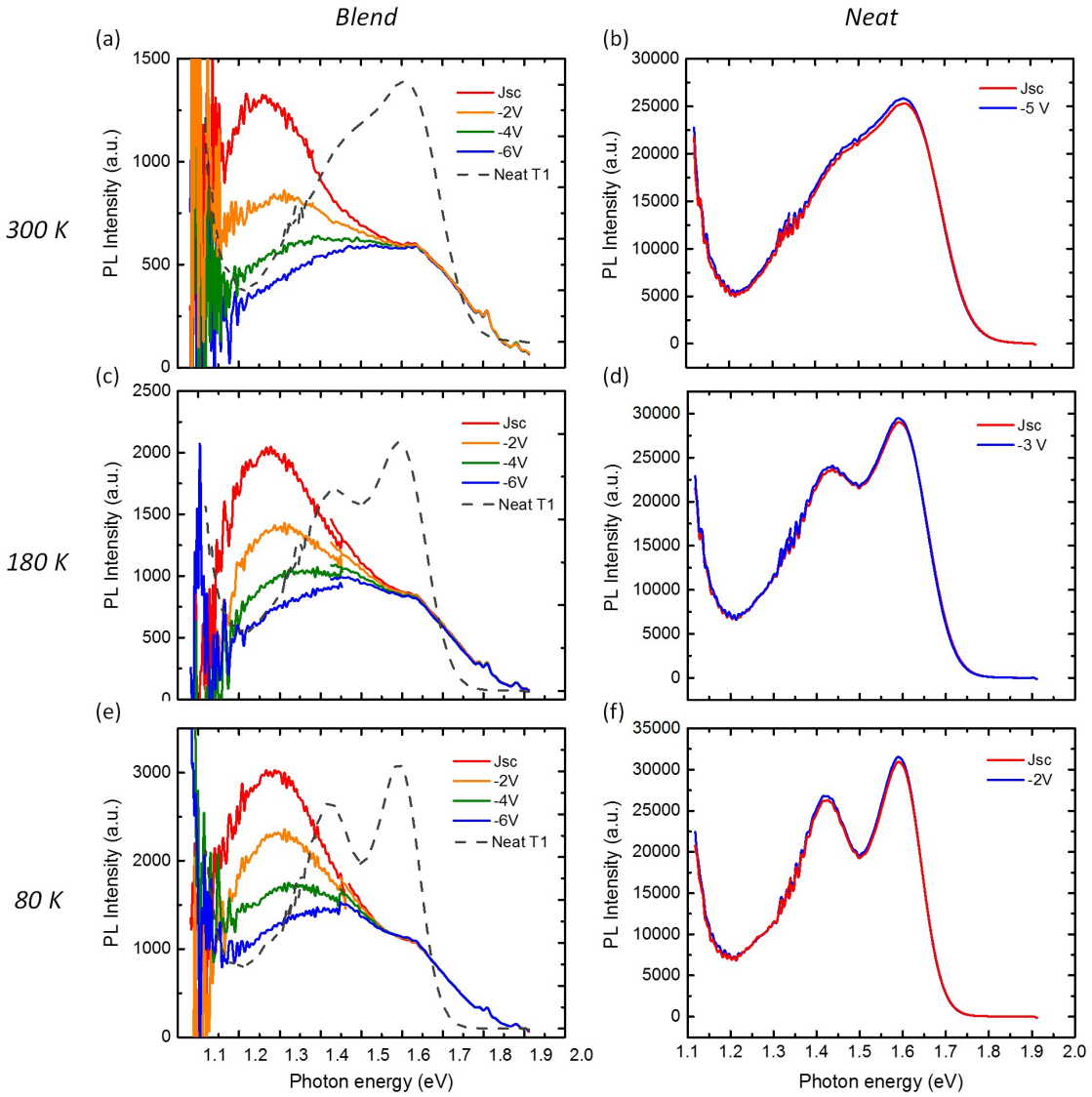

Figure 2.14: Bias- and temperature-dependent PL from as-cast p-DTS(FBTTh$_2$)$_2$:PC$_{71}$BM (a,c,e) and neat p-DTS(FBTTh$_2$)$_2$ (b,d,f) devices. The spectra of neat p-DTS(FBTTh$_2$)$_2$ was overlain on the bias-dependent PL plots of the as-cast blend p-DTS(FBTTh$_2$)$_2$:PC$_{71}$BM devices, at the appropriate temperature. The PL spectra were collected under temperatures of 295 K (a,b), 180 K (c,d), and 80 K (e,f).

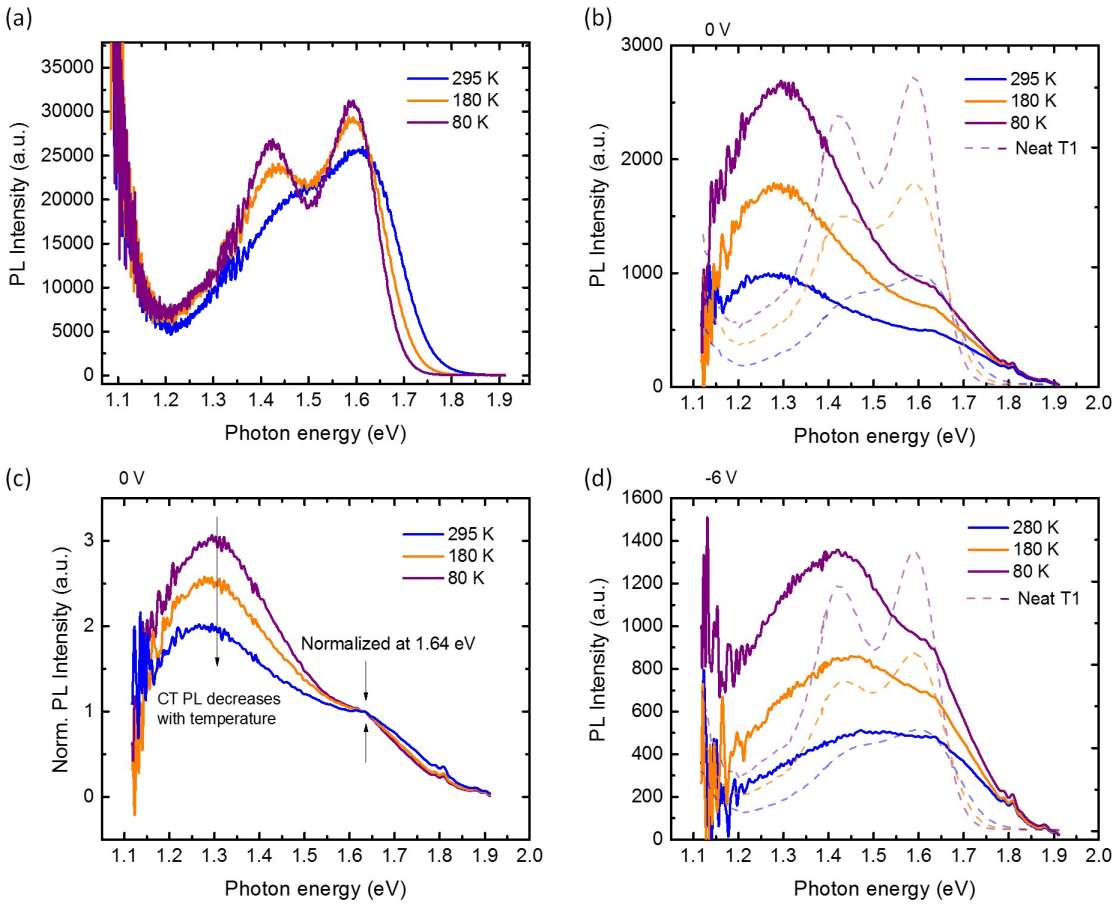

Figure 2.15: (a) Temperature dependent PL from neat p-DTS($FBTTh_2$)$_2$, and (b) blend as-cast p-DTS($FBTTh_2$)$_2$:$PC_{71}BM$ devices, under no applied bias. (c) Normalized temperature-dependent PL spectra at no applied voltage (from (b)). (d) Temperature-dependent PL spectra of as-cast p-DTS($FBTTh_2$)$_2$:$PC_{71}BM$ devices, under a reverse bias of -6 V.

to limited exciton diffusion (as may be expected in an as-cast blend, where the donor and acceptor are intimately mixed[12]), but is instead the result of either an equilibrium between the CT state and singlet state, or some process that additionally involves charge separation prior to the radiative recombination.

2.10 Conclusions and outlook

To summarize, we observe CT states as well as singlet exciton EL from blends of three high-performing solution-processed molecular solar cells. The contribution of singlet emission in the EL of these solar cells is present only in the optimized blends, and can be detected from emission onset. EQE and EL measurements confirm that in all cases the CT states is energetically distinct from the singlet state, suggesting that singlet emission is not due to coherence between the two states. Temperature-dependence of the EL spectra suggests that thermal activation may account in part for singlet emission in DPP(TBFu)$_2$ and p-SIDT(FBTTh$_2$)$_2$ blends with PC$_{71}$BM, while singlet emission from optimized p-DTS(FBTTh$_2$)$_2$:PC$_{71}$BM is temperature independent. In all cases singlet emission is present upon increased order and phase separation, and in DPP(TBFu)$_2$:PC$_{71}$BM we show a direct correlation between onset of singlet emission with formation of separate phases and donor crystallinity.[63] While it is clear that any recombination represents photoconversion losses, it appears that the emergence of singlet emission from these narrow-bandgap molecular donors, as well as PCPDTBT,[65] blended with fullerene derivatives is indicative of conditions favorable to photovoltaic performance. Understanding of interfacial properties such as molecular orientation, crystallinity, and charge delocalization will play a critical role in pushing organic photovoltaics towards higher efficiencies, especially as we design materials towards high V_{OC} values and minimum losses due to energetic offset between donor and acceptor.

2.11 Experimental

2.11.1 Material and film processing

DPP(TBFu)$_2$, p-DTS(FBTTh$_2$)$_2$, and p-SIDT(FBTTh$_2$)$_2$ were synthesized according to previously described procedures.[60, 61, 61] PC$_{71}$BM was purchased from Solenne BV and used as-received. DPP(TBFu)$_2$ and p-DTS(FBTTh$_2$)$_2$ were both blended with PC$_{71}$BM at a ratio of 3:2, p-SIDT(FBTTh$_2$)$_2$ was blended with PC$_{71}$BM at a ratio of 1:1, corresponding with optimal photovoltaic response. DPP(TBFu)$_2$ blends were dissolved at 21 mg mL^{-1} in chloroform and heated at 60 °C overnight prior to casting from room temperature at a spin speed of 2000 RPM. Half of the films were annealed at 110 °C for 10 minutes. p-DTS(FBTTh$_2$)$_2$ blends were dissolved at 35 mg mL^{-1} in chlorobenzene and heated at 90 °C overnight prior to casting from 70 °C at a spin speed of 1750 RPM. The same procedure was followed for DIO-processed devices with the addition of 0.4% DIO by volume. After casting from DIO containing solutions, the films was annealed at 70 °C to remove residual solvent additive. p-SIDT(FBTTh$_2$)$_2$ blends were dissolved at 40 mg mL^{-1} in chlorobenzene and heated at 90 °C overnight prior to casting from RT at a spin speed of 1750 RPM. Typical device thicknesses are about 100 nm for all blend films. Neat materials DPP(TBFu)$_2$, p-DTS(FBTTh$_2$)$_2$, p-SIDT(FBTTh$_2$)$_2$, and PC$_{71}$BM were dissolved at 15 mg mL^{-1} chloroform, 21 mg mL^{-1} chlorobenzene, 30 mg mL^{-1} chlorobenzene, and 25 mg mL^{-1} chlorobenzene, respectively.

2.11.2 Solar cell device fabrication

All samples were fabricated with the architecture ITO(140 nm)/PEDOT:PSS(35 nm)/active layer/Ca(15 nm)/Al(100 nm). Glass substrates patterned with 140 nm ITO were cleaned by sonication in water, acetone, and isopropanol, followed by UV-ozone

treatment. PEDOT:PSS layers were cast and dried at 140 °C, followed by active layer deposition under nitrogen environment as described above. Devices were finalized by thermal sublimation of 15 nm calcium and 100 nm aluminum electrodes. The device area used for all samples is 15 mm^2.

2.11.3 Photovoltaic and EQE measurements

Solar cell device properties were measured under illumination by simulated 1000 mW cm^{-2} AM1.5G light source using a 300 W Xe arc lamp with an AM 1.5 global filter. The irradiance was calibrated with a standard silicon photovoltaic calibrated by the National Renewable Energy Laboratory. EQE characteristics were measured with a 75 W Xe light source, monochromator, optical chopper, lock-in amplifier, and a National Institute of Standards and Technology calibrated silicon photodiode for power-density calibration.

2.11.4 EL and PL measurements

A Si CCD array cooled to -70°C was used as the detector for all EL emission spectra. Emission from the devices was aligned to the CCD entrance slit with a series of focusing lenses. A Si photodiode was used for luminescence-voltage (L-V) measurements. Low temperatures EL measurements were performed using a cryostat cooled with liquid N_2 and the CCD Si array. PL was measured using a HeNe laser (633 nm) excitation at a 90° angle to the detector, and the sample at a 45° angle to the detector. Bias-dependent PL was measured in the same setup, while applying a voltage to the device

2.12 Bonus: discovering trap-assisted *vs.* bimolecular recombination through emission

As noted in the preface, we began this study on the EL form the singlet state of optimized solar cells by first trying to characterize the recombination behavior in these devices using the relationship between EL intensity normalized for injected current, as a function of applied voltage. This technique was developed by Gert-Jan Wetzelaer and Martijn Kuik, as is described in reference [32]. By and large, when geminate recombination is eliminated, charge-carrier recombination can occur bimolecularly, when two free and oppositely-charged carriers meet and recombine, or *via* charge traps, where one charge is 'trapped' in an energetic state that is within the effective gap where it waits for a free charge-carrier to come by, and the charges recombine. Bimolecular recombination is a second order recombination process, while trap-assisted recombination is a first order process. Trap-assisted recombination, also termed as Shockley-Read-Hall (SRH) recombination is commonly considered non-radiative recombination, and can significantly reduce the efficiency of light emitting diodes.[31] Here, I would refer the reader to literature written by Martijn Kuik, who's PhD thesis title is "Trap Assisted Recombination in Polymer Light-Emitting Diodes". The expectation that SRH recombination is non-radiative is borrowed from the field of inorganic semiconductors, where it was established that SRH recombination is non-radiative, however this is not always necessarily true, and will be discussed more below. However, moving forward in this section, it is valid to consider SRH recombination as non-radiative recombination.

SRH recombination rate is described according to Equation 2.1, and is linearly de-

pendent on charge carrier density, it is a monomolecular process.

$$R_{SRH} = \frac{C_n C_p N_t (np - n_i^2)}{C_n(n + n_1) + C_p(p + p_1)} \propto n \tag{2.1}$$

Here, C_n and C_p are the capture coefficients for electrons and holes, respectively; N_t is the density of electron traps; n and p are the electron and hole densities, respectively; n_i is the intrinsic carrier concentration and is equal to $n_i = p_1 n_1$.

Bimolecular recombination can be described according to the Langevin recombination rate (although the Langevin recombination coefficient does not always predict recombination in organic solar cell devices,[88] it is a good approximation of recombination in organic light-emitting diodes), described in Equation 2.2

$$R_{BMR} = \gamma \frac{q}{\epsilon}(\mu_n + \mu_p)(np - n_i^2) \propto n^2 \tag{2.2}$$

Here, γ is the reduced recombination prefactor(which corrects for the deviation between the Langevin recombination coefficient and the experimentally determined coefficient); q is the elementary charge; ϵ is the dielectric constant; and μ_n and μ_p are the electron and hole charge-carrier mobilities, respectively.

Recombination current is determined by both bimolecular and trap-assisted recombination. As we have defined the two recombination types, however, radiative recombination will only be determined by bimolecular recombination. As charge carrier density is increased, the two recombination pathways will increase differently: since bimolecular recombination depends on the square of the charge carrier density and trap-assisted recombination depends linearly on the charge carrier density, as the carrier density is increased, bimolecular recombination will dominate over trap-assisted recombination. Given these characteristics, we can use the relationship between emission intensity and current to identify the recombination pathways in the device.

When a device is operated at voltages larger than the turn-on voltage of the device, charge carriers will be injected into the active layer where they are expected to recombine. This recombination can be radiative or non-radiative, and will increase in intensity as the voltage is increased and more charges are recombining in the actrive layer. The emission intensity can be recorded with a photodiode, and normalized by the current density, to give an EL efficiency. If the emission (radiative recombination) and current are dictated by the same recombination behavior (or at least recombination that has the same dependence on carrier density), then as the voltage across the devices is increased, the EL efficiency should not change. However, if the current, for example, is determined by both bimolecular recombination and trap-assisted recombination, but as we have established the emission can only be determined by bimolecular recombination, then the EL efficiency will change with the carrier density (applied voltage)- in this case the EL efficiency is expected to increase as bimolecular recombination will grow faster with carrier density than trap-assisted recombination.

The above is illustrated according to the following relationship, 2.3

$$EL_{eff} \propto \frac{R_L}{R_L + R_{SRH}} \tag{2.3}$$

It is possible to characterize the quality of charge recombination from the diffusion regime of a dark *J-V* curve for a diode device, such as the solar cell. At relatively low carrier densities current in the diode is diffusion limited, and is described as an exponential grown in current with voltage. Once the applied voltage surpasses the V_{bi} and carrier density is relatively large, current in the solar cell begins to be limited by recombination (assuming very low contact resistance), and is termed drift current. From the diffusion regime, it is possible to extract the ideality factor, which describes the voltage dependence of charge carrier recombination, and may provide information on

the dominant types of recombination providing information about the recombination routes.[89, 90, 91] The ideality factor, η, is found in the denominator of the exponent in the non-ideal Shockley diode equation:

$$J_D = J_0[exp(\frac{qV}{\eta kT}) - 1] \tag{2.4}$$

Where J_D is the dark current, J_0 is the saturation current, q is the elementary charge, V is the applied voltage, η is the ideality factor , k the Boltzmann constant, and T temperature. The addition of an ideality factor to the ideal Shockley diode equation comes to correct for the fact that recombination current does not only depend exponentially on the temperature, voltage, and the bandgap as would be predicted based on Boltzmann population, or depends on these factors differently from direct band-to-band recombination. Recently, it has been suggested that this deviation is due to the added non-ideal non-radiative recombination contribution to recombination current.[89] The same reference, a study by Kristofer Tvingstedt, reports a details study on the ideality factor determined by various methods. Tvingstedt *et al.* conclude that the ideality factor determined by dark J-V current, as was done here, is in fact not the most accurate way due to resistive losses. The argument is, in part, based on the wide range of ideality factors, from less than 1 all the way to 20. However, the ideality factors we determined here are low and comparable to values which Tvingstedt *et al.* find as accurate, and may not be so distorted by resistive losses.

A method that has been widely used to characterize the ideality of recombination, and also suggested by Tvingstedt *et al.* as a better method compared to the dark J-V method,[89] is to determine the relationship between the V_{OC} and light intensity.[92, 93, 94] First, we define the current under illumination, J_L, as the current due to photocurrent

(J_{ph}) on top of the dark current (J_D):

$$J_L = J_{ph} + J_D \tag{2.5}$$

Under V_{OC} conditions, the current (J_L) is equal to zero, by definition, and therefore $J_D = J_{ph}$. Starting with the Shockley diode equation, we can next derive the following relationship for the V_{OC}:

$$V_{OC} = \eta(\frac{kT}{q})ln(\frac{J_{ph}}{J_s} + 1) \tag{2.6}$$

If the photocurrent is linearly proportional to the light intensity (I), which is often the case, then we can get a relationship for the V_{OC} with light intensity:

$$V_{OC} \propto \eta(\frac{kT}{q})ln(I + 1) \tag{2.7}$$

From here we can extract that the V_{OC} should have an exponential relationship with light intensity, with a slope of $\eta\frac{kT}{q}$. The ideality factor, η, will be 1 if all recombination is bimolecular, and 2 if recombination is heavily trap-assisted.

To complete this analysis, blend devices of DTS($FBTTh_2$)$_2$:$PC_{71}BM$ and DPP($TBFu$)$_2$:$PC_{71}BM$ were fabricated, using the same processing methods outlined above: as-cast as unoptimized, processed with DIO (p-DTS($FBTTh_2$)$_2$), or thermally annealed (DPP($TBFu$)$_2$). In addition, as a control we also fabricated a DPP($TBFu$)$_2$:$PC_{71}BM$ with a semiconductor especially chosen with energy levels that would act as an electron trap: TCNQ. TCNQ was added as a 1:250 mole ratio with $PC_{71}BM$. First, we look at the relationship between EL_{eff} and V for the solar cell blends: while running an J-V scan, a silicon photodiode was placed in front of the solar cell (glass side), and the response of the silicon photodiode was recorded. The J-V curve and the response of the photodiode are shown in Figure 2.16. Dividing the photodiode response

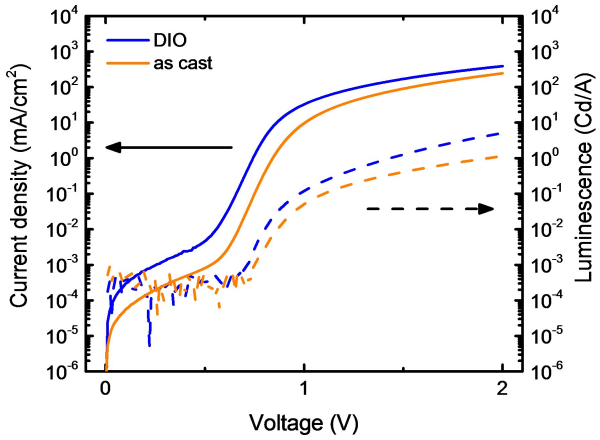

Figure 2.16: Current and the corresponding emission intensity as a function of applied voltage.

(radiative recombination) by the current (radiative + non-radiative recombination) gives the EL_{eff}. The EL_{eff} for as-cast DTS(FBTTh$_2$)$_2$:PC$_{71}$BM and DPP(TBFu)$_2$:PC$_{71}$BM, as well as optimized films of the same blends is shown in Figure 2.17.

The EL_{eff} of as-cast DTS(FBTTh$_2$)$_2$:PC$_{71}$BM, as-cast DPP(TBFu)$_2$:PC$_{71}$BM, and annealed DPP(TBFu)$_2$:PC$_{71}$BM are all independent of voltage, which implies that current and luminescence are governed by recombination with the same carrier-density dependence. The EL_{eff} of DIO-processed DTS(FBTTh$_2$)$_2$:PC$_{71}$BM, however, is increasing with applied voltage, which implies that this device suffers from trap-assisted recombination. This is a very surprising especially considering that among these four blends and processing conditions, DIO-processed DTS(FBTTh$_2$)$_2$:PC$_{71}$BM has the highest PCE (Figure 2.2). It is well expected that trap-assisted recombination will significantly reduce solar cell performance.[92, 93] Note, however, that no emission was detected from the blend with the intentional addition of traps (DPP(TBFu)$_2$:PC$_{71}$BM:TCNQ).

Next, we characterized the ideality factor for these solar cell devices. The ideality factor is determined from the diffusion regime of the dark J-V curve, and therefore requires devices of very high quality, with very low leakage current (high shunt resistance).

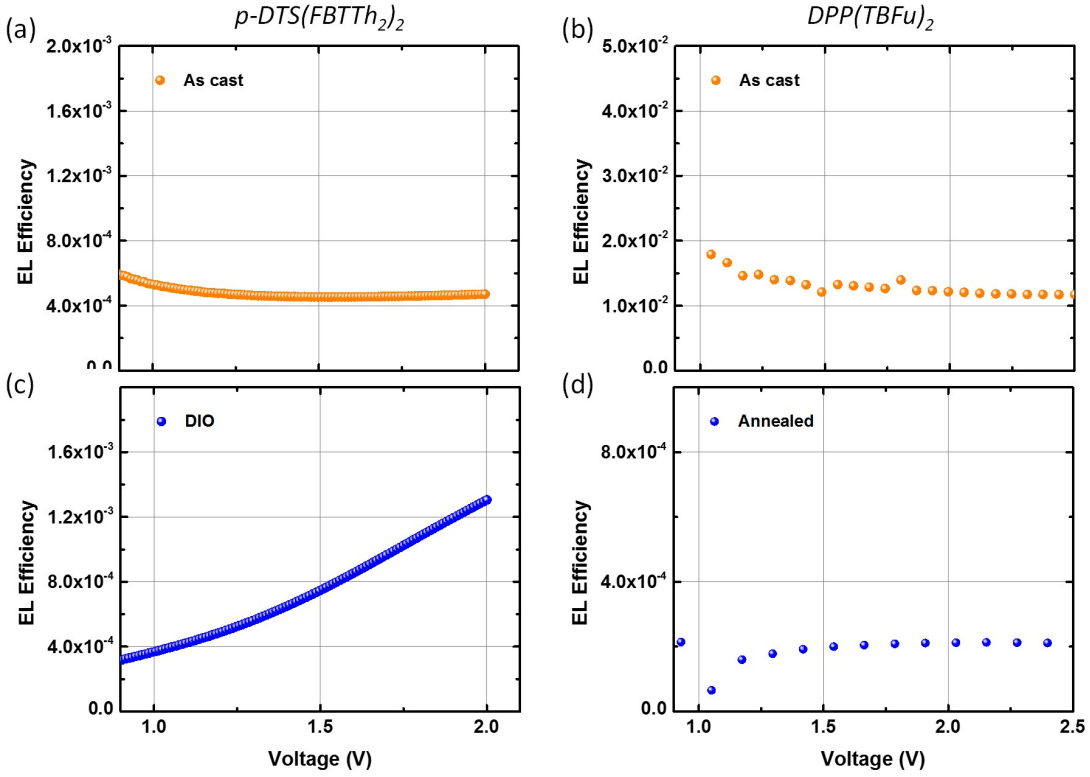

Figure 2.17: EL_{eff} for as cast (a) DTS(FBTTh$_2$)$_2$:PC$_{71}$BM and (b) DPP(TBFu)$_2$:PC$_{71}$BM, (c) DIO-processed DTS(FBTTh$_2$)$_2$:PC$_{71}$BM, and (d) annealed DPP(TBFu)$_2$:PC$_{71}$BM.

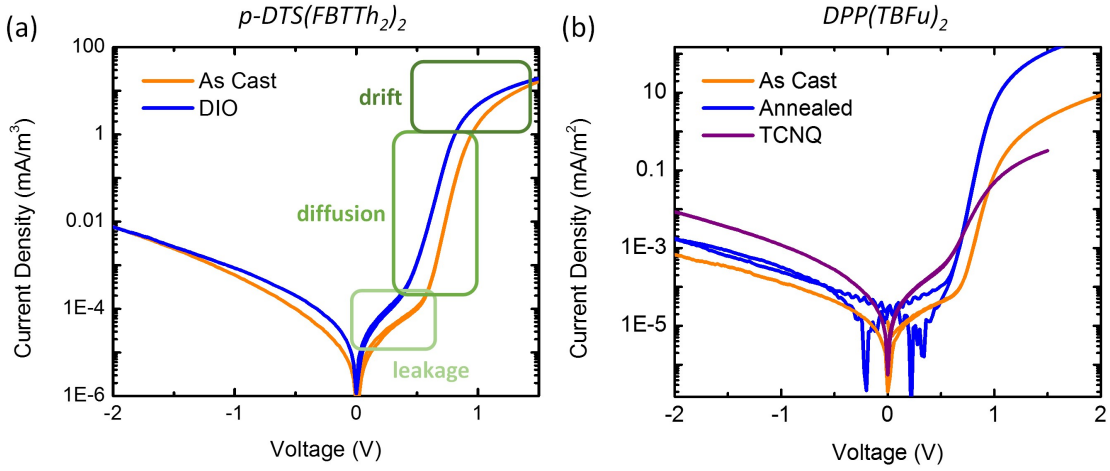

Figure 2.18: J-V curves under dark for (a) DTS(FBTTh$_2$)$_2$:PC$_{71}$BM and (b) DPP(TBFu)$_2$:PC$_{71}$BM.

The dark curves for these devices are shown in Figure 2.18, with the different regimes outlined. Rearranging the non-ideal Shockley diode equation, we can calculate η as a function of applied voltage. We are most interested in the slope (under log-lin) of the diffusion regime, which will be represented as a minimum plateau in η *vs.* V. η is expected to be determined by the fastest charge carrier, which for most OPV blends is the electron transport in PCBM. It has been shown that the dark current J-V η in organic solar cells is rarely below 1.3, which is a characteristic η of PCBM.[90] The η values obtained for the blends studied here are shown in Figure 2.19.

As-cast p-DTS(FBTTh$_2$)$_2$ and annealed DPP(TBFu)$_2$ blend films both have a low ideality factor, at about 1.3, which is consistent with good electron transport through PC$_{71}$BM.[90] DIO-processed p-DTS(FBTTh$_2$)$_2$ and as-cast DPP(TBFu)$_2$ blends, on the other hand have, have an ideality factor of about 1.6. As noted, the ideality factor should be dictated by the fastest charge carrier. This means that in DIO-processed p-DTS(FBTTh$_2$)$_2$ blends it is possible that hole transport through p-DTS(FBTTh$_2$)$_2$ is in fact faster than electron transport through PC$_{71}$BM. Given that this blend has the highest PCE, this is a more reasonable conclusion than that electron transport is hindered. Indeed, single-carrier hole and electron mobilities confirm that the hole mobility is equivalent to- or higher than- the electron mobility in this blend film.[79] In the case of as-cast DPP(TBFu)$_2$, however, hole mobility is nearly an order of magnitude smaller than the electron mobility, and the electron mobility is not significantly lower than in DIO-processed p-DTS(FBTTh$_2$)$_2$ (and it is worth noting that as-cast p-DTS(FBTTh$_2$)$_2$ has much lower hole and electron mobilities). It is important to revisit the dark J-V curves, however, to verify that each curve has a significant diffusion regime: if the regime is too short, the ideality factor can be distorted by leakage current or the effect of contact resistance in the drift regime. The as-cast DPP(TBFu)$_2$ blend and especially the DPP(TBFu)$_2$ mixed with TCNQ, both have a limited diffusion regime . Given the dark

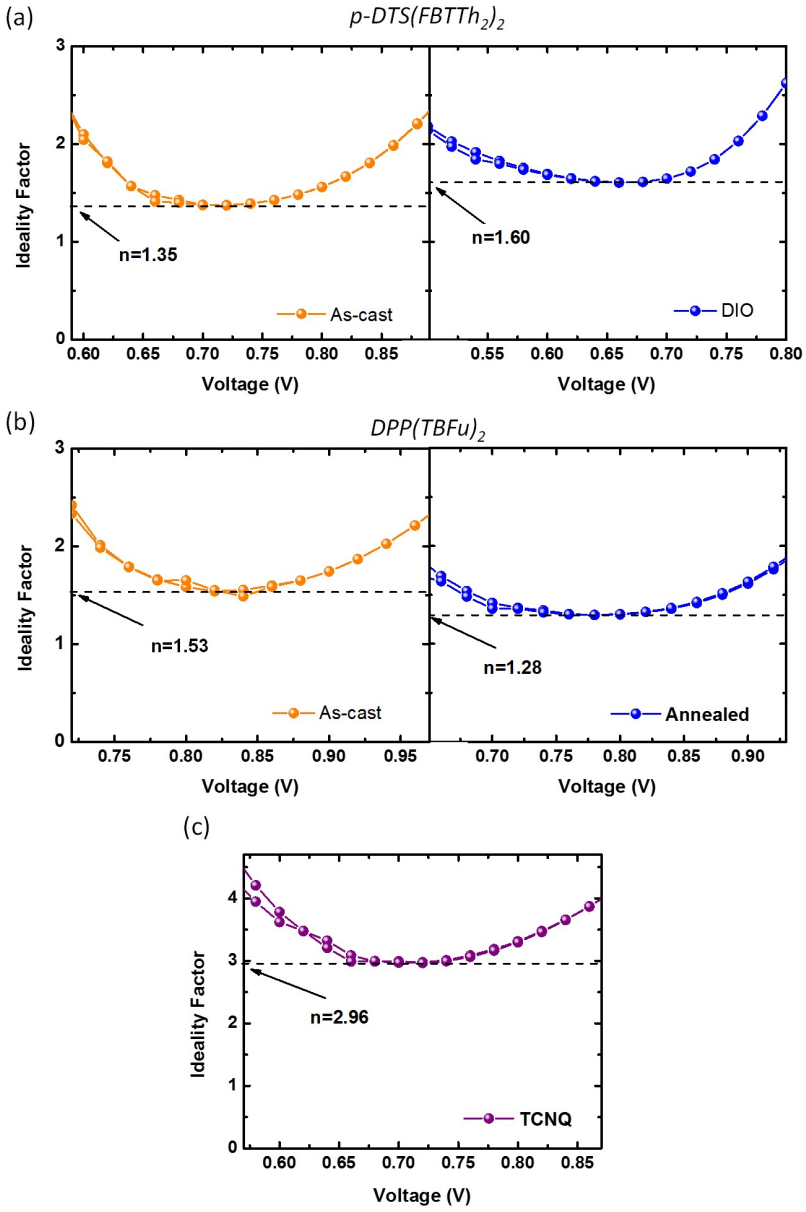

Figure 2.19: Ideality factors for (a) DTS(FBTTh$_2$)$_2$:PC$_{71}$BM and (b) DPP(TBFu)$_2$:PC$_{71}$BM, as-cast (left) and optimized (right), and for (c) DPP(TBFu)$_2$:PC$_{71}$BM:TCNQ.

J-V curve of DPP(TBFu)$_2$ with TCNQ, the ideality factor extracted from this blend is particularly not trust worthy. Indeed, the ideality factor of this blend is approaching 3, and we would expect the ideality factor to be on higher than 2.

The ideality factors shown in Figure 2.19 did not explain the results shown in Figure 2.17, and are in themselves complicated to discern. To understand if recombination in these blends is truly dictated by bimolecular or trap-assisted recombination we recorded the dependence of the V_{OC} on light intensity, a method that is well accepted and has been demonstrated on many systems. In these measurements, J-V curves are measured at a range of illumination intensities. The V_{OC} values as measured at each light intensity are shown in Figure 2.20. The V_{OC} *vs.* light intensity in all blend systems, with the exception of the TCNQ-added blend, has a slope, S, of kT/q, and therefore an ideality factor of 1. Only the blend to which we intentionally added electron traps, in the form of 1:250 equivalents TCNQ:$PC_{71}BM$, has a slope of 1.9 kT/q, implying that transport in this blend is heavily electron trapped. This means that our experimental setup was good, except that the TCNQ had such a severe effect on transport and emission in the blend that it hindered even the analysis.

It is most interesting to note, however, that the DIO-processed p-DTS(FBTTh$_2$)$_2$ blend clearly shows that emission and current have different charge recombination contributions to them, while the V_{OC} *vs.* light intensity relationship suggests bimolecular recombination without any trap-assisted recombination. This is the point where we first arrived when we started studying the emission in the solar cell blends. As was established above, we now know that the DIO-processed p-DTS(FBTTh$_2$)$_2$ blend shows EL from both the CT state as well as the p-DTS(FBTTh$_2$)$_2$ S1 singlet state. The emission from the CT state and the singlet state follow a different carrier-density dependence, modulated by applied bias. To illustrate, Figure 2.21 shows EL spectra from a DIO-processed p-DTS(FBTTh$_2$)$_2$ blend film, at different applied voltages (and therefore dif-

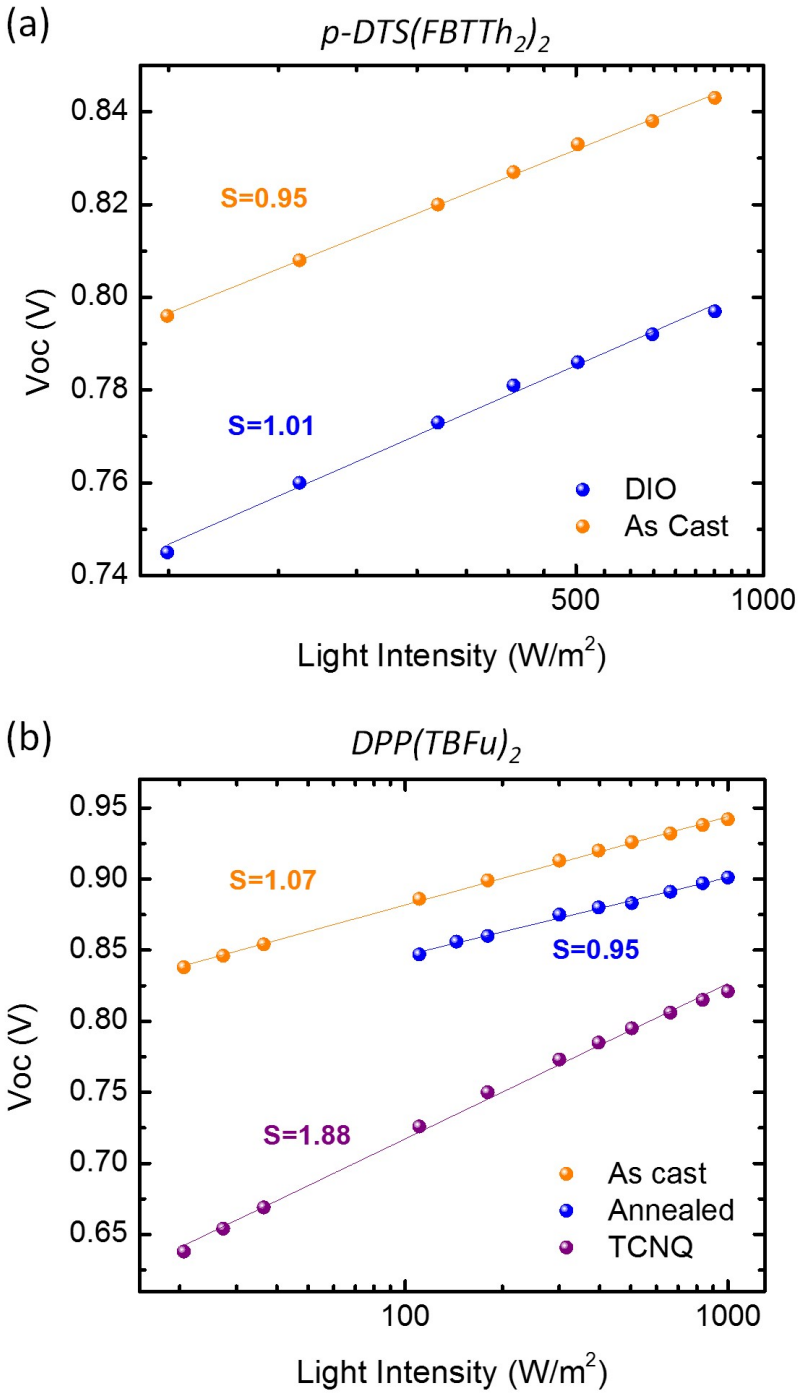

Figure 2.20: V_{OV} *vs.* light intensity (a) DTS$(FBTTh_2)_2$:$PC_{71}BM$ and (b) DPP$(TBFu)_2$:$PC_{71}BM$ films at varying processing conditions.

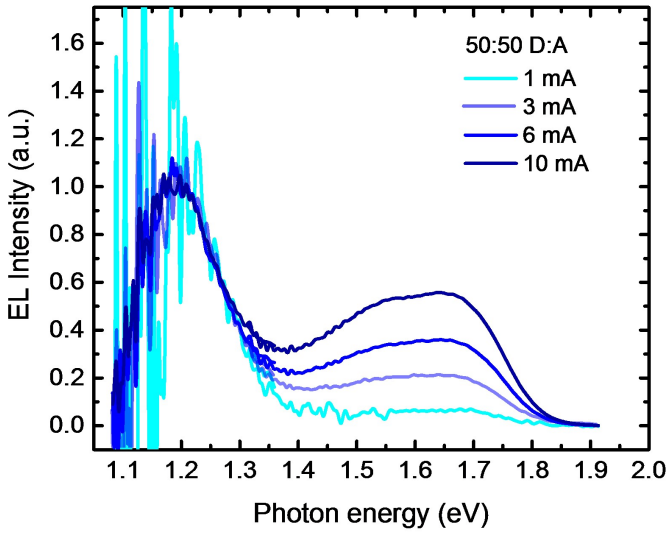

Figure 2.21: Bias-dependent emission from optimized p-DTS(FBTTh$_2$)$_2$:PC$_{71}$BM, normalized to the CT state peak.

ferent currents), normalized to the CT state peak. Starting from a current across the device of 1 mA, most of the radiative emission is through the CT state. As the voltage (and therefore current) are increased, the singlet emission grows faster than the CT state emission. This observation alone is enough to suggest that recombination in DIO-processed DTS(FBTTh$_2$)$_2$:PC$_{71}$BM blends can take place *via* a few routs: radiative CT state, radiative singlet state, and non-radiative recombination which can have a few more distinct routs.

From Figures 2.21 and 2.17 we know that the DIO-processed p-DTS(FBTTh$_2$)$_2$ blend device has a number of recombination pathways, with different dependence on voltage (carrier density). The expected pathway is through the CT state, and the surprising pathway through the donor singlet state. However, the presence of two pathways alone does not explain the difference in carrier-density dependence. We therefore examined the EL_{eff} from neat p-DTS(FBTTh$_2$)$_2$ films. The emission spectrum for p-DTS(FBTTh$_2$)$_2$ is shown in Figure 2.5.

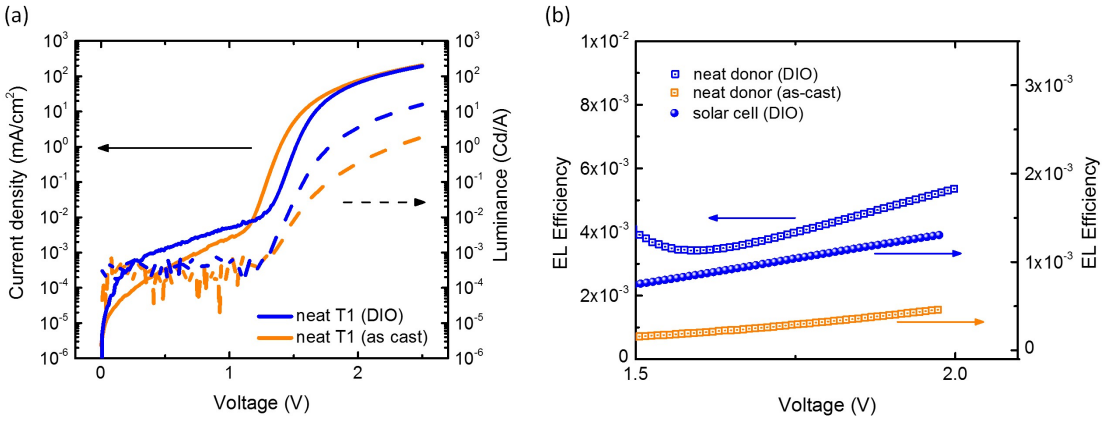

Figure 2.22: EL_{eff} of neat p-DTS(FBTTh$_2$)$_2$. (a) J-V and EL-V for neat p-DTS(FBTTh$_2$)$_2$ as-cast and with 0.4% DIO. (b) EL_{eff} for neat p-DTS(FBTTh$_2$)$_2$ with and without DIO, compared with the EL_{eff} of the blend film with DIO.

Figure 2.22a shows the J-V curve for a neat p-DTS(FBTTh$_2$)$_2$ film processed as-cast or with DIO (as was done for the blend films), alone with the emission intensity as a function of applied voltage. Figure 2.22b shows the EL_{eff} for the neat films as-cast or with DIO, as well as the EL_{eff} of the DIO-processed blend film. First, it is evident that emission from neat p-DTS(FBTTh$_2$)$_2$ alone has two pathways for recombination, since the EL_{eff} for both neat films is increasing with applied voltage. The shape of the EL spectra for neat p-DTS(FBTTh$_2$)$_2$ is not, however, dependent on voltage: the intensity grows, but no new peaks emerge. This means that there is only one radiative recombination pathway, and an additional non-radiative pathway. Furthermore, the dependence on applied voltage is greater in the p-DTS(FBTTh$_2$)$_2$ device, while the dependence in the as-cast neat device resembles the DIO-processed blend device. This may imply a morphological dependence of trap-assisted recombination: while as-cast p-DTS(FBTTTh$_2$)$_2$ is crystalline, the addition of DIO increases the crystallinity of the film. A greater dependence on carrier density suggests of a stronger contribution of trap-assisted recombination. Interestingly, exciton diffusion measurements on neat p-DTS(FBTTh$_2$)$_2$ films

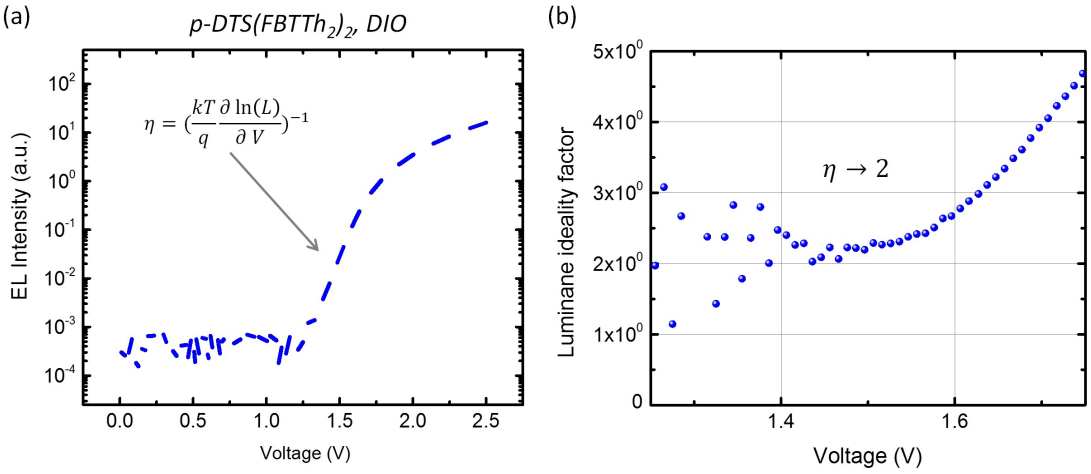

Figure 2.23: EL ideality factor for neat p-DTS(FBTTh$_2$)$_2$ (a) $EL - V$ for p-DTS(FBTTh$_2$)$_2$ with DIO. (b) The ideality factor, η, extracted from the $EL - V$ relationship in (a).

also show that exciton diffusion of as-cast p-DTS(FBTTh$_2$)$_2$ (6.8±0.4 nm) is significantly reduced when the films are annealed or processed with DIO (4.9±0.3 nm) or thermal annealing (2.8±0.2 nm). The authors suggest that there may be exciton traps that emerge at grain boundaries, with a density on the order of f 1.2×10^{18} cm^{-3}.[86]

To confirm that recombination in neat p-DTS(FBTTh$_2$)$_2$ is indeed trap-assisted, we return now to the ideality factor. However, instead of extracting the ideality factor from J-V measurements, it is possible to extract η from the diffusion regime of EL intensity *vs.* V. This requires, however, that EL intensity *vs.* V also have a long diffusion regime, which is not a trivial task. The EL intensity *vs.* applied voltage curve of the DIO-processed p-DTS(FBTTh$_2$)$_2$ film is shown in Figure 2.23a, and the ideality factor extracted from the same curve is shown in Figure 2.23b. The luminance ideality factor for this film is approaching a plateau at 2, confirming that the radiative recombination through the singlet of p-DTS(FBTTh$_2$)$_2$ is in competition with another non-radiative recombination pathway. Therefore, it may be that the behavior indicating of trap-assisted recombination, in

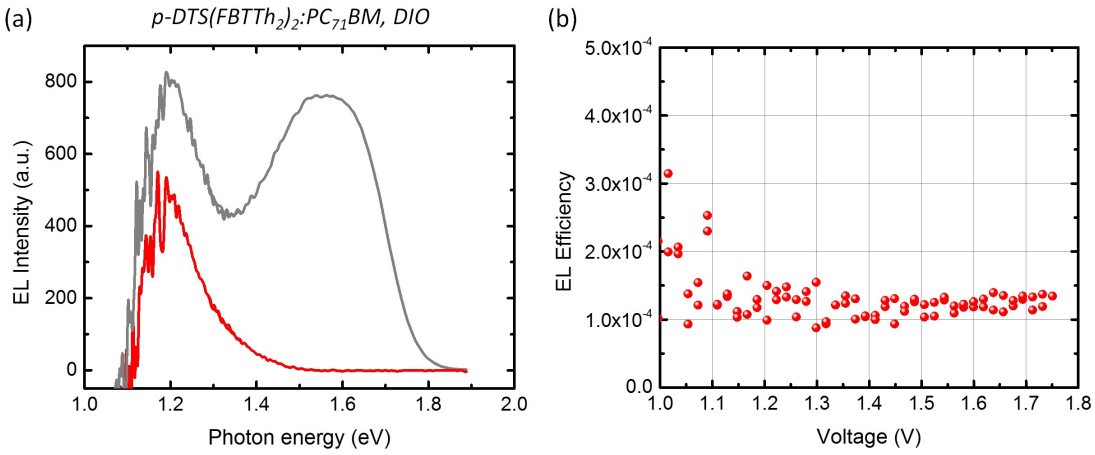

Figure 2.24: EL_{eff} for CT state emission from p-DTS(FBTTh$_2$)$_2$:PC$_{71}$BM with DIO. (a) EL spectra from a blend film of p-DTS(FBTTh$_2$)$_2$:PC$_{71}$BM processed with dio DIO (grey) and EL of the same device, under the same applied voltage, using a 1000 nm long-pass filter, to eliminate signal from the singlet emission. (b) EL_{eff} of the same device in (a), using the long-pass filter.

Figure 2.17 is in fact only due to the fact that recombination in p-DTS(FBTTh$_2$)$_2$ alone is characterized by competing radiative and non-radiative recombination pathways. [91]

Finally, we now return to the DIO-processed p-DTS(FBTTh$_2$)$_2$:PC$_{71}$BM device, and decouple the behavior of the CT state emission and p-DTS(FBTTh$_2$)$_2$ emission. We accomplish this by performing the EL_{eff} measurements, but using a high-pass 1000 nn optical density filter to remove the contribution of singlet emission. The emission spectra with and without the filter are shown in Figure 2.24a, where the emission without the filter is only at energies corresponding to the CT state. EL_{eff} collected using the filter, shown in Figure 2.24b, shows an independence to the applied voltage, confirming that recombination *via* the CT state has the same voltage (carrier-density) dependence as the current. Therefore, the current and recombination that govern CT state emission cannot include trap-assisted recombination, and must be bimolecular in nature. This is in agreement with the V_{OC} dependence on illumination intensity, which suggests that at

V_{OC}, recombination is well described by bimolecular recombination.

The process of trap assisted recombination can be radiative, and in fact describes the emissive recombination of polymer light emitting diodes in a host polymer,[91] where polymers of varying bandgaps are combined in a host chromophore, to produce a combined white emission. The traps in these cases provide the lower-energy emission. However, in light-emitting diodes made of a single active material, trap assisted recombination is still present, and has been shown to be non-radiative. [95, 96, 31] In the materials studied here, emission that would indicate of the expected bimolecular recombination should arise form the CT states. The CT states of the blends here have emission that is at the low-energy detection edge of the detectors used (silicon photodectros have a bandgap of 1.2 eV) and any emission of lower energy cannot be detected. Therefore, if there are some emissive trap states in our blend materials, their radiative decay would be not detected, and can be treated as non-radiative contribution to the recombination in the solar cells.

Chapter 3

Impact of Interfacial Molecular Orientation on Radiative Recombination and Charge Generation Efficiencies

Sometimes it's not enough to know what things mean,

sometimes you have to know what things don't mean.

– Bob Dylan

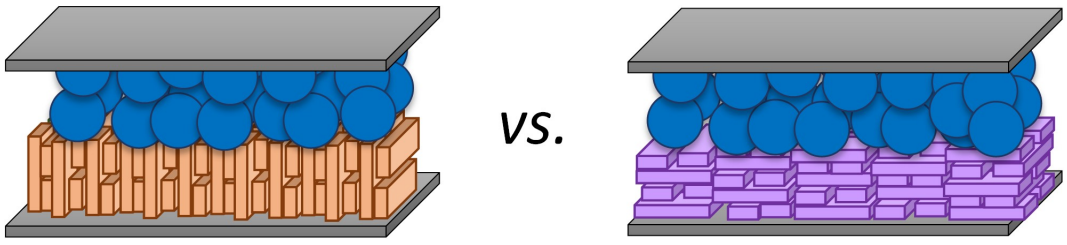

3.1 Preface

The study of the importance of interfacial molecular orientation that is presented here was only possible because Dr. Jack Love and Dr. Chris Takacs were using TEM and GIWAXS to study a molecule synthesized in Prof. Gui Bazan's lab by Dr. Ikuhiro Nagao. Through some inconsistent data, Chris and Jack realized that if this molecules, called colloquially H1 around the lab (named after Ikuhiro Nagao), is processed from a solution of chlorobenzene or chlorobenzene with DIO, the resulting TEM images and GIWAXS spectra look entirely different. After some careful studies Chris and Jack understood that H1 in fact adopts different molecular orientations with respect to the substrate in the two cases. The great moment of discovery is really owned by Jack and Chris, and I feel very fortunate that I got to work on this material system - it's been a pleasure working on this project. And it is Quyen who oversaw all the advancements and discoveries in the group, and directed me to work on this project from the point of view of my focus on donor/acceptor

From the inception of this study I worked closely with Jack, who is inspiring and creative to work with. We thought of, talked about, and tried a large range of ideas and directions that are related to the importance of molecular orientation. Although we worked on this project together, Jack was also very generous throughout, saying that he is trying to stay removed from this project and let me lead it (even though he is among the two people who made the discovery of the orientation change).

Due to the expertise on and instrumentation in Prof. Dieter Neher's lab, we reached out to them to ask if they would like to collaborate with us on this project: it may be that field-dependence of generation, the origin of which is not understood (and thus how to mitigate it), is a function of orientation. Steffen Roland was the student whom Dieter put us in touch with. Steffen was a really great collaborator, even overseas and with

the limitation of email for communication. Steffen and I exchanged many emails back and forth, and discussed what the results mean and what we should do further - Steffen took a much more active role in this than many other 2nd co-authors. Steffen was the first to think of checking for differences in the non-radiative recombination of the two orientations! He did the TDCF and the temperature-dependent V_{OC} measurements, as well as repeated many of the measurements I did here for confidence (J-V, EQE, EL, radiative and non-radiative voltage losses, bias-dependent EQE).

Jack taught me how to do the TEM on H1 films, which are the images shown in this chapter. But Jack did all the FIB and coss-sectional TEM, which are very work- and time-intensive. Chris Takacs, who is also intimately familiar with H1, joined us at some of the TEM sessions when we were looking at the cross-section samples, and it is thanks to his proficiency over the TEM that we were able to resolve lattice planes in the cross-section TEM of the edge-on sample! I cannot stress how impressive this feat is, and how much luck and expertise it requires. Moreover, we did not only see lattice planes in the small imaged area shown here, with the help of a program Chris wrote, we were able to get a 'panorama' image of the entire cross-section sample (20 μm long). And even more moreover, we collected some higher-resolution TEM images that night, in which we can resolve the π-stacking of the H1 molecules! I hope these data will all be published soon in a manuscript that Chris is writing on the structural characterization of H1. Chris had also done some MD simulations, back calculating from TEM and GIWAXS spectra what the molecular packing of H1 must be. It is really thanks to Chris that we had such a good handle on the packing and morphology of H1 starting out.

Victoria Savikhin, in Mike Toney's group, did all the GIWAXS characterization of H1 to quantify the molecular orientation of the crystalline material, and the characterization of the interface quality in the H1/C_{60} bilayer samples. Yao-Tsung Fu, Hong Li, and Vaceslav (Slava) Coropceanu, in Jean-Luc Bréda's group were the team responsible for

the electronic-structure calculations, which they were able to get started on thanks to the MD simulations that Chris had done to get a starting point for the unit cell of H1. Xiaofen Liu is the one we have to thank for making a good batch of H1, which proved to be very difficult to synthesize well (leaving us with some H1 batches that are different from the characteristics we have measured thus far).

During the process of writing this paper, a few people really made a large impact. Once again, Gui had some really insightful comments on the structure and presentation of the story which upped the quality of the manuscript. Slava read the paper very carefully and debated with me about a few of the points I was making. He was even so kind to meet with me over skype and have a long discussion about these points until we were both in agreement. I really appreciate this time and the discussion, through which I even learned a good amount. Most of the co-authors of this paper took an active role in the writing of this paper, with really good comments form Steffen, Jack, Victoria, Chris, Slava, Jean-Luc, Gui, Mike, Dieter, and Quyen.

This chapter is the result of a collaborative effort by: myself, Steffen Roland, Dr. John Love, Victoria Savikhin, Dr. Chris Takacs, Dr. Yao-Tsung Fu, Dr. Hong Li, Dr. Veaceslav Coropceanu, Dr. Xiaofen Liu, Prof. Jean-Luc Brdas, Prof. Gui Bazan, Prof. Mike Toney, Prof. Dieter Neher, and Prof. Thuc-Quyen Nguyen.

3.2 Introduction

The efficiencies of charge generation and recombination at a donor acceptor heterojunction depend on parameters such as distance and molecular orientation of the donor and acceptor molecules at the interface. These processes dictate the performance of electronic devices such as light emitting diodes (LEDs), photodetectors, and photovoltaics. It is therefore critical to understand the properties of the donor/acceptor interface which

affect the efficiencies of charge generation and recombination. The properties of the donor/acceptor interface can be studied from the point of view of photovoltaics, with implications on the performance of other devices which depend on donor/acceptor interfaces.

A fundamental issue under much debate in the organic photovoltaic literature involves the geometry of the donor/acceptor interface: whether a *face-on* geometry (one where the π-faces of the donor and acceptor π-conjugated molecules or polymer chains are in parallel) is favorable compared to an *edge-on* geometry (where the π-faces are orthogonal). Theoretical calculations have long suggested that the nature of the donor-acceptor interface will have a large effect on the rates of charge transfer and recombination,[97, 98, 99] as well as charge delocalization.[99, 100] Other calculations have found that molecular orientation affects interfacial quadrupoles and consequently the ease of charge separation.[101, 102] A number of experimental researchers have attempted to resolve this question with the use of controlled donor and/or acceptor orientations in planar heterojunction solar cells.[97, 103, 104, 105, 106, 107, 108, 66, 109] In general, most studies have found that within the same material system, *face-on* solar cells have a superior power coversion efficiency (PCE) when compared to the *edge-on* orientation.[103, 110] This has been attributed primarily to changes in the donor ionization potential (IP) (or, to a first approximation, highest occupied molecular orbital (HOMO) energy level), which directly affects the open circuit voltage (V_{OC}),[103, 110, 104, 105, 107, 111, 112] but has also been explained by differences in recombination rates.[97, 103, 108, 110]

Despite significant efforts, it has remained very challenging to fabricate high-quality planar heterojunctions with identical active layers and contacts, but opposite molecular orientations. Most studies settle for comparisons between one orientation and a mixed orientation, or modified contacts to induce changes in orientation. Furthermore, it was demonstrated that molecular diffusion in planar heterojunctions can happen

spontaneously,[113] and to varying extents for different orientations.[114] Interfacial mixing will lead to unfair comparisons and erroneous conclusions if not properly taken into account. To date, experimental studies in which the effects of molecular orientation have truly been isolateda single materials system in which the two extremes of *face-on* and *edge-on* orientations can be accessed while maintaining abrupt donor/acceptor interfaces and identical contactshave not been reported.

In this work, we begin by establishing that we are able to precisely control molecular orientation of p-SIDT(FBTTh$_2$)$_2$[62] (structure shown in Figure 3.1a) in neat films, and fabricate bilayer heterojunctions with sharp, well-defined interfaces of known molecular orientations. We then analyze the photovoltaic performance, which reveals that molecular orientation has a profound effect on the V_{OC} and short-circuit current (J_{SC}). The higher V_{OC} of the solar cells with *face-on* p-SIDT(FBTTh$_2$)$_2$ is attributed to a higher charge transfer (CT) state energy (E_{CT}) and lower non-radiative recombination losses. However, the *edge-on* solar cells are more efficient at charge generation illustrated by a higher internal quantum efficiency (IQE). Electronic-structure calculations predict that the *face-on* bilayers have a larger electronic coupling between the CT state and ground state (GS), suggesting that they suffer from greater geminate recombination. In addition, charge generation in *face-on* bilayers is significantly more temperature-dependent than *edge-on* bilayers, which may be a consequence of a larger barrier to charge generation or favorable polarization at the *edge-on* donor/acceptor interface.

From the point of view of molecular orientation, our study addresses two topics that have been gaining significant attention in the literature: non-radiative recombination losses to the V_{OC},[99, 17, 19, 115, 34, 116, 117] and the driving force for charge generation.[118, 119, 120] It is thought that non-radiative recombination plays a significant role in efficiency losses in photovoltaics and LEDs, and it is only when non-radiative pathways have been eliminated that organic solar cells become competitive

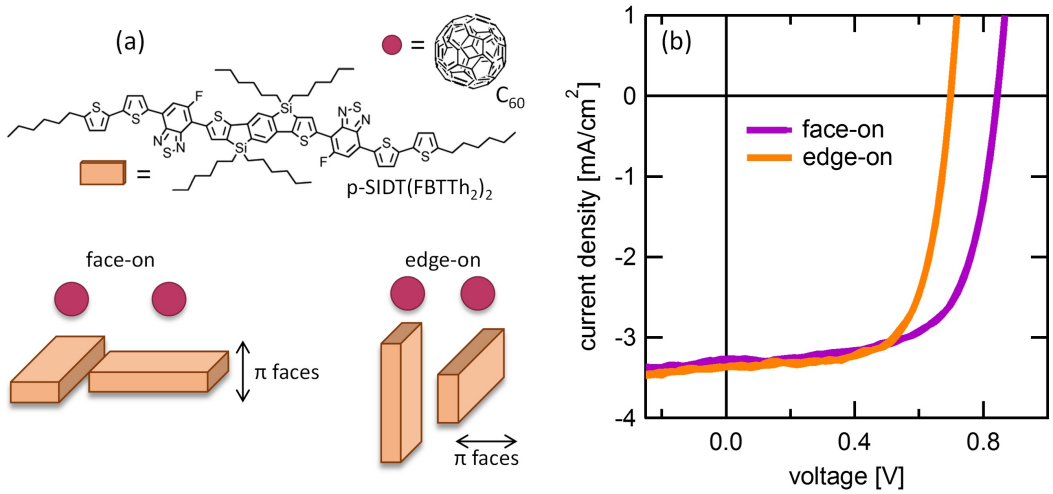

Figure 3.1: Molecular orientation and solar cell performance. (a) Molecular structures of p-SIDT(FBTTh$_2$)$_2$ and C$_{60}$; (b) J-V characteristics of bilayer devices under 1 sun illumination.

with high performance inorganic materials.[19, 34, 121, 122] A recent theoretical study by Chen *et al.* on pentacene/C$_{60}$ interfaces predicts that *face-on* interactions result in less non-radiative recombination, due to reduced vibronic coupling between the CT state and the GS.[99] To date, little is understood about the origin of non-radiative recombination in organic solar cells, how it relates to molecular orientation, or how to curtail this recombination pathway. Furthermore, the driving force for charge generation has remained a disputed topic in the literature, with researchers quoting the need for energetic offsets,[58, 47] hot charges,[51, 123] delocalization,[124, 57] low reorganization energies,[125] electric fields,[126, 127] energetic cascades and disorder,[128, 129] and entropy,[130, 118] to achieve efficient charge generation. Our study presents important experimental evidence pertaining to the effect of molecular orientation on non-radiative recombination and the efficiency of charge generation.

3.3 Structural characterization: molecular orientation and interface quality

To begin, films of neat p-SIDT(FBTTh$_2$)$_2$ were characterized to quantify bulk and interfacial molecular orientation. Preferential orientation can be measured using grazing incidence wide-angle x-ray scattering (GIWAXS), by comparing intensities of in-plane and out-of-plane π-stacking peaks (at q 1.7 -1). The amount of *face-on* vs. *edge-on* charcter is calculated from the anistropy of the π-stacking peak, as a function of the polar angle, χ, from the substrate plane, shown in Figure 3.2. The intensity must be corrected for solid angle effects using: $intensity \times |sin(\chi - 90)|$. While the signal from the GIWAXS scans originates only from the ordered portions of the films, both *face-on* and *edge-on* films are thin (45 nm) and significantly crystalline, justifying orientation assignment for the bulk films by crystalline scattering. When cast from chlorobenzene (CB), films of p-SIDT(FBTTh$_2$)$_2$ show a ratio of 99.5:0.5 *face-on*:*edge-on* orientation. When cast from CB with 0.4% v/v diiodooctane (DIO), films of p-SIDT(FBTTh$_2$)$_2$ show a ratio of 94:6 *edge-on*:*face-on* orientation. The two orientations also have distinctly different structures seen by high-resolution transmission electron microscope (HR-TEM) images. Figure 3.3 show HR-TEM and GIWAXS images of p-SIDT(FBTTh$_2$)$_2$ films cast from CB (*face-on*) and CB+DIO (*edge-on*).

The quality of the p-SIDT(FBTTh$_2$)$_2$ interface was verified by cross-section HR-TEM and GIWAXS. The miscibility of C_{60} into p-SIDT(FBTTh$_2$)$_2$ was determined by monitoring the GIWAXS signal of varying thicknesses of C_{60} evaporated on p-SIDT(FBTTh$_2$)$_2$ (Figure 3.4). A linear increase in C_{60} scattering intensity with C_{60} thickness indicates that C_{60} molecules are not diffusing into the p-SIDT(BFTTh2)2 layer beneath. Figure 3.5c shows a linear signal growth with C_{60} thickness for the *face-on* device, confirming that the interface is sharp. The trace for the *edge-on* device, Figure 3.5d, shows a

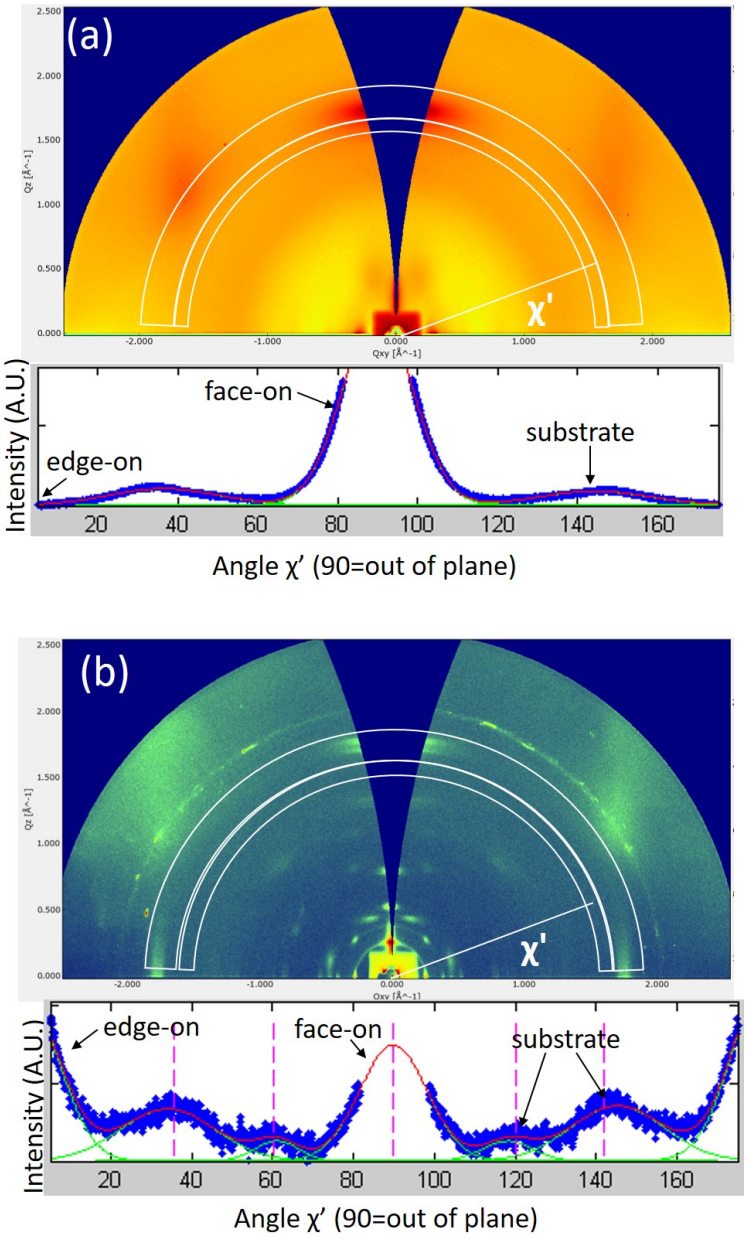

Figure 3.2: Quantifying the molecular orientation in p-SIDT(FBTTh$_2$)$_2$ films. GI-WAXS of p-SIDT(FBTTh$_2$)$_2$ cast from (a)chlorobenzene or from (b) chlorobenzene with 0.4% w/w diiodooctane.

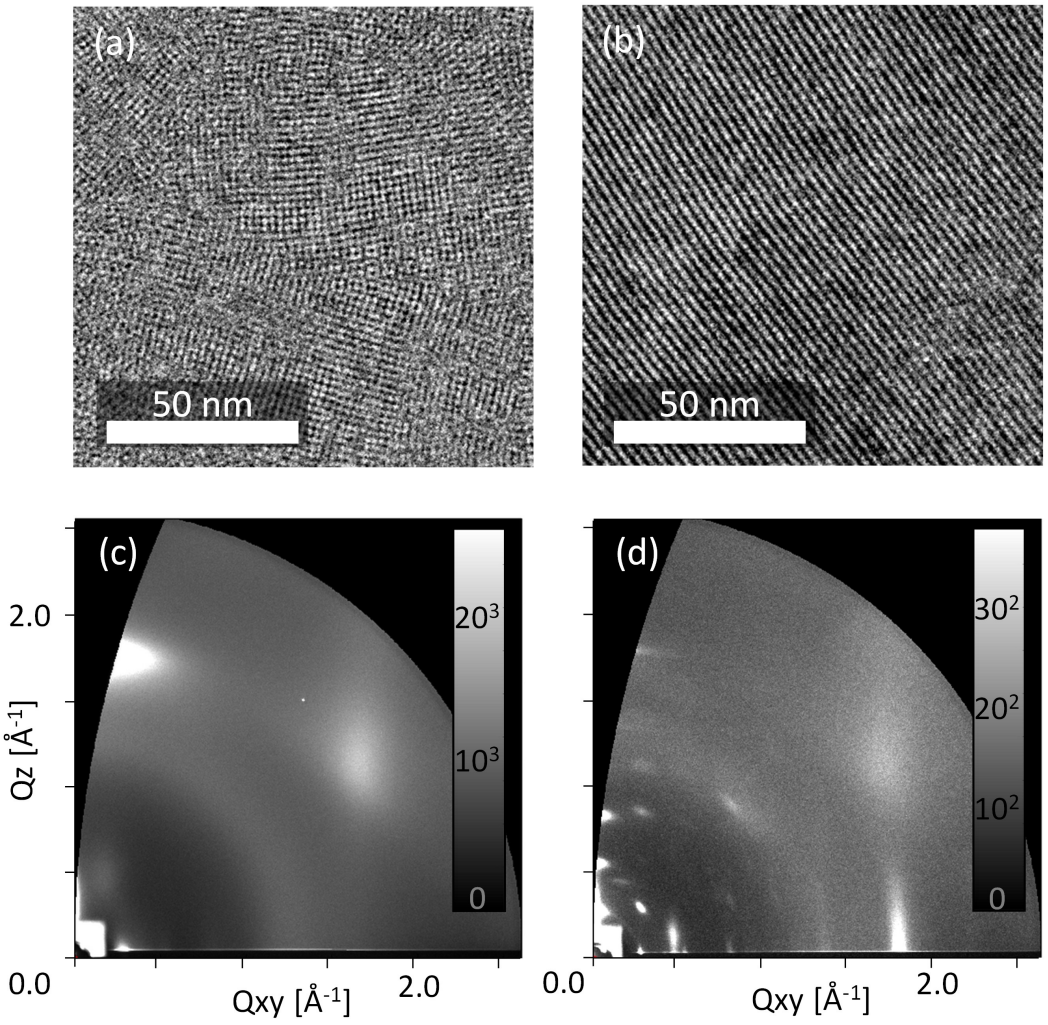

Figure 3.3: HR-TEM images (a,b) and GIWAXS spectra (c,d) of *face-on* (a,c) and *edge-on* (b,d) p-SIDT(FBTTh$_2$)$_2$ films used to characterize molecular orientation.

slight deviation from linearity at small amounts of C_{60}. However, this can be explained by deposition of C_{60} into pinholes in the *edge-on* p-SIDT(FBTTh$_2$)$_2$ film which are not present in the *face-on* film (Figure 3.6). In addition to reducing the actual film thickness from the nominal predicted film thickness, the surface topography presented by pinholes may have an unpredictable effect on the X-ray scattering. Cross-section TEM (Figure 3.5a,b) shows no evidence of interdiffusion for either *face-on* or *edge-on* bilayers. In fact, lattice planes can be well resolved in the cross-section TEM of the *edge-on* sample for the entire thickness of the p-SIDT(FBTTh$_2$)$_2$ layer (Figure 3.5b). The lattice planes further confirm that the donor layers retain their orientation through the bulk of the film to the interface with C_{60}, and that deposition of the C_{60} layer does not disrupt the packing of p-SIDT(FBTTh$_2$)$_2$. Thus, it can be concluded that the donor/acceptor interface is abrupt for *edge-on* and *face-on* p-SIDT(FBTTh$_2$)$_2$.

3.4 Solar cell characteristics as a function of molecular orientation

The *J-V* characteristics of the *edge-on* and *face-on* bilayers, using identical contacts (ITO/PEDOT:PSS/active layer/BCP/Al), under 1 sun illumination, are presented in Figure 3.1b and Table 3.1. The J_{SC} and the *FF* are very similar for both molecular orientations of the donor layer. The V_{OC}, on the other hand, is a substantial 150 mV larger when the donor molecules are *face-on* compared to *edge-on*.

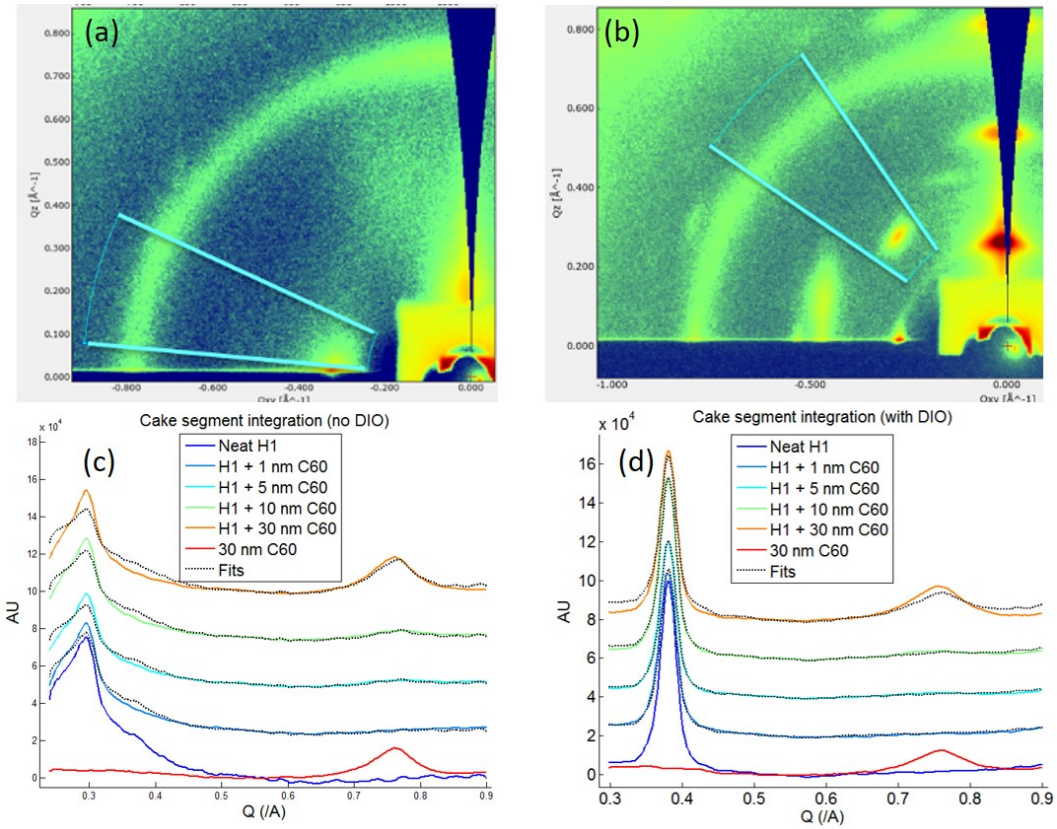

Figure 3.4: GIWAXS of face-on (a) and edge-on (b)p-SIDT(FBTTh$_2$)$_2$ with C_{60} evaporated on top, showing signal for p-SIDT(FBTTh$_2$)$_2$ and C_{60}. The cake slices in (a) and (b) show where the signal for p-SIDT(FBTTh$_2$)$_2$ and C_{60} was fit for the two samples. (c,d) show the scattered intensity for *face-on* and *edge-on* p-SIDT(FBTTh$_2$)$_2$, respectively, with varying thicknesses of evaporated C_{60}, as a function of q, which were used to generate Figures 3.5c,d.

Table 3.1: Solar cell characteristics of p-SIDT(FBTTh$_2$)$_2$/C_{60} devices with *face-on* or *edge-on* donor molecular orientation.

	V_{OC} [V]	J_{SC} [mA/cm^2]	*FF* [%]
Face-on	0.84±0.03	-2.97±0.3	66±5
Edge-on	0.69±0.04	-3.03±0.4	68±3

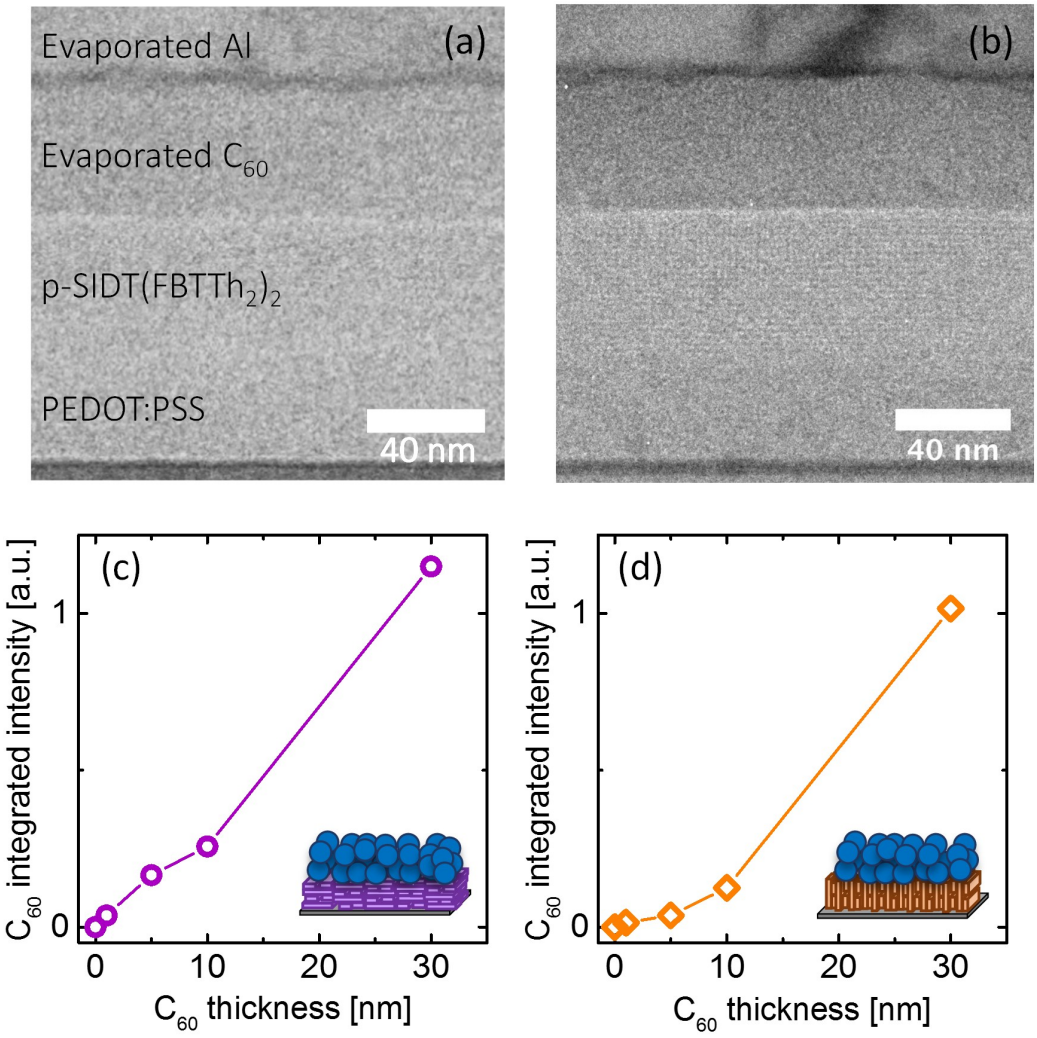

Figure 3.5: Cross-section HR-TEM of (a) *face-on* and (b) *edge-on* bilayers. Correlation of peak intensity fitting with C_{60} thickness evaporated on films of p-SIDT(FBTTh$_2$)$_2$ for (c) *face-on* and (d) *edge-on* samples.

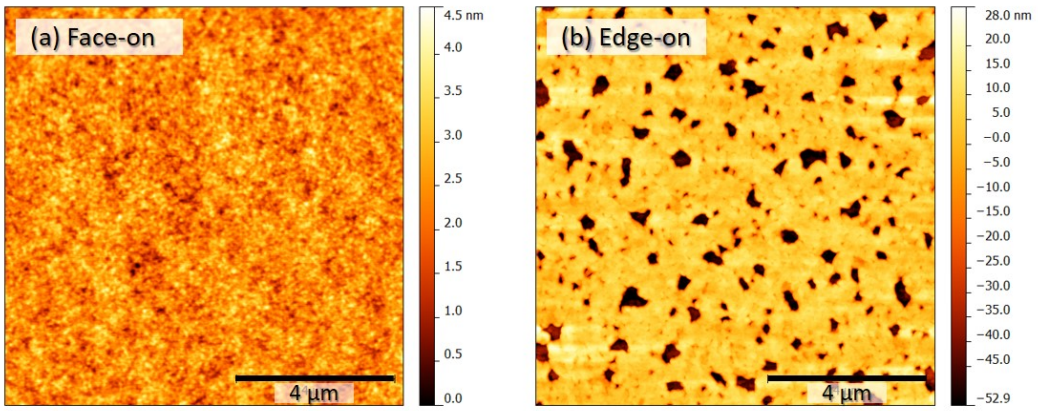

Figure 3.6: AFM images for (a)*face-on* and (b)*edge-on* p-SIDT(FBTTh$_2$)$_2$ films.

3.5 Open circuit voltage: E_{CT} and non-radiative recombination

There are several factors that can account for the change in the V_{OC}, and we will explore each in turn: IP and E_{CT}, radiative recombination, and non-radiative recombination.

A number of studies have demonstrated that changing molecular orientation in a film can lead to differences in the material energy levels,[103, 104, 105, 107, 111, 112] which can have a direct effect on the V_{OC}. Indeed, ultraviolet photoelectron spectroscopy (UPS) measurements of p-SIDT(FBTTh$_2$)$_2$ films show an increase on the order of 60 meV in the IP of p-SIDT(FBTTh$_2$)$_2$ when it is *face-on* (Figure 3.7). In good agreement, electronic-structure calculations performed on p-SIDT(FBTTh$_2$)$_2$ also found that the *face-on* orientation has a deeper work function (Figure 3.8). However, as the V_{OC} varies by 150 mV, changing the molecular orientation has altered more than just the IP value.

It has been demonstrated numerous times that E_{CT} and V_{OC} tend to correlate according to: E_{CT} qV_{OC} = 0.6±0.1 eV.[19, 34] The CT state is routinely studied with

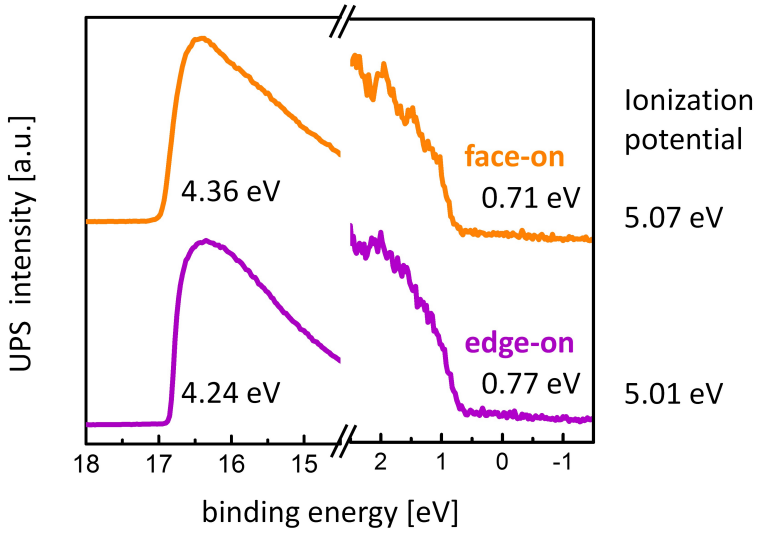

Figure 3.7: UPS measurements of *face-on* and *edge-on* p-SIDT(FBTTh$_2$)$_2$ films.

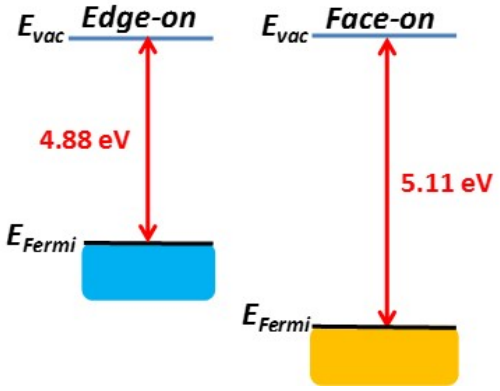

Figure 3.8: Work function (evaluated from the vacuum level to the top valence bands) of *edge-on* (left) and *face-on* (right) p-SIDT(FBTTh$_2$)$_2$ slabs, estimated at the DFT/HSE level.

highly sensitive absorption techniques (here, we use external quantum efficiency, EQE), where it is identified as a shoulder at sub-bandgap energies.[18] The CT state can also be studied by emission spectra (here we use electroluminescence, EL), where it is identified as a featureless emission spectrum at low energies.[24] The E_{CT}, defined as the midpoint between absorption and emission of the CT state, can be determined by a simultaneous fit to the measured absorption (Equation 4.1) and emission spectra (Equation 4.2):[29]

$$\sigma(E) = \frac{f}{E\sqrt{4\pi\lambda kT}} exp(\frac{-(E_{CT} + \lambda - E)^2}{4\lambda kT}) \tag{3.1}$$

$$I(E) = \frac{Ef}{\sqrt{4\pi\lambda kT}} exp(\frac{-(E_{CT} - \lambda - E)^2}{4\lambda kT}) \tag{3.2}$$

In these equations, k denotes Boltzmanns constant; T, temperature; and E, photon energy. The fit parameters are E_{CT} (energy of the CT state), λ (reorganization energy), and f (a parameter proportional to the number of CT states and the square of their coupling matrix element with the GS). Using Equations 4.1 and 4.2, fit simultaneously to the EQE and EL spectra, we obtain that E_{CT} is 1.38±0.02 eV when p-SIDT(FBTTh$_2$)$_2$ is *face-on* vs. 1.32±0.03 eV for the *edge-on* orientation. The EQE, EL and their corresponding fits are shown in Figure 4.8a-b. The 60 meV higher E_{CT} is in excellent agreement with the higher ionization energy of the *face-on* p-SIDT(FBTTh$_2$)$_2$ layer, implying vacuum alignment at the interface to C$_{60}$. However, it does not explain the full difference in V_{OC} upon changing molecular orientation.

Another estimate for the E_{CT} can be obtained by temperature-dependent V_{OC} measurements extrapolated to 0 K,[29, 30] where the deviation from E_{CT} to V_{OC} at room temperature (RT) should correlate with losses in the solar cell. One model that has been demonstrated on a number of systems separates the losses from E_{CT} into radiative and

non-radiative recombination, shown in Equation 3.3:[29]

$$V_{OC}(T) = \frac{E_{CT}}{q} - \Delta V_{rad}(T) - \Delta V_{nonrad}(T) \tag{3.3}$$

With $\Delta V_{rad}(T)$ and $\Delta V_{nonrad}(T)$ the temperature-dependent radiative and non-radiative recombination losses given by Equations 3.4,3.5:

$$\Delta V_{rad}(T) = -\frac{kT}{q} ln(\frac{J_{SC} h^3 c^2}{f q 2\pi (E_{CT} - \lambda)}) \tag{3.4}$$

$$\Delta V_{nonrad}(T) = -\frac{kT}{q} ln(EQE_{EL}) \tag{3.5}$$

In these equation, J_{SC} represents the short circuit current; h, Plancks constant; c, speed of light; E_{CT}, f, λ are fit parameters from Equations 1, 2 (Figure 3a,b); and EQE_{EL} is the total external quantum efficiency of electroluminescence.

The V_{OC} values of each bilayer were measured at different light intensities and temperatures ranging from 190 K to 310 K, and extrapolated to 0 K, as shown in Figure 4.8c. For all light intensities the V_{OC} extrapolated to 0 K is 1.40±0.02 V for the *face-on* compared to 1.31±0.02 V for the *edge-on* solar cells, which is in close agreement to the E_{CT} values obtained from the fits of the EQE and EL spectra. This confirms our interpretation from above that the difference in V_{OC} is not solely due to energetics. In fact, from the temperature-dependent slopes in Figure 4.8c, it is evident that the overall V_{OC} loss is smaller in *face-on* than in *edge-on* bilayers.

As shown by Equation 3.3, the voltage loss can be quantified into radiative and non-radiative recombination contributions, as has been outlined by Rau30 and Vandewal *et al.*.[29] Radiative recombination can be estimated according to Equation 3.4. We find that at room temperature ΔV_{rad} is very similar, 199±2 mV and 197±4 mV for the *face-*

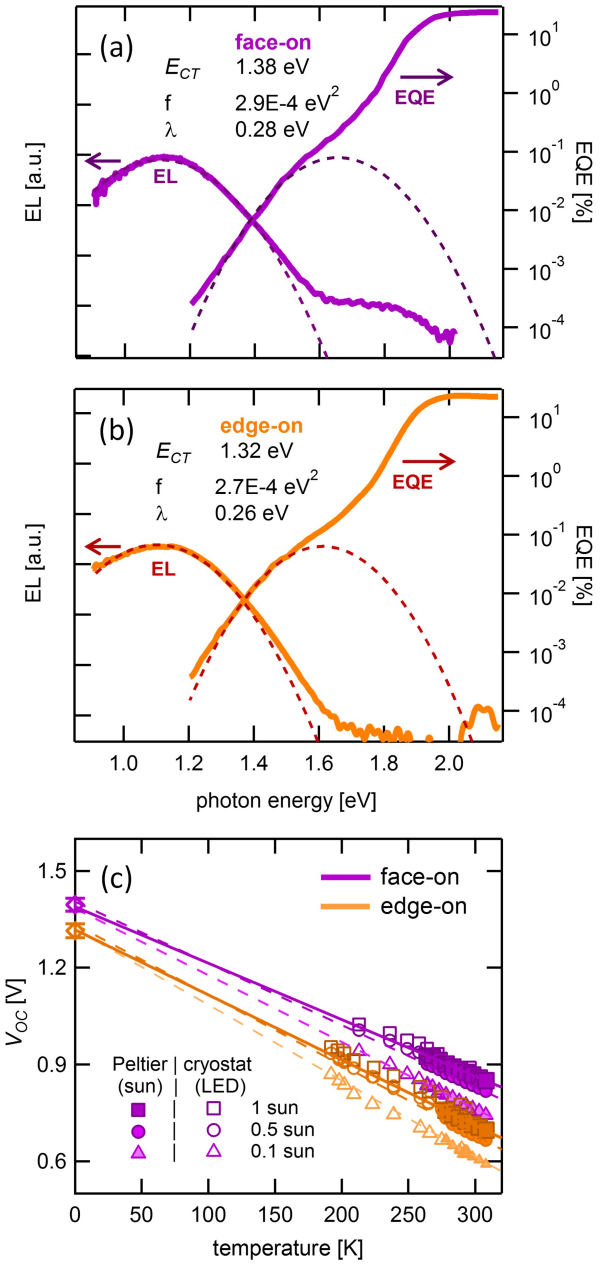

Figure 3.9: Characterization of the CT state in the bilayers. (a,b) EQE spectra of the sub-bandgap absorption and the corresponding EL spectra for *face-on* (a) and *edge-on* (b) bilayers. Dashed lines are fits to the EQE using Equations 4.1,4.2. Fit parameters are reported in the figures. (c) Temperature-dependent V_{OC} at 1, 0.5 and 0.1 suns, extrapolated to 0 K represented on the axis with the corresponding standard deviations.

Table 3.2: Summary of E_{CT} and recombination voltage losses for the bilayer solar cells.

	E_{CT} [eV]	Radiative loss [mV]	Non-radiative loss [mV]	$V_{OC,calc}$ [V]	$V_{OC,exp}$ [V]
Face-on	1.38±0.02	199±2	316±10	0.87	0.84±0.03
Edge-on	1.32±0.03	197±4	382±28	0.74	0.69±0.04

on and *edge-on* bilayers, respectively, leading to the important conclusion that losses due to radiative recombination are not a function of molecular orientation.

Non-radiative recombination remains poorly understood, yet it is considered to be among the primary reasons that the overall V_{OC} loss has not decreased significantly in recent years.[34] Most organic blends reported in the literature lose 300-400 mV to non-radiative recombination, constituting 60% or more of the lost potential.[34, 29] To estimate the effect of orientation on non-radiative recombination, we refer to EQE_{EL}, defined as photons emitted per electrons injected into the device. The lower the radiative efficiency, the more non-radiative decay channels contribute to the overall recombination. Equation 3.5 relates EQE_{EL} to the voltage loss.

Importantly, the measured EQE_{EL} values differ by more than an order of magnitude between the two samples, with $3.2\times10^{-6}\pm1.4\times10^{-6}$ for the *face-on* and $2.3\times10^{-7}\pm3.5\times10^{-7}$ for the *edge-on* bilayers. Using Equation 3.5, we find that voltage losses due to non-radiative recombination are 316±10 mV and 382±28 mV for the *face-on* and *edge-on* solar cells, respectively.

Table 3.2 summarizes the energetic and recombination differences between the bilayers with the two orientations. The estimated differences in ΔV_{OC},calc values calculated from E_{CT}, and corrected for losses due to radiative and non-radiative recombinations are in very good agreement with the measured ΔV_{OC}.

The significance of these findings lies in the differences in non-radiative recombination:

on average, the *edge-on* solar cells lose 66 mV more voltage than *face-on* cells due to non-radiative recombination. Using the same system but flipping the donor molecular orientation, the non-radiative recombination pathway has been altered, implying it is sensitive to the molecular alignment at the donor/acceptor interface. Interestingly, these experimental results are fully consistent with a recent theoretical study: Chen *et al.*[99] found that the higher E_{CT} value and greater hole delocalization and migration away from a *face-on* pentacene/C_{60} interface caused a decrease in vibronic coupling of the CT state to the GS, thus reducing the non-radiative recombination rate. While the results by Chen *et al.*[99] refer to model molecular packings of pentacene, the similarity to our findings on p-SIDT(FBTTh$_2$)$_2$/C_{60}, namely a smaller E_{CT} and more non-radiative recombination in the *edge-on* bilayers, is striking.

3.6 Short circuit current: electronic coupling and charge generation barriers

In contrast to the V_{OC}, the J_{SC} appears independent of molecular orientation (Figure 3.1). However, due to alignment of the molecular transition dipoles, the absorption strength of the two bilayers toward normal incident light is significantly different: *face-on* p-SIDT(FBTTh$_2$)$_2$ films have a two times higher absorbance as *edge-on* films (Figure 4.2). The similar J_{SC} values are in agreement with the EQE (quantum efficiency per *incident* photons) of the bilayers, both peaking at about 25% on average. However, when the EQE spectra are corrected for absorption of the active layer (device absorption corrected for parasitic absorption, more detail in Figure 3.11), we obtain quantum efficiency spectra per *absorbed* photons, i.e. internal quantum efficiency (IQE). EQE and IQE spectra of the bilayers are shown in Figure 3.12a. For reference, the unitless absorption spectra of

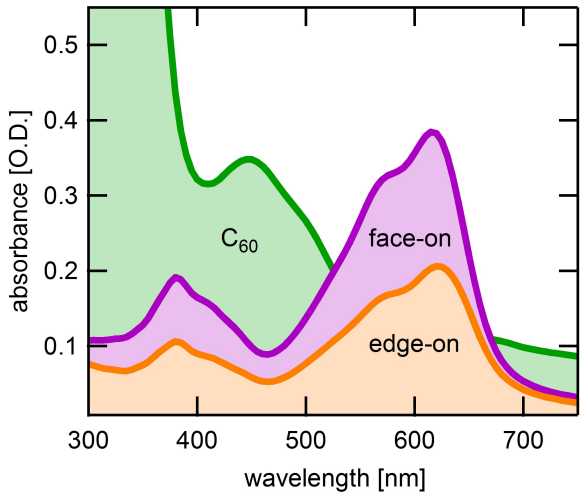

Figure 3.10: Absorption spectra of neat C_{60}, *face-on* and *edge-on* p-SIDT(FBTTh$_2$)$_2$ films.

p-SIDT(FBTTh$_2$)$_2$ and C_{60} are shown in the background.

IQE of the *edge-on* bilayers is higher than the *face-on* bilayers (Figure 3.12). This indicates that in *edge-on* bilayers fewer excitons and charges recombine at short circuit. In other words, the *edge-on* solar cells have more efficient charge generation. This finding is consistent with the results of our electronic-structure calculations, which indicate that electronic coupling between CT state and GS is weaker in the *edge-on* configuration than in the *face-on* configuration (Figure 3.13). A smaller electronic coupling is expected to decrease the rate of geminate recombination as the CT state tends to dissociate, shifting the generation-recombination balance towards free charge formation, as seen here.[98]

For a deeper understanding of the differences in IQE, we measured the EQE under varying electric fields and temperatures. These measurements are complex, since they reflect the combination of many processes such as exciton diffusion, charge transfer, charge generation, bimolecular recombination, and charge transport. However, with the appropriate conditions and analysis, EQE measurements can be used to gain insight into charge generation/geminate recombination. Specifically, to eliminate effects of exciton diffusion

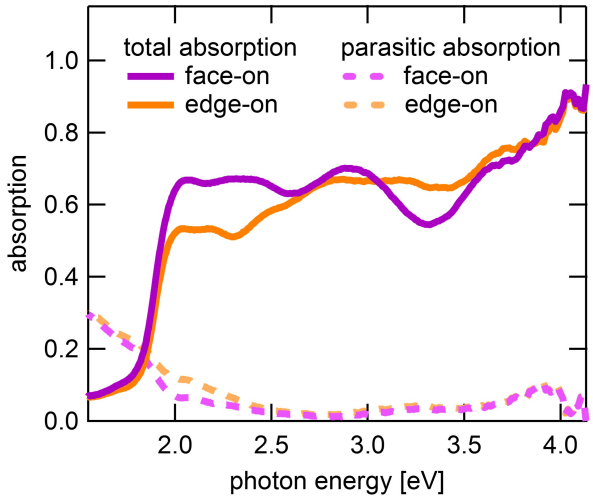

Figure 3.11: Total absorption, as measured with an integrating sphere, corrected for by parasitic absorption calculated using transfer matrix modeling. To calculate the parasitic absorption we used the Matlab program written by Burkhard *et al.* For more detail, see [131].

and charge transfer, EQE spectra can be analyzed at energies corresponding to CT state absorption. Also, since these devices are bilayers and the measurements are carried out at low light intensities and under an internal field (J_{SC} conditions, unless otherwise stated), bimolecular recombination is expected to be negligible. Under these conditions, our EQE measurements should reflect the dependence of charge generation/geminate recombination on electric field and temperature.

First, we asked if changing interfacial molecular orientation has an impact on the Coulomb binding energy of the CT state. The binding energy, a consequence of the electrostatic attraction between opposite charge carriers, depends on the electron-hole separation and the dielectric constant.[132] The binding energy can be overcome with the assistance of a field,[126, 133] and thus it may follow that the field-dependence of generation would be different for the two bilayers.[134] Figure 3.12b shows the effect of an electric field on the EQE of *face-on*/*edge-on* devices: both have a very similar dependence on the electric field. The EQE values in Figure 3.12b are normalized to the

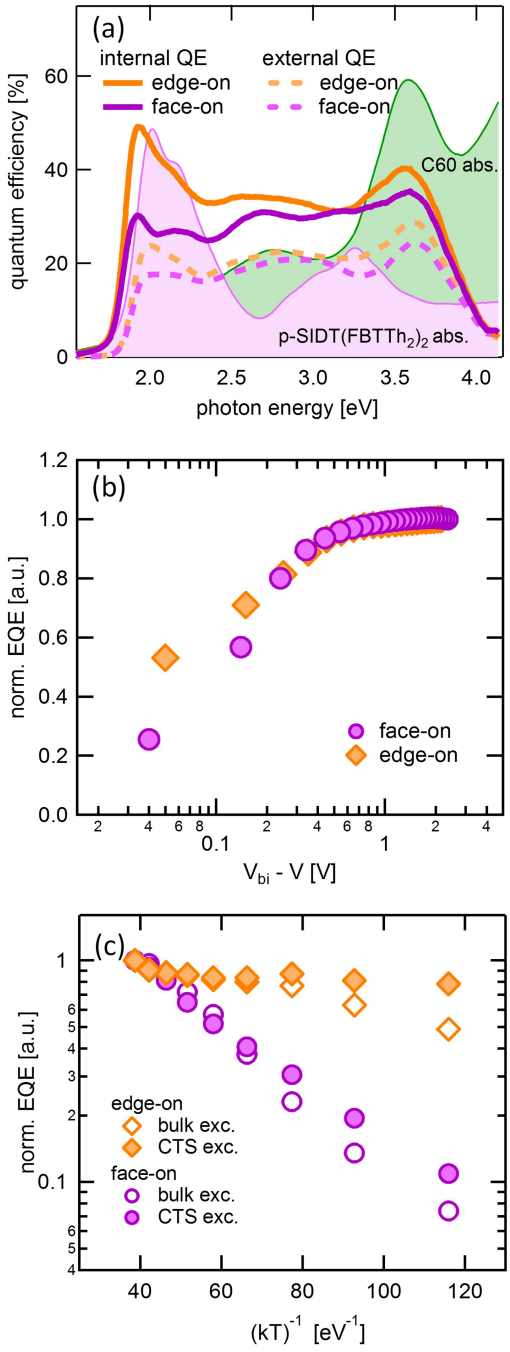

Figure 3.12: Efficiency of charge generation. (a) EQE (dashed lines) and IQE (continuous lines) spectra of bilayer solar cells with varying orientation. The absorption spectra of p-SIDT(FBTTh$_2$)$_2$ and C_{60} are plotted in the background for reference. (b) Bias-dependent EQE values corresponding to p-SIDT(FBTTh$_2$)$_2$ absorption, integrated and normalized to the value under the highest field. Bias was corrected for the built-in potential. (c) Temperature-dependent EQE values, integrated and normalized. Open symbols are EQE values integrated over bulk absorption, and full symbols are EQE values integrated only for CT state absorption.

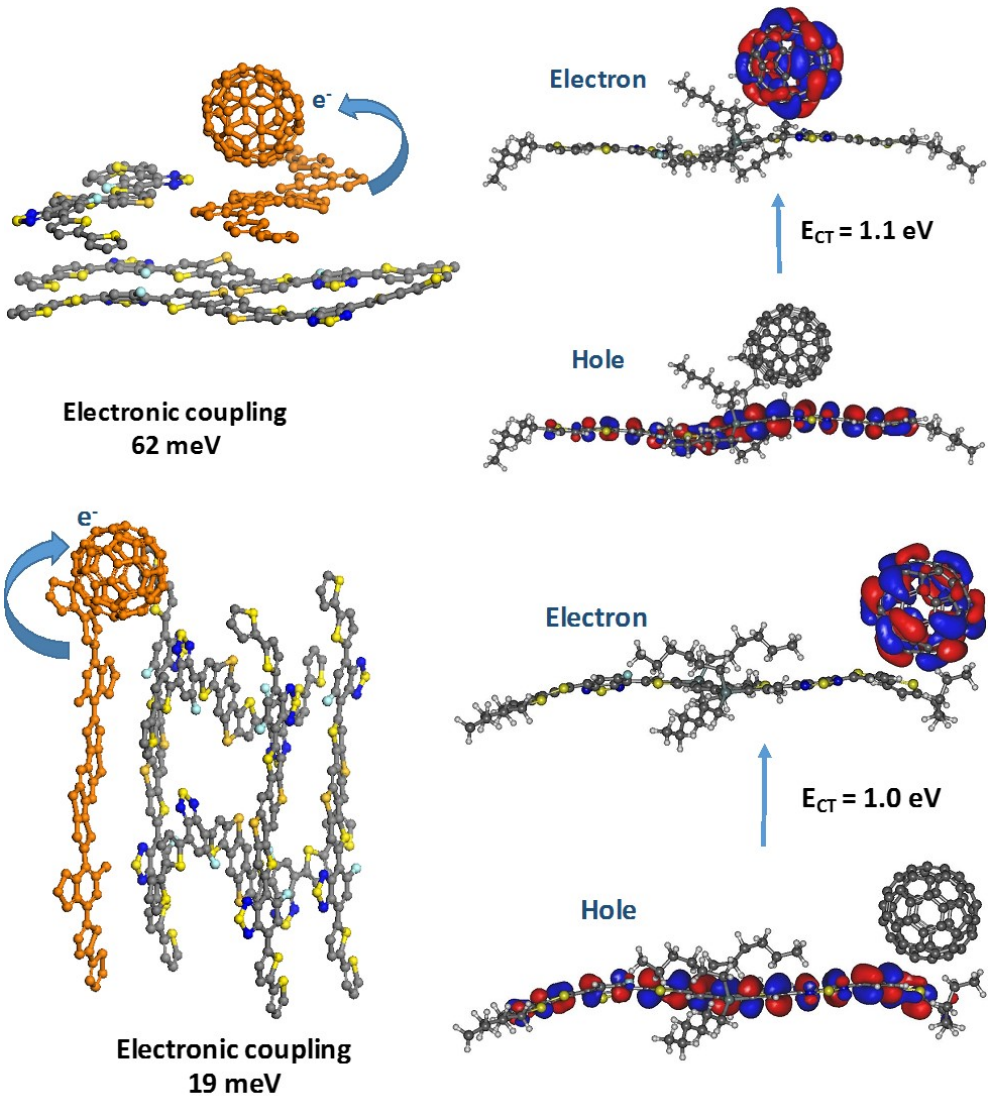

Figure 3.13: Electronic coupling between the lowest CT state and the ground state in p-SIDT(FBTTh$_2$)$_2$/C$_{60}$. Illustration of the *face-on* (top) or *edge-on* (bottom) p-SIDT(FBTTh$_2$)$_2$/C$_{60}$ configurations that exhibit the largest electronic couplings between the lowest CT state and the ground state. Left: Donor and acceptor molecules used in the calculations. Right: Natural transition orbitals describing the charge transfer states.

efficiency at the strongest applied bias, and the field across the device is corrected by the built-in voltage, analogous to photocurrent analysis. The unnormalized bias-dependent EQE spectra, are shown in Figure 3.14. Time Delayed Collection Field (TDCF) measurements confirm no significant differences in the field dependence of generation between the two orientations (Figure 3.15). Furthermore, by TDCF there is no difference in field-dependence of generation for excitations at 350 nm, 600 nm, or 650 nm, ruling out any effects of hot-exciton generation. . All these results indicate that the binding energy of the CT state is not a function of molecular orientation.

Bias-dependent EQE. EQE spectra collected under bias ranging from VOC to -1.5 V. In the background are unitless absorption spectra of p-SIDT(FBTTh2)2 and C60 for reference.

Next, we turned our attention to the temperature-dependence of charge generation. Figure 3.12c shows EQE values normalized to the EQE at RT, as a function of temperature. For temperature-dependent EQE spectra, see Figure 5.7. The temperature dependence is shown for absorption over all energies, as well as absorption corresponding only to the CT state (1.2-1.5 eV). Overall, while charge generation in both bilayers is temperature-dependent, the temperature-dependence in the *face-on* bilayers is much stronger, indicating a larger activation energy for charge generation. To illustrate this point, if we make crude simplifications and extrapolate the EQE values to the limit of temperature$\rightarrow$0 K, we find that generation in the *face-on* bilayer becomes negligible, while the *edge-on* bilayer can still generate about 10-40% carriers (as compared to carrier generation at RT). Charge generation resulting from bulk and direct CT state excitations follows similar temperature dependences, as a function of p-SIDT(FBTTh$_2$)$_2$ orientation. The contrast in temperature dependence is therefore not due to differences in exciton diffusion or electron transfer, but is instead a function of interfacial molecular orientation. This can be explained by a larger barrier to charge generation in the *face-on*

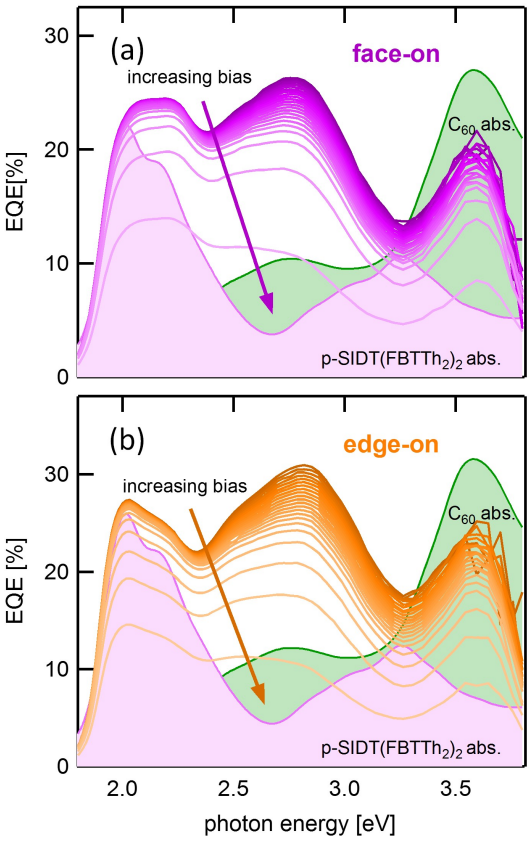

Figure 3.14: EQE spectra collected under an applied bias, ranging from V_{OC} to -1.5 V. Untiless absorption spectra of p-SIDT(FBTTh$_2$)$_2$ and C_{60} are shown in the background for reference.

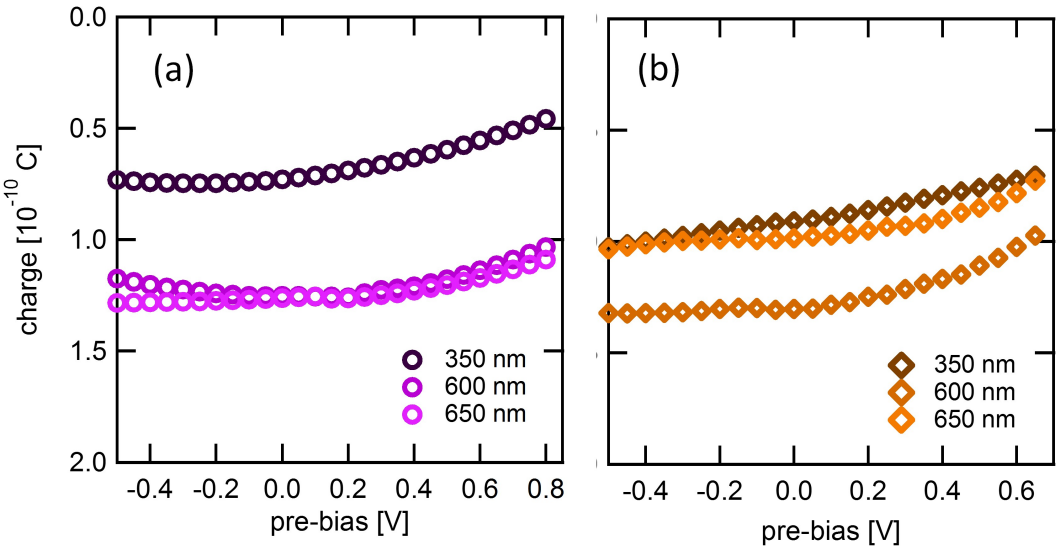

Figure 3.15: TDCF measurements of (a) *face-on* and (b) *edge-on* bilayers excited at varying wavelengths.

bilayer due to elements such as electronic coupling between the CT states and separated states or polarization at the donor/acceptor interface.

3.7 Conclusions and outlook

In conclusion, we have been able to fabricate donor-acceptor bilayers with sharp interfaces and well-defined p-SIDT(FBTTh$_2$)$_2$ molecular orientations: either *face-on* or *edge-on* with respect to the substrate. These orientations are preserved through the donor film to the interface with C_{60}, with none-to-minimal diffusion at the donor/acceptor interface. This unprecedented precise morphological control reveals the genuine effects of molecular orientation on photovoltaic performance. Edge-on p-SIDT(FBTTh$_2$)$_2$ bilayers suffer from greater non-radiative recombination and a reduced E_{CT}, which result in a substantial V_{OC} loss of 150 mV. However, charge generation is more efficient when the donor/acceptor interface is *edge-on*, evidenced by a higher IQE. This is attributed to

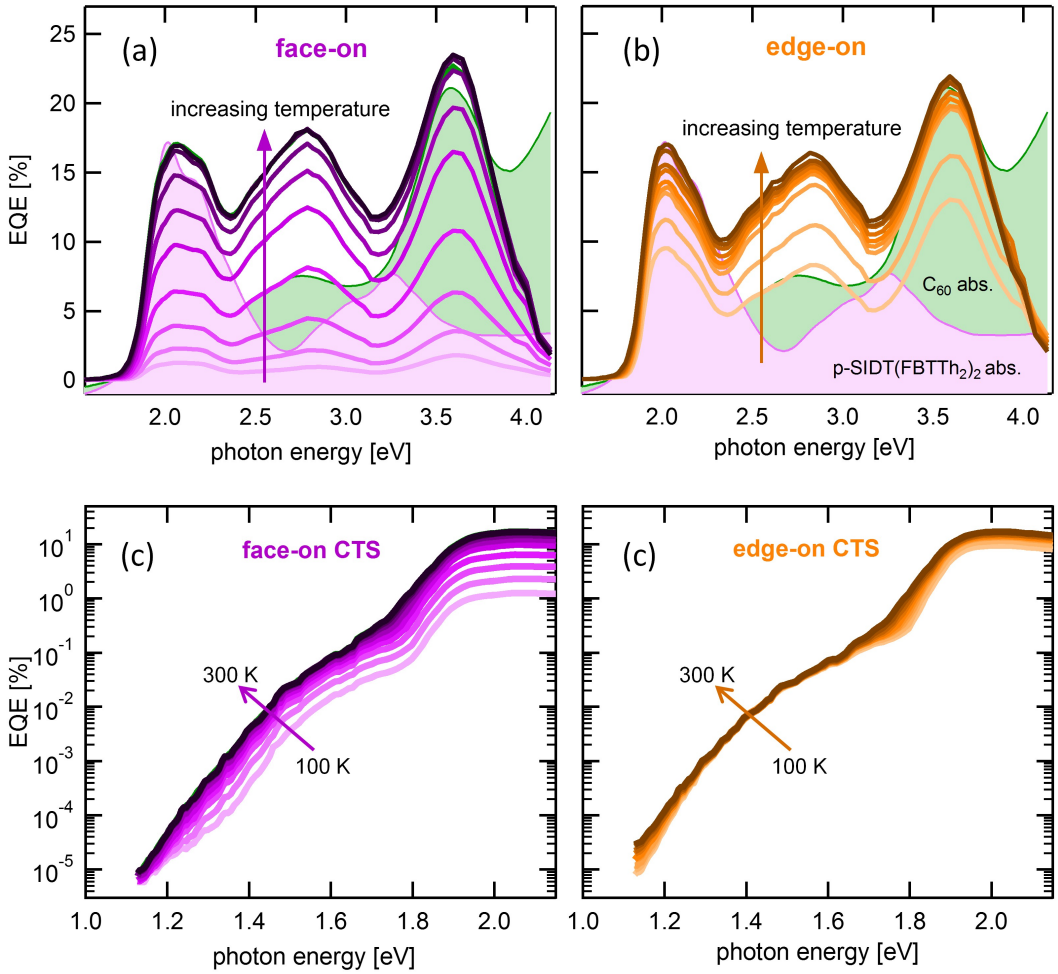

Figure 3.16: EQE spectra collected at varying temperatures ranging from 300 K to 100 K. In the background of (a,b) are unitless absorption spectra of p-SIDT(FBTTh$_2$)$_2$ and C_{60} for reference. (a,b) are the linear EQE spectra over the whole absorption spectrum for face-on and edge-on bilayers, respectively. (c,d) are the EQE spectra on a log-lin scale, at energies corresponding to CTS absorption for the face-on and edge-on bilayers, respectively.

reduced CT state-GS electronic coupling as well as smaller activation energy for charge generation in the *edge-on* bilayer, which may be a consequence of a reduced barrier between CT state and separated states or favorable polarization at the donor/acceptor interface.

The lessons learned from p-SIDT(FBTTh$_2$)$_2$/C$_{60}$ bilayers can be summarized into two major points:

1) In applications which benefit from high radiative efficiency (such as LEDs and OPVs), interfacial molecular orientation should reduce non-radiative recombination (by reducing charge recombination through triplet states or through vibronic coupling of the CT state to the GS). Our results establish that *face-on* molecular orientations would achieve higher radiative efficiency.

2) In applications where charge separation is important (such as photodetectors and OPVs), the electronic couplings between the CT state and the GS, as well as the activation energy for charge generation should both be minimized. This can perhaps be accomplished by beneficial polarization effects. This could be favored by beneficial polarization effects. Thus, our results determine that interfacial molecular orientation should be *edge-on* for intrinsic, efficient charge generation.

Overall, in the case of OPV, these two lessons go in opposite directions. These results highlight that to achieve high performance in OPV, the electronic coupling for *face-on* donor/acceptor interactions must be reduced to eliminate geminate recombination. Conversely, more research on non-radiative recombination is necessary in order to curtail the resulting losses to benefit from the improved charge generation in an *edge-on* donor/acceptor interaction. It may be possible to tackle both problems from the perspectives of molecular design and clever device engineering.

3.8 A few more interesting notes and unanswered questions

3.8.1 Singlet emission

Among the first findings when we first started studying the effect of molecular orientation was that when the bilayers are forward biased, the *face-on* bilayer has p-SIDT(FBTTh$_2$)$_2$ singlet emission in the EL, while EL from the *edge-on* is only at energies of the CT state for all applied voltages, as is shown in Figure 3.17a. We still do not underatnd why and how it is possible to observe singlet emission at very low applied voltages (much lower than the energy of emission), but the difference due to molecular orientation can give us some clues. First, this suggests that perhaps also in in the BHJ device the singlet EL that is observed originates from *face-on* p-SIDT(FBTTh$_2$)$_2$:C$_{60}$ interfaces (Figure 3.17b). The dependence of the singlet emission on molecular orientation may be explained by anisotropy in exciton diffusion. If excitons traverse along the π-stacking direction, it may be that even if an electron were to transfer to the p-SIDT(FBTTh$_2$)$_2$ LUMO and form an excited singlet state with a hole in the *edge-on* configuration, that the exciton would isotropically travel along the interface (along the $\pi - \pi$ stacking direction, where it would have a high probability of transferring the electron back to the CT state and recombine through the CT state. In contrast, if the same were to happen in the *face-on* configuration, and the exciton traveled along the $\pi - \pi$ stacking direction, it would travel away from the interface and thus have a lower probability to undergo electron transfer, and recombine through the p-SIDT(FBTTh$_2$)$_2$ singlet state.

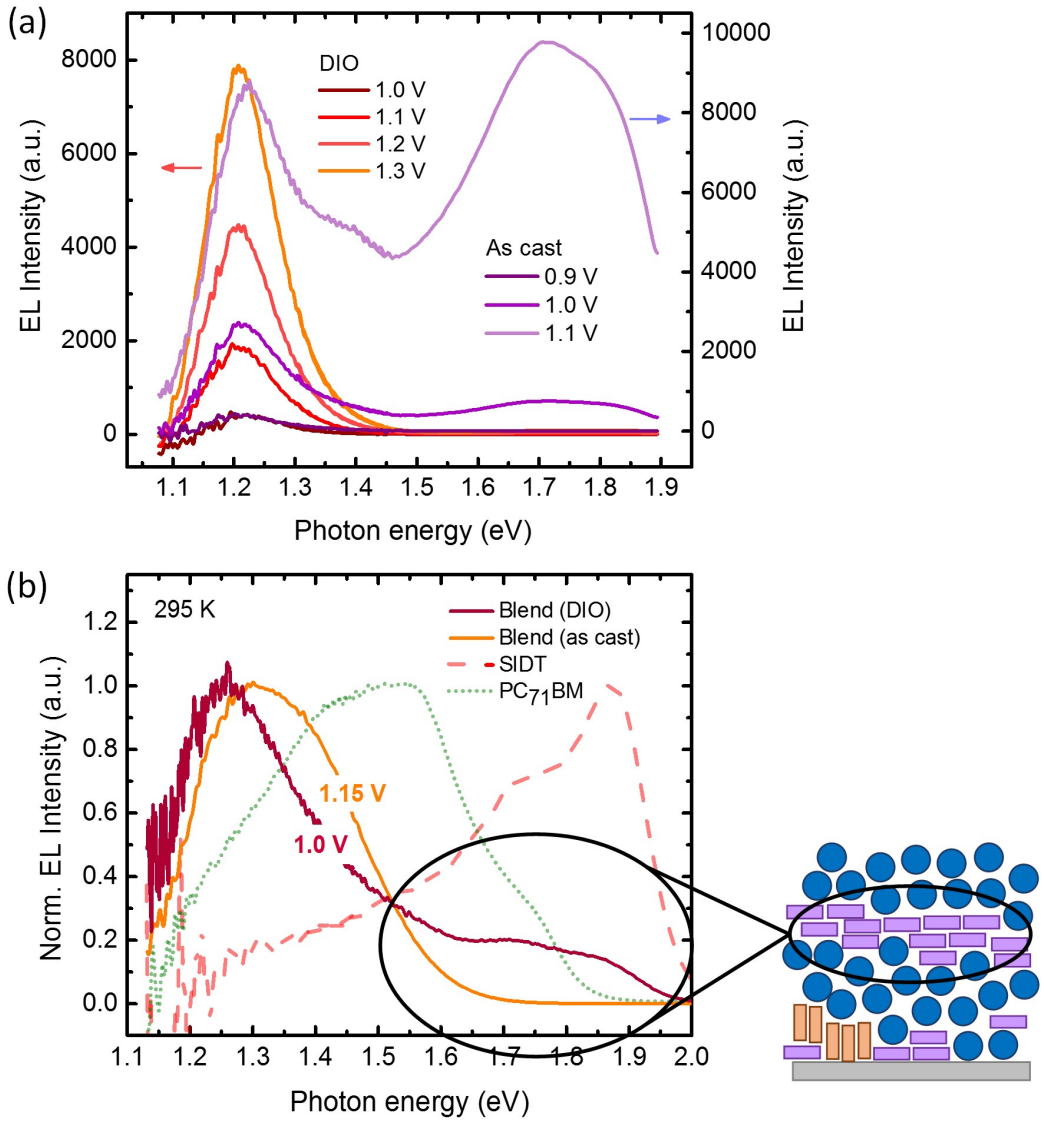

Figure 3.17: Singlet emission from *face-on* bilayers. (a) EL spectra from *face-on* and *edge-on* bilayers at varying applied voltages. (b) EL spectra of a p-SIDT(FBTTh$_2$)$_2$:PC$_{71}$BM BHJ processed with DIO, along with the as-cast blend and the neat donor and acceptor spectra.

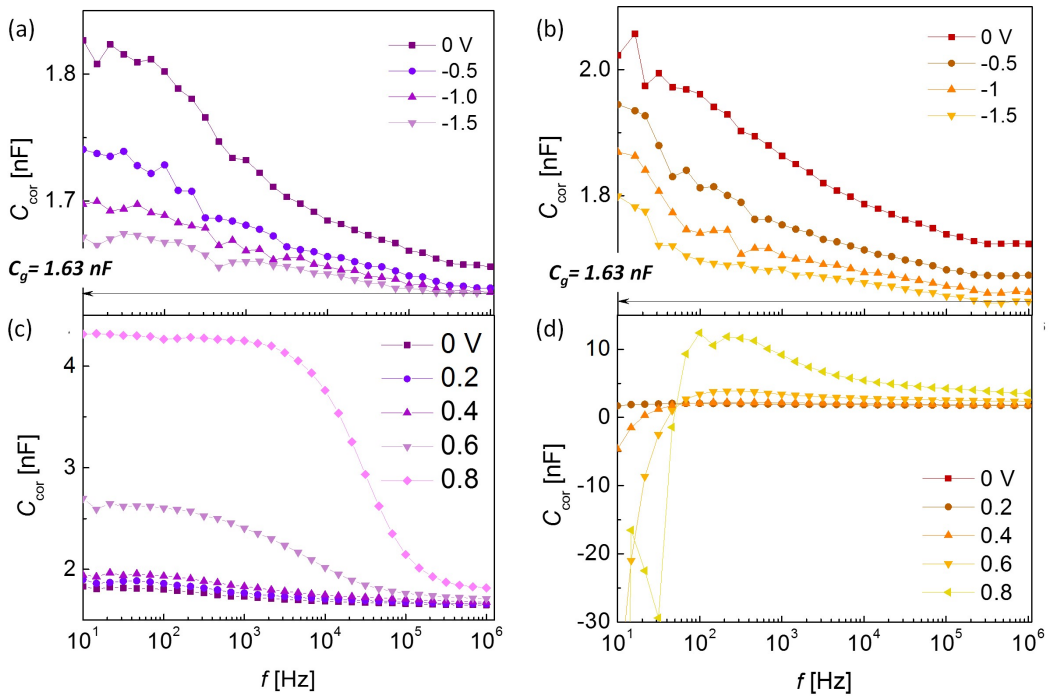

Figure 3.18: Impedance analysis of *face-on* (a,c) and *edge-on* (b,d) bilayers under reverse bias (a,b) and forward bias (c.d).

3.8.2 Impedance analysis

Under reverse bias, as charges are extracted from the devices, the *face-on* and the *edge-on* bilayers have similar capacitance spectra which plateau at a similar geometrical capacitance value (thus indicating the bilayers may have the same dielectric constant, or that dielectric constant is not a function of orientation). In forward bias, however, there is a big difference with orientation. The *face-on* bilayer shows the expected response to forward applied voltage, where the capacitance increases, especially at low frequencies, as voltage increases because there is an increasing concentration of charge carriers in the device. In the *edge-on* bilayer, however, the capacitance spectra drop to negative capacitance even for low applied voltages. This indicates that in the edge-on bilayer the charges are note able to respond fast enough to the alternative voltage signal that is applied to the device at the specified frequencies. This may be an indication of an interfacial dipole or of shallow charge-carrier traps. It is also interesting to consider this in light of the greater non-radiative recombination that was characterized for *edge-on* bilayers. These measurements were done by Dr. Viktor Brus.

3.8.3 DIO content and orientation control

So far we have established that addition of 0.4% DIO v/v to a 15 mg/mL solution of p-SIDT(FBTTh$_2$)$_2$ flips the molecules from *face-on* to *edge-on* orientation. We can measure a difference in the resulting V_{OC} and the E_{CT} of devices made with the two opposite orientations, and in addition we have measured a difference in the Fermi level of neat p-SIDT(FBTTh$_2$)$_2$ films. The relationship of the effect of molecular orientation on the E_{CT}, V_{OC}, and the Fermi level is shown in Figure 3.19. It is important to recall that the measured energy levels can have a strong dependence on the DOS filling, and the three measurements reported in Figure 3.19 relate to different carrier densities, which

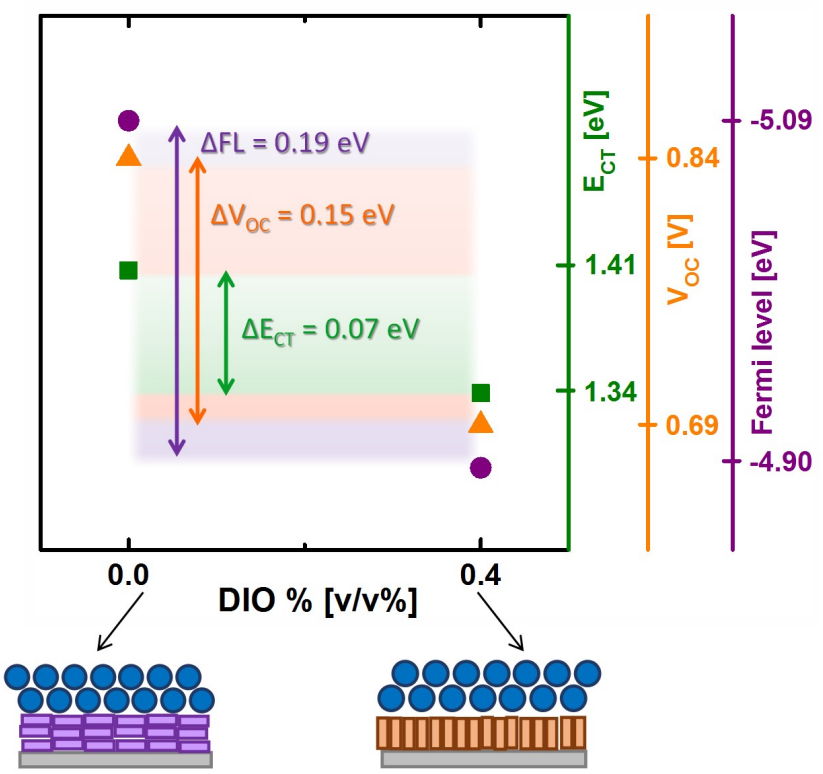

Figure 3.19: Difference in the Fermi level, V_{OC}, and E_{CT} with molecular orientation.

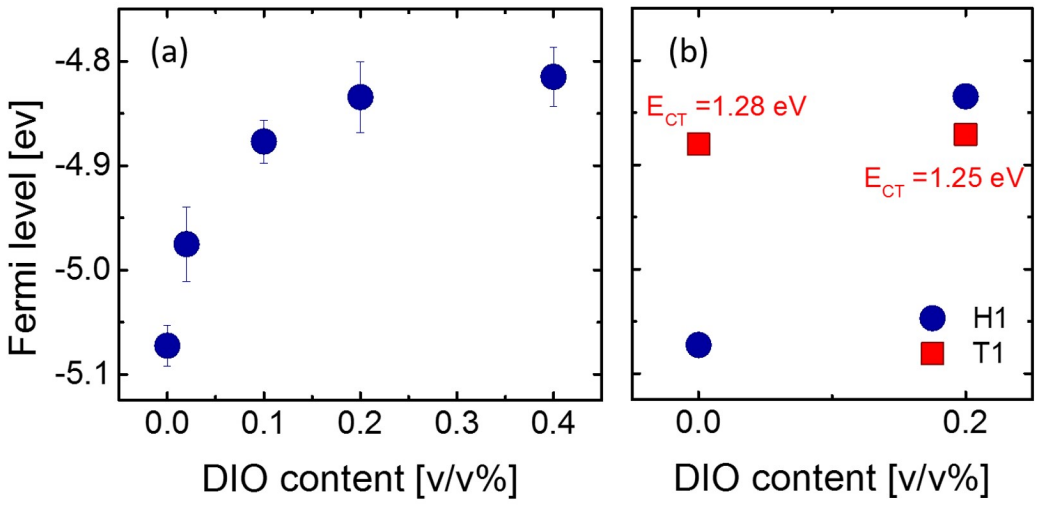

Figure 3.20: Changes in the Fermi level of p-SIDT(FBTTh$_2$)$_2$ with % DIO content. (a) Fermi level measured for 40 nm thick films cast from solutions with varying DIO concentration, but constant solids concentration. (b) Control measurements of the effect of DIO on the Fermi level of p-DTS(FBTTh$_2$)$_2$.

explains the variety in difference.

However, the more exciting measurements we completed with the Kelvin Probe are shown in Figure 3.20. By varying the concentration of DIO in the solution, we were able to gradually change the Fermi level of the p-SIDT(FBTTh$_2$)$_2$. Jack Love did TEM on a film processed with 0.2% DIO, and found structure that indicated of both *face-on* and *edge-on* orientation in the same film. We were not able to repeat this, however, and due to the limited availability of p-SIDT(FBTTh$_2$)$_2$ we did not put much effort into repeating this work. As a control, we also show here that the presence of DIO alone does not alter the Fermi level of a semiconductor, using the molecule p-DTS(FBTTh$_2$)$_2$ (Figure 3.20).

3.8.4 Orientation control with diCN-TIPS-Pn

Dr. Oleksandr Mikhnenko suggested that we should try to remove signal from singlet excitons in the EQE by mixing an exciton quencher in the p-SIDT(FBTTh$_2$)$_2$ layer. We

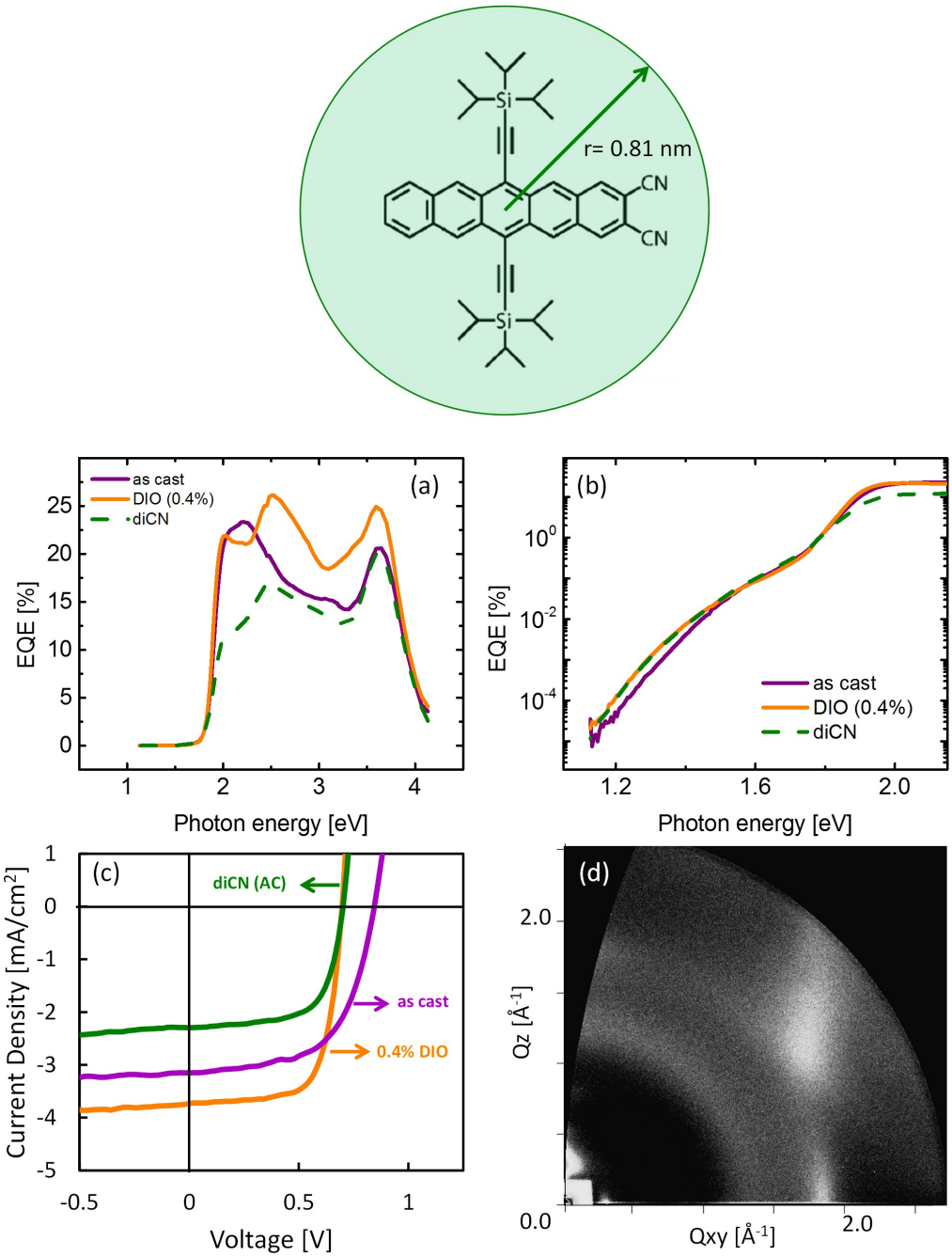

Figure 3.21: The effect of adding an exciton quencher (diCN-TIPS-Pn, structure shown at top of the Figure) to p-SIDT(FBTTh$_2$)$_2$ films. (a) EQE spectra of as-cast (*face-on*), DIO-procesesd (*edge-on*), and diCN-TIPS-Pn processed bilayers. (b) CT state region of the EQE spectra for hte same three bilayers. (c) *J*-*V* curves for the three bilayers. (d) GIWAXS measurements of a p-SIDT(FBTTh$_2$)$_2$ film cast from a solution containing a small amount of diCN-TIPS-Pn.

chose to use a TIPS-pentacene derivative, which Alex had used in a previous study and had characterized to have a larger quenching radius than PCBM. The TIPS-pentacene derivative is diCN-TIPS-Pn, and its structure is shown in Figure 3.21. In the EQE spectra, there appears to be a significant portion of the photocurrent missing, coinciding with energies of p-SIDT($FBTTh_2$)$_2$ absorption (Figure 3.21a), corresponding very well with a reduction in the J_{SC} (Figure 3.21c). This is a promising result, but it implies that more diCN-TIPS-Pn must be used. However, the CT state region of the EQE (Figure 3.21b), as well as the V_{OC} (Figure 3.21c) of the p-SIDT($FBTTh_2$)$_2$ film (dissolved only in chlorobenzene, without any DIO, expected to be *face-on*) mixed with a small amount of diCN-TIPS-Pn both greatly resemble the behavior of and edge-on solar cell. Finally, GIWAXS measurements of this film confirm that the addition of a minute amount of diCN-TIPS-Pn to p-SIDT($FBTTh_2$)$_2$ is enough to flip the molecules edge-on (Figure 3.21d).

3.9 Methods

3.9.1 Sample preparation

p-SIDT($FBTTh_2$)$_2$ was synthesized according to the previously reported scheme.20 p-SDIT(FBTTh2)2 was dissolved at a concentration of 15 mg/mL in pristine chlorobenzene (CB), or CB with 0.4% diiodooctane (DIO) v/v. In the CB+DIO solution, the conditions correspond to a ratio of 2 molecules DIO for every 1 molecule of p-SIDT($FBTTh_2$)$_2$.51 Bi-layer devices were fabricated on glass substrates sputtered with ITO, and coated with 35 nm poly(3,4-ehtylenedioxythiophene):poly(styrenesulfonate) (PEDOT:PSS). A C_{60} layer was thermally evaporated on p-SIDT($FBTTh_2$)$_2$, followed by bathocuproine (BCP) and Al. The final device structure for nearly all measurements reported herein is as follows:

ITO/PEDOT (35 nm)/p-SIDT(FBTTh$_2$)$_2$ (45 nm)/C_{60} (45 nm)/BCP (4 nm)/Al (80 nm).

3.9.2 GIWAXS analysis

GIWAXS was performed at Stanford Synchrotron Radiation Lightsource (SSRL) beamline 11-3 with a MAR345 image plate. The data was calibrated and reduced using WxDiff software package.52 To characterize the amount of *edge-on* vs. *face-on* material, a cake slice around the π-stacking peak, between Q=1.8/ and 2.0/, was reduced to a pole figure. An adjacent cake slice between Q=1.7/ and 1.8/ was subtracted from the data to account for background scattering (see Figure S1). The data was fit to two in-plane π-stacking peaks at about -90 and +90, one out-of-plane π-stacking peak at 0, and four peaks around $\pm$30 and $\pm$55 representing the SiO2 substrate background. The out-of-plane peak area was compared to the average of the two in-plane peak areas to arrive at the *face-on* to *edge-on* ratio for each sample. Samples for GIWAXS were prepared on cleaned SiO2 substrates, coated with PEDOT:PSS and p-SIDT(FBTTh$_2$)$_2$ cast from 15 mg/mL CB or CB+DIO.

The C_{60} scattering as a function of C_{60} thickness was tracked by reducing cake slices shown in Figure S2 to I vs. Q. We selected these specific cake slices for analysis because they contain non-overlapping peaks from both the small molecule and the C_{60}, allowing a simultaneous comparison of contributions from both materials. This data was fit to a linear combination of neat p-SIDT(FBTTh$_2$)$_2$ and neat C_{60} data, and the fit coefficient for C_{60} was reported. Fits are shown in Figure S2 along with the neat data. Fits have some discrepancy due to small changes in peak shape but are reasonably accurate in depicting overall trends. Samples for these measurements were prepared on cleaned SiO2 substrates, coated with PEDOT:PSS and p-SIDT(FBTTh$_2$)$_2$ cast from 15 mg/mL CB

or CB+DIO, with C_{60} evaporated for thicknesses of 0 30 nm.

3.9.3 Current-Voltage characteristics

Solar-cell device properties were measured under illumination by a simulated 100 mW cm2 AM1.5G light source using a 300 W Xe arc lamp with an AM 1.5 global filter. The irradiance was adjusted to one sun with a standard silicon photovoltaic calibrated by the National Renewable Energy Laboratory. Temperature dependent V_{OC} in the range of 275-300 K was collected using a custom Peltier cooled sample holder under illumination from the above described light source in combination with optical density filters to reduce the intensity. In the range of temperatures below 275 K, a helium cryostat was used for temperature control and illumination was achieved with a high power 1W, 445 nm laser diode (fluence was tuned with the DC bias applied to the laser diode to match light intensity used in the solar simulator).

3.9.4 TEM and cross-sectional TEM

TEM samples were prepared by casting a layer of p-SIDT(FBTTh$_2$)$_2$ from CB or CB+DIO on PEDOT:PSS, and floating pieces of the film on DI water. Film pieces were transferred to TEM grids and allowed to dry overnight. High-resolution images were taken with an FEI Titan FEG High Resolution microscope. The TEM images were collected using a low-dose electron beam (spot size 6) to avoid beam damage, and a small defocus to enhance the contrast in the images.

Using an FEI focused ion-beam (FIB) microscope, a 20 um long slice with a thickness of about 200 nm was cut from a bilayer device (prepared as described above), and mounted on a TEM grid. The donor/acceptor interface in the bilayers was then imaged by HR-TEM. The procedure followed has been described in detail previously.53,54 Care-

ful attention was devoted to minimize exposure of the sample to high-energy electron and ion beams, thereby reducing damage as much as possible.

3.9.5 External and internal quantum efficiencies

EQE characteristics were measured in a nitrogen-filled glovebox using a setup at UCSB and in Potsdam University. At UCSB, the EQE setup consisted of a 75 W Xe light source, monochromator, optical chopper, lock-in amplifier, and a National Institute of Standards and Technology calibrated silicon photodiode for power-density calibration. At Potsdam University, the EQE setup is similar, but used a 200 W halogen lamp (Philips), and a UV enhanced silicon photodiode to calibrate the visible spectra, or a germanium photodiode to calibrate the near infrared spectra. Both photodiodes were calibrated by Newport. For the sub-bandgap EQE, higher sensitivity settings were used with a longer time delay between measurement points. Bias-dependent EQE was collected on the setup in Potsdam University, coupled to a Keithley source-measure-unit used to apply a bias while the EQE spectra were recorded. Temperature-dependent EQE measurements were collected with a setup at UCSB, following a similar procedure, using a nitrogen-cooled cryostat.

Total absorption of solar cell devices was measured with an integrating sphere, and corrected for parasitic absorption as determined for the bilayers using a transfer matrix model.55 Subtracting the parasitic absorption from the total device absorption then gives the active layer absorption, and dividing EQE spectra by the corresponding active layer absorption gives the IQE spectra of the device.

3.9.6 Electroluminescence and electroluminescence efficiency

Electroluminescence spectra for the bilayers were collected directly from the solar cell devices, by applying a bias that is close to the turn-on voltage of the devices. The resulting emission was collected with an Andor SR393i-B spectrometer provided with a cooled silicon detector DU420ABR-DD and a cooled InGaAs DU491A-1.7 detector. The spectra were corrected for detector response using a blackbody spectrum.

The EL efficiency was collected by applying a small bias to the bilayer devices, and placing a calibrated silicon photodiode directly in front of the device to collect the resulting emission. The angle between the calibrated silicon photodiode and the device was varied to account for anisotropy in emission intensity.

3.9.7 Time-delayed collection field measurements

Excitation is realized by a laser system consisting of a Libra USP-1K-HE with a pulse energy of 4.0 mJ at 1kHz and an OPerA Solo for wavelength selection. The pre- and collection voltage is applied via an Agilent 81150A pulse generator in combination with a home-built amplifier. Currents through the devices are measured via a 50 resistor and recorded with an Yokogawa DL9140 oscilloscope.

3.9.8 Electronic-structure calculations

The p-SIDT(FBTTh$_2$)$_2$ bulk structure and C$_{60}$/p-SIDT(FBTTh$_2$)$_2$ bilayer structure were generated by a combination of Monte Carlo (MC) and molecular dynamics (MD) simulations. The MD simulations were run for 200 ps at 300 K with under the NVT ensemble using the Verlet integrator with a time step of 1 fs. The temperature was maintained by the Nose-Hoover thermostat. A spherical cutoff of 1.25 nm for the summation of van der Waals interactions and the Ewald solver for long-range Coulomb interactions

was used throughout. The COMPASS force field as implemented in the Forcite program of Materials Studio was used for the MD simulations.[**?**] Density-functional theory calculations using the range-separated HSE functional were then carried out for *face-on* and *edge-on* p-SIDT(FBTTh$_2$)$_2$ slabs under periodic boundary conditions using the plane-wave based Vienna Ab-initio Simulation Package (VASP). [135, 136, 137, 138]

The electron coupling between diabatic CT state and the GS of p-SIDT(FBTTh$_2$)$_2$/C$_{60}$ complexes were evaluated by means of the generalized Mulliken-Hush approach at the MD generated geometry. These calculations were performed with the B3LYP functional and 6-31G(d,p) basis set, using the Q-Chem package.[139]

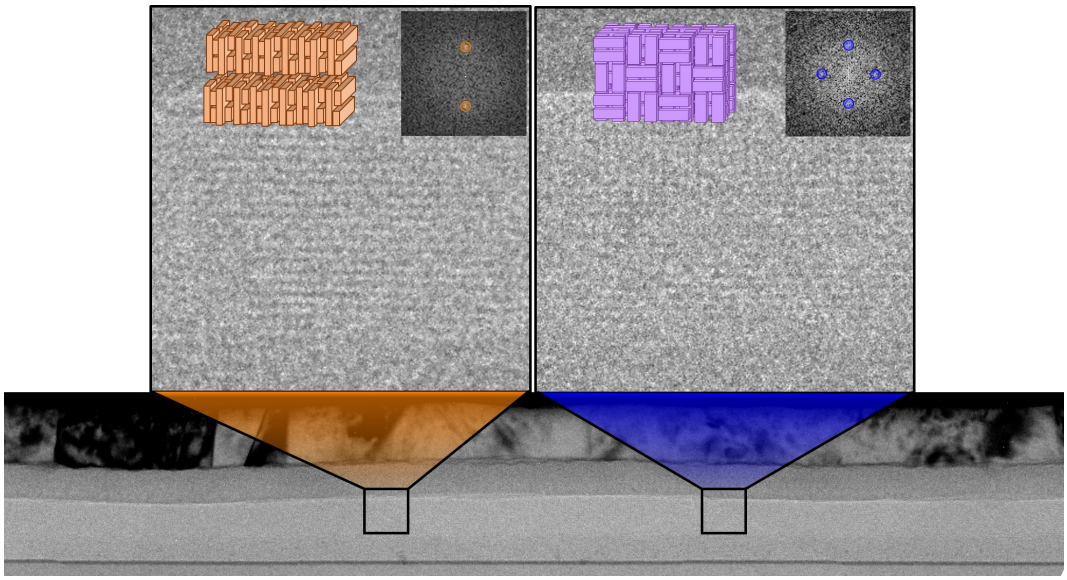

Chapter 4

Harvesting the Full Potential of Photons with Organic Solar Cells

Life is a beautiful magnificent thing, even to a jellyfish.

– Charlie Chaplin

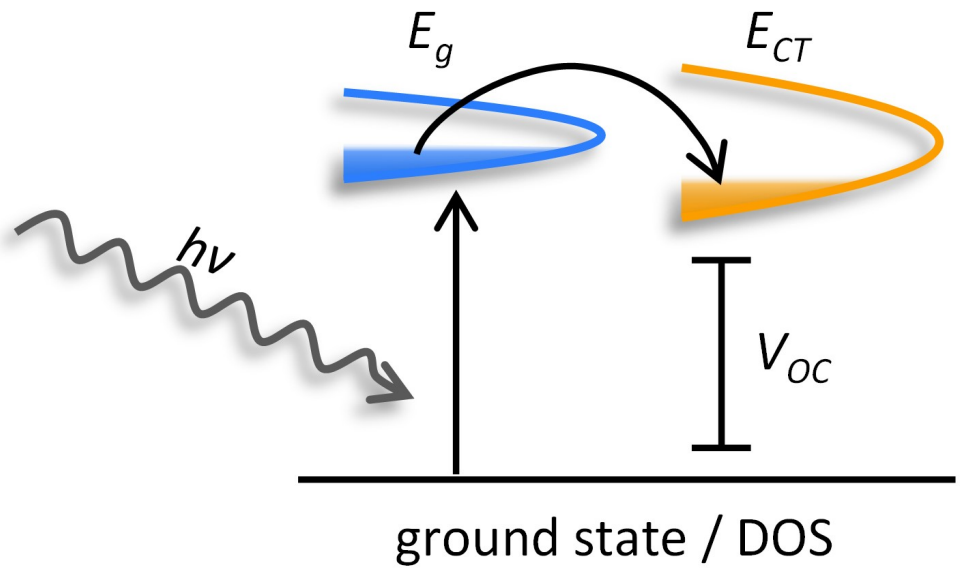

4.1 Preface

My involvement with this project started as a 'quick measurement' to estimate the E_{CT} in PIPCP:$PC_{61}BM$. Ming is the one I have to thank for getting me involved in a project that spanned into two large collaborations on a material system that has since geared much interest in the community. When Ming had asked that I look at the system, I did EL measurements on the system (and two other polymers which Ming had synthesized, blended with PCBM), and saw that the E_{CT} was very difficult to distinguish due to its proximity to the PIPCP singlet. The data lay dormant until we had our kick-off MURI meeting in Atlanta, GA, where I learned that also the Friend group was looking at PIPCP:$PC_{61}BM$, doing some similar measurements to what I had done. The discussion also stimulated me to email Sam the same night, and suggest that we should do Kelvin probe measurements of these polymers (and their blends), since there is something interesting happening with the V_{OC} and the energy levels. When we returned from Georgia, there was a good amount of excitement about PIPCP:$PC_{61}BM$, and we started to try and organize the data collected to that point and synthesize a story out of it. Jessica (Ye) Huang was the primary device fabricator, and had been trying a slew of ways to increase the performance of PIPCP as a donor polymer. At this point, I got much more involved with this project, as I helped to put all the data (and there was a lot of it) into a single document for our reference, and started collaborating with Jessica: she would make devices and I would measure the properties I was interested in. During this time, Jack was also getting more involved with PIPCP from the side of measuring its mobility. Shortly after, Jessica got a job with Dow Chemical and left the group, leaving the project to Jack and me. Following a meeting with Prof. Richard Friend, who was at UCSB for a day or two, we conducted a plan that we will write two papers about PIPCP: one focused on the V_{OC} and the other on the FF.

The story told in this chapter came together by a process of some iterations with Prof. Guillermo Bazan. I put together one version of the manuscript, then Gui looked at it, made many changes, I implemented them, then Gui read through again, made more changes, I implemented them, then Gui read through and suggested we rearrange the whole story, which I did, and so on. Unlike my first paper, the writing process of this paper was much more collaborative and enjoyable. I think Gui's style and talent in writing papers really made this paper far better than it would have been otherwise. throughout the process of writing Jack also took an active role in giving comments and thinking about the physics of the story that was unfolding.

Richard Friend's group pointed out two things that we had not seen before: the absorption of PIPCP red-shifts in the blend, and the absorption edge is very sharp, corresponding to a very low Urbach energy. These two details were key in this first part of our exploration of PIPCP. I believe it was Simon Gélinas who first did PDS and transient absorption on PIPCP:$PC_{61}BM$, but he also finished his tenure in the Friend group. Aditya Sadhanala took over the PDS measurements in the Friend group. Chris Takacs, who we are all to thank for teaching Jack, who then taught me, how to do TEM on organic films, is the one who collected the TEM in this chapter. I started to do Kelvin probe measurements on PIPCP, but an undergrad, Justin Beavers joined our group and needed a project. Sam trained Justin on doing Kelvin probe measurements, and Justin collected and fit the Kelvin probe data in Figure 4.9 of this chapter. Jessica Huang had found the optimized condition that was used in this study, and Ming Wang synthesized the material. I'd also like to emphasize that my analysis at the end of this chapter, where I estimate the $lUMO_D$-$LUMO_A$ offset, was inspired by the picture I got form the work that Sam has published in reference [140].

This chapter is therefore the collaborative effort of a number of people: myself, Dr. John Love, Dr. Chris Takacs, Dr. Aditya Sadhanala, Justin Beavers, Sam Collins, Dr. Ye

Huang, Dr. Ming Wang, Prof. Richard Friend, Prof. Gui Bazan, and Prof. Thuc-Quyen Nguyen.

4.2 Introduction

The power conversion efficiency (PCE) of solar cells and their open circuit voltage (V_{OC}) are directly related. In the majority of conjugated polymer:fullerene bulk heterojunction (BHJ) organic photovoltaics (OPV) the eV_{OC} is significantly lower than the energy of photons absorbed, as determined by the donor material bandgap (E_g). Due to the excitonic nature of organic semiconductors, donor and acceptor materials with cascading energy levels are used to provide a driving force for charge separation. As a first approximation, eV_{OC} is governed by the photovoltaic gap of the solar cell, defined as the energy difference between the lowest unoccupied molecular orbital (LUMO) of the acceptor (LUMO_A) and the highest occupied molecular orbital (HOMO) of the donor (HOMO_D).

Wavefunction overlap between LUMO_A and HOMO_D can lead to an interfacial state that has been correlated to eV_{OC}, referred to as the charge transfer (CT) state.[19] The energy the CT state (E_{CT}) has been shown to track linearly with eV_{OC} at a constant offset, and even to extrapolate to the same value as temperature approaches 0 K, suggesting that the E_{CT} may set the upper limit for the eV_{OC}.[29] Minimizing E_g to eV_{OC} energy losses could appreciably increase the PCE in organic solar cells. Considerable efforts are thus under way to determine the electronic and morphological factors that reduce the V_{OC}, but improvements in the V_{OC} values in high performing systems remain limited.[47, 141, 18]

Here we define energy losses related to the V_{OC} as $E_{loss} = E_g$ eV_{OC}. We note that in this manuscript we use the optical bandgap as an estimate for E_g, to provide a straight-

forward comparison between the results we report and those previously described by others.[142, 58] E_{loss} can be split into two categories. First, E_{loss} is determined by variations in energetic offset, specifically between $LUMO_D$ and $LUMO_A$. A number of works have highlighted the importance of the $LUMO_D$-$LUMO_A$ (and also the $HOMO_A$-$HOMO_D$) energy offsets for efficient charge transfer,[58, 143, 144] while other theoretical and empirical efforts have emphasized the need for reduced offsets to achieve maximal V_{OC} .[47, 143, 145, 146, 37] DPP-based donor acceptor polymers introduced by Li *et al.*[142] are a good example in the context of low E_{loss} values, demonstrating the fine balance between energetic offsets and charge generation and extraction. From the polymer donor series introduced by Li *et al.*, BHJ blends with an E_{loss} 0.55 eV had poor efficiencies, while blends with E_{loss} 0.59 eV could achieve fair external quantum efficiencies (EQE).[142] We consider losses due to energetic offset and charge transfer as the differences between E_g and E_{CT}. Second, literature precedence has shown an empirical relationship of E_{CT} - eV_{OC} = 0.6±0.1 eV, that is valid for a large variation of BHJ blends.[19, 47, 18] In the literature, this voltage loss has been attributed to a range of recombination losses,[29, 141, 115, 92, 147] which are affected by factors such as band bending near the contacts,[148, 149] energetic disorder,[141, 28, 150, 151, 152] electronic coupling at the donor/acceptor interface,[141, 66] and interfacial area between donor and acceptor phases.[147]

The recently reported regioregular conjugated polymer, PIPCP (see Figure 4.1a), was examined within the context of BHJ systems with low E_{loss}. From absorption spectroscopy, films of neat PIPCP show a value for E_g of 1.47 eV. The optical gap, E_g, is determined by the energy corresponding to the onset of absorption, as is shown in more detail in Figure 4.2. For PIPCP:PC_{61}BM blends Wang *et al.* found that V_{OC} = 0.86 V, corresponding to E_{loss} = 0.61 eV.[153] The low E_{loss} in PIPCP:PC_{61}BM solar cells prompted us to examine in more detail the energetic characteristics and morphological

details of PIPCP:$PC_{61}BM$ blends. As reported herein, we find that the effective E_g of PIPCP in the blend films is in fact lower than for PIPCP in neat films, and in combination with slightly improved processing conditions we obtain an $E_{loss} = 0.52 \pm 0.02$ eV. This loss is amongst the lowest reported in the literature for a device with PCE above 6%. We find that the E_g of PIPCP in the blend and the E_{CT} are nearly of equal energy, eliminating losses attributed to an energetic cascade. A schematic demonstrating the relationship between E_{loss} and E_g, E_{CT}, and V_{OC} is shown in Figure 4.1b. Despite these considerations it is not yet possible to design, a priori, a blend for which E_{loss} is close to the thermodynamic limit, while allowing for efficient charge generation and ultimately high short circuit current (J_{SC}). From absorption measurements, PIPCP in neat films and in the blend demonstrates very low Urbach energies, supported by low energetic disorder values extracted from Kelvin probe measurements of band bending. Structural characterization of the blend films show crystalline features not often observed in polymer:fullerene blends, illustrating a high degree of structural order in the system. These observations provide insight into a BHJ system that is able to efficiently generate charge carriers despite marginal energetic offsets.

4.3 Optical energy levels

We sought to understand differences in optical properties between PIPCP and the blend, first by using photothermal deflection spectroscopy (PDS). PDS is a highly sensitive absorption technique that is particularly useful for characterizing optical transitions at sub-bandgap energies,[154] and is therefore used to identify the presence of the CT state in BHJ solar cells.[20] As shown in Figure 4.2, upon blending with $PC_{61}BM$ the PIPCP absorption redshifts by 60 meV. Typically, features in the absorption spectrum of a blend film that are lower in energy than for the individual neat components are

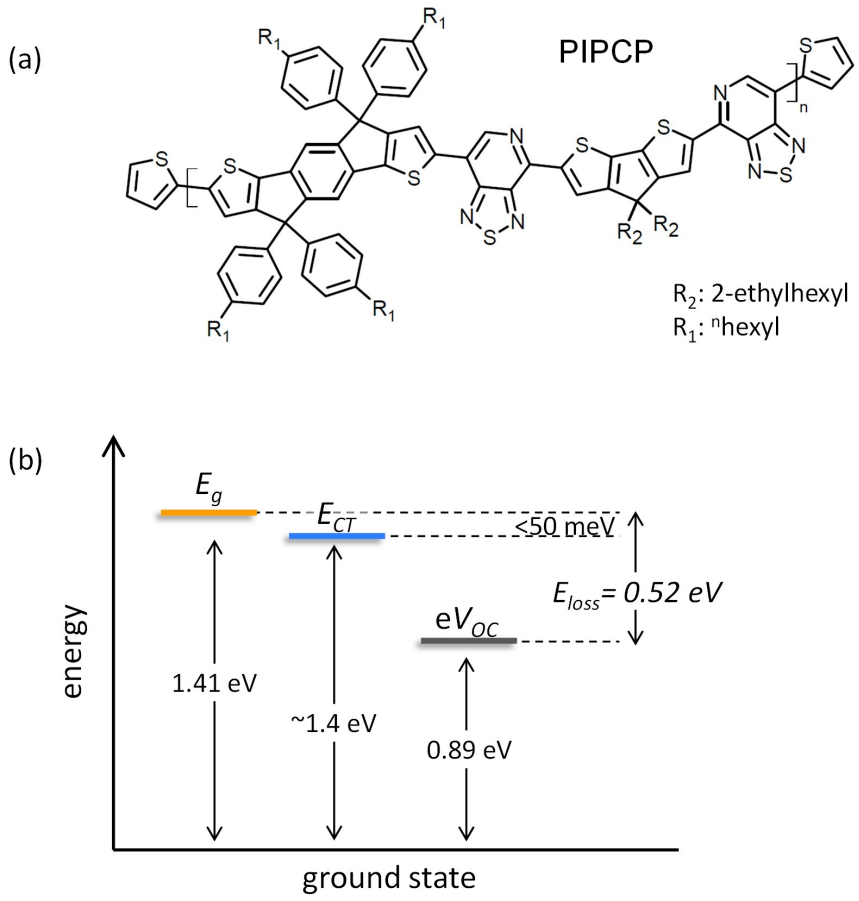

Figure 4.1: (a) Chemical structure of PIPCP. (b) Schematic diagram of the energy levels in a solar cell to illustrate voltage losses incurred from photon absorption to V_{OC}. Approximate values relevant to the work presented here are included. The ¡50 meV value reported for the energetic offset between the donor E_g and the E_{CT} is shown as an upper limit for the offset, extracted from Marcus theory fitting to the absorption by EQE and emission by EL, simultaneously, described for Figure 4.8

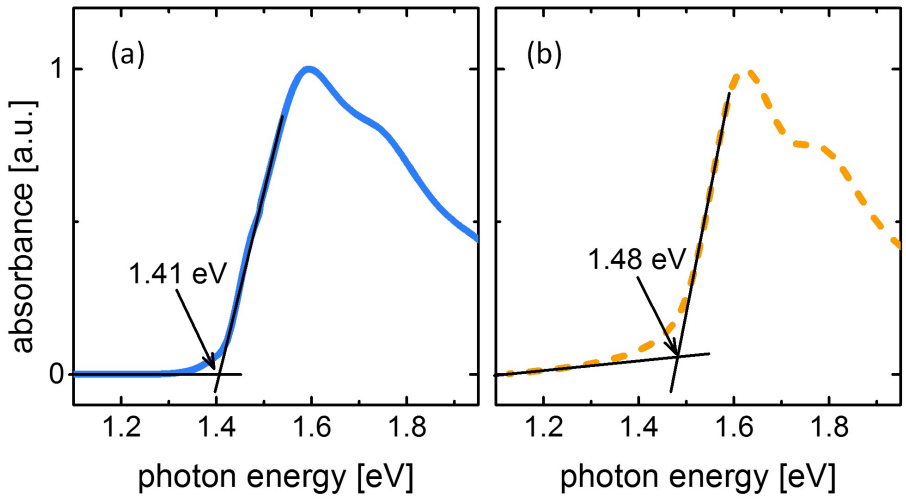

Figure 4.2: Absorption spectra of (a) blend PIPCP:$PC_{61}BM$ films and (b) neat PIPCP films. E_g is defined as the absorption onset, determined by the intersection of the lines as shown in the figure.

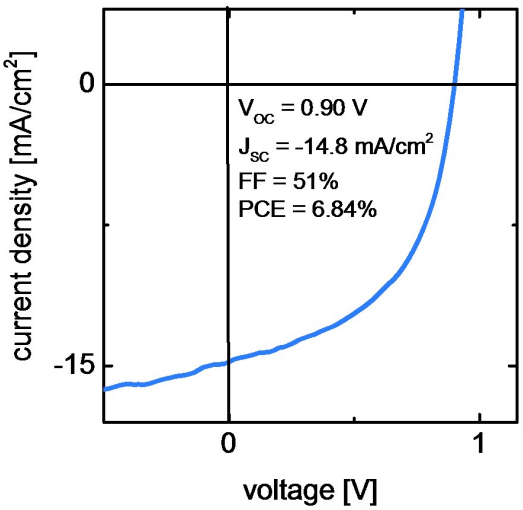

Figure 4.3: J-V characteristics of PIPCP:$PC_{61}BM$ devices under 1-sun illumination.

attributed to direct CT state absorption.[18] However, because the absorption strength of the CT state is normally 2-4 orders of magnitude lower with respect to the S_0-S_1 of the donor or acceptor in the blend,[115] it is unlikely that the red-shifted absorption of the blend film is due to CT state absorption alone. Instead, we attribute the red-shift to changes in structure and/or environment of the PIPCP backbone within the blend environment that lead to a higher degree of electronic delocalization. From Figure 4.2, the E_g of PIPCP in the blend is 1.41±0.01 eV, which compared with a V_{OC} of 0.89±0.01 V leads to an E_{loss} of 0.52±0.02 eV.

4.4 Morphology by TEM

Insight into possible structural differences that may account for the red-shifted absorption of PIPCP in blend films may be achieved using high resolution transmission electron microscopy (HR-TEM). The resulting images of PIPCP:$PC_{61}BM$ show fiber like phases with well-defined lattice planes (Figure 4.2), suggesting highly crystalline features which are uncommon in polymer:fullerene systems. Indeed, this morphology is not observed in neat PIPCP films and is reminiscent of the structural order in small-molecule solar cell blends prepared with processing condition that induce crystallinity.[12]

4.5 Voltage losses: E_g, E_{CT} and energetic order

Due to its high sensitivity, PDS has been utilized to detect the presence of the CT state in organic solar cells. External quantum efficiency (EQE) measurements of solar cells are another common way to obtain information about the CT state.[29, 18] However, due to the weak absorption of the CTS, the absorption/charge generaiton curves must be on a log-lin scale. Figure 4.5 provides the PDS and the EQE curves for the

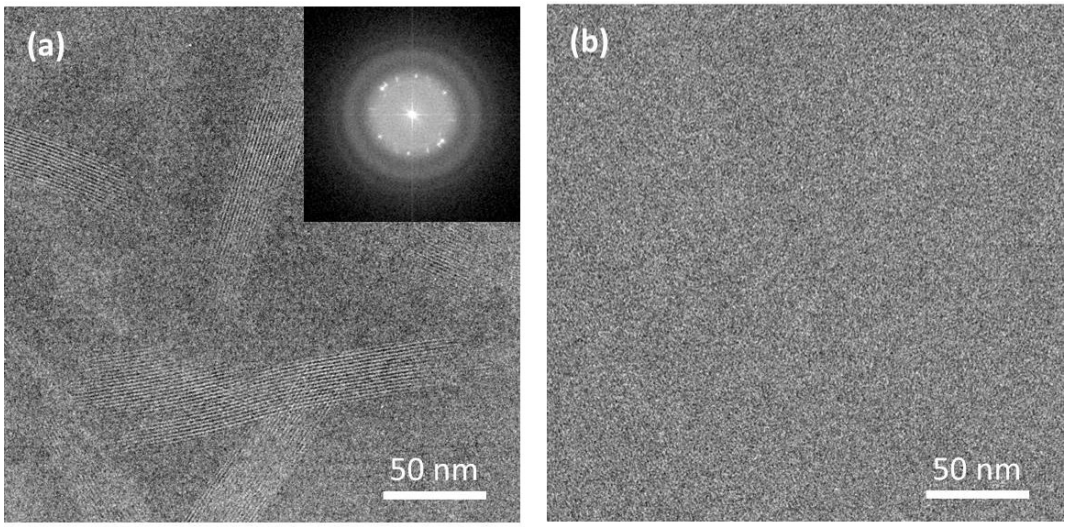

Figure 4.4: High resolution-TEM images of a (a) PIPCP:$PC_{61}BM$ blend film, and (b) neat PIPCP film.

PIPCP:$PC_{61}BM$ blend films along with neat PIPCP films, on a log-lin scale. In both PDS and EQE methods the CT state is generally distinguished by a shoulder of low intensity at sub-bandgap energies that deviates from the band shape of the individual BHJ blend components. The CT state in PIPCP:$PC_{61}BM$ blends is of particular interest within the context of the E_{CT} eV_{OC} = 0.6±0.1 eV relationship often discussed in the literature.[19, 47, 18] We emphasize that the 0.6±0.1 eV voltage loss is only with respect to the E_{CT}, and if losses from E_g eV_{OC} were taken into account the voltage loss in those systems are anticipated to be greater. The E_{loss} of 0.52±0.02eV reported herein is calculated from the bandgap of PIPCP, E_g. Thus we sought to understand if PIPCP:$PC_{61}BM$ has achieved low voltage losses with respect to the CT state (E_{CT} eV_{OC}), or whether losses from exciton to CT state (E_g E_{CT}) have been eliminated.

Comparison of the PDS spectra and the EQE traces reveals that they show similar results, both confirming the red-shifted absorption of the blend. Importantly, the normalized EQE measurements demonstrate that the entire absorption profile contributes to charge generation, including the absorption gained by the red-shift. However, neither

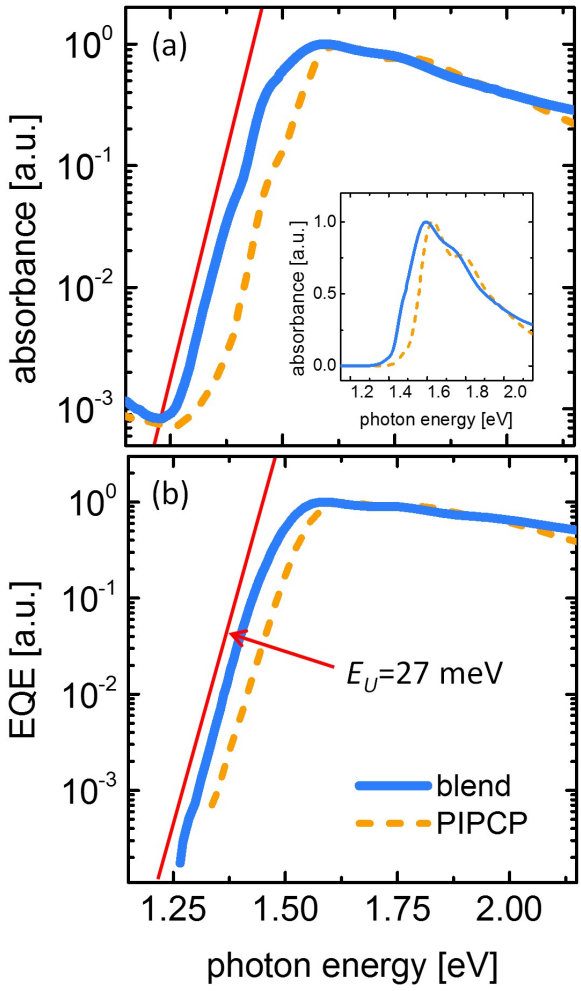

Figure 4.5: Sub-bandgap absorption in PIPCP:$PC_{61}BM$ films. (a) Normalized log-lin PDS spectra of PIPCP neat (dashed line) and blend (solid line) films. Inset shows the PDS spectra on a linear scale. (b) EQE spectra of neat and blend PIPCP:$PC_{61}BM$. Red lines demonstrate an absorption edge with an Urbach energy of 27 meV, as determined from Equation 4.3.

the PDS nor the EQE spectra of the blend exhibit a shoulder characteristic of the CT state. These data suggest that the PIPCP exciton in a PIPCP:$PC_{61}BM$ blend must be nearly of equal energy to the CT state, such that the E_{CT} absorption band is buried within the polymer absorption and therefore not apparent by both PDS and EQE.

4.6 Proximity of E_g and E_{CT} by emission spectroscopy

The close proximity between the values of E_{CT} and E_g is also supported by emission measurements. Electroluminescence (EL) (Figure 4.6) and photoluminescence (PL) (Figure 4.6b) were recorded for blend PIPCP:$PC_{61}BM$ and neat PIPCP devices. EL measurements were performed by applying a small forward bias directly to solar cell devices and collecting the resulting emission; PL measurements were carried out on the same devices with a laser excitation at 633 nm.

The EL spectra of neat PIPCP and the blend overlap to a great extent with emission peaking at 1.39 eV for the neat film and at 1.37 eV for the blend. When compared to the EL spectrum of neat PIPCP, emission from PIPCP:$PC_{61}BM$ is broader, with a shoulder to the emission spectrum at low energies. Of note, the EL spectrum from neat PIPCP has a shoulder at 1.49 eV that is not present in the PIPCP:$PC_{61}BM$ EL spectrum (Figure 4.6a). Upon increasing the applied bias, the EL spectrum of PIPCP:$PC_{61}BM$ does not change in shape, suggesting the whole emission spectrum originates from one state or multiple states with the same carrier density dependence (Figure 4.7).[22]

From PL measurements, the blend emission is similarly featureless and broad, although the shoulder at low energies is not as pronounced as in the EL spectra (Figure 4.6b). The neat PIPCP shoulder at 1.49 eV is more prominent by PL than EL, and is absent in the PL of the blend, as also seen by EL. CT state emission is most generally characterized as a featureless, relatively broad spectrum, at lower energies when

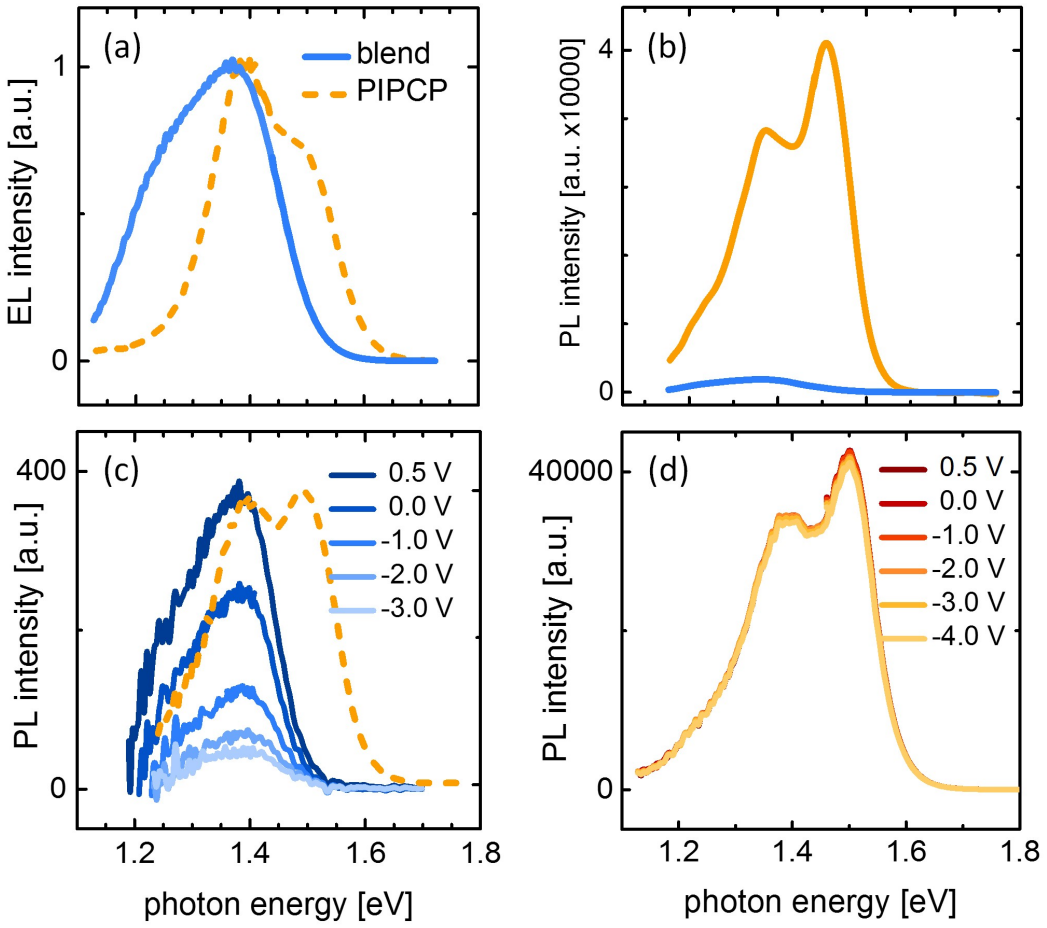

Figure 4.6: a) Normalized electroluminescence spectra of neat PIPCP and PIPCP:$PC_{61}BM$ devices. (b) PL quenching in PIPCP:$PC_{61}BM$ films, with respect to neat PIPCP; excited at 633 nm. (c) Bias-dependent PL of PIPCP:$PC_{61}BM$ device excited at 633 nm; the PL of neat PIPCP is shown for reference as a dashed spectrum. (d) Bias-dependent PL of neat PIPCP films, excited at 633 nm.

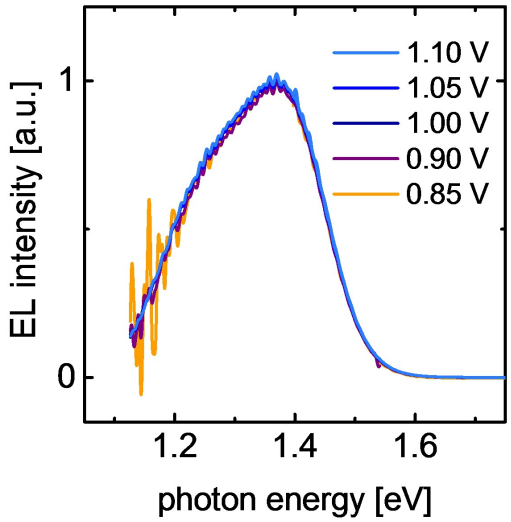

Figure 4.7: Normalized EL spectra of PIPCP:$PC_{61}BM$ blend films with varying applied bias.

compared to the emission of the individual blend components.[24] However, the close proximity between the emission peaks of PIPCP and PIPCP:$PC_{61}BM$, and the large degree of overlap between the spectra make it difficult to determine with confidence whether this emission originates from the CT state or from PIPCP. In EL measurements opposite charges are injected from the respective electrodes, and are expected to recombine at the lowest energy states available, namely the CT state in most OPV blends. However, blends that have very small energetic offsets may sometimes have back-electron transfer from the CT state to an exciton singlet.

We confirm that the observed emission from PL of PIPCP:$PC_{61}BM$ is not from bulk PIPCP singlet states recombining geminately, by examining the bias-dependence of the PL. To do this, solar cell devices were excited from the glass/ITO side within the cathode electrode area by a laser excitation at 633 nm, while a bias was applied to the electrodes. PL spectra were collected at a forward bias of 0.5 V (below the threshold for EL), at 0 V, and at reverse bias of -1 V, -2 V, and -3 V. It is important to note that at the highest forward bias applied (0.5 V), no EL can be detected, confirming that the emission shown

in Figure 4.6b originates from PL due to absorption, not injected charges. As seen in Figure 4.6c, when the bias is varied from 0.5 V to -3.0 V, the PL is significantly quenched without changes to the spectral shape. If the emission observed by PL were solely due to singlet geminate recombination in the polymer bulk, an external field would have no effect on the PL intensity as the exciton is a charge neutral species. This is illustrated in Figure 4.6d, by similarly recording the bias-dependent PL of a neat PIPCP device with the same electrodes (ZnOx and MoOx/Ag) and thickness (100 nm) as the blend. If photoexcitation of PIPCP leads to CT state formation and/or free charge carriers, the presence of an applied electric field would induce dissociation of the CT state as well as prevent reformation of the CT state from free charges, therefore reducing the PL intensity.[23] The results in Figure 4.6 indicate that the emission observed from PIPCP:$PC_{61}BM$ blends is due to radiative recombination from CT state at the donor/acceptor interface or back-electron transfer from the CT state to a PIPCP singlet.

If the emission observed by PL and EL from the blend is purely CT state emission, this allows for a direct comparison between the emission of PIPCP singlet and the CT state in PIPCP:$PC_{61}BM$ blends. If the emission from the blend includes exciton recombination due to back-electron transfer, this suggests that the CT state and PIPCP singlet must be close enough in energy for the exciton to be thermally populated from the CT state. The CT state, as an interfacial state formed due to wave function overlap of the donor and acceptor orbitals, can be approximated as a state between the energy levels of $HOMO_D$ and $LUMO_A$. That an electron on the CT state ($LUMO_A$-$HOMO_D$) is able to undergo back-electron transfer to the singlet exciton ($LUMO_D$ $HOMO_D$) suggests that $LUMO_A$ is energetically close to $LUMO_D$. On the other hand, the observed PL quenching from PIPCP:$PC_{61}BM$ blend devices does suggest sufficient driving force for charge transfer (Figure 4.6b. Thus, either picture supports the close proximity between E_{CT} and E_g, and in fact emphasizes that PIPCP:$PC_{61}BM$ blends are able to achieve high solar cell

efficiencies with J_{SC} = 14.0±0.1 mA/cm^2 and FF = 51±2%, under conditions where many other blends lose photovoltaic response.[58, 144, 59, 39]

4.7 Esitamting E_g-E_{CT} using Marcus theory

If we take the view that emission from the blend is due to back-electron transfer from the CT state to PIPCP singlet states at the donor/acceptor interface, as has been observed for systems with low LUMO$_D$-LUMO$_A$ (or HOMO$_D$-HOMO$_A$) offsets,[58, 144] we can use the EL and EQE spectra for additional analysis. It is possible to fit equations originating from Marcus theory for absorption and emission (Equations 4.1 and 4.2, respectively) simultaneously, using the EQE and EL spectra of the blend devices, and from that extract the band gap of the emitting state.[29]

$$\sigma(E) = \frac{f}{E\sqrt{4\pi\lambda kT}} exp(\frac{-(E_{CT} + \lambda - E)^2}{4\lambda kT}) \tag{4.1}$$

$$I(E) = \frac{Ef}{\sqrt{4\pi\lambda kT}} exp(\frac{-(E_{CT} - \lambda - E)^2}{4\lambda kT}) \tag{4.2}$$

Specifically, one can fit the low-energy shoulder of the EL as the CT state shoulder, and the higher-energy peak as the PIPCP singlet peak. The result of the fits may thus provide an upper limit estimate for the energetic difference between E_g and E_{CT}, which comes out to be 50 meV (Figure 4.8). Here it is important to note that different techniques will probe the solar cells under different conditions. Using fits as done in Figure 4.8, the bandgap energy is defined as the mid-point between the absorption and emission spectra, corresponding to an estimation of band gap energies at maximum density of states (DOS). For this reason, the bandgap that is estimated by absorption spectroscopy and the value from the Marcus theory fits differ by a few tens of meV. Furthermore,

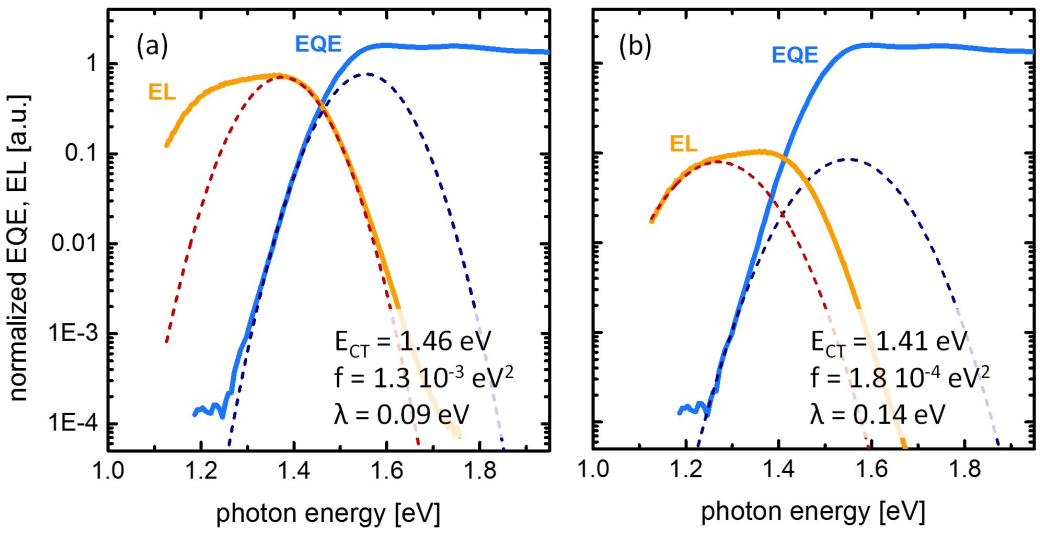

Figure 4.8: EQE and EL spectra of PIPCP:$PC_{61}BM$ devices on a log-lin scale, fit simultaneously with Equations 4.1 and 4.2 to the (a) high energy EL peak and the (b) low energy EL peak. The dashed lines are simultaneous fits using Equations 4.1 and 4.2.

since solar cell operation usually takes place at charge carrier densities that do not reach the maximum of the DOS, instead often estimated at 10^16 cm$^-3$,[151] the transport and charge transfer under solar cell operation will occur through the tail of the density of states (DOS) distribution.

One explanation for the high solar cell efficiency in PIPCP:$PC_{61}BM$ despite the very low energetic offsets estimated by the EQE an EL fits could be a broader DOS distribution of the CT state compared to the DOS of PIPCP. While PIPCP in the blend may be highly ordered, as is suggested by the red-shifted absorption of the blend, the CT state is composed of orbital overlap between the two blend components and is thus affected by disorder originating from both phases. Thus, although E_{CT} and E_g may not be very different in energy at maximum DOS, the tail states of the PIPCP singlet can be higher in energy than the tail states of the CT state, and this alone may provide enough driving force for charge transfer and generation.

4.8 The DOS distribution in PIPCP:$PC_{61}BM$

To better understand the DOS broadening in PIPCP blends one can refer back to the absorption measurements shown in Figure 4.5. Franz Urbach reported on an exponential dependence of the optical transitions of AgBr crystals at long wavelengths.[155] This behavior was later demonstrated on other classes of materials, and became known as the Urbach rule.[156] The absorption described by the Urbach rule includes a fit parameter called the Urbach energy (E_U), which in the case of disordered semiconductors has been related to DOS tails in the gap.[157] E_U is a function of temperature, structural and energetic disorder, and thus of the DOS broadening, and can be extracted from the dependence of absorption on photon energies below the band-edge of a semiconductor as measured by sensitive techniques such as PDS and EQE.[158] The relationship between E_U and absorption is shown in Equation 4.3, where E is the photon energy, α_0 and E_0 are constants.

$$\alpha(E) = a_0 exp(\frac{E - E_0}{E_u}) \tag{4.3}$$

From a fit to the PDS and EQE spectra, PIPCP has an Urbach energy close to thermal energy, at 27 meV, both in the neat and blend films, where thermal energy, kT = 25 meV, sets the lower limit for energetic order. For comparison, Venkateshvaran *et al.* recently reported on a series of semiconducting polymers, most with Urbach energies on the order of 40 meV or higher, but one with an indacenodithiophene-co-benzothiadiazole (IDTBT) backbone that demonstrated a very sharp Urbach tail that reached E_U below kT as well as low disorder by field effect transistor parameters.[159] Simulations of the conformation that IDTBT adopts when crystalline, amorphous, and disordered suggest the polymer is able to retain a near-planar backbone conformation in all cases, and maintain a narrow DOS. As suggested by Venkateshvaran *et al.*, it may be that the conjugated IDT unit,

present both in IDTBT and regioregular PIPCP adds resilience to torsional deformations of the backbone, thus reducing DOS broadening from structural disorder.

For another measure of the electronic ordering of PIPCP when in the neat and blend films we referred to Kelvin probe measurements. Kelvin probe is a technique that measures the contact potential difference between a calibrated tip and a film of interest, from which one can extract the work function or Fermi level of the sample.[160] Due to charge diffusion from Ohmic contacts, organic semiconductors exhibit band bending, which manifests as a shift in the measured Fermi level as a function of film thickness. Band bending can be related to the width of the DOS, and thus the energetic disorder in the film. When the active layer is cast on a high work function electrode, band bending occurs due to the transfer of holes into the HOMO, and similarly when the active layer is cast on a low work function electrode, band bending results from electron transfer into the LUMO. Using the relationship between band bending and film thickness from the model of charge transfer into a DOS, the energetic disorder can be extracted by means of an analytical expression derived by Ottinger, *et al.*

$$d = \sqrt{\frac{2E_t\epsilon_r\epsilon_0}{q^2N_r}}exp(\frac{|V(d)-V(0)|}{2E_t}) \times arccos[exp(\frac{-|V(d)-V(0)|}{2E_t})] \tag{4.4}$$

In this expression, the shape of the DOS tail is represented by an exponential function with disorder parameter E_t, and maximum DOS value N_t, while d is the film thickness, *V(d)* is the Fermi level of the film at a thickness d, and *V(0)* is the Fermi level of the film at d=0 nm.

PIPCP and PIPCP:$PC_{61}BM$ films were cast on MoOx and Al electrodes with a range of thicknesses, and the Fermi level for each film thickness on the respective electrode was measured. The results from these studies are shown in Figure 4.9. Both PIPCP and PIPCP:$PC_{61}BM$ show the expected change in Fermi level with film thickness and

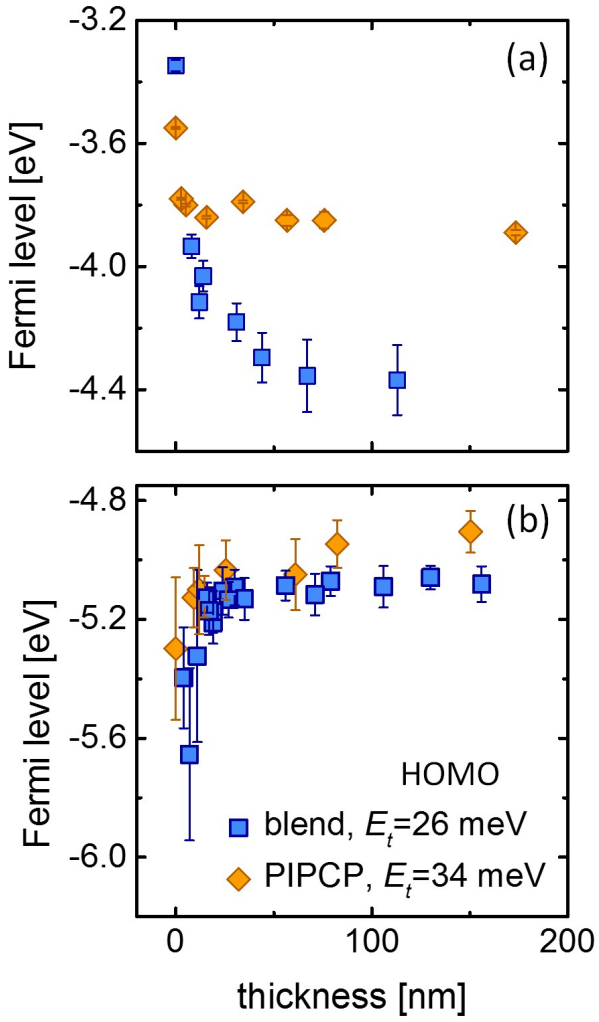

Figure 4.9: Band bending profiles of PIPCP:$PC_{61}BM$ and neat PIPCP as measured by Kelvin probe on films with varying thicknesses for (a) films cast on Al for the LUMO and (b) films cast on MoOx for the HOMO. The disorder values, E_t, are extracted for blend and neat films from fits using Equation 4.4.

an eventual plateau. The Fermi level of the HOMO of PIPCP:$PC_{61}BM$ (Figure 4.9b), as well as the Fermi level of the LUMO of PIPCP (Figure 4.9a), both have a particularly sharp plateau at small thicknesses. Previous reports have shown that it is difficult to obtain complete fits to the band bending profile when E_t is below 30 meV, but a quick plateau of the Fermi level at thicknesses of 10-20 nm, as is the case here, is a signature of a highly ordered film.[161]

Since charge transfer occurs only when energetically favorable to the lowest available states, it is expected that the band bending of the blend films on MoOx give a measure of the PIPCP $HOMO_D$ disorder in the blend film, and similarly that the band bending of the blend on Al give a measure of $LUMO_A$.[151] Using Equation 4.4 to fit the data, disorder values of 34 meV and 26 meV were obtained for the HOMO of neat PIPCP and PIPCP:$PC_{61}BM$, respectively. Along with the E_U and a disorder value of 26 meV for the blend $HOMO_D$, we deduce that the $LUMO_D$ of PIPCP in the blend is also highly energetically ordered. These considerations, along with the E_U, are consistent with PIPCP having exceptionally low energetic disorder and a narrow DOS.

4.9 Energetic offsets in PIPCP:$PC_{61}BM$ under solar cell operation

The Kelvin probe data for thick films can also be used to estimate the LUMO level of PIPCP and $PC_{61}BM$ in the blend, which is of particular interest given the discussion above about the low driving force for charge generation in this system. Neat PIPCP films on Al plateau at a Fermi level of 3.89 eV, while the $LUMO_A$ in the blend plateaus at 4.36 eV (Figure 4.9a). From absorption spectroscopy, E_g of PIPCP is reduced by 60 meV, which should be taken into account when estimating the $LUMO_D$ of PIPCP in

the blend. As seen in Figure 4.9b, the $HOMO_D$ of PIPCP deepens upon blending with $PC_{61}BM$, from -4.91 eV to -5.07 eV. Accounting for the reduction in the bandgap and the deeper PIPCP $HOMO_D$ in the blend, we estimate the PIPCP $LUMO_D$ in the blend, in the dark, at -4.11 eV. This analysis thus provides an estimate for the difference between the $LUMO_D$ of PIPCP and $LUMO_A$ of $PC_{61}BM$, in situ in the blend films, to be 260 meV.

Thus far we have shown that the difference in $LUMO_D$ $LUMO_A$ by Kelvin probe is 260 meV, while the difference by the EL/EQE fits is only 50 meV. This is because the energy level extracted by EL/EQE fits corresponds to a charge carrier density at maximum DOS, which we will assume to be 10^{20} cm^{-3},[162] while Kelvin probe measurements, performed in the dark, correspond to a much lower charge carrier density, which we will assume to be on the order of 10^{14}-10^{15} cm^{-3}.[151] If we assume that the Fermi level is exponentially dependent on charge carrier density, we can interpolate to get an estimate of the $LUMO_D$ $LUMO_A$ offset at a charge carrier density of 10^{16}-10^{17} cm^{-3}, corresponding to devices at 1 sun illumination.[151] Applying this analysis, we arrive at a $LUMO_D$ $LUMO_A$ offset of 150-190 meV under 1 sun. This offset between the tail states of the $LUMO_D$ and $LUMO_A$ may be the reason that PIPCP:$PC_{61}BM$ solar cells are able to perform so well, despite the very close proximity between E_{CT} and E_g.

4.10 V_{OC} *vs.* the J_{SC} and the *FF*

An important question that can be raised in light of these results is whether there exists a trade-off between maximizing the V_{OC} and the yield of photogenerated charges. This has been a central question in many studies, but to date there is no consensus on the topic.[17] PIPCP:$PC_{61}BM$ solar cells are pushing the limits of photogeneration in light of low energetic differences as a driving force for charge separation, clearly illustrated also

by Li *et al.*[142] It should be emphasized here that when compared to many other blends with similar energetic offsets, PIPCP:$PC_{61}BM$ blends have a high photogeneration yield with a $J_{SC} = 14.0 \pm 0.1$ mA/cm^2. However, the maximum EQE value for PIPCP:$PC_{61}BM$ solar cells is 62%, which is lower than the highest performing blends. Similarly, the *FF* of PIPCP:$PC_{61}BM$ remains low at $FF = 51 \pm 2$ % despite many attempts at device optimization, which may point at issues of field-dependence of generation.

4.11 Conclusions and outlook

In summary, PIPCP is able to achieve very low losses from photon absorption (E_g) to V_{OC}, with $E_{loss} = 0.52 \pm 0.02$eV. E_{CT} and E_g appear to be nearly equal in energy, suggesting that PIPCP:$PC_{61}BM$ BHJs have eliminated losses from photon absorption to charge transfer, other than the relatively small offset between $LUMO_D$ and $LUMO_A$ tail states. Evidence of high morphological order in the PIPCP:$PC_{61}BM$ films, a low Urbach energy, and low energetic disorder by Kevlin probe, suggest that reducing disorder (energetic and morphological) can allow for minimized voltage losses, as has been proposed by recent theoretical contributions.[141] Using Klelvin probe measurements, the proximity between E_{CT} and E_g, and the assumed charge carrier densities, we estimated the offset between the $LUMO_D$-$LUMO_A$ tails for charge transfer in PIPCP:$PC_{61}BM$ to be 150-190 meV. Furthermore, if E_{CT} is estimated by the E_g of PIPCP in the blend (1.41 ± 0.01 eV), then also E_{CT} $V_{OC} = 0.52 \pm 0.02$eV, which is slightly lower than the typical empirical relationship between E_{CT} and V_{OC}. While the high energetic and morphological order observed in PIPCP:$PC_{61}BM$ may facilitate achieving low voltage losses from photon absorption to E_{CT}, further work is necessary to understand and reduce losses from E_{CT} to V_{OC} in order to approach thermodynamic limits of efficiency in organic solar cells. Finally, our results suggest that by the use of polymers with high energetic order, the

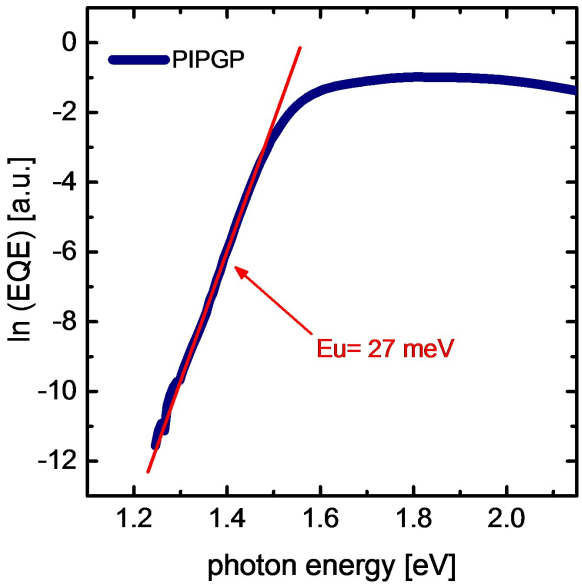

Figure 4.10: ELow energy EQE spectrum of PIPGP:$PC_{61}BM$, with a fit to the tail to extract the Urbach energy.

necessity of an appreciable energetic offset in OPV devices for high PCEs may need to be reconsidered and that high V_{OC} values can be achieved in organic solar cells. There may be more potential to organic solar cells than had been assumed in the past.

4.12 Effects of molecular modifications: notes and unanswered questions

4.12.1 PIPGP and Urbach energy

Dr. Ming Wang synthesized a very similar analog to PIPCP: PIPGP, where the carbon bridge is replaced with a Germinium bridge. This modification has been done in the past, and generally results in improved performance. While in this caes the Ge substitution did not improve solar cell performance, we recorded the EQE sepctra for the device to see if the modification of the carbon bridge altered the sub-bandgap region.

As shown in Figure 4.10, the low-energy tail of PiPGP retains the high energetic order reported for PIPCP, with an Urbach energy of 27 meV. The bridge atom substitution does not seem to affect the energetic order of the overall molecule.

4.12.2 PT to FBT, and IDT to SiIDT: charge transfer state and energy loss

Dr. Jianyu Yuan synthesized four polymer derivatives of PIPCP. First, he substituted the PT in PIPCP to an FBT unit. Then, in two of the polymers Jianyu also altered the solubilizing chains of PIPCP to reduce the bulkyness: he changed the IDT group into an SiIDT group. Here, we will talk about PIFCF (PT to FBT substitution) and PSFCF (PT to FBT, and IDT to SiIDT substitution).

The E_{loss} in PIPCP:$PC_{61}BM$ (E_{loss} with PIPCP:$PC_{71}BM$ is similar) is among the lowest obtained for a solar cell blend system that can achieve a PCE ¿ 6%. The analysis on PIPCP:$PC_{61}BM$ revealed that the E_{CT} and polymer singlet are very close in energy, differing only by 50 meV, thereby reducing potential losses associated with charge transfer.6b However, as is shown in Table 2, the E_{loss} values of both PIFCF and PSFCF solar cells are significantly higher than what was achieved with PIPCP. In order to address this critical difference in performance, we therefore examine the impact of chemical structure on E_{CT} and thereby probe its relationship to qV_{OC}.

As noted, it has been demonstrated on number photovoltaic blend systems that the V_{OC} is tracks linearly with the E_{CT}, according to E_{CT} e$V_{OC} = 0.6 \pm 0.1$ eV. Therefore, to decouple the source of the larger E_{loss} in the FBT polymers, we determined the E_{CT} of for the polymers blended with $PC_{71}BM$ solar cells studied here. We determined E_{CT} using Marcus theory equations for absorption (Equation 4.1) and emission (Equation 4.2), fit simultaneously to EQE and EL spectra collected from working solar cell devices.As was

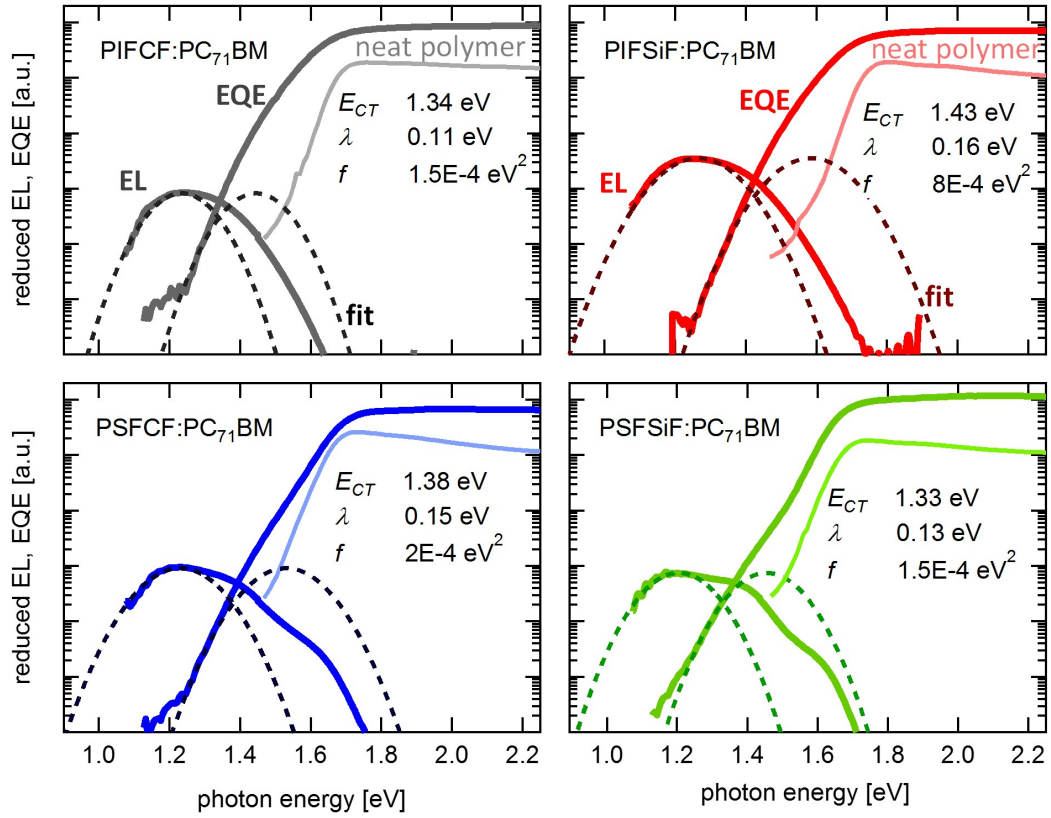

Figure 4.11: EQE and EL spectra of PIPCP analogs: PIFCF, PIFSiF, PSFCF, and PSFSiF blended with $PC_{71}BM$. The dashed lines are simultaneous fits using Equations 4.1 and 4.2 fit to the low-energy tail of the EQE and low-energy peak of the EL. The light-colored spectra are the EQE response of the neat polymer. The obtained fit parameters are reported for each blend.

the case in PIPCP, it is paramount that the fitting to obtain E_{CT} is done on both the EQE and the EL, instead of only the EQE, in order to reduce the degrees of freedom in the fits.

For reference, the EQE of the neat polymers are also provided in the figure. It is paramount that the fitting to obtain E_{CT} is done on both the EQE and the EL, instead of only the EQE, in order to reduce the degrees of freedom in the fits. The E_{CT} values obtained by this analysis are summarized in the Table 4.1.

Examination of Figure 4.11 reveals that PIFCF shows significant charge generation

at energies that are well below the EQE response of the neat polymer, while the characteristic signature of the CT state is absent. This resembles the EQE of PIPCP:$PC_{61}BM$, which also shows significant charge generation at sub-bandgap energies, and no obvious CT state shoulder to the EQE. However, the E_{loss} of PIFCF-based solar cells (0.82 eV) is much higher than the E_{loss} of PIPCP:$PC_{61}BM$ solar cells (0.52 eV). The reason the E_{loss} in PIFCF-based solar cells is greater lies in E_g-E_{CT} = 0.31 eV, compared to E_g-E_{CT} = 0.05 eV in PIPCP-based solar cells (see Table 4.1). This increased loss due to E_g-E_{CT} correlates well with the shallow LUMO level of PIFCF compared to PIPCP (-3.55 vs. -3.79 eV). The difference between E_g-E_{CT} of PIPCP and PIFCF is also predicted using density functional theory calculations, as will be elaborated below.

It is interesting to note that the E_{CT}-qV_{OC} of PIPCP- and PIFCF-based solar cells is very low, at 0.51 eV for both. This may suggest of a relationship between the molecular structure similarities between PIPCP and PIFCF, and low voltage losses from E_{CT}-qV_{OC}. However, further modifications to the structure are necessary, since both PIFCF and PIPCP have a low FF. In PIFCF:PC71BM solar cells it is unlikely that the FF is low due to insufficient energetic offsets, as may be suggested in the case of PIPCP:$PC_{61}BM$ solar cells, given the increased LUMO of PIFCF. Instead, the issue may lie in factors such as charge transport, morphology, etc.

In contrast to PIPCP and PIFCF, PSFCF shows EQE spectra that track in shape the EQE response of the neat polymer and exhibits a clear (albeit small) shoulder in the low energy regime, which is characteristic of CT state contribution. Nonetheless, PSFCF solar cells also have a larger E_{loss} (0.78 eV) when compared to PIPCP solar cells (0.51 eV). The larger E_{loss} in PSFCF solar cells is a result of a larger E_g-E_{CT}=0.19 eV, as well as a larger E_{CT}-qV_{OC}=0.59 eV. The LUMO of PSFCF (-3.59 eV) is more shallow compared to PIPCP (-3.79 eV), correlating, as may be expected, with the E_g-E_{CT} differences. However, it is not currently understood what factors control the loss

Table 4.1: Energy levels of the polymer:fullerene BHJ solar cells.

Polymer	E_g [eV]	qV_{OC} [eV]	E_{CT} [eV]	E_{loss} [eV]	E_g - E_{CT} [eV]	E_{CT} - qV_{OC} [eV]
PIPCP	1.41	0.89	1.40	0.52	0.05	0.51
PIFCF	1.65	0.83	1.34	0.82	0.31	0.51
PSFCF	1.57	0.79	1.38	0.78	0.19	0.59

from E_{CT}-qV_{OC}.

Table 4.1 summarizes the obtained E_{CT} values and their relation to E_g and V_{OC}. It is clear that the large E_{loss} (0.78 - 0.82 eV) in the FBT analogues compared to the E_{loss} of PIPCP (0.52 eV), originates in part from a large E_g - E_{CT} (0.19 - 0.31 eV). The FBT analogues lose more potential in the process of electron transfer between the donor and acceptor, thus increasing E_g - qV_{OC}. Interestingly, the greater E_g - E_{CT} values in FBT analogues relative to PIPCP are approximatively consistent with the their LUMO level changes, which is a translation of the LUMO influence on the E_{loss}. Small LUMO-LUMO offsets between the donor materials and fullerene acceptors might potentially induce small E_g - E_{CT} values, which is important in recent low E_{loss} systems.

While it may be tempting to tie the results in Table 4.1 back to the superior PCE of PSFCF relative to PIFCF, it is evident that energy levels alone cannot account for the difference. PSFCF-based solar cells have superior FF and J_{sc} values compared to PIFCF-based solar cells. As is illustrated by E_g - E_{CT} in Table 4.1, this is not due to a superior driving force for charge transfer in PSFCF. Instead, the key for the enhanced FF and J_sc may lie in the improved charge carrier mobility of PSFCF (which may improve extraction vs. bimolecular recombination) or perhaps morphological details such as phase separation and phase purity (which may affect charge generation vs. geminate recombination, as well as transport). Indeed, the hole mobility of PSFCF is significantly higher than that of PIFCF and PIPCP. It may be that the phenyl groups connecting the

solubilizing chains to the IDT units in PIFCF and PIPCP disrupt close $\pi - \pi$ reducing favorable intermolecular interactions for charge transport.

4.13 Methods and experimental

PIPCP was synthesized as reported previously.[153] All films were prepared as follows: neat PIPCP samples were cast from solutions of 8 mg/mL in 4:6 v/v chlorobenzene:chloroform, and the blend films were deposited from a 1:2 PIPCP:$PC_{61}BM$ w/w solution with a total solids concentration of 18 mg/mL, in 4:6 v/v chlorobenzene:chloroform. The device structure for both neat and blend devices was ITO/ZnOx (35 nm)/active layer/MoOx (6 nm)/Ag (80 nm). These conditions lead to the following device characteristics: $V_{OC} = 0.89 \pm 0.01$ V, $J_{SC} = 14.0 \pm 0.1$ mA/cm^2, FF = 51±2%, PCE = 6.4±0.3%, which are a slight improvement over the original report, see Figure 4.3.

4.13.1 Daevice preparation

All solar cell devices fabricated had an inverted structure. 35 nm ZnOx films were cast on ITO-sputtered glass substrates, and annealed at 200 °C in air for 20 minutes. ZnOx was prepared according to the sol-gel method, as described by Sun *et al.*[42] PIPCP:$PC_{61}BM$ or PIPCP films were cast on ZnOx films at a spin speed of 2000 RPM to avhieve a thickness of about 100 nm, unless otherwise specified. Top contacts of MoOx (6 nm)/Ag (100 nm) contacts were thermally evaporated to complete the devices. For luminescence measurements, which are done in air, devices were encapsulated with epoxy and a glass slide.

4.13.2 Luminescence:

PL and EL spectra were collected with a silicon CCD array detector cooled to -70 °C. Emission from the devices was aligned to the CCD entrance slit with a series of focusing lenses. EL measurements were performed by applying a small forward bias to solar cells. PL measurements were done on the same device using a HeNe laser with an excitation at 633 nm. Bias-dependent PL is accomplished by exciting the film from the glass side, in an area underneath the MoOx/Ag anode, while simultaneously applying a bias to the electrodes. All emission spectra were corrected for detector sensitivity with a black body spectrum.

4.13.3 Kelvin probe:

For Kelvin probe measurements films of PIPCP and PIPCP:$PC_{61}BM$ were cast on ITO/(70 nm) MoOx. Solutions of varying concentrations were used to cast films with a range of thicknesses. Contact potential difference (CPD) values were measured with an SKP 5050 (KP Technology, UK) Kelvin probe with a stainless steel tip 2 mm in diameter. The probe work function was calibrated against freshly cleaved HOPG, which was assumed to have a work function of 4.6 eV.[43] All measurements were done under inert conditions.

4.13.4 External quantum efficiency

External quantum efficiency (EQE) for all solar cells was measured using a 75 W Xe light source, monochromator, optical chopper, and a lock-in amplifier. Power-density calibration of the EQE characteristics was achieved using a calibrated National Institute of Standards and Technology silicon photodiode. For the sub-bandgap EQE, higher sensitivity settings were used with a longer time delay between measurement points.

4.13.5 Transmission electron micrsocopy

TEM samples were prepared casting an active layer of PIPCP or PIPCP:$PC_{61}BM$ on PEDOT:PSS, and floating pieces of the film on DI water. Film pieces were transferred to the TEM grids and allowed to dry overnight. High resolution images were taken on an FEI Titan FEG High Resolution microscope. The TEM images were collected using a low-dose electron beam (spot size 6) to avoid damaging the samples, and a small defocus to enhance the contrast between PIPCP and $PC_{61}BM$.

4.13.6 Photothermal deflection spectroscopy

PDS is a scatter-free surface sensitive absorption measurement capable of measuring 5-6 orders of magnitude weaker absorbance than the band edge absorption. For the measurements, a monochromatic Pump light beam is shined on the sample (film on Quartz substrate), which on absorption produces a thermal gradient near the sample surface via nonradiative-relaxation-induced heating. This results in a refractive index gradient in the area surrounding the sample surface. This refractive index gradient is further enhanced by immersing the sample in an inert liquid FC-72 Fluorinert (3M Company) which has a high refractive index change per unit change in temperature. A fixed wavelength CW laser probe beam is passed through this refractive index gradient producing a deflection proportional to the absorbed light at that particular wavelength, which is detected by a photo-diode and lockin amplifier combination. Scanning through different wavelengths gives us the complete absorption spectra. Because this technique makes use of the non-radiative relaxation processes in the sample, it is immune to optical effects like interference and scattering.

Chapter 5

Charge Generation and Recombination in an Organic Solar Cell with Low Energetic Offsets

I don't know anything, but I do know that everytying
is interesting if you go into it deeply enough.
– Richard Feynman

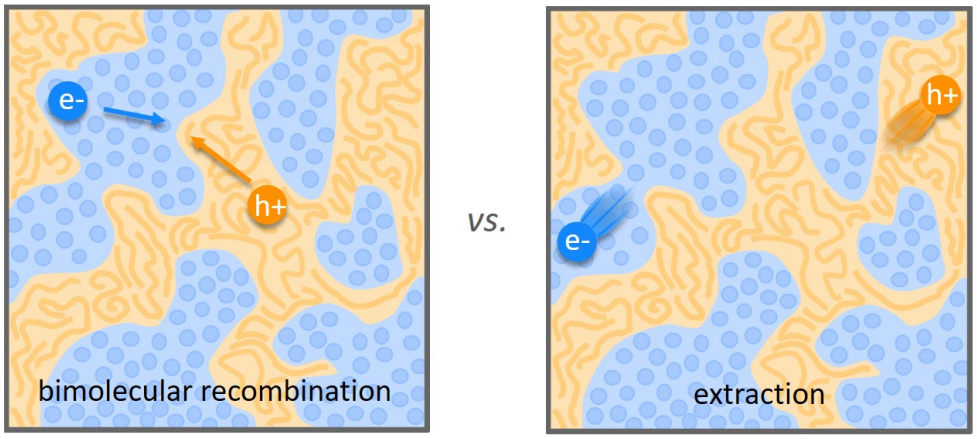

5.1 Preface

This chapter is the continuation of the work of Chapter 5. Initially, the plan was for Jack to write the paper on the low FF in PIPCP, but Jack has since graduated and since I have been so involved with PIPCP, I continued to research it. Through the MURI that we are involved with and the enthusiasm of the program officer, and through the responses to conference presentations that Quyen has given, it became evident that PIPCP:$PC_{61}BM$ is a system that many people are interested in. Since publishing the first PIPCP paper on the low potential losses, it has become very "hot" to discuss and study the topic of V_{OC} losses, and in particular to focus on systems that have low V_{OC} losses. This new focus in the field is not necessarily due to the publication of the PIPCP V_{OC} paper, as it appears many people were already thinking in that direction, but it was certainly good timing to get the paper out as everyone was getting more interested in the topic. The question that was always on our mind, from the onset of working on PIPCP, was why the FF remained so perpetually low. Admittedly, this was also one of the questions the reviewers of the PIPCP V_{OC} paper asked us to comment on. Furthermore, a few other "low V_{OC} loss" systems reported in the literature have low FF values. It may be that we have pushed the $LUMO_D/LUMO_A$ offset too close, and we are beginning to lose the beneficial thermodynamic driving force for charge generation that the donor/acceptor heterojunction was meant to solve in the first place.

During the time that I started working on understanding the recombination losses in PIPCP:$PC_{61}BM$, we were running into many issues with device fabrication- all our PIPCP devices (made in an inverted structure), were coming out short, and with V_{OC}, J_{SC}, and FF values that were far lower than they should have been. Michael Hughes was my partner in armor in trying to figure this out. We spent perhaps a month or so, getting very frustrating, inconsistent results, leading to no advancements. At the same

time, our evaporator malfunctioned (turns out the cryo-pump needed to be rebuilt), and so we were operating with the 'old evaporator.' Given the push of time to get results and publish this work, I got in touch with Hengbin Wang, a scientist working for Mitsubishi Chemical at UCSB (as part of the Mitsubishi Chemical Center for Advanced Materials), who had originally worked on PIPCP when Ming synthesized it. Hengbin was so kind as to agree to help us out and make devices as we needed them, and has since made a large number of batches for us to do a range of tests and reproduce those tests. It has been such a pleasure to work with Hengbin, and I really appreciate his willingness to help and fabricate devices whenever we needed them.

Michael Hughes was a first-year student when Jack was working on measuring the mobility and then trying to improve it using nucleating agents. Since Jack was training Michael, Michael's first project (or second?) was the mobility study using DMDBS. I should note, that the inspiration to use DMDBS in this system is based on the work by Alex Sharenko, in reference [163]. However, as mentioned, Michael was my partner in frustration when we tried to fabricated good devices unsuccessfully, but moreover, Michael has also always been very enthusiastic to jump up and do small measurements (like obtain the absorption spectrum of $PC_{61}BM$) if he wasn't otherwise very busy. Jack, while having done the DMDBS study, also got involved in this study of PIPCP from another angle: this time, as a post-doc in Dieter Neher's group in Potsdam. There, Jack has been studying the recombination behavior in PIPCP:$PC_{61}BM$ using the specialized instruments the Neher group is known for. Here we are showing the basic TDCF results Jack collected, but there are more nuanced and interesting results to come form them as a separate study. During the last few months when Viktor Brus was a post-doc in our lab, Viktor (with the help of Alexander Mikhailovsky), built an open-circuit voltage decay (OCVD) setup which we use in this chapter to study recombination. Viktor and I took the first OCVD scan of PIPCP:$PC_{61}BM$ solar cell devices. During his time here Viktor

also infected the lab with the gift of impedance spectroscopy, which has spawned the project that Michael (Hughes) is working on for his PhD, and an integral part to gain information about the recombination coefficient from the OCVD setup. Mike Heiber, who is also doing a post-doc with us, has taken the OCVD/impedance combination, upgraded the hardware and the method, to focus on studying recombination dynamics in many solar cell systems. It has taken time, understanding, and innovation on Mike's part, but he's taken it now to the next level. Mike did the full analysis of recombination in PIPCP:$PC_{61}BM$, having to go through a number of iterations of measurements to learn how to do it and trust his results (since especially with impedance you have to know precisely what you're doing).

One of the questions that has remained unanswered about PIPCP:$PC_{61}BM$ is a good understanding of the morphology of the blend. To answer this, Quyen got in touch with Prof. Harald Ade in North Carolina, to invite him to collaborate with us. Quyen has a great skill at identifying when a collaboration would be helpful, and making it happen very quickly. Harald was indeed interested to collaborate, and set his student Xuechen Jiao to do STXM and RSoXS measurements on PIPCP:$PC_{61}BM$. Xuechen and Harald have been gracious in explaining and answering our questions about the techniques and the samples that we should make. The RSoXS data and χ calculations here were done by Xuechen. Around this time, Ben Luginbuhl got involved in the project as well, as he helped me prepare some of the samples we sent to Xuechen to measure. There should be another manuscript from Harald's group, with a more in-depth study of the morphology and self-assembly of PIPCP and $PC_{61}BM$. During this time, Quyen suggested that Akchheta do some pc-AFM of PIPCP:$PC_{61}BM$ blend films- the results of the regular films are shown here. She also did pcAFM of films that were solvent annealed, and processed with DMDBS, which are not shown here. Finally, Bernard Kippelen's group has also studied PIPCP, using different electrodes. Their results also

agree with our light-intensity results, showing that the FF does not improve with lower light intensities. Bernard was also so kind as to offer us thorough comments on the manuscript we put together based on this work.

This chapter is the result of a collaborative effort by: myself, Michael Hughes, Dr. Michael Heiber,Dr. John Love, Xuechen Jiao, Akchheta Karki, Dr. Hengbin Wang, Dr. Ming Wang, Dr. Viktor Brus, Prof. Dieter Neher, Prof. Harald Ade,Prof. Gui Bazan, and Prof. Thuc-Quyen Nguyen.

5.2 Introduction

Studies on organic bulk heterojunction (BHJ) photovoltaics (OPV) have suggested that if the energetic offset is below 100-300 meV, the efficiency of charge generation and extraction is severely diminished, resulting in decreased short circuit currents (J_{SC}) and fill factors (FF). However, a number of groups have recently reported BHJ blends that are pushing at the accepted limits of energetic offsets necessary for efficient solar cell devices.[117, 164, 165, 35, 142] Active layers with low energetic offsets are desirable in order to achieve solar cells with high open circuit voltages (V_{OC}). However, many of these blends are only able to achieve modest FF values.[165, 35, 142]

The FF is among the three parameters used to assess the power conversion efficiency (PCE) of solar cells, and provides insight into the efficiency of charge generation and collection across the operating voltages of the solar cell. In the absence of charge recombination losses, the FF is only limited by the series and shunt (parallel) resistances in the solar cell device,[166] as is the case for inorganic solar cells where the FF can achieve values above 80%. However, in OPVs charge generation and extraction are known to be hindered by geminate and/or bimolecular charge recombination losses, and thus the FF of OPVs is often lower.[127] As a consequence of these recombination losses, the

FF in organic solar cell has been described as a field-dependent competition between charge extraction and charge recombination.[127, 167, 168] It is notable, however, that in recent years there have been a number of reports of organic solar cells that achieve very impressive *FF* values, approaching 80%.[169, 170, 171, 13, 172, 172, 173]

Although a simplified description, the V_{OC} and the J_{SC} are determined by the hole and electron quasi-Fermi level separation, and the efficiency of the solar cell to absorb photons and generate photocurrent under the internal field of the device (also described by the external quantum efficiency, EQE), respectively. Recently we have introduced a low-bandgap regioregular polymer, PIPCP (Figure 5.1a), that can achieve a high V_{OC} in BHJ solar cells when blended with the electron acceptor $PC_{61}BM$.[153] PIPCP contains a backbone comprised of CPDT-PT-IDT-PT repeat units (CPDT=cyclopentadithiophene, PT=pyridyl[2,1,3]thiadiazole, IDT=indacenodithiophene) and strictly organized PT orientations, such that the pyridyl N-atoms point toward the CPDT fragment. The energy loss, E_{loss}, defined as the difference between the polymer bandgap and the V_{OC}, E_{loss} = E_g qV_{OC}, was determined to be among the lowest losses reported in the literature (0.52 eV), for a system with a PCE ¿ 6%. The low E_{loss} was attributed to a minimal offset between the E_g and the charge transfer (CT) state energy (E_{CT}), E_g - E_{CT} ¡ 50 meV. However, the *FF* of PIPCP:$PC_{61}BM$ BHJs has remained low, at ≈54%, despite multiple attempts at device optimization.[35] Given that this blend system is pushing the accepted limits of operational OPVs,[142] we asked: why is the *FF* in PIPCP:$PC_{61}BM$ low and whether this is a direct consequence of the low energetic offset? Answering this question has fundamental importance for the field of organic photovoltaics, as we need to simultaneously maximize all parameters that determine the PCE.

Figure 5.1 sshows a characteristic current-voltage (J-V) curve for a PIPCP:$PC_{61}BM$ BHJ solar cell under 1 sun illumination shows a high V_{OC}=0.89 V but limited *FF*=54%. The low *FF* denotes that as the field across the active layer decreases (i.e. the applied

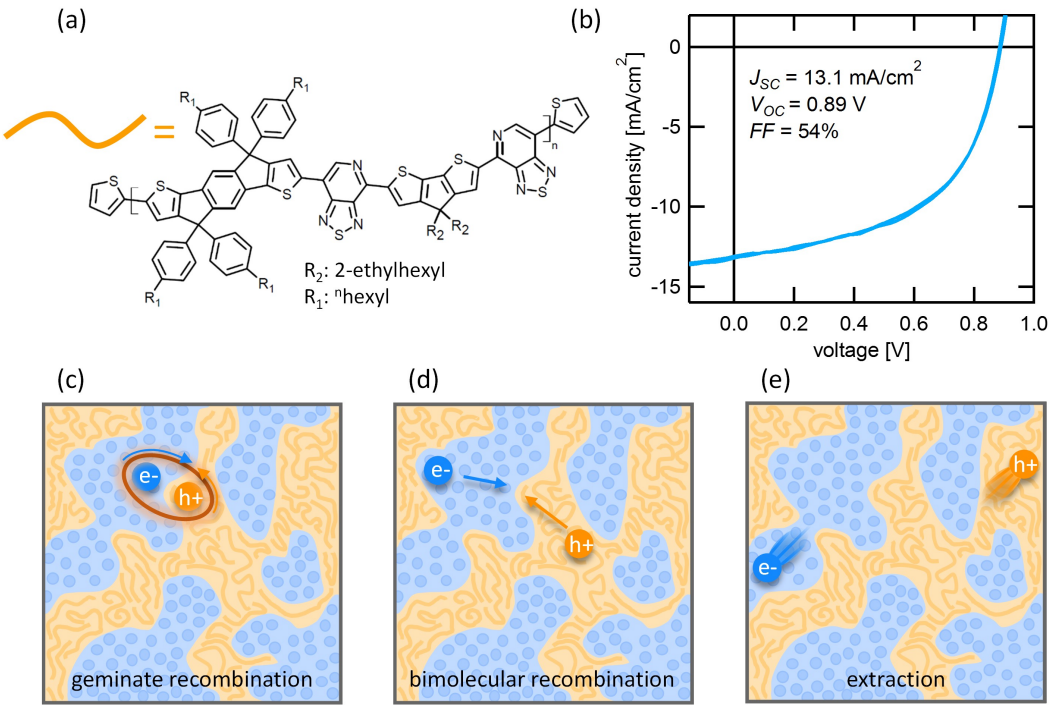

Figure 5.1: (a) The molecular structure of PIPCP. (b) Representative J-V of PIPCP:$PC_{61}BM$ solar cells under 1-sun illumination. Cartoon representation of (c) geminate recombination, (d) bimolecular recombination, and (e) extraction.

bias approaches V_{OC}), the balance between charge recombination and charge extraction shifts towards recombination losses. It has been suggested that the low energetic driving force for charge separation in PIPCP:$PC_{61}BM$ may give rise to field-dependent generation, thus reducing the *FF*.[35] On the other hand, Menke *et al.* have shown that PIPCP:$PC_{61}BM$ blends are characterized by fast triplet formation. Triplet recombination can thus lead to poor charge extraction (bimolecular recombination).[174] As described below, we now explore the possible effects of contact limitations, report new insights on the blend morphology,[35] and determine the contributions of geminate recombination, bimolecular recombination, temperature and charge transport in the limited performance of PIPCP:$PC_{61}BM$. Geminate recombination, bimolecular recombination, and charge extraction are schematically represented in Figure 5.1c-e.

5.3 Contact limitations

Non-Ohmic contacts may cause a reduced electric field and space-charge buildup, which would lead to increased charge recombination.[175, 176, 177, 178] To ensure that the *FF* in PIPCP:$PC_{61}BM$ solar cells is not limited by extraction barriers at the contacts or by the need for hole/electron transport interlayers, we fabricated PIPCP:$PC_{61}BM$ solar cells with various device architectures. Inverted solar cells were fabricated with zinc oxide and PEIE as the bottom contact (cathode), and silver-caped molybdenum oxide as the top contact (anode). Regular solar cells were fabricated with PEDOT:PSS and molybdenum oxide as the bottom contacts (anode), topped with calcium, lithium fluoride, and bathocuporoine capped with aluminum. Despite the various architectures, there was no improvement in device performance. The *FF* in PIPCP:$PC_{61}BM$ does not seem to be limited due to contact barriers, though dark carriers diffusing from the contacts may have an effect on the performance, as will be discussed below in the section

about bimolecular recombination.

5.4 The morphology of PIPCP:$PC_{61}BM$ and consequent changes in energy levels

Achieving an optimal BHJ morphology is critical for high device performance. For this reason, we begin with a characterization of the morphology in PIPCP:$PC_{61}BM$. Specifically, we sought to understand the mixing between PIPCP and $PC_{61}BM$ BHJ films. The morphology of PIPCP:$PC_{61}BM$ was investigated using resonant soft x-ray scattering (RSoXS) and photoconductive atomic force microscopy (pc-AFM). If film thickness is uniform, the scattering contrast in RSoXS results from separate material domains due to differences in the complex index of refraction at a specific photon energy.[179] Soft x-rays used in RSoXS are particularly well-suited for the absorption of elements such as C, N, etc., which are prevalent in organic semiconductors. RSoXS can therefore be used to provide valuable information about phase separation in organic BHJ solar cells.[16, 85]In pc-AFM, the surface morphology is imaged using contact-mode AFM, collecting simultaneously a topographic image and a photocurrent image of the same area. The photocurrent is collected by illuminating the sample with white light, and applying a bias to the sample to induce an electric field in the device. This technique has been used to identify donor and acceptor phases in BHJ films, determined by the sign of the current collected by the pc-AFM tip.[180, 181, 182]

Figure 5.2a shows RSoXS scans of PIPCP:$PC_{61}BM$ blend films as-cast (the condition relevant for the best performing solar cells), and annealed at 200 °C for different times (annealing was meant to induce different degrees of phase separation). RSoXS data for the as-cast blend show a weak signal that indicates phase separation on the order of ≈30

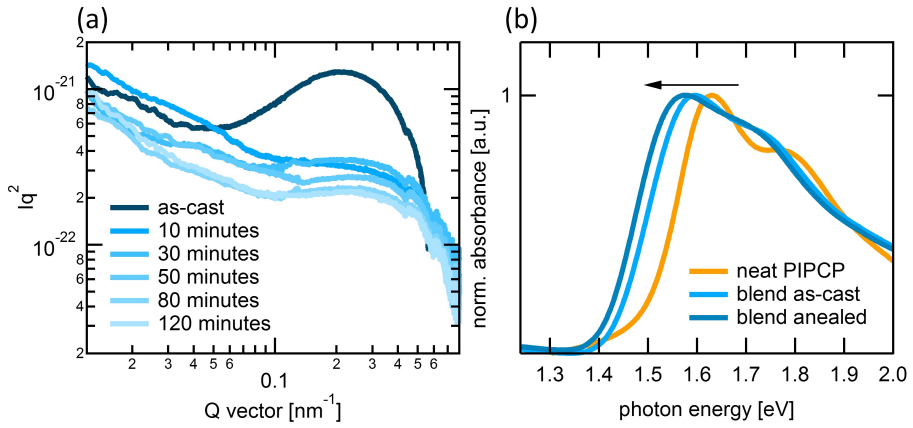

Figure 5.2: Morphological Characterization. (a) RSoXS spectra of PIPCP:$PC_{61}BM$ BHJ blends pristine, and annealed at 200 °C for a range of times. (b) Film absorption spectra of neat PIPCP, pristine PIPCP:$PC_{61}BM$ blend, and PIPCP:$PC_{61}BM$ blend annealed at 200 °C for 10 minutes.

nm. Upon annealing the films at 200 °C for 10 minutes, any signal indicating phase separation disappears. This suggests that PIPCP and $PC_{61}BM$ are highly miscible with each other, and given thermal energy they form a highly mixed morphology instead of pure, separate phases.[179] Furthermore, χ calculations for PIPCP and $PC_{61}BM$ also indicate that the two materials have a high propensity to mix, with a χ of about 0.54. These calculations are based on the Hansen solubility parameters of the functional groups in PIPCP and $PC_{61}BM$,[183] using the additive functional group method as described below.

The cohesive energy density can be decomposed into three Hansen solubility parameters (HSP): dispersive interaction, δD, polar interaction, δP, and hydrogen bonding interaction, δH.

$$CED = \delta_D^2 + \delta_P^2 + \delta_H^2 \tag{5.1}$$

Accordingly, the χ can be estimated by the following:

$$\chi = \alpha \frac{V_s}{RT}((\delta_{Dp} - \delta_{Ds})^2 + \frac{1}{4}(\delta_{Pp} - \delta_{Ps})^2 + \frac{1}{4}(\delta_{Hp} - \delta_{Hs})^2) \tag{5.2}$$

Here, V_S is the molar volume of the solvent (herein, PCBM) and α is a correction term which is usually set at 0.5. The HSP can be experimentally determined by solubility studies in multiple solvents. In this study, the HSPs of a given material are calculated by functional group additive methods, where the given material is decomposed into functional groups with known HSPs.

$$\delta_d = \frac{\Sigma F_{di}}{V}, \delta_p = \frac{\Sigma F_{pi}}{V}, \delta_h = \frac{\Sigma F_{hi}}{V} \tag{5.3}$$

F_{di}, F_{pi}, and F_{hi} correspond to the dispersive interaction, polar interaction, and hydrogen bonding interaction of cohesive energy density, respectively. All contributions to the cohesive energy density can be found in Properties of polymers, their estimation and correlation with chemical structure, 1976. It is important to consider that the solubility parameter method only considers the collective effect of all functional moieties, without considering the relative arrangement of the functional moieties, such as regioregular or regiorandom arrangements.

With the knowledge that PIPCP and $PC_{61}BM$ are highly miscible, we revisited the absorption data.[35] Upon blending PIPCP with $PC_{61}BM$, the absorption edge red-shifts, corresponding to a reduction in the bandgap of PIPCP. Thermal annealing of PIPCP:$PC_{61}BM$ causes a further red-shift in the absorption (Figure 5.2b). In lieu of the RSoXS results, the red-shift in absorption may be an indication of mixing between PIPCP and $PC_{61}BM$. A red-shift in absorption upon mixing is in contrast to what is generally observed for polymers: more often, PCBM disrupts polymer interchain packing and may even decrease the effective polymer conjugation, resulting in blue-shifted

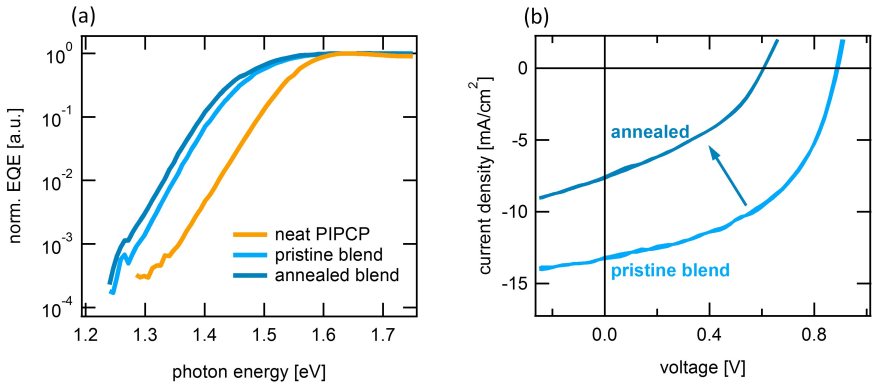

Figure 5.3: (a) Normalized EQE spectra of neat PIPCP, pristine PIPCP:$PC_{61}BM$, and annealed PIPCP:$PC_{61}BM$ blend films, on a log-lin scale showing the sharp Urbach energy retained in all cases. (b) 1-sun J-V curves of a pristine PIPCP:$PC_{61}BM$ blend film, and a PIPCP:$PC_{61}BM$ blend film annealed at 200°C.

absorption. It is worth noting that while PIPCP and $PC_{61}BM$ are highly miscible and can be driven to a fully mixed morphology, PIPCP retains a very high energetic order. This is illustrated by an Urbach energy of ≈27 meV true for neat PIPCP, the pristine BHJ, and the annealed BHJ (Figure 5.3a). However, the annealed film has lower FF and the J_{SC} compared to the pristine BHJ blend (Figure 5.3b).

Further evidence for the mixed morphology of PIPCP:$PC_{61}BM$ solar cells was sought by using pc-AFM (Figure 5.4). Figure 5.4a shows a representative height image of a PIPCP:$PC_{61}BM$ film; Figures 5.4b-d are the current scans of the same area, with increasing extraction bias. Under the chosen experimental conditions, the pc-AFM Cr/Pt tip is expected to collect holes, which which transport through PIPCP domains. As the extraction bias is increased, the current over the entire imaged area increases, instead of only from certain regions that would then be identified as PIPCP. In fact, domains that have relatively higher current at the lower applied bias change shape and grow in size as the applied bias is increased. This is unlike what has been seen with pc-AFM in other systems that have well-defined phase separation.[180, 181, 182]These data illustrate that holes can be extracted from the entire imaged-area, thus giving no indication

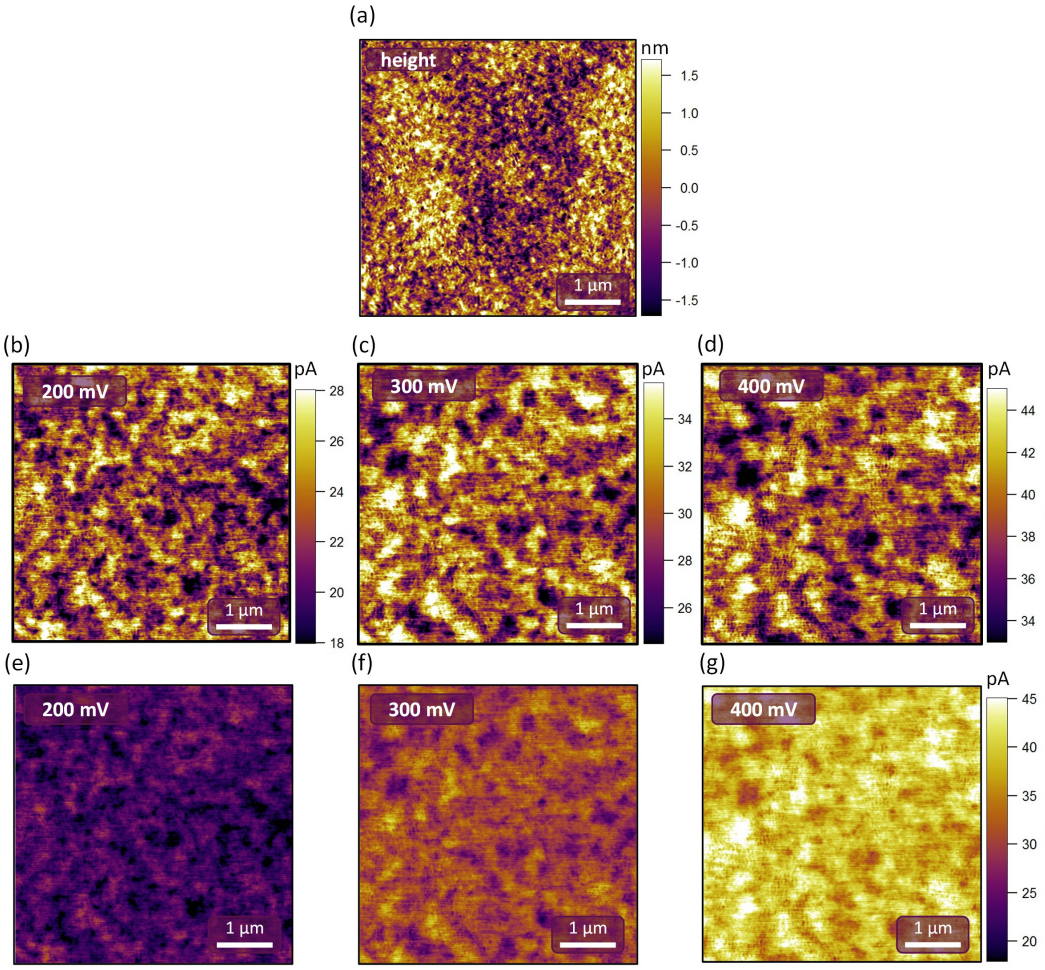

Figure 5.4: (a) Contact-mode topography AFM image for a pristine PIPCP:$PC_{61}BM$ blend film. (b-d) Photocurrent images collected under voltages of (b) 200 mV, (c) 300 mV, and (d) 400 mV applied to the substrate (ITO/ZnO). (e-g) same as images (b-d), redrawn with a normalized current scale, to the right of (g).

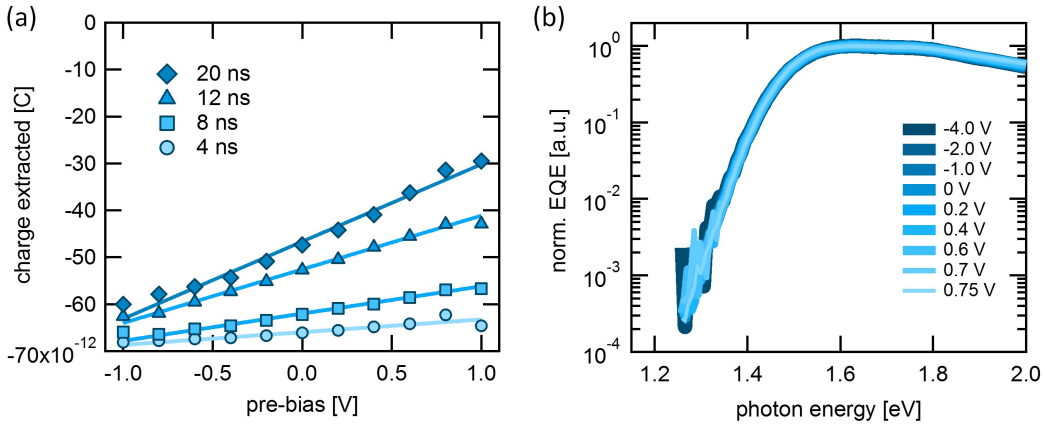

Figure 5.5: (a) TDCF data for PIPCP:$PC_{61}BM$ at different delay times. (b) Normalized bias-dependent EQE at low photon energies, for full spectra refer to 5.6.

of clear phase separation between PIPCP and $PC_{61}BM$, in agreement with the RSoXS data. The two techniques are therefore in agreement with a mixed PIPCP:$PC_{61}BM$ BHJ blend and have low domain purity. Such an intimately mixed BHJ morphology is expected to cause recombination losses. Even in systems that have sufficient energetic driving force for charge generation, a highly-mixed morphology has been shown to be detrimental to device performance.[85, 80] Below we investigate the recombination losses in PIPCP:$PC_{61}BM$ and determine the impact of the low-energetic offset and the highly-mixed morphology on the recombination.

5.5 Field-dependent generation

The poor *FF* of PIPCP:$PC_{61}BM$ may indicated of geminate recombination, defined as relaxation of bound hole-electron pairs, which originate from the same photon absorption (schematically represented in Figure 5.1c).

To determine whether PIPCP:$PC_{61}BM$ blends suffer from field-dependent generation, we referred to time-delayed collection-field (TDCF) measurements. In TDCF measure-

ments the solar cell is held at a particular bias (called the pre-bias) while excitons are generated with a laser pulse. After a specified delay-time, a strong-reverse bias is applied in order to quickly collect all charges that remain. With a short enough time delay, such that no charges have recombined before the collection voltage is applied, TDCF can be used to measure the field dependence of charge generation.[80, 126]

Figure 5.5a shows the TDCF results for PIPCP:$PC_{61}BM$, excited at 532 nm, for delay times varying from 20 ns down to 4 ns, and across a range of pre-bias conditions. With a delay of 20 ns between excitation and extraction, one observes a very strong dependence of extracted charge on the pre-bias. The steep dependence might suggest that the generation of charges is indeed field dependent. However, as the delay time is shortened, the dependence on the pre-bias decreases, until at a delay of 4 ns (at the limit of the instrument capability), the collected charge shows a weak dependence on the pre-bias. These results illustrate two findings. First, the strong field dependence seen at 20 ns, suggests exceptionally fast bimolecular recombination. At low fields, that is at a pre-bias close to V_{OC}, one can see that after 20 ns nearly half of the charge has already recombined. Second, the TDCF results at a delay of 4 ns suggest that generation can, in fact, happen equally efficiently at all fields. In other words, these results indicate that PIPCP:$PC_{61}BM$ blends do not suffer from field-dependent charge generation.

It is worth pointing out that the photocurrent (dark current subtracted from current under illumination) of PIPCP:$PC_{61}BM$ continues to climb, even up to an effective bias (applied voltage subtracted by the built-in voltage) of 10 V, where the photocurrent is nearly 20 mA/cm^2 (Figure 5.6).This increase indicates that also the J_{SC} would be significantly increased if the field-dependence of the photocurrent were resolved. Bias-dependent EQE spectra show that excitation over the entire absorption spectrum of PIPCP:$PC_{61}BM$ results in a similar field-dependence (Figure 5.5 and Figure 5.6b,c). Overcoming the binding energy to achieve charge separation is not dependent on ex-

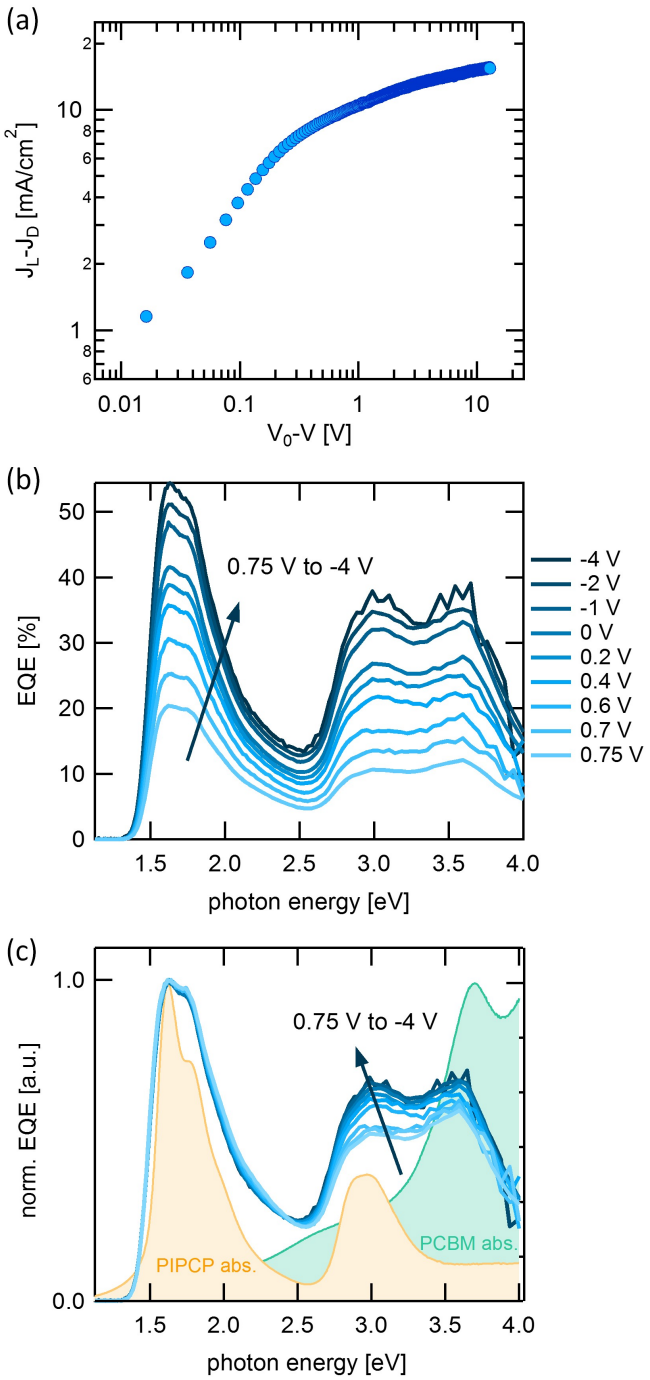

Figure 5.6: (a) Photocurrent (light current corrected for dark current) of PIPCP:$PC_{61}BM$ *vs.* V_0 (applied bias corrected for the built-in voltage. (b) Unnormalized EQE spectra under varying applied voltages. (c) Normalized bias-dependent EQE curves form (b).

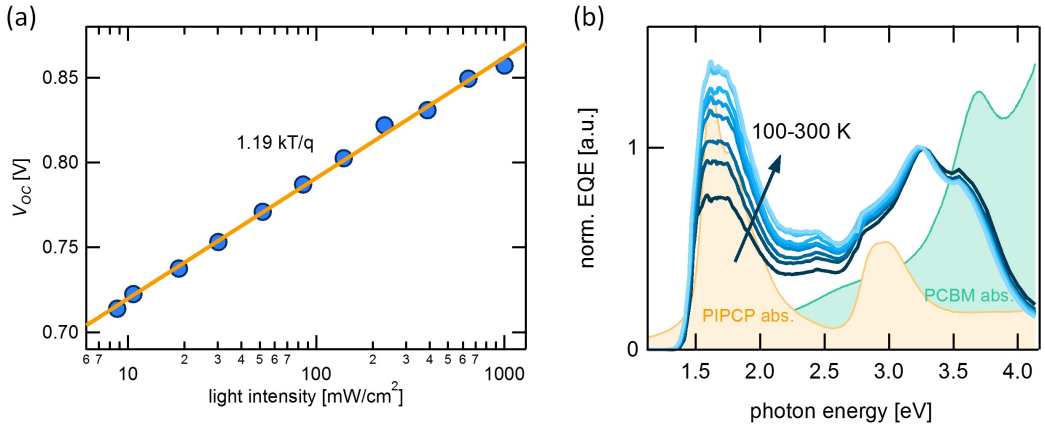

Figure 5.7: Intensity and temperature-dependence. (a) V_{OC} *vs.* light intensity, showing an exponential relationship with a slope of $\approx 1kT/q$. (b) Temperature dependent EQE curves, normalized to the EQE at 3.3 eV. Unitless absorption spectra of PIPCP and $PC_{61}BM$ are shown in the background for reference.

citation energy, even at energies corresponding to the CT state or low-energy PIPCP absorption. This behavior is opposite to observations using EQE analysis for another low-bandgap polymer system, where excitation energy was suggested to play a significant role in dissociating excitons generated on the polymer.[184]

5.6 Shallow traps in PIPCP:$PC_{61}BM$

Having established that charge generation in PIPCP:$PC_{61}BM$ is not limited due to field-dependent generation at all photon energies, despite the very low energetic offset, we investigated the carrier-density dependence of the V_{OC} and the role of temperature on photocurrent generation.

Figure 5.7a shows the V_{OC} of PIPCP:$PC_{61}BM$ as a function of light intensity. As was noted in Chapter 2, for a trap-free cell where recombination is well described by bimolecular recombination, the V_{OC} should depend on light intensity (and thus the carrier-density) with an exponential relationship and a slope of kT/q. If the slope is larger than kT/q,

this is an indication of trap-assisted recombination. For the case of PIPCP:$PC_{61}BM$, the slope is indeed larger, at $1.2kT/q$, indicating of some trap-assisted recombination. Figure 5.7b shows EQE spectra collected at temperatures ranging from 100-300 K, normalized to the EQE at 3.3 eV. Interestingly, the EQE spectra show that charge generation from excitation at energies associated with PIPCP is more temperature-dependent than generation from excitation at energies corresponding to $PC_{61}BM$ absorption. Using a simple Arrhenius relationship it is possible to extract an activation energy for charge generation from temperature-dependent EQE, as was recently shown by Gao *et al.*[87]The activation energies for charge generation from PIPCP excitations (1.5-2.7 eV) and $PC_{61}BM$ excitations (2.7-4.0 eV) come out to be 32 meV and 24 meV, respectively. This indicates the presence of a barrier for electron transfer from PIPCP.

The temperature dependence suggests that excitons originated on PIPCP are extracted less efficiently, and depend more on thermal activation to escape recombination. Here we recall that mixing between PIPCP and $PC_{61}BM$ reduces the bandgap of PIPCP (absorption data in Figure 5.2b), deepens the ionization potential (IP) of PIPCP, and in so doing also deepens the electron affinity (EA) of PIPCP.[35] Together, these two effects create an energetic landscape that is different from the picture often used to describe the benefits to the mixed phase between pure phases, according to which the mixed phase creates an energetic cascade that may obstruct recombination.[185] One possibility is that the deepening of the EA of PIPCP creates PIPCP states with an EA that is even deeper than $PC_{61}BM$, thereby creating shallow electron trap-states. Indeed, time-dependent density functional theory (TD-DFT) calculations on the PIPCP Frenkel exciton and the CT state at the interface with $PC_{61}BM$, show that at certain PIPCP/$PC_{61}BM$ configurations the E_{CT} is higher in energy than the PIPCP S_1.[174] Thermal energy at room-temperature may be sufficient for most carriers to escape the shallow traps, but as thermal energy is reduced the energetic landscape increasingly

impedes charge generation.

5.7 Bimolecular recombination: transport, charge-carrier densities, and the recombination coefficient

While the data presented so far suggest that PIPCP:$PC_{61}BM$ blends do not suffer from field-dependent generation, the data do suggest of field-dependent recombination losses. In particular, that the results in Figure 5.5a indicate of very fast bimolecular recombination, prompted us to investigate if we can increase the *FF* of PIPCP:$PC_{61}BM$ by improving charge extraction or by reducing the probability of charge encounter and the consequent bimolecular recombination.

Bimolecular recombination occurs as free electrons (holes) diffuse through the film and encounter holes (electrons) generated from a different photon, form a CT state, and recombine, as is illustrated in Figure 5.1d. Since bimolecular recombination is a second order process, its effect on solar cell performance may depend on factors such as charge-carrier density (bimolecular recombination depends on the product between the hole, p, and electron, n, charge-carrier densities, see Equation 5.4), film thickness (will influence charge-carrier extraction times), and mobility (will dictate how fast charge-carriers encounter each other as well as how fast they can be extracted from the film).

Figure 5.8 shows the effects of charge carrier mobility, charge-carrier density, and film thickness on the *FF* in PIPCP:$PC_{61}BM$ solar cells, as well as the rate coefficient for bimolecular recombination, k_{rec}. The bimolecular recombination rate, R, is described as the product between a recombination coefficient (k_{rec}), the hole (p) and electron (n)

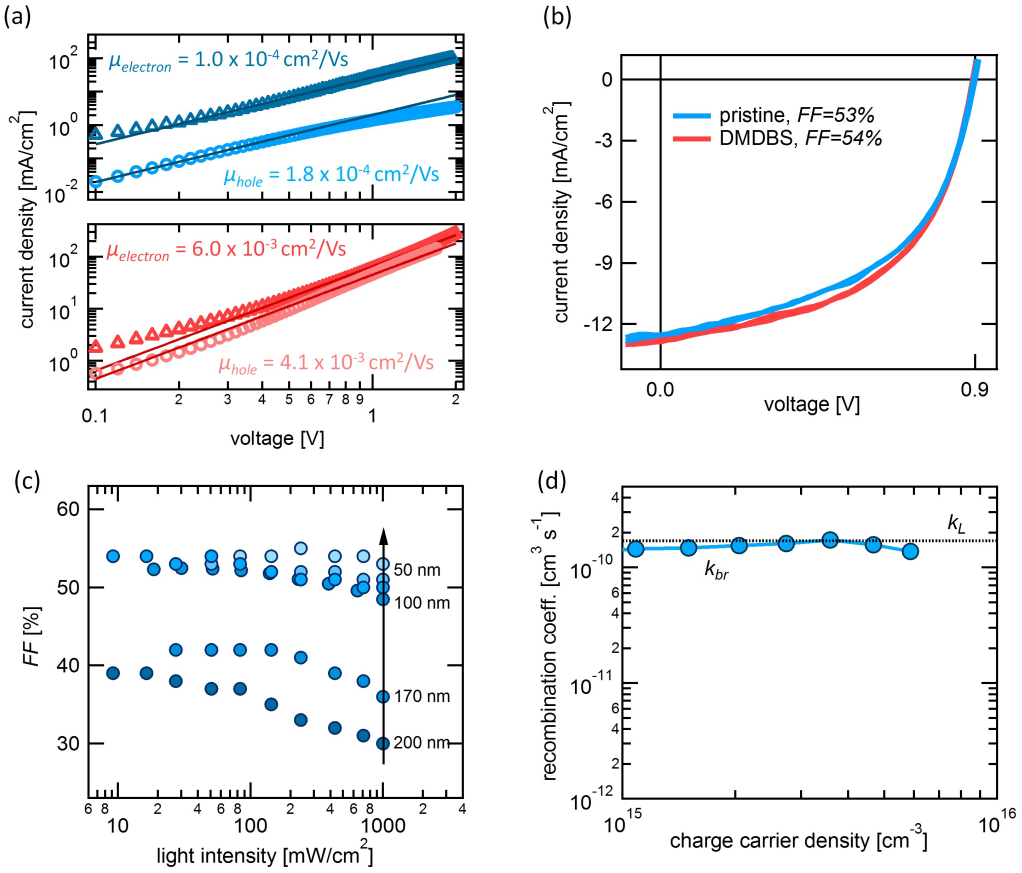

Figure 5.8: (a) SCLC fits to hole- and electron-only diode current from pristine PIPCP:$PC_{61}BM$ devices (top, blue) and PIPCP:$PC_{61}BM$ devices fabricated with DMDBS (bottom, red). (b) *J-V* characteristics of pristine PIPCP:$PC_{61}BM$ BHJ and PIPCP:$PC_{61}BM$ BHJ fabricated with DMDBS, under 1-sun illumination. (c) light intensity dependent *FF* values for PIPCP:$PC_{61}BM$ devices with varying active area thicknesses. (d) recombination coefficient, k_{rec}, for PIPCP:$PC_{61}BM$ solar cells, at varying initial light intensities. The Langevin recombination coefficient, k_L, calculated using the hole and electron mobilities in (a), is shown for reference by a dotted line.

charge-carrier densities, as shown in Equation 5.4:

$$R = \frac{dn}{dt} = k_{rec} np \tag{5.4}$$

Electron and hole mobilities of PIPCP:PC_{61}BM blends, extracted from hole- and electron-only diodes using the SCLC model, are balanced but modest, at best 2×10^{-4} cm^2 V^{-1} s^{-1} (Figure 5.8a, top). It has been established that low charge carrier mobilities will increase charge recombination and the field-dependence of extraction, and thereby reduce the *FF*.[177, 186, 187][22,40,41] Attempts to process PIPCP:PC_{61}BM solar cells with thermal annealing or the use of the solvent additive, 1,8-diiodooctane, were unsuccessful in improving the *FF*. Therefore, we turned to using a nucleating agent, 1,3:2,4-bis(3,4-dimethylbenzylidene)sorbitol (DMDBS; Millad 3988), which has been used in a number of solar cell blends to improve solar cell performance.[163, 188]Indeed, casting blend films of PIPCP:PC_{61}BM with 3% DMDBS w/w achieved an order of magnitude increase in both the electron (6×10^{-3} cm^2 V^{-1} s^{-1}) and hole mobilities (4×10^{-3} cm^2 V^{-1} s^{-1}) (Figure 5.8a, bottom). However, even with these high mobilities, PIPCP:PC_{61}BM devices showed no improvement in *FF* (Figure 5.8b), suggesting that the charge carrier mobilities are not the limiting factor for the *FF* in PIPCP:PC_{61}BM.[186, 187, 189]

Light intensity can be used to modulate charge-carrier density in organic solar cells, and in cases where the *FF* is limited by bimolecular recombination, the *FF* has been shown to increase as light-intensity (and by that, charge-carrier density) decreased.[80, 190, 191] Similarly, thick BHJ films often suffer from low *FF* due to increase in extraction times.[186, 192] The *FF* of thick PIPCP:PC_{61}BM devices is indeed significantly reduced, most likely due to an increase in bimolecular recombination (Figure 5.8c).As light intensity is reduced, the *FF* of the thick devices increases, though the increase is modest (10% increase in *FF* with two orders of magnitude decrease in light intensity). The *FF* of the

thin devices appears nearly independent of light intensity, reaching a plateau near 56%. It should be noted here that Figure 5.8c only shows data for conditions where dark leakage current (resulting from low shunt resistance) did not influence device performance. If a solar cell device has poor diode characteristics (low shunt resistance), leakage current may distort device performance, especially at low light intensities.[193]

Bimolecular recombination losses in solar cells can be directly probed by kinetics of V_{OC} decay. In these measurements, the photovoltage generated by the solar cell is recorded as illumination is turned-off. Because the devices are kept under open circuit conditions, any changes in the photovoltage must be due to recombination losses and the consequent reduction in quasi Fermi level splitting. Using impedance analysis, we can extract the relationship between charge-carrier density and the corresponding photovoltage.[194, 84, 140] Finally, provided with the dynamics of charge-carrier density decay in the solar cell, we derive the recombination rate coefficient, k_{rec}, using Equation 5.4. More detail on this method is available in the experimental section and Figure 5.9.

From this analysis, two particular results are salient: the charge-carrier density at maximum power point is low (9×10^{-15} cm^{-3}), and the recombination coefficient, krec, is very high (1.6×10^{-10} cm^{-3} s^{-1}), compared to range that has been reported for other blends. Our measurements indicate that the charge-carrier density in PIPCP:$PC_{61}BM$ under 1-sun illumination and at V_{OC} conditions is 9×10^{-15} cm^{-3} (Figure 5.9), compared to $\approx 5 \times 10^{-16}$ cm^{-3} measured in other systems.[140, 151] The k_{rec} in PIPCP:$PC_{61}BM$ at 1-sun is 1.6×10^{-10} cm^{-3} s^{-1}, with very little dependence on charge-carrier density (Figure 5.8d). This is recombination coefficient is very high: most organic solar cell blends have k_{rec} values that range between 1×10^{-12} and 1×10^{-10} cm^{-3} s^{-1}.[195, 186] This range is illustrated in the scale of Figure 5.8d. To put k_{rec} in context, it is often compared to the recombination coefficient as predicted by the Langevin model, k_L, given

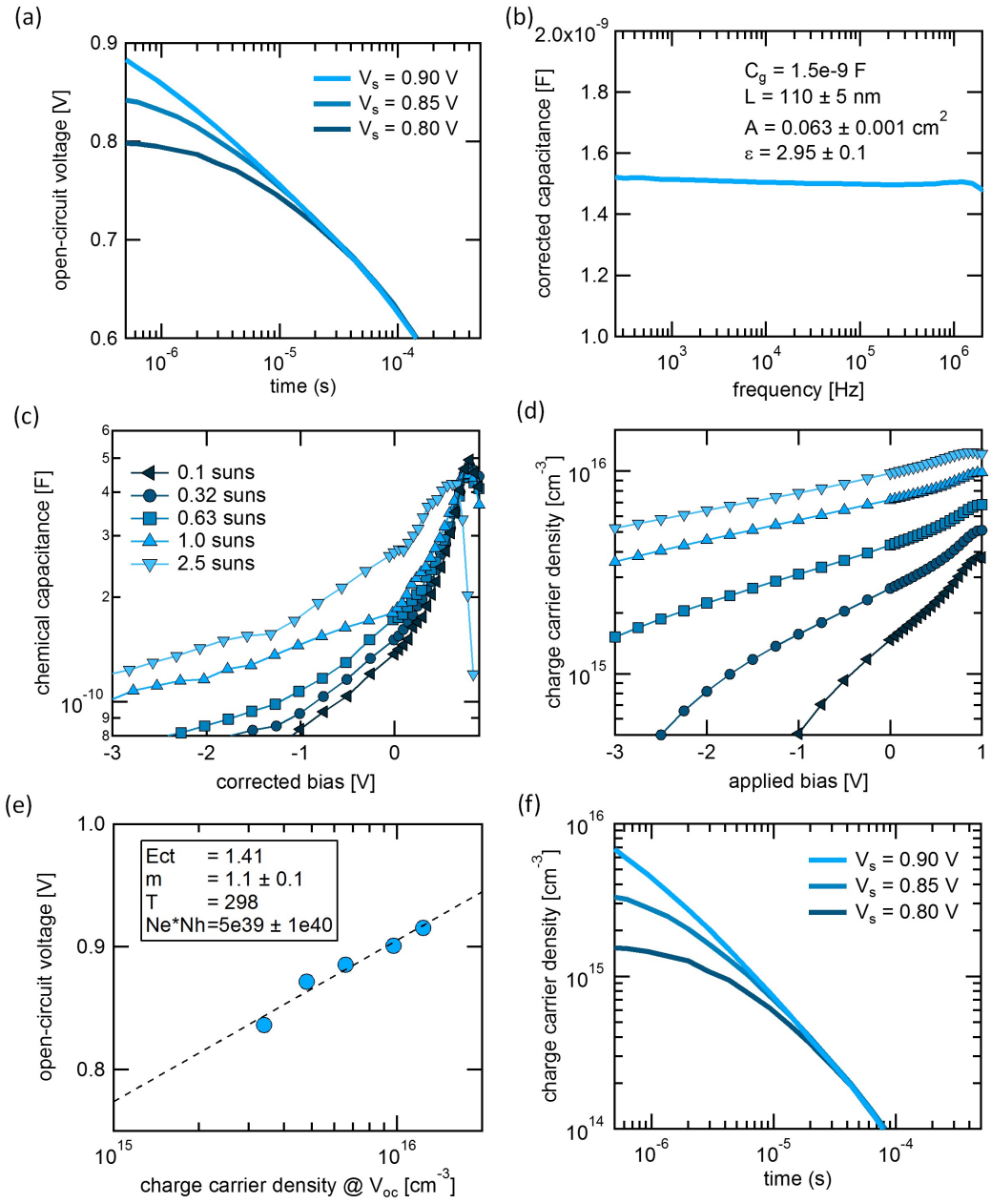

Figure 5.9: The method to determine k_{rec}. (a) OCVD data for varying light intensities. (b) geometrical capacitance for PIPCP:$PC_{61}BM$ derived from impedance spectroscopy, performed under reverse bias and in the dark to ensure the film is depleted of charge-carriers. (c) Chemical capacitance vs. applied bias, extracted from impedance spectroscopy at different light intensities. (d) Charge carrier density at light intensities corresponding to (c) *vs.* applied bias, obtained from the capacitance data in (c). (e) V_{OC} *vs.* charge carrier density, obtained by the carrier density (d) and J-V measurements at the corresponding light intensities. (f) Carrier density decay dynamics, arrived at by using the relationship in (e) and the V_{OC} decay dynamics from (a).

by Equation 5.5, below:

$$k_L = \frac{q}{(\epsilon\epsilon_0}(\mu_n + \mu_p) \tag{5.5}$$

Here, q- elementary charge;ϵ, ϵ_0 relative, and vacuum permittivity, respectively; μ_n, μ_p-electron and hole mobilities, respectively. The Langevin model can be taken as the upper limit of recombination in solar cells, as it describes that recombination occurs instantly upon encounter of opposite charges, and is limited only by the rate of encounter. Deviations from the Langevin model have been used as evidence for an equilibrium between CT states and free charge carriers, where charges form CT states and dissociate many times before they are finally extracted or lost to recombination.[141, 196] Furthermore, the Langevin model was originally derived to describe recombination in a single-phase system, and deviations from the Langevin rate coefficient are sometimes attributed to the presence of separate phases for hole and electron transport in BHJ solar cells.[88, 197]

Using the pristine blend SCLC mobilities from Figure 5.8a (top), and a dielectric constant that is obtained for this blend using the capacitance spectra (Figure 5.9b), we obtain a k_L of 1.7×10^{-10} cm^{-3} s^{-1}, shown as a dotted line across all charge-carrier densities in Figure 5.8d. In this system k_{rec} and k_L are in very close agreement, yielding a reduction factor (defined as k_{rec}/k_L), of over 0.9. The agreement between k_{rec} and k_L implies that recombination in PIPCP:$PC_{61}BM$ is closely described by the Langevin model. Given that charge generation from primary CT states is efficient, it might then be expected that re-dissociation of nongeminate CT states would also be efficient. However, due to spin statistics, nongeminate CT states will mostly be in a triplet spin state. Recent measurements by Menke *et al.* indicate that triplet CT states in PIPCP:$PC_{61}BM$ decay very quickly to the triplet state, much faster than singlet CT states decay to the ground state.[174] This blend exhibits a relatively unique situation in which charge generation

is very efficient, but bimolecular recombination rate is very close to the Langevin limit.

That recombination in PIPCP:$PC_{61}BM$ is encounter-limited can explain why increasing the hole- and electron-mobilities did not increase the *FF* (Figure 5.8a,b). In the scenario where recombination and extraction are both proportional to the mobilities, it follows that increasing the charge carrier mobilities would not shift the balance towards superior extraction, and therefore would not increase the *FF*. Furthermore, the low charge-carrier density may explain the plateau of the *FF* in thin devices at low light-intensities (Figure 5.8c). As the photogenerated charge-carrier density decreases, the presence of dark carriers that diffuse from the contacts[161] becomes increasingly influential. At low photogenerated charge-carrier densities, recombination has been shown to be dominated by non-uniform charge-carrier densities, which results in recombination of minority charge-carriers with majority charge-carriers near the contacts.[195, 198] This can explain a plateau in the *FF* with decreasing charge-carrier density, as is seen in Figure 5.8c, though this is rarely observed at *FF* values as low as in PIPCP:$PC_{61}BM$.

Although the rate of recombination may be large in PIPCP:$PC_{61}BM$, if the rate of charge extraction is significantly faster, then all solar cell parameters (J_{SC}, V_{OC}, and the *FF*) can be high. Analysis of the recombination and extraction lifetimes in PIPCP:$PC_{61}BM$, based on the V_{OC} decay kinetics, shows that under 1 sun illumination, the charge recombination lifetime (2×10^{-6} s) is very close to the charge extraction lifetime (9×10^{-7} s), see Equations 5.6,5.7.

The recombination lifetime, at maximum power point (and therefore carrier density at maximum power point, n_{mp}), is related to the recombination coefficient, k_{rec} according to Equation 5.6:

$$\tau_{rec} = \frac{1}{k n_{mp}} \tag{5.6}$$

For comparison, the extraction life time is determined under maximum power point conditions using film thickness (L), charge-carrier mobility (μ), open-circuit voltage (V_{OC}), and voltage at maximum power point (V_{mp}):

$$\tau_{ex} = \frac{L^2}{2\mu(V_{OC} - Vmp)} \tag{5.7}$$

To illustrate the meaning of these lifetimes, Bartesaghi *et al.* recently demonstrated a dependence between the *FF* of many experimental and simulated devices and a dimensionless parameter, θ, which describes the ratio between the recombination lifetime and extraction lifetime.[195] In PIPCP:$PC_{61}BM$ θ comes out to be 6.7×10^{-1}, while to ensure high *FF* values θ should be on the order of 10^{-3} or smaller.

5.8 PIPCP bilayer solar cells achieve high *FF*

Highly mixed morphologies have been shown to be detrimental to device performance, and the importance of pure domains has been demonstrated in a number of systems.[179, 85, 199, 200] Therefore, in an attempt to decouple effects of energetics and morphology, we fabricated bilayer solar cells by spin-coating a PIPCP layer topped with thermally evaporated C_{60}. Before contact deposition, some PIPCP/C_{60} bilayers were thermally annealed at varying temperatures for 5 minutes to induce mixing at the donor/acceptor interface.[113] Pristine bilayers of PIPCP/C_{60}, where phase separation is maximized, indeed achieve a very high *FF* of 72% (Figure 5.10a). Upon thermal annealing, however, the *FF* of the bilayers decreases down to 56%, on par with PIPCP:$PC_{61}BM$ BHJs. The increase in field-dependent recombination losses in PIPCP/C_{60} with thermally-induced mixing suggests that intimate mixing between PIPCP and $PC_{61}BM$ can be responsible for the low *FF* in the bilayer and in the BHJ.

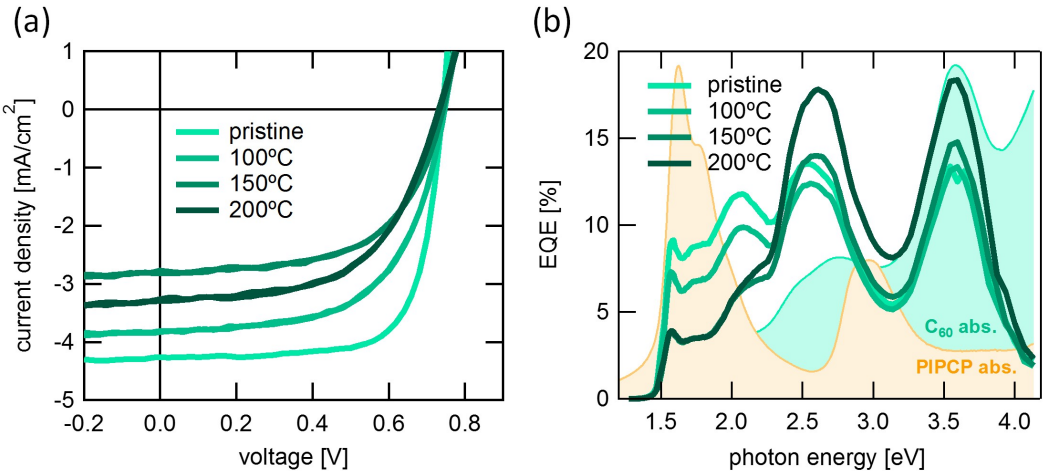

Figure 5.10: (a) 1-sun illuminated J-V curves and (b) EQE spectra of pristine PIPCP/C_{60} bilayers, and bilayers annealed at increasingly high temperatures. Unitless absorption spectra of PIPCP and C_{60} are shown in the background for reference.

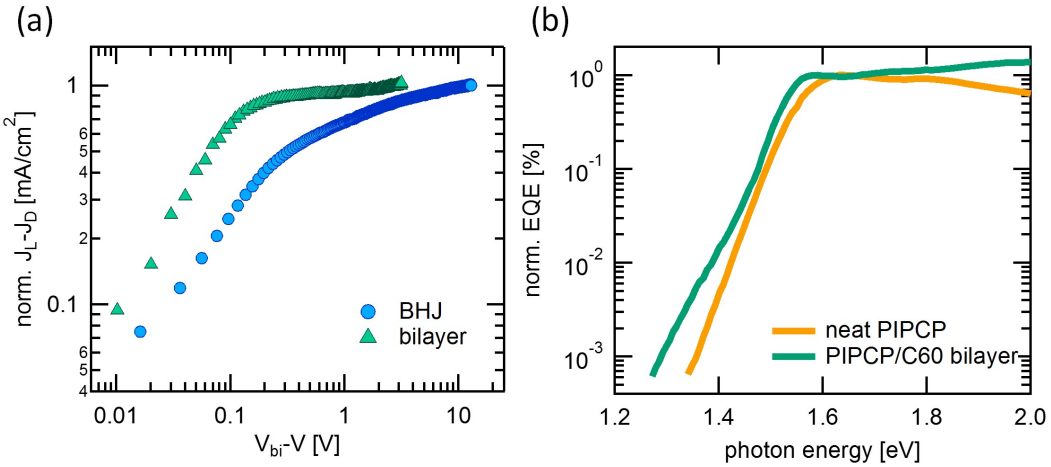

Figure 5.11: (a) photocurrent of PIPCP/C_{60} compared to PIPCP:PC_{61}BM, (b) EQE spectra of PIPCP/C_{60} bilayers, compared to PIPCP:PC_{61}BM.

Mixing at the interface in bilayers is expected to increase the J_{SC} due to the increase in surface area for charge generation.[114, 201] Interestingly, in the case of PIPCP/C_{60}, the J_{SC} in fact decreases with thermal annealing. EQE spectra of the bilayers (Figure 5.10b) show that the decrease in J_{SC} from pristine bilayers to bilayers annealed at 100 °C, is due to a reduction in current generation from PIPCP absorption (1.5-2.7 eV), while generation primarily from $PC_{61}BM$ absorption (2.7-4.0 eV) remains unchanged. Upon annealing at 150 °C, current generation from PIPCP absorption further decreases, while generation from C_{60} begins to increase, perhaps due to increased order in the C_{60} layer. Overall, these data suggest that intimate mixing of PIPCP with C_{60} results in high recombination losses, specifically for excitons generated on PIPCP. This is despite the fact that the EA of neat PIPCP is closer to vacuum than in mixed PIPCP,[35] thereby providing a larger energetic offset for charge separation in the bilayers. Therefore, these results suggest that intimate mixing in PIPCP:$PC_{61}BM$ is the primary reason for the low *FF* in the BHJ devices.

5.9 Conclusions and outlook

With the information discussed above, we now present a more pertinent cartoon depicting the recombination, morphology, and energetic landscape in PIPCP:$PC_{61}BM$ (Figure 5.12). The low energetic offset of PIPCP and $PC_{61}BM$ does not result in field-dependent charge generation. Instead, the field-dependence which limits the *FF* stems from very fast field-dependent bimolecular recombination that is equivalent to- or even faster than- charge extraction. Within the view of a balance between charge recombination and charge extraction, in the absence of a field (at V_{OC} conditions) charge recombination dominates (Figure 5.12a), but as the field increases, the balance shifts towards charge collection (Figure 5.12b). In addition, our characterization suggests that

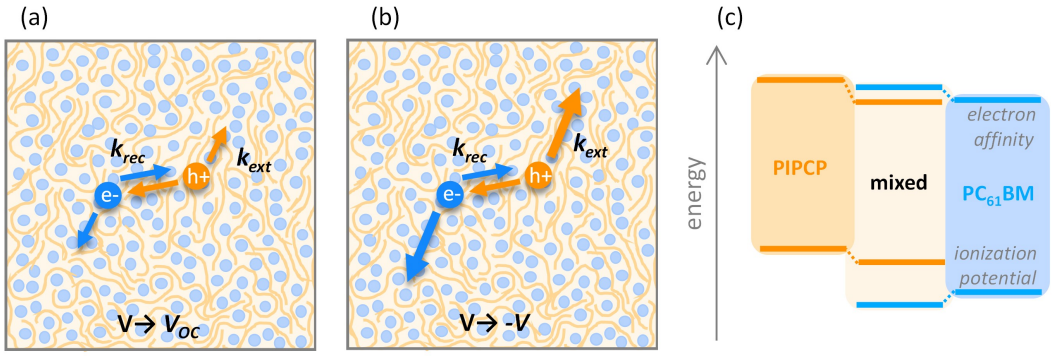

Figure 5.12: Charge separation and recombination illustrated as competing processes under varying electric fields: (a) under no internal field (near V_{OC}), (b) at fields approaching the internal field (near J_{SC}), and (c) at fields that promote charge extraction (reverse bias). k_{rec} and k_{ext} in this figure represent the recombination rate coefficient and extraction rate coefficient, respectively. (d) suggested energetic landscape of a primarily mixed PIPCP:$PC_{61}BM$ film.

mixing between PIPCP and $PC_{61}BM$ decrease the E_g of PIPCP. Since ΔEA of PIPCP and $PC_{61}BM$ is already very low, this may lead to the formation of shallow electron traps which require the assistance of thermal energy to escape.

Slowing down charge recombination in PIPCP:$PC_{61}BM$ is paramount to improve efficiency. Menke *et al.* estimate that as much as 90% of all recombination events in PIPCP:$PC_{61}BM$ occur via triplet decay pathways.[174] There is evidence in the literature that charge delocalization, achieved by fullerene aggregates, significantly reduces triplet recombination losses, shown by transient absorption.[76, 75] In fact, there is a growing body of work emphasizing the importance of aggregation and charge delocalization,[76, 75, 202, 51, 203, 204, 205, 206, 100, 99, 57] and the necessity for high purity in the separate donor/acceptor domains.[179, 207, 199, 200] Thus it may be that in order to slow down bimolecular recombination it is necessary to induce pure, separate PIPCP and $PC_{61}BM$ domains (to enhance charge delocalization and escape from the triplet states), without mixed phases (where electron traps may lower photocurrent generation efficiency). Indeed, bilayers fabricated from PIPCP/C_{60} achieve a very high FF=72%.

PIPCP holds promise for understanding the fundamentals of charge generation and recombination, given that it retains excellent energetic order in the solid state, even when intimately mixed with $PC_{61}BM$. PIPCP:$PC_{61}BM$ can generate up to 14 mA cm^{-2} under unfavorable conditions of high mixing and little energetic driving force for charge generation, with a high V_{OC} of 0.90 V. A number of studies have been drawing attention to results which indicate that efficient charge generation and collection can be achieved also with minimal energetic offsets.[205, 208] While some highlight the importance of highly ordered donor and acceptor domains and high dielectric constants,[208] others focus on an entropic driving force for charge generation.[205] If it were possible to fabricate a BHJ with pure PIPCP and $PC_{61}BM$ phases, there is good reason to believe that the FF and the J_{SC} would increase, leading to a BHJ device with very high performance.

To improve the performance of PIPCP as a donor material in OPV we must therefore find the appropriate methods to control BHJ morphology. To achieve this, a few routes may be possible: (i) it may be that film-formation techniques which do not rely on the self-assembly of the donor and acceptor materials from a homogeneous solution, such as sequential processing of the donor and acceptor, can achieve improved BHJ morphologies.[209] (ii) PIPCP could be combined with a non-fullerene acceptor which does not have such a high χ of mixing. Furthermore, if that acceptor does not cause changes in the energy levels of PIPCP, and has an EA closer to vacuum than $PC_{61}BM$, the blend may also benefit from a high V_{OC}. (iii) modifying the solubility of PIPCP by side-chain engineering may afford the use of solvents better suited for PIPCP or $PC_{61}BM$, as was demonstrated for a series of semiconductors by Liu *et al.*.[16] Alternatively, it may be possible to fabricate BHJ films from solvent blends, in which the two solvents are each better suited for PIPCP or $PC_{61}BM$. These considerations for morphological control are not specific to PIPCP:$PC_{61}BM$, and should be at the forefront of our attention as we design new materials for efficient OPVs.

5.10 Methods

5.10.1 Sample preparation

PIPCP was synthesized according to the previously reported scheme.[153] PIPCP:$PC_{61}BM$ solutions were prepared at a ratio of 1:2 w/w, dissolved at 18 mg/mL in 3:2 CF:CB v/v. To achieve devices of varying thicknesses, solution concentration and spin speeds were varied, but solids ratio and solvents ratio were kept constant. BHJ devices were fabricated in inverted structures on ZnO. The ZnO layer was prepared on ITO sputtered glass substrates according to the sol-gel method, described in a previous publication.[210] BHJ active layers were spin-coated from the blend solution at a spin speed of 1500 RPM. The devices were completed with a thermally deposited MoOx/Ag top-contact. The final BHJ device structure for most measurements reported herein is as follows: ITO/ZnO (40 nm)/PIPCP:$PC_{61}BM$ (100-110 nm)/MoOx (6 nm)/Ag (100 nm). Active layers with DMDBS were fabricated using the same procedure as described above, with one exception: DMDBS was added to the blend solution prior to casting, at 3% by weight with respect to total solids concentration. Note that 3% w/w DMDBS is the condition under which we achieved the highest single-carrier diode mobilities. Bilayer devices were fabricated on ITO sputtered glass substrates, coated with thermally evaporated MoOx (10 nm). PIPCP was dissolved at 6 mg/mL in 3:2 CF:CB v/v, and spin-coated at 2000 RPM, followed by a thermally evaporated C_{60} layer. Annealed bilayer devices were placed directly on a hot plate at the specified temperature for 5 minutes. Devices were completed by evaporating a top contact: bathocuproine (BCP) and Al. The final bilayer device structure is as follows: ITO/MoOx (10 nm)/PIPCP (60 nm)/C_{60} (45 nm)/BCP (5 nm)/Al (100 nm).

5.10.2 Current-voltage characteristics

Solar-cell device properties were measured under illumination by a simulated 100 mW cm^{-2} AM1.5G light source using a 300 W Xe arc lamp with an AM 1.5 global filter. The irradiance was adjusted to 1-sun using a standard silicon photovoltaic cell with a protective KG1 filter calibrated by the National Renewable Energy Laboratory.

5.10.3 External and internal quantum efficiency measurements

EQE characteristics were measured in a nitrogen-filled glovebox using a 75 W Xe light source, monochromator, optical chopper, lock-in amplifier, and a National Institute of Standards and Technology calibrated silicon photodiode for power-density calibration. Bias-dependent EQE was collected on the same setup, coupled to a Keithley source-measure-unit which was used to apply a bias while the EQE spectra were recorded. Temperature-dependent EQE measurements were collected following a similar procedure, using a nitrogen-cooled cryostat. Total absorption of solar cell devices was measured with a Perkin Elmer integrating sphere, and corrected for parasitic absorption as determined using a transfer matrix model.[131] Subtracting the parasitic absorption from the total device absorption then gives the active layer absorption, and dividing EQE spectra by the corresponding active layer absorption gives the IQE spectra of the device.

5.10.4 Time-Delayed Collection Field measurements

Time-Delayed Collection Field measurements. Excitation is realized by a laser system consisting of an Ekspla NT-242-500 Laser operating at 500 Hz. The beam is attenuated via neutral density filters to a fluence of 0.06 $\mu J/cm^2$. The pre- and collection voltage is applied via an Agilent 81150A pulse generator in combination with a home-built amplifier. Currents through the devices are measured via a 50 Ω resistor and recorded with an

Agilent Infiniium DSO9054H oscilloscope.

5.10.5 Electroluminescence

Electroluminescence spectra were collected in air from encapsulated solar cell devices, by applying a bias that is close to the turn-on voltage of the devices. The resulting emission was collected with a CCD Si detector, cooled to -70°C. The spectra were corrected for detector response using a blackbody spectrum.

5.10.6 Single-carrier diodes

Solutions for single-carrier diode measurements were prepared using the same blend ratio and solvent ratio as the solar cell devices, but at a solids concentration of 30 mg/mL. This was done to increase the accuracy of the space-charge limited current analysis, which has a cubed dependence on film thickness. Hole-only diodes were fabricated using the following device structure: ITO/MoOx (10 nm)/PIPCP:$PC_{61}BM$ (300 nm)/MoOx (10 nm)/Ag (100 nm). Electron only diodes had the following device structure: ITO/ZnO (40 nm)/PIPCP:$PC_{61}BM$ (300 nm)/Ca (10 nm)/Al (100 nm).

5.10.7 Open-circuit voltage decay

Measurements were performed on BHJ devices loaded into a nitrogen filled cryostat. Devices were illuminated with a single, high-power white LED (CREE XT-E W130) controlled by a square wave function generator (Stanford Research Systems) attached to a diode switch. Using a focusing lens, illumination intensity can reach above 1 sun. With an LED turn-off time of 200 ns, the setup has a time resolution of 500 ns. The device photovoltage was measured using a high-impedance voltage follower and an oscilloscope (Techtronix) set with a 200 ns resolution. The repetition rate of the function generator

and was set so that the photovoltage produced by the device reached less than 50 mV after each pulse to prevent the possibility of device charging. Impedance analysis. Devices were illuminated with an AM1.5 solar simulator (300 W Xe arc lamp with an AM 1.5 global filter) that was attenuated using neutral density filters. The solar simulator irradiance was calibrated using a standard silicon photovoltaic cell with a protective KG1 filter calibrated by the National Renewable Energy Laboratory. Light and dark J-V curves were measured using a source-meter (Keithley 2602), and the device impedance response in the dark and under illumination was measured with an impedance analyzer (Solartron SI 1255, SI 1287) with an AC amplitude of 100 mV.

5.10.8 Resonant soft x-ray scattering

R-SoXS transmission measurements were performed at beamline 11.0.1.2 at the ALS30. Samples for R-SoXS measurements were prepared on a PSS modified Si substrate under the same conditions as those used for device fabrication, and then transferred by floating in water to a 1.5 × 1.5mm, 100-nm thick Si3N4 membrane supported by a 5 × 5mm, 200m thick Si frame (Norcada Inc.). Two dimensional scattering patterns were collected on an in-vacuum CCD camera (Princeton Instrument PI-MTE). The beam size at the sample is ≈100m by 200m. The composition variation (or relative domain purity) over the length scales probed can be extracted by integrating scattering profiles to yield the total scattering intensity. The purer the average domains are, the higher the total scattering intensity. Owing to a lack of absolute flux normalization, the absolute composition cannot be obtained by only R-SoXS.

5.10.9 Photoconductive atomic force microscopy

pc-AFM measurements were performed with an Asylum Research MFP-3D microscope sitting atop an inverted optical microscopy (Olympus, IX71). All measurements were done under inert atmosphere. In this work, the bias was applied to the substrate, and the current was recorded by internal preamplifier (Asylum Research ORCA head model). Chromium/Platinum-coated silicon probes with a spring constant of 0.2 N m^{-1} and resonant frequency of 13 kHz (Budget Sensors) were used. A white light source with a power of 30 W cm^{-2} was used for photocurrent imaging. The light was focused on the sample through an inverted optical microscope (Olympus) and then the tip was positioned at the center of the illumination spot. The illuminated spot size at the sample surface was measured to be approximately 160 m in diameter.

Bibliography

[1] "U.S. Energy Facts - Energy Explained, Your Guide To Understanding Energy - Energy Information Administration." http://www.eia.gov/energyexplained/?page=us_energy_home.

[2] O. US EPA, "Overview of Greenhouse Gases." https://www.epa.gov/ghgemissions/overview-greenhouse-gases.

[3] "IPCC Working Group II." http://ipcc-wg2.gov/AR5/.

[4] J. E. Coughlin, Z. B. Henson, G. C. Welch, and G. C. Bazan, *Design and Synthesis of Molecular Donors for Solution-Processed High-Efficiency Organic Solar Cells*, *Accounts of Chemical Research* **47** (Jan., 2014) 257–270.

[5] H. Shirakawa, E. J. Louis, A. G. MacDiarmid, C. K. Chiang, and A. J. Heeger, *Synthesis of electrically conducting organic polymers: Halogen derivatives of polyacetylene, (CH)x*, .

[6] "The Nobel Prize in Chemistry 2000." https://www.nobelprize.org/nobel_prizes/chemistry/laureates/2000/.

[7] mzentgraad, "Photovoltaics Report (Slides) — Fraunhofer ISE." https://www.ise.fraunhofer.de/en/downloads-englisch/pdf-files-englisch/photovoltaics-report-slides.pdf.

[8] A. Köhler and H. Bässler, *The Electronic Structure of Organic Semiconductors*, in *Electronic Processes in Organic Semiconductors*, pp. 1–86. Wiley-VCH Verlag GmbH & Co. KGaA, 2015.

[9] C. W. Tang, *Two-layer organic photovoltaic cell*, *Applied Physics Letters* **48** (Jan., 1986) 183–185.

[10] O. V. Mikhnenko, P. W. M. Blom, and T.-Q. Nguyen, *Exciton diffusion in organic semiconductors*, .

[11] G. Yu, J. Gao, J. C. Hummelen, F. Wudl, and A. J. Heeger, *Polymer Photovoltaic Cells: Enhanced Efficiencies via a Network of Internal Donor-Acceptor Heterojunctions*, *Science* **270** (Dec., 1995) 1789–1791.

[12] J. A. Love, C. M. Proctor, J. Liu, C. J. Takacs, A. Sharenko, T. S. van der Poll, A. J. Heeger, G. C. Bazan, and T.-Q. Nguyen, *Film Morphology of High Efficiency Solution-Processed Small-Molecule Solar Cells*, *Advanced Functional Materials* **23** (Oct., 2013) 5019–5026.

[13] M. Li, F. Liu, X. Wan, W. Ni, B. Kan, H. Feng, Q. Zhang, X. Yang, Y. Wang, Y. Zhang, Y. Shen, T. P. Russell, and Y. Chen, *Subtle Balance Between Length Scale of Phase Separation and Domain Purification in Small-Molecule Bulk-Heterojunction Blends under Solvent Vapor Treatment*, *Advanced Materials* **27** (Oct., 2015) 6296–6302.

[14] C. Cui, X. Guo, J. Min, B. Guo, X. Cheng, M. Zhang, C. J. Brabec, and Y. Li, *High-Performance Organic Solar Cells Based on a Small Molecule with Alkylthio-Thienyl-Conjugated Side Chains without Extra Treatments*, *Advanced Materials* **27** (Dec., 2015) 7469–7475.

[15] S. Badgujar, G.-Y. Lee, T. Park, C. E. Song, S. Park, S. Oh, W. S. Shin, S.-J. Moon, J.-C. Lee, and S. K. Lee, *High-Performance Small Molecule via Tailoring Intermolecular Interactions and its Application in Large-Area Organic Photovoltaic Modules*, *Advanced Energy Materials* **6** (June, 2016) n/a–n/a.

[16] Y. Liu, J. Zhao, Z. Li, C. Mu, W. Ma, H. Hu, K. Jiang, H. Lin, H. Ade, and H. Yan, *Aggregation and morphology control enables multiple cases of high-efficiency polymer solar cells*, *Nature Communications* **5** (Nov., 2014).

[17] C. Deibel, T. Strobel, and V. Dyakonov, *Role of the Charge Transfer State in Organic Donor–Acceptor Solar Cells*, *Advanced Materials* **22** (2010), no. 37 4097–4111.

[18] K. Vandewal, A. Gadisa, W. D. Oosterbaan, S. Bertho, F. Banishoeib, I. Van Severen, L. Lutsen, T. J. Cleij, D. Vanderzande, and J. V. Manca, *The Relation Between Open-Circuit Voltage and the Onset of Photocurrent Generation by Charge-Transfer Absorption in Polymer : Fullerene Bulk Heterojunction Solar Cells*, *Advanced Functional Materials* **18** (2008), no. 14 2064–2070.

[19] K. Vandewal, K. Tvingstedt, A. Gadisa, O. Inganäs, and J. V. Manca, *On the origin of the open-circuit voltage of polymer–fullerene solar cells*, *Nature Materials* **8** (Nov., 2009) 904–909.

[20] J. J. Benson-Smith, L. Goris, K. Vandewal, K. Haenen, J. V. Manca, D. Vanderzande, D. D. C. Bradley, and J. Nelson, *Formation of a Ground-State Charge-Transfer Complex in Polyfluorene//[6,6]-Phenyl-C61 Butyric Acid Methyl Ester (PCBM) Blend Films and Its Role in the Function of Polymer/PCBM Solar Cells*, *Advanced Functional Materials* **17** (2007), no. 3 451–457.

[21] K. Vandewal, L. Goris, I. Haeldermans, M. Nesládek, K. Haenen, P. Wagner, and J. Manca, *Fourier-Transform Photocurrent Spectroscopy for a fast and highly sensitive spectral characterization of organic and hybrid solar cells*, *Thin Solid Films* **516** (Aug., 2008) 7135–7138.

[22] N. A. Ran, M. Kuik, J. A. Love, C. M. Proctor, I. Nagao, G. C. Bazan, and T.-Q. Nguyen, *Understanding the Charge-Transfer State and Singlet Exciton Emission from Solution-Processed Small-Molecule Organic Solar Cells*, *Advanced Materials* **26** (Sept., 2014) 7405–7412.

[23] K. Tvingstedt, K. Vandewal, F. Zhang, and O. Inganäs, *On the Dissociation Efficiency of Charge Transfer Excitons and Frenkel Excitons in Organic Solar Cells: A Luminescence Quenching Study*, *The Journal of Physical Chemistry C* **114** (Dec., 2010) 21824–21832.

[24] K. Tvingstedt, K. Vandewal, A. Gadisa, F. Zhang, J. Manca, and O. Inganäs, *Electroluminescence from Charge Transfer States in Polymer Solar Cells*, *Journal of the American Chemical Society* **131** (Aug., 2009) 11819–11824.

[25] A. Köhler and H. Bässler, *Electronic Processes in Organic Semiconductors*. Wiley-VCH Verlag GmbH & Co. KGaA, Weinheim, Germany.

[26] J.-L. Bredas, *Mind the gap!*, .

[27] A. Kahn, *Fermi level, work function and vacuum level*, *Materials Horizons* **3** (2016), no. 1 7–10.

[28] J. C. Blakesley and D. Neher, *Relationship between energetic disorder and open-circuit voltage in bulk heterojunction organic solar cells*, *Physical Review B* **84** (Aug., 2011) 075210.

[29] K. Vandewal, K. Tvingstedt, A. Gadisa, O. Inganäs, and J. V. Manca, *Relating the open-circuit voltage to interface molecular properties of donor:acceptor bulk heterojunction solar cells*, *Physical Review B* **81** (Mar., 2010) 125204.

[30] U. Hörmann, J. Kraus, M. Gruber, C. Schuhmair, T. Linderl, S. Grob, S. Kapfinger, K. Klein, M. Stutzman, H. J. Krenner, and W. Brütting, *Quantification of energy losses in organic solar cells from temperature-dependent device characteristics*, *Physical Review B* **88** (Dec., 2013) 235307.

[31] M. Kuik, L. Koster, A. Dijkstra, G. Wetzelaer, and P. Blom, *Non-radiative recombination losses in polymer light-emitting diodes*, *Organic Electronics* **13** (June, 2012) 969–974.

[32] G.-J. A. H. Wetzelaer, M. Kuik, and P. W. M. Blom, *Identifying the Nature of Charge Recombination in Organic Solar Cells from Charge-Transfer State Electroluminescence*, *Advanced Energy Materials* **2** (Oct., 2012) 1232–1237.

[33] P. C. Y. Chow, S. Gélinas, A. Rao, and R. H. Friend, *Quantitative Bimolecular Recombination in Organic Photovoltaics through Triplet Exciton Formation*, *Journal of the American Chemical Society* **136** (Mar., 2014) 3424–3429.

[34] J. Yao, T. Kirchartz, M. S. Vezie, M. A. Faist, W. Gong, Z. He, H. Wu, J. Troughton, T. Watson, D. Bryant, and J. Nelson, *Quantifying Losses in Open-Circuit Voltage in Solution-Processable Solar Cells*, *Physical Review Applied* **4** (July, 2015) 014020.

[35] N. A. Ran, J. A. Love, C. J. Takacs, A. Sadhanala, J. K. Beavers, S. D. Collins, Y. Huang, M. Wang, R. H. Friend, G. C. Bazan, and T.-Q. Nguyen, *Harvesting the Full Potential of Photons with Organic Solar Cells*, *Advanced Materials* (Dec., 2015) 1482–1488.

[36] H. Zhou, L. Yang, and W. You, *Rational Design of High Performance Conjugated Polymers for Organic Solar Cells*, *Macromolecules* **45** (Jan., 2012) 607–632.

[37] M. C. Scharber and N. S. Sariciftci, *Efficiency of bulk-heterojunction organic solar cells*, *Progress in Polymer Science* **38** (Dec., 2013) 1929–1940.

[38] N. S. Sariciftci, L. Smilowitz, A. J. Heeger, and F. Wudl, *Photoinduced Electron Transfer from a Conducting Polymer to Buckminsterfullerene*, *Science* **258** (Nov., 1992) 1474–1476.

[39] T. M. Clarke and J. R. Durrant, *Charge Photogeneration in Organic Solar Cells*, *Chemical Reviews* **110** (Nov., 2010) 6736–6767.

[40] C. Piliego and M. A. Loi, *Charge transfer state in highly efficient polymer–fullerene bulk heterojunction solar cells*, *Journal of Materials Chemistry* **22** (Feb., 2012) 4141–4150.

[41] C. L. Braun, *Electric field assisted dissociation of charge transfer states as a mechanism of photocarrier production*, *The Journal of Chemical Physics* **80** (May, 1984) 4157–4161.

[42] C. M. Proctor, M. Kuik, and T.-Q. Nguyen, *Charge carrier recombination in organic solar cells*, *Progress in Polymer Science* **38** (Dec., 2013) 1941–1960.

[43] G. Lakhwani, A. Rao, and R. H. Friend, *Bimolecular Recombination in Organic Photovoltaics*, *Annual Review of Physical Chemistry* **65** (2014), no. 1 null.

[44] K. Vandewal, K. Tvingstedt, J. V. Manca, and O. Inganäs, *Charge-Transfer States and Upper Limit of the Open-Circuit Voltage in Polymer:Fullerene Organic Solar Cells*, *IEEE Journal of Selected Topics in Quantum Electronics* **16** (2010), no. 6 1676–1684.

[45] T. Drori, C.-X. Sheng, A. Ndobe, S. Singh, J. Holt, and Z. V. Vardeny, *Below-Gap Excitation of π-Conjugated Polymer-Fullerene Blends: Implications for Bulk Organic Heterojunction Solar Cells*, *Physical Review Letters* **101** (July, 2008) 037401.

[46] M. A. Loi, S. Toffanin, M. Muccini, M. Forster, U. Scherf, and M. Scharber, *Charge Transfer Excitons in Bulk Heterojunctions of a Polyfluorene Copolymer and a Fullerene Derivative*, *Advanced Functional Materials* **17** (2007), no. 13 2111–2116.

[47] D. Veldman, S. C. J. Meskers, and R. A. J. Janssen, *The Energy of Charge-Transfer States in Electron Donor–Acceptor Blends: Insight into the Energy Losses in Organic Solar Cells*, *Advanced Functional Materials* **19** (2009), no. 12 1939–1948.

[48] F. Piersimoni, S. Chambon, K. Vandewal, R. Mens, T. Boonen, A. Gadisa, M. Izquierdo, S. Filippone, B. Ruttens, J. D'Haen, N. Martin, L. Lutsen, D. Vanderzande, P. Adriaensens, and J. V. Manca, *Influence of Fullerene Ordering on the Energy of the Charge-Transfer State and Open-Circuit Voltage in Polymer:Fullerene Solar Cells*, *The Journal of Physical Chemistry C* **115** (June, 2011) 10873–10880.

[49] A. E. Jailaubekov, A. P. Willard, J. R. Tritsch, W.-L. Chan, N. Sai, R. Gearba, L. G. Kaake, K. J. Williams, K. Leung, P. J. Rossky, and X.-Y. Zhu, *Hot charge-transfer excitons set the time limit for charge separation at donor/acceptor interfaces in organic photovoltaics*, *Nature Materials* **12** (Jan., 2013) 66–73.

[50] S. D. Dimitrov, A. A. Bakulin, C. B. Nielsen, B. C. Schroeder, J. Du, H. Bronstein, I. McCulloch, R. H. Friend, and J. R. Durrant, *On the Energetic Dependence of Charge Separation in Low-Band-Gap Polymer/Fullerene Blends*, *Journal of the American Chemical Society* **134** (Nov., 2012) 18189–18192.

[51] A. A. Bakulin, A. Rao, V. G. Pavelyev, P. H. M. van Loosdrecht, M. S. Pshenichnikov, D. Niedzialek, J. Cornil, D. Beljonne, and R. H. Friend, *The Role of Driving Energy and Delocalized States for Charge Separation in Organic Semiconductors*, *Science* **335** (Mar., 2012) 1340–1344.

[52] K. Vandewal, S. Albrecht, E. T. Hoke, K. R. Graham, J. Widmer, J. D. Douglas, M. Schubert, W. R. Mateker, J. T. Bloking, G. F. Burkhard, A. Sellinger, J. M. J. Fréchet, A. Amassian, M. K. Riede, M. D. McGehee, D. Neher, and A. Salleo, *Efficient charge generation by relaxed charge-transfer states at organic interfaces*, *Nature Materials* **13** (Jan., 2014) 63–68.

[53] S. Albrecht, K. Vandewal, J. R. Tumbleston, F. S. U. Fischer, J. D. Douglas, J. M. J. Fréchet, S. Ludwigs, H. Ade, A. Salleo, and D. Neher, *On the Efficiency*

of Charge Transfer State Splitting in Polymer:Fullerene Solar Cells, *Advanced Materials* (2014) 2533–2539.

[54] K. Paudel, B. Johnson, A. Neunzert, M. Thieme, B. Purushothaman, M. M. Payne, J. E. Anthony, and O. Ostroverkhova, *Small-Molecule Bulk Heterojunctions: Distinguishing Between Effects of Energy Offsets and Molecular Packing on Optoelectronic Properties*, *The Journal of Physical Chemistry C* (Oct., 2013).

[55] M. J. Kendrick, A. Neunzert, M. M. Payne, B. Purushothaman, B. D. Rose, J. E. Anthony, M. M. Haley, and O. Ostroverkhova, *Formation of the Donor–Acceptor Charge-Transfer Exciton and Its Contribution to Charge Photogeneration and Recombination in Small-Molecule Bulk Heterojunctions*, *The Journal of Physical Chemistry C* **116** (Aug., 2012) 18108–18116.

[56] J. Widmer, M. Tietze, K. Leo, and M. Riede, *Open-Circuit Voltage and Effective Gap of Organic Solar Cells*, *Advanced Functional Materials* **23** (2013), no. 46 5814–5821.

[57] B. Bernardo, D. Cheyns, B. Verreet, R. D. Schaller, B. P. Rand, and N. C. Giebink, *Delocalization and dielectric screening of charge transfer states in organic photovoltaic cells*, *Nature Communications* **5** (Feb., 2014).

[58] M. A. Faist, T. Kirchartz, W. Gong, R. S. Ashraf, I. McCulloch, J. C. de Mello, N. J. Ekins-Daukes, D. D. C. Bradley, and J. Nelson, *Competition between the Charge Transfer State and the Singlet States of Donor or Acceptor Limiting the Efficiency in Polymer:Fullerene Solar Cells*, *Journal of the American Chemical Society* **134** (Jan., 2012) 685–692.

[59] K. Vandewal, Z. Ma, J. Bergqvist, Z. Tang, E. Wang, P. Henriksson, K. Tvingstedt, M. R. Andersson, F. Zhang, and O. Inganäs, *Quantification of Quantum Efficiency and Energy Losses in Low Bandgap Polymer:Fullerene Solar Cells with High Open-Circuit Voltage*, *Advanced Functional Materials* **22** (2012), no. 16 3480–3490.

[60] B. Walker, A. B. Tamayo, X.-D. Dang, P. Zalar, J. H. Seo, A. Garcia, M. Tantiwiwat, and T.-Q. Nguyen, *Nanoscale Phase Separation and High Photovoltaic Efficiency in Solution-Processed, Small-Molecule Bulk Heterojunction Solar Cells*, *Advanced Functional Materials* **19** (2009), no. 19 3063–3069.

[61] T. S. van der Poll, J. A. Love, T.-Q. Nguyen, and G. C. Bazan, *Non-Basic High-Performance Molecules for Solution-Processed Organic Solar Cells*, *Advanced Materials* **24** (2012), no. 27 3646–3649.

[62] J. A. Love, I. Nagao, Y. Huang, M. Kuik, V. Gupta, C. J. Takacs, J. E. Coughlin, L. Qi, T. S. van der Poll, E. J. Kramer, A. J. Heeger, T.-Q. Nguyen, and G. C. Bazan, *Silaindacenodithiophene-Based Molecular Donor: Morphological Features and Use in the Fabrication of Compositionally Tolerant, High-Efficiency Bulk Heterojunction Solar Cells*, *Journal of the American Chemical Society* **136** (Mar., 2014) 3597–3606.

[63] A. Sharenko, M. Kuik, M. F. Toney, and T.-Q. Nguyen, *Crystallization-Induced Phase Separation in Solution-Processed Small Molecule Bulk Heterojunction Organic Solar Cells*, *Advanced Functional Materials* **24** (June, 2014) 3543–3550.

[64] D. Veldman, Ö. İpek, S. C. J. Meskers, J. Sweelssen, M. M. Koetse, S. C. Veenstra, J. M. Kroon, S. S. van Bavel, J. Loos, and R. A. J. Janssen, *Compositional and Electric Field Dependence of the Dissociation of Charge Transfer Excitons in Alternating Polyfluorene Copolymer/Fullerene Blends*, *Journal of the American Chemical Society* **130** (June, 2008) 7721–7735.

[65] M. C. Scharber, C. Lungenschmied, H.-J. Egelhaaf, G. Matt, M. Bednorz, T. Fromherz, J. Gao, D. Jarzab, and M. A. Loi, *Charge transfer excitons in low band gap polymer based solar cells and the role of processing additives*, *Energy & Environmental Science* **4** (Nov., 2011) 5077–5083.

[66] K. R. Graham, P. Erwin, D. Nordlund, K. Vandewal, R. Li, G. O. Ngongang Ndjawa, E. T. Hoke, A. Salleo, M. E. Thompson, M. D. McGehee, and A. Amassian, *Re-evaluating the Role of Sterics and Electronic Coupling in Determining the Open-Circuit Voltage of Organic Solar Cells*, *Advanced Materials* **25** (2013), no. 42 6076–6082.

[67] A. S. Dhoot, J. A. Hogan, A. C. Morteani, and N. C. Greenham, *Electromodulation of photoinduced charge transfer in polyfluorene bilayer devices*, *Applied Physics Letters* **85** (Sept., 2004) 2256.

[68] A. C. Morteani, R. H. Friend, and C. Silva, *Endothermic exciplex–exciton energy-transfer in a blue-emitting polymeric heterojunction system*, *Chemical Physics Letters* **391** (June, 2004) 81–84.

[69] A. Morteani, A. Dhoot, J.-S. Kim, C. Silva, N. Greenham, C. Murphy, E. Moons, S. Ciná, J. Burroughes, and R. Friend, *Barrier-Free Electron–Hole Capture in Polymer Blend Heterojunction Light-Emitting Diodes*, *Advanced Materials* **15** (2003), no. 20 1708–1712.

[70] A. C. Morteani, P. K. H. Ho, R. H. Friend, and C. Silva, *Electric field-induced transition from heterojunction to bulk charge recombination in bilayer polymer light-emitting diodes*, *Applied Physics Letters* **86** (Apr., 2005) 163501.

[71] A. C. Morteani, R. H. Friend, and C. Silva, *Exciton trapping at heterojunctions in polymer blends*, *The Journal of Chemical Physics* **122** (June, 2005) 244906.

[72] A. C. Morteani, P. Sreearunothai, L. M. Herz, R. H. Friend, and C. Silva, *Exciton Regeneration at Polymeric Semiconductor Heterojunctions*, *Physical Review Letters* **92** (June, 2004) 247402.

[73] H. J. Snaith, A. C. Arias, A. C. Morteani, C. Silva, and R. H. Friend, *Charge Generation Kinetics and Transport Mechanisms in Blended Polyfluorene Photovoltaic Devices*, *Nano Letters* **2** (Dec., 2002) 1353–1357.

[74] I. Riisness and M. J. Gordon, *Electronic structure disorder, vibronic coupling, and charge transfer excitons in poly(fluorene-alt-bithiophene):fullerene films*, *Applied Physics Letters* **102** (Mar., 2013) 113302.

[75] S. Gélinas, A. Rao, A. Kumar, S. L. Smith, A. W. Chin, J. Clark, T. S. van der Poll, G. C. Bazan, and R. H. Friend, *Ultrafast Long-Range Charge Separation in Organic Semiconductor Photovoltaic Diodes*, *Science* **343** (Jan., 2014) 512–516.

[76] A. Rao, P. C. Y. Chow, S. Gélinas, C. W. Schlenker, C.-Z. Li, H.-L. Yip, A. K.-Y. Jen, D. S. Ginger, and R. H. Friend, *The role of spin in the kinetic control of recombination in organic photovoltaics*, *Nature* **500** (Aug., 2013) 435–439.

[77] B. M. Savoie, A. Rao, A. A. Bakulin, S. Gelinas, B. Movaghar, R. H. Friend, T. J. Marks, and M. A. Ratner, *Unequal Partnership: Asymmetric Roles of Polymeric Donor and Fullerene Acceptor in Generating Free Charge*, *Journal of the American Chemical Society* (Jan., 2014).

[78] C. W. Schlenker, K.-S. Chen, H.-L. Yip, C.-Z. Li, L. R. Bradshaw, S. T. Ochsenbein, F. Ding, X. S. Li, D. R. Gamelin, A. K.-Y. Jen, and D. S. Ginger, *Polymer Triplet Energy Levels Need Not Limit Photocurrent Collection in Organic Solar Cells*, *Journal of the American Chemical Society* **134** (Dec., 2012) 19661–19668.

[79] P. Zalar, M. Kuik, N. A. Ran, J. A. Love, and T.-Q. Nguyen, *Effects of Processing Conditions on the Recombination Reduction in Small Molecule Bulk Heterojunction Solar Cells*, *Advanced Energy Materials* **4** (Oct., 2014) n/a–n/a.

[80] C. M. Proctor, S. Albrecht, M. Kuik, D. Neher, and T.-Q. Nguyen, *Overcoming Geminate Recombination and Enhancing Extraction in Solution-Processed Small Molecule Solar Cells*, *Advanced Energy Materials* (Mar., 2014) n/a–n/a.

[81] J. J. Benson-Smith, J. Wilson, C. Dyer-Smith, K. Mouri, S. Yamaguchi, H. Murata, and J. Nelson, *Long-Lived Exciplex Formation and Delayed Exciton Emission in Bulk Heterojunction Blends of Silole Derivative and Polyfluorene*

Copolymer: The Role of Morphology on Exciplex Formation and Charge Separation, *The Journal of Physical Chemistry B* **113** (June, 2009) 7794–7799.

[82] T. Hahn, S. Tscheuschner, C. Saller, P. Strohriegl, P. Boregowda, T. Mukhopadhyay, S. Patil, D. Neher, H. Bässler, and A. Köhler, *Role of Intrinsic Photogeneration in Single Layer and Bilayer Solar Cells with C60 and PCBM*, *The Journal of Physical Chemistry C* **120** (Nov., 2016) 25083–25091.

[83] Y. Zou and R. J. Holmes, *The Role of Exciton Ionization Processes in Bulk Heterojunction Organic Photovoltaic Cells*, *Advanced Energy Materials* **5** (June, 2015) 1500019.

[84] C. M. Proctor, C. Kim, D. Neher, and T.-Q. Nguyen, *Nongeminate Recombination and Charge Transport Limitations in Diketopyrrolopyrrole-Based Solution-Processed Small Molecule Solar Cells*, *Advanced Functional Materials* **23** (2013), no. 28 3584–3594.

[85] S. Mukherjee, C. M. Proctor, G. C. Bazan, T.-Q. Nguyen, and H. Ade, *Significance of Average Domain Purity and Mixed Domains on the Photovoltaic Performance of High-Efficiency Solution-Processed Small-Molecule BHJ Solar Cells*, *Advanced Energy Materials* **5** (Nov., 2015) 1500877.

[86] J. D. A. Lin, O. V. Mikhnenko, T. S. van der Poll, G. C. Bazan, and T.-Q. Nguyen, *Temperature Dependence of Exciton Diffusion in a Small-Molecule Organic Semiconductor Processed With and Without Additive*, *Advanced Materials* **27** (Apr., 2015) 2528–2532.

[87] F. Gao, W. Tress, J. Wang, and O. Inganäs, *Temperature Dependence of Charge Carrier Generation in Organic Photovoltaics*, *Physical Review Letters* **114** (Mar., 2015) 128701.

[88] M. C. Heiber, C. Baumbach, V. Dyakonov, and C. Deibel, *Encounter-Limited Charge-Carrier Recombination in Phase-Separated Organic Semiconductor Blends*, *Physical Review Letters* **114** (Apr., 2015) 136602.

[89] K. Tvingstedt and C. Deibel, *Temperature Dependence of Ideality Factors in Organic Solar Cells and the Relation to Radiative Efficiency*, *Advanced Energy Materials* **6** (May, 2016) n/a–n/a.

[90] G. A. H. Wetzelaer, M. Kuik, M. Lenes, and P. W. M. Blom, *Origin of the dark-current ideality factor in polymer:fullerene bulk heterojunction solar cells*, *Applied Physics Letters* **99** (Oct., 2011) 153506–153506–3.

[91] G. A. H. Wetzelaer, M. Kuik, H. T. Nicolai, and P. W. M. Blom, *Trap-assisted and Langevin-type recombination in organic light-emitting diodes*, *Physical Review B* **83** (Apr., 2011) 165204.

[92] M. M. Mandoc, F. B. Kooistra, J. C. Hummelen, B. de Boer, and P. W. M. Blom, *Effect of traps on the performance of bulk heterojunction organic solar cells*, *Applied Physics Letters* **91** (Dec., 2007) 263505.

[93] S. R. Cowan, A. Roy, and A. J. Heeger, *Recombination in polymer-fullerene bulk heterojunction solar cells*, *Physical Review B* **82** (Dec., 2010) 245207.

[94] L. J. A. Koster, V. D. Mihailetchi, R. Ramaker, and P. W. M. Blom, *Light intensity dependence of open-circuit voltage of polymer:fullerene solar cells*, *Applied Physics Letters* **86** (Mar., 2005) 123509.

[95] M. Kuik, H. T. Nicolai, M. Lenes, G.-J. A. H. Wetzelaer, M. Lu, and P. W. M. Blom, *Determination of the trap-assisted recombination strength in polymer light emitting diodes*, *Applied Physics Letters* **98** (Feb., 2011) 093301.

[96] M. Kuik, L. J. A. Koster, G. A. H. Wetzelaer, and P. W. M. Blom, *Trap-Assisted Recombination in Disordered Organic Semiconductors*, *Physical Review Letters* **107** (Dec., 2011) 256805.

[97] B. P. Rand, D. Cheyns, K. Vasseur, N. C. Giebink, S. Mothy, Y. Yi, V. Coropceanu, D. Beljonne, J. Cornil, J.-L. Brédas, and J. Genoe, *The Impact of Molecular Orientation on the Photovoltaic Properties of a Phthalocyanine/Fullerene Heterojunction*, *Advanced Functional Materials* **22** (2012), no. 14 2987–2995.

[98] Y. Yi, V. Coropceanu, and J.-L. Brédas, *Exciton-Dissociation and Charge-Recombination Processes in Pentacene/C60 Solar Cells: Theoretical Insight into the Impact of Interface Geometry*, *Journal of the American Chemical Society* **131** (Nov., 2009) 15777–15783.

[99] X.-K. Chen, M. K. Ravva, H. Li, S. M. Ryno, and J.-L. Brédas, *Effect of Molecular Packing and Charge Delocalization on the Nonradiative Recombination of Charge-Transfer States in Organic Solar Cells*, *Advanced Energy Materials* (Aug., 2016) 1601325.

[100] B. Yang, Y. Yi, C.-R. Zhang, S. G. Aziz, V. Coropceanu, and J.-L. Bredas, *Impact of Electron Delocalization on the Nature of the ChargeTransfer States in Model Pentacene/C60 Interfaces: A Density Functional Theory Study*, *Journal of Physical Chemistry C* **118** (2014) 27648–27656.

[101] S. Verlaak, D. Beljonne, D. Cheyns, C. Rolin, M. Linares, F. Castet, J. Cornil, and P. Heremans, *Electronic Structure and Geminate Pair Energetics at Organic–Organic Interfaces: The Case of Pentacene/C60 Heterojunctions*, *Advanced Functional Materials* **19** (Dec., 2009) 3809–3814.

[102] J. Idé, S. Mothy, A. Savoyant, A. Fritsch, P. Aurel, R. Méreau, L. Ducasse, J. Cornil, D. Beljonne, and F. Castet, *Interfacial dipole and band bending in model pentacene/C60 heterojunctions*, *International Journal of Quantum Chemistry* **113** (Feb., 2013) 580–584.

[103] J. R. Tumbleston, B. A. Collins, L. Yang, A. C. Stuart, E. Gann, W. Ma, W. You, and H. Ade, *The influence of molecular orientation on organic bulk heterojunction solar cells*, *Nature Photonics* **8** (May, 2014) 385–391.

[104] L. Zhang, S. S. Roy, R. J. Hamers, M. S. Arnold, and T. L. Andrew, *Molecular Orientation-Dependent Interfacial Energetics and Built-in Voltage Tuned by a Template Graphene Monolayer*, *The Journal of Physical Chemistry C* (2014) 45–54.

[105] W. Chen, D.-C. Qi, H. Huang, X. Gao, and A. T. S. Wee, *Organic–Organic Heterojunction Interfaces: Effect of Molecular Orientation*, *Advanced Functional Materials* **21** (2011), no. 3 410–424.

[106] D. M. Alloway and N. R. Armstrong, *Organic heterojunctions of layered perylene and phthalocyanine dyes: Characterization with UV-photoelectron spectroscopy and luminescence quenching*, *Applied Physics A* **95** (Jan., 2009) 209–218.

[107] B. Kitchen, O. Awartani, R. J. Kline, T. McAfee, H. Ade, and B. T. O'Connor, *Tuning Open-Circuit Voltage in Organic Solar Cells with Molecular Orientation*, *ACS Applied Materials Interfaces* **7** (2015), no. 24 13208–13216.

[108] A. Ojala, A. Petersen, A. Fuchs, R. Lovrincic, C. Pölking, J. Trollmann, J. Hwang, C. Lennartz, H. Reichelt, H. W. Höffken, A. Pucci, P. Erk, T. Kirchartz, and F. Würthner, *Merocyanine/C60 Planar Heterojunction Solar Cells: Effect of Dye Orientation on Exciton Dissociation and Solar Cell Performance*, *Advanced Functional Materials* **22** (Jan., 2012) 86–96.

[109] A. L. Ayzner, D. Nordlund, D.-H. Kim, Z. Bao, and M. F. Toney, *Ultrafast Electron Transfer at Organic Semiconductor Interfaces: Importance of Molecular Orientation*, *The Journal of Physical Chemistry Letters* **6** (Jan., 2015) 6–12.

[110] U. Hörmann, C. Lorch, A. Hinderhofer, A. Gerlach, M. Gruber, J. Kraus, B. Sykora, S. Grob, T. Linderl, A. Wilke, A. Opitz, R. Hansson, A. S. Anselmo, Y. Ozawa, Y. Nakayama, H. Ishii, N. Koch, E. Moons, F. Schreiber, and W. Brütting, *Voc from a Morphology Point of View: The Influence of Molecular Orientation on the Open Circuit Voltage of Organic Planar Heterojunction Solar Cells*, *The Journal of Physical Chemistry C* (Oct., 2014) 26462–26470.

[111] H.-C. Lin, G. A. MacDonald, Y. Shi, N. W. Polaske, D. V. McGrath, S. R. Marder, N. R. Armstrong, E. L. Ratcliff, and S. S. Saavedra, *Influence of*

Molecular Orientation on Charge-Transfer Processes at Phthalocyanine/Metal Oxide Interfaces and Relationship to Organic Photovoltaic Performance, *The Journal of Physical Chemistry C* **119** (2015) 10304–10313.

[112] S. Duhm, G. Heimel, I. Salzmann, H. Glowatzki, R. L. Johnson, A. Vollmer, J. P. Rabe, and N. Koch, *Orientation-dependent ionization energies and interface dipoles in ordered molecular assemblies*, *Nature Materials* **7** (Apr., 2008) 326–332.

[113] N. D. Treat, M. A. Brady, G. Smith, M. F. Toney, E. J. Kramer, C. J. Hawker, and M. L. Chabinyc, *Interdiffusion of PCBM and P3HT Reveals Miscibility in a Photovoltaically Active Blend*, *Advanced Energy Materials* **1** (Jan., 2011) 82–89.

[114] G. O. Ngongang Ndjawa, K. R. Graham, R. Li, S. M. Conron, P. Erwin, K. W. Chou, G. F. Burkhard, K. Zhao, E. T. Hoke, M. E. Thompson, M. D. McGehee, and A. Amassian, *Impact of Molecular Orientation and Spontaneous Interfacial Mixing on the Performance of Organic Solar Cells*, *Chemistry of Materials* **27** (Aug., 2015) 5597–5604.

[115] M. Gruber, J. Wagner, K. Klein, U. Hörmann, A. Opitz, M. Stutzman, and W. Brütting, *Thermodynamic Efficiency Limit of Molecular Donor-Acceptor Solar Cells and its Application to Diindenoperylene/C60-Based Planar Heterojunction Devices*, .

[116] U. Rau, U. W. Paetzold, and T. Kirchartz, *Thermodynamics of light management in photovoltaic devices*, *Physical Review B* **90** (July, 2014) 035211.

[117] J. Liu, S. Chen, D. Qian, B. Gautam, G. Yang, J. Zhao, J. Bergqvist, F. Zhang, W. Ma, H. Ade, O. Inganäs, K. Gundogdu, F. Gao, and H. Yan, *Fast charge separation in a non-fullerene organic solar cell with a small driving force*, *Nature Energy* **1** (June, 2016) 16089.

[118] F. Gao and O. Inganäs, *Charge generation in polymer–fullerene bulk-heterojunction solar cells*, *Physical Chemistry Chemical Physics* **16** (Sept., 2014) 20291–20304.

[119] S. Few, J. M. Frost, and J. Nelson, *Models of charge pair generation in organic solar cells*, *Physical Chemistry Chemical Physics* **17** (Dec., 2014) 2311–2325.

[120] H. Bässler and A. Köhler, *"Hot or cold": How do charge transfer states at the donor–acceptor interface of an organic solar cell dissociate?*, *Physical Chemistry Chemical Physics* **17** (Oct., 2015) 28451–28462.

[121] U. Rau, *Reciprocity relation between photovoltaic quantum efficiency and electroluminescent emission of solar cells*, *Physical Review B* **76** (Aug., 2007) 085303.

[122] O. D. Miller, E. Yablonovitch, and S. R. Kurtz, *Strong Internal and External Luminescence as Solar Cells Approach the Shockley #x2013;Queisser Limit*, *IEEE Journal of Photovoltaics* **2** (July, 2012) 303–311.

[123] D. A. Vithanage, A. Devižis, V. Abramavičius, Y. Infahsaeng, D. Abramavičius, R. C. I. MacKenzie, P. E. Keivanidis, A. Yartsev, D. Hertel, J. Nelson, V. Sundström, and V. Gulbinas, *Visualizing charge separation in bulk heterojunction organic solar cells*, *Nature Communications* **4** (Aug., 2013) 2334.

[124] F. C. Jamieson, E. B. Domingo, T. McCarthy-Ward, M. Heeney, N. Stingelin, and J. R. Durrant, *Fullerene crystallisation as a key driver of charge separation in polymer/fullerene bulk heterojunction solar cells*, *Chemical Science* **3** (Jan., 2012) 485–492.

[125] A. J. Ward, A. Ruseckas, M. M. Kareem, B. Ebenhoch, L. A. Serrano, M. Al-Eid, B. Fitzpatrick, V. M. Rotello, G. Cooke, and I. D. W. Samuel, *The Impact of Driving Force on Electron Transfer Rates in Photovoltaic Donor–Acceptor Blends*, *Advanced Materials* **27** (Apr., 2015) 2496–2500.

[126] S. Albrecht, W. Schindler, J. Kurpiers, J. Kniepert, J. C. Blakesley, I. Dumsch, S. Allard, K. Fostiropoulos, U. Scherf, and D. Neher, *On the Field Dependence of Free Charge Carrier Generation and Recombination in Blends of PCPDTBT/PC70BM: Influence of Solvent Additives*, *The Journal of Physical Chemistry Letters* **3** (Mar., 2012) 640–645.

[127] G. F. A. Dibb, F. C. Jamieson, A. Maurano, J. Nelson, and J. R. Durrant, *Limits on the Fill Factor in Organic Photovoltaics: Distinguishing Nongeminate and Geminate Recombination Mechanisms*, *The Journal of Physical Chemistry Letters* **4** (Mar., 2013) 803–808.

[128] P. K. Nayak, K. L. Narasimhan, and D. Cahen, *Separating Charges at Organic Interfaces: Effects of Disorder, Hot States, and Electric Field*, *The Journal of Physical Chemistry Letters* **4** (May, 2013) 1707–1717.

[129] J. A. Bartelt, Z. M. Beiley, E. T. Hoke, W. R. Mateker, J. D. Douglas, B. A. Collins, J. R. Tumbleston, K. R. Graham, A. Amassian, H. Ade, J. M. J. Fréchet, M. F. Toney, and M. D. McGehee, *The Importance of Fullerene Percolation in the Mixed Regions of Polymer–Fullerene Bulk Heterojunction Solar Cells*, *Advanced Energy Materials* **3** (2013), no. 3 364–374.

[130] N. R. Monahan, K. W. Williams, B. Kumar, C. Nuckolls, and X.-Y. Zhu, *Direct Observation of Entropy-Driven Electron-Hole Pair Separation at an Organic Semiconductor Interface*, *Physical Review Letters* **114** (June, 2015) 247003.

[131] G. F. Burkhard, E. T. Hoke, and M. D. McGehee, *Accounting for Interference, Scattering, and Electrode Absorption to Make Accurate Internal Quantum Efficiency Measurements in Organic and Other Thin Solar Cells*, *Advanced Materials* **22** (Aug., 2010) 3293–3297.

[132] A. Köhler and H. Bässler, *Electronic and Optical Processes of Organic Semiconductors*, in *Electronic Processes in Organic Semiconductors*, pp. 193–305. Wiley-VCH Verlag GmbH & Co. KGaA, 2015.

[133] B. Schweitzer, V. I. Arkhipov, and H. Bässler, *Field-induced delayed photoluminescence in a conjugated polymer*, *Chemical Physics Letters* **304** (May, 1999) 365–370.

[134] C. Schwarz, S. Tscheuschner, J. Frisch, S. Winkler, N. Koch, H. Bässler, and A. Köhler, *Role of the effective mass and interfacial dipoles on exciton dissociation in organic donor-acceptor solar cells*, *Physical Review B* **87** (Apr., 2013) 155205.

[135] G. Kresse and J. Furthmüller, *Efficiency of ab-initio total energy calculations for metals and semiconductors using a plane-wave basis set*, *Computational Materials Science* **6** (July, 1996) 15–50.

[136] G. Kresse and J. Furthmüller, *Efficient iterative schemes for \textit{ab Initio} total-energy calculations using a plane-wave basis set*, *Physical Review B* **54** (Oct., 1996) 11169–11186.

[137] J. Heyd and G. E. Scuseria, *Efficient hybrid density functional calculations in solids: Assessment of the Heyd–Scuseria–Ernzerhof screened Coulomb hybrid functional*, *The Journal of Chemical Physics* **121** (July, 2004) 1187–1192.

[138] J. Heyd, J. E. Peralta, G. E. Scuseria, and R. L. Martin, *Energy band gaps and lattice parameters evaluated with the Heyd-Scuseria-Ernzerhof screened hybrid functional*, *The Journal of Chemical Physics* **123** (Nov., 2005) 174101.

[139] Y. Shao, L. F. Molnar, Y. Jung, J. Kussmann, C. Ochsenfeld, S. T. Brown, A. T. B. Gilbert, L. V. Slipchenko, S. V. Levchenko, D. P. O'Neill, R. A. D. Jr, R. C. Lochan, T. Wang, G. J. O. Beran, N. A. Besley, J. M. Herbert, C. Y. Lin, T. V. Voorhis, S. H. Chien, A. Sodt, R. P. Steele, V. A. Rassolov, P. E. Maslen, P. P. Korambath, R. D. Adamson, B. Austin, J. Baker, E. F. C. Byrd, H. Dachsel, R. J. Doerksen, A. Dreuw, B. D. Dunietz, A. D. Dutoi, T. R. Furlani, S. R. Gwaltney, A. Heyden, S. Hirata, C.-P. Hsu, G. Kedziora, R. Z. Khalliulin, P. Klunzinger, A. M. Lee, M. S. Lee, W. Liang, I. Lotan, N. Nair, B. Peters, E. I. Proynov, P. A. Pieniazek, Y. M. Rhee, J. Ritchie, E. Rosta, C. D. Sherrill, A. C. Simmonett, J. E. Subotnik, H. L. W. Iii, W. Zhang, A. T. Bell, A. K. Chakraborty, D. M. Chipman, F. J. Keil, A. Warshel, W. J. Hehre, H. F. S. Iii,

J. Kong, A. I. Krylov, P. M. W. Gill, and M. Head-Gordon, *Advances in methods and algorithms in a modern quantum chemistry program package*, .

[140] S. D. Collins, C. M. Proctor, N. A. Ran, and T.-Q. Nguyen, *Understanding Open-Circuit Voltage Loss through the Density of States in Organic Bulk Heterojunction Solar Cells*, *Advanced Energy Materials* (Nov., 2015) 1501721.

[141] T. M. Burke, S. Sweetnam, K. Vandewal, and M. D. McGehee, *Beyond Langevin Recombination: How Equilibrium Between Free Carriers and Charge Transfer States Determines the Open-Circuit Voltage of Organic Solar Cells*, *Advanced Energy Materials* **5** (Apr., 2015) 1500123.

[142] W. Li, K. H. Hendriks, A. Furlan, M. M. Wienk, and R. A. J. Janssen, *High Quantum Efficiencies in Polymer Solar Cells at Energy Losses below 0.6 eV*, *Journal of the American Chemical Society* **137** (Feb., 2015) 2231–2234.

[143] L. J. A. Koster, S. E. Shaheen, and J. C. Hummelen, *Pathways to a New Efficiency Regime for Organic Solar Cells*, *Advanced Energy Materials* **2** (Oct., 2012) 1246–1253.

[144] E. T. Hoke, K. Vandewal, J. A. Bartelt, W. R. Mateker, J. D. Douglas, R. Noriega, K. R. Graham, J. M. J. Fréchet, A. Salleo, and M. D. McGehee, *Recombination in Polymer:Fullerene Solar Cells with Open-Circuit Voltages Approaching and Exceeding 1.0 V*, *Advanced Energy Materials* **3** (Feb., 2013) 220–230.

[145] B. P. Rand, D. P. Burk, and S. R. Forrest, *Offset energies at organic semiconductor heterojunctions and their influence on the open-circuit voltage of thin-film solar cells*, *Physical Review B* **75** (Mar., 2007) 115327.

[146] U. Würfel, D. Neher, A. Spies, and S. Albrecht, *Impact of charge transport on current-voltage characteristics and power-conversion efficiency of organic solar cells*, *Nature Communications* **6** (Apr., 2015).

[147] K. Vandewal, J. Widmer, T. Heumueller, C. J. Brabec, M. D. McGehee, K. Leo, M. Riede, and A. Salleo, *Increased Open-Circuit Voltage of Organic Solar Cells by Reduced Donor-Acceptor Interface Area*, *Advanced Materials* **26** (June, 2014) 3839–3843.

[148] V. D. Mihailetchi, P. W. M. Blom, J. C. Hummelen, and M. T. Rispens, *Cathode dependence of the open-circuit voltage of polymer:fullerene bulk heterojunction solar cells*, *Journal of Applied Physics* **94** (Nov., 2003) 6849–6854.

[149] M. Kemerink, J. M. Kramer, H. H. P. Gommans, and R. a. J. Janssen, *Temperature-dependent built-in potential in organic semiconductor devices*, *Applied Physics Letters* **88** (May, 2006) 192108.

[150] J. C. Blakesley and N. C. Greenham, *Charge transfer at polymer-electrode interfaces: The effect of energetic disorder and thermal injection on band bending and open-circuit voltage*, *Journal of Applied Physics* **106** (Aug., 2009) 034507.

[151] I. Lange, J. Kniepert, P. Pingel, I. Dumsch, S. Allard, S. Janietz, U. Scherf, and D. Neher, *Correlation between the Open Circuit Voltage and the Energetics of Organic Bulk Heterojunction Solar Cells*, *The Journal of Physical Chemistry Letters* **4** (2013), no. 22 3865–3871.

[152] T. Heumueller, T. M. Burke, W. R. Mateker, I. T. Sachs-Quintana, K. Vandewal, C. J. Brabec, and M. D. McGehee, *Disorder-Induced Open-Circuit Voltage Losses in Organic Solar Cells During Photoinduced Burn-In*, *Advanced Energy Materials* **5** (May, 2015) 1500111.

[153] M. Wang, H. Wang, T. Yokoyama, X. Liu, Y. Huang, Y. Zhang, T.-Q. Nguyen, S. Aramaki, and G. C. Bazan, *High Open Circuit Voltage in Regioregular Narrow Band Gap Polymer Solar Cells*, *Journal of the American Chemical Society* **136** (Sept., 2014) 12576–12579.

[154] L. Goris, K. Haenen, M. Nesládek, P. Wagner, D. Vanderzande, L. D. Schepper, J. D'haen, L. Lutsen, and J. V. Manca, *Absorption phenomena in organic thin films for solar cell applications investigated by photothermal deflection spectroscopy*, *Journal of Materials Science* **40** (Mar., 2005) 1413–1418.

[155] F. Urbach, *The Long-Wavelength Edge of Photographic Sensitivity and of the Electronic Absorption of Solids*, *Physical Review* **92** (Dec., 1953) 1324–1324.

[156] M. V. Kurik, *Urbach rule*, *physica status solidi (a)* **8** (Nov., 1971) 9–45.

[157] V. Sa-Yakanit and N. R. Glyde, *Urbach tails and disorder*, *Comments Cond. Mat. Phys.* **13** (1987), no. 1 35–48.

[158] B. R. Weinberger, C. B. Roxlo, S. Etemad, G. L. Baker, and J. Orenstein, *Optical Absorption in Polyacetylene: A Direct Measurement Using Photothermal Deflection Spectroscopy*, *Physical Review Letters* **53** (July, 1984) 86–89.

[159] D. Venkateshvaran, M. Nikolka, A. Sadhanala, V. Lemaur, M. Zelazny, M. Kepa, M. Hurhangee, A. J. Kronemeijer, V. Pecunia, I. Nasrallah, I. Romanov, K. Broch, I. McCulloch, D. Emin, Y. Olivier, J. Cornil, D. Beljonne, and H. Sirringhaus, *Approaching disorder-free transport in high-mobility conjugated polymers*, *Nature* **515** (Nov., 2014) 384–388.

[160] L. Kelvin, *V. Contact electricity of metals*, *Philosophical Magazine Series 5* **46** (July, 1898) 82–120.

[161] I. Lange, J. C. Blakesley, J. Frisch, A. Vollmer, N. Koch, and D. Neher, *Band Bending in Conjugated Polymer Layers*, *Physical Review Letters* **106** (May, 2011) 216402.

[162] G. Garcia-Belmonte and J. Bisquert, *Open-circuit voltage limit caused by recombination through tail states in bulk heterojunction polymer-fullerene solar cells*, *Applied Physics Letters* **96** (Mar., 2010) 113301–113301–3.

[163] A. Sharenko, N. D. Treat, J. A. Love, M. F. Toney, N. Stingelin, and T.-Q. Nguyen, *Use of a commercially available nucleating agent to control the morphological development of solution-processed small molecule bulk heterojunction organic solar cells*, *Journal of Materials Chemistry A* **2** (Sept., 2014) 15717–15721.

[164] Y. Li, X. Liu, F.-P. Wu, Y. Zhou, Z.-Q. Jiang, B. Song, Y. Xia, Z.-G. Zhang, F. Gao, O. Inganäs, Y. Li, and L.-S. Liao, *Non-fullerene acceptor with low energy loss and high external quantum efficiency: Towards high performance polymer solar cells*, *Journal of Materials Chemistry A* **4** (2016), no. 16 5890–5897.

[165] K. Kawashima, Y. Tamai, H. Ohkita, I. Osaka, and K. Takimiya, *High-efficiency polymer solar cells with small photon energy loss*, *Nature Communications* **6** (Dec., 2015) 10085.

[166] M.-H. Jao, H.-C. Liao, and W.-F. Su, *Achieving a high fill factor for organic solar cells*, *Journal of Materials Chemistry A* **4** (2016), no. 16 5784–5801.

[167] P. Kaienburg, U. Rau, and T. Kirchartz, *Extracting Information about the Electronic Quality of Organic Solar-Cell Absorbers from Fill Factor and Thickness*, *Physical Review Applied* **6** (Aug., 2016) 024001.

[168] T. Kirchartz, T. Agostinelli, M. Campoy-Quiles, W. Gong, and J. Nelson, *Understanding the Thickness-Dependent Performance of Organic Bulk Heterojunction Solar Cells: The Influence of Mobility, Lifetime, and Space Charge*, *The Journal of Physical Chemistry Letters* **3** (Dec., 2012) 3470–3475.

[169] N. Zhou, X. Guo, R. P. Ortiz, T. Harschneck, E. F. Manley, S. J. Lou, P. E. Hartnett, X. Yu, N. E. Horwitz, P. M. Burrezo, T. J. Aldrich, J. T. López Navarrete, M. R. Wasielewski, L. X. Chen, R. P. H. Chang, A. Facchetti, and T. J. Marks, *Marked Consequences of Systematic Oligothiophene Catenation in Thieno[3,4-c]pyrrole-4,6-dione and Bithiopheneimide Photovoltaic Copolymers*, *Journal of the American Chemical Society* **137** (Oct., 2015) 12565–12579.

[170] N. Gasparini, X. Jiao, T. Heumueller, D. Baran, G. J. Matt, S. Fladischer, E. Spiecker, H. Ade, C. J. Brabec, and T. Ameri, *Designing ternary blend bulk heterojunction solar cells with reduced carrier recombination and a fill factor of 77%*, *Nature Energy* **1** (Aug., 2016) 16118.

[171] F. Liu, W. Zhao, J. R. Tumbleston, C. Wang, Y. Gu, D. Wang, A. L. Briseno, H. Ade, and T. P. Russell, *Understanding the Morphology of PTB7:PCBM Blends in Organic Photovoltaics*, *Advanced Energy Materials* **4** (Apr., 2014) n/a–n/a.

[172] J.-L. Wang, F. Xiao, J. Yan, Z. Wu, K.-K. Liu, Z.-F. Chang, R.-B. Zhang, H. Chen, H.-B. Wu, and Y. Cao, *Difluorobenzothiadiazole-Based Small-Molecule Organic Solar Cells with 8.7% Efficiency by Tuning of π-Conjugated Spacers and Solvent Vapor Annealing*, *Advanced Functional Materials* **26** (Mar., 2016) 1803–1812.

[173] K. Sun, Z. Xiao, S. Lu, W. Zajaczkowski, W. Pisula, E. Hanssen, J. M. White, R. M. Williamson, J. Subbiah, J. Ouyang, A. B. Holmes, W. W. H. Wong, and D. J. Jones, *A molecular nematic liquid crystalline material for high-performance organic photovoltaics*, *Nature Communications* **6** (Jan., 2015) 6013.

[174] S. M. Menke, A. Sadhanala, M. Nikolka, N. A. Ran, M. K. Ravva, S. Abdel-Azeim, H. L. Stern, M. Wang, H. Sirringhaus, T.-Q. Nguyen, J.-L. Brédas, G. C. Bazan, and R. H. Friend, *Limits for Recombination in a Low Energy Loss Organic Heterojunction*, *ACS Nano* (Nov., 2016).

[175] A. Kumar, G. Lakhwani, E. Elmalem, W. T. S. Huck, A. Rao, N. C. Greenham, and R. H. Friend, *Interface limited charge extraction and recombination in organic photovoltaics*, *Energy & Environmental Science* (May, 2014).

[176] Z.-K. Tan, Y. Vaynzof, D. Credgington, C. Li, M. T. L. Casford, A. Sepe, S. Huettner, M. Nikolka, F. Paulus, L. Yang, H. Sirringhaus, N. C. Greenham, and R. H. Friend, *In-Situ Switching from Barrier-Limited to Ohmic Anodes for Efficient Organic Optoelectronics*, *Advanced Functional Materials* **24** (May, 2014) 3051–3058.

[177] W. Tress, K. Leo, and M. Riede, *Optimum mobility, contact properties, and open-circuit voltage of organic solar cells: A drift-diffusion simulation study*, *Physical Review B* **85** (Apr., 2012) 155201.

[178] B. E. Lassiter, G. Wei, S. Wang, J. D. Zimmerman, V. V. Diev, M. E. Thompson, and S. R. Forrest, *Organic photovoltaics incorporating electron conducting exciton blocking layers*, *Applied Physics Letters* **98** (June, 2011) 243307–243307–3.

[179] B. A. Collins, Z. Li, J. R. Tumbleston, E. Gann, C. R. McNeill, and H. Ade, *Absolute Measurement of Domain Composition and Nanoscale Size Distribution Explains Performance in PTB7:PC71BM Solar Cells*, *Advanced Energy Materials* **3** (Jan., 2013) 65–74.

[180] M. Guide, X.-D. Dang, and T.-Q. Nguyen, *Nanoscale Characterization of Tetrabenzoporphyrin and Fullerene-Based Solar Cells by Photoconductive Atomic Force Microscopy*, *Advanced Materials* **23** (May, 2011) 2313–2319.

[181] X.-D. Dang, A. Mikhailovsky, and T.-Q. Nguyen, *Measurement of nanoscale external quantum efficiency of conjugated polymer:fullerene solar cells by photoconductive atomic force microscopy*, *Applied Physics Letters* **97** (Sept., 2010) 113303.

[182] X.-D. Dang, A. B. Tamayo, J. Seo, C. V. Hoven, B. Walker, and T.-Q. Nguyen, *Nanostructure and Optoelectronic Characterization of Small Molecule Bulk Heterojunction Solar Cells by Photoconductive Atomic Force Microscopy*, *Advanced Functional Materials* **20** (Oct., 2010) n/a–n/a.

[183] E. M. Pearce, *Properties of polymers, their estimation and correlation with chemical structure – (2nd rev. ed.), D. W. Van Krevelen, Elsevier, Amsterdam – Oxford – New York, 1976, 620 pp.*, *Journal of Polymer Science: Polymer Letters Edition* **15** (Jan., 1977) 56–56.

[184] T. Hahn, J. Geiger, X. Blase, I. Duchemin, D. Niedzialek, S. Tscheuschner, D. Beljonne, H. Bässler, and A. Köhler, *Does Excess Energy Assist Photogeneration in an Organic Low-Bandgap Solar Cell?*, *Advanced Functional Materials* **25** (Feb., 2015) 1287–1295.

[185] S. Sweetnam, K. R. Graham, G. O. Ngongang Ndjawa, T. Heumüller, J. A. Bartelt, T. M. Burke, W. Li, W. You, A. Amassian, and M. D. McGehee, *Characterization of the Polymer Energy Landscape in Polymer:Fullerene Bulk Heterojunctions with Pure and Mixed Phases*, *Journal of the American Chemical Society* **136** (Oct., 2014) 14078–14088.

[186] J. A. Bartelt, D. Lam, T. M. Burke, S. M. Sweetnam, and M. D. McGehee, *Charge-Carrier Mobility Requirements for Bulk Heterojunction Solar Cells with High Fill Factor and External Quantum Efficiency >90%*, *Advanced Energy Materials* **5** (Aug., 2015) n/a–n/a.

[187] C. M. Proctor, J. A. Love, and T.-Q. Nguyen, *Mobility Guidelines for High Fill Factor Solution-Processed Small Molecule Solar Cells*, *Advanced Materials* **26** (Sept., 2014) 5957–5961.

[188] N. D. Treat, J. A. Nekuda Malik, O. Reid, L. Yu, C. G. Shuttle, G. Rumbles, C. J. Hawker, M. L. Chabinyc, P. Smith, and N. Stingelin, *Microstructure formation in molecular and polymer semiconductors assisted by nucleation agents*, *Nature Materials* **12** (July, 2013) 628–633.

[189] X. Guo, N. Zhou, S. J. Lou, J. Smith, D. B. Tice, J. W. Hennek, R. P. Ortiz, J. T. L. Navarrete, S. Li, J. Strzalka, L. X. Chen, R. P. H. Chang, A. Facchetti, and T. J. Marks, *Polymer solar cells with enhanced fill factors*, *Nature Photonics* **7** (Oct., 2013) 825–833.

[190] L. Wu, H. Zang, Y.-C. Hsiao, X. Zhang, and B. Hu, *Origin of the fill factor loss in bulk-heterojunction organic solar cells*, *Applied Physics Letters* **104** (Apr., 2014) 153903.

[191] R. Mauer, I. A. Howard, and F. Laquai, *Effect of Nongeminate Recombination on Fill Factor in Polythiophene/Methanofullerene Organic Solar Cells*, *The Journal of Physical Chemistry Letters* **1** (Dec., 2010) 3500–3505.

[192] M. Lenes, L. J. A. Koster, V. D. Mihailetchi, and P. W. M. Blom, *Thickness dependence of the efficiency of polymer:fullerene bulk heterojunction solar cells*, *Applied Physics Letters* **88** (June, 2006) 243502.

[193] C. M. Proctor and T.-Q. Nguyen, *Effect of leakage current and shunt resistance on the light intensity dependence of organic solar cells*, *Applied Physics Letters* **106** (Feb., 2015) 083301.

[194] V. V. Brus, C. M. Proctor, N. A. Ran, and T.-Q. Nguyen, *Capacitance Spectroscopy for Quantifying Recombination Losses in Nonfullerene Small-Molecule Bulk Heterojunction Solar Cells*, *Advanced Energy Materials* **6** (June, 2016) 1502250.

[195] D. Bartesaghi, I. d. C. Pérez, J. Kniepert, S. Roland, M. Turbiez, D. Neher, and L. J. A. Koster, *Competition between recombination and extraction of free charges determines the fill factor of organic solar cells*, *Nature Communications* **6** (May, 2015).

[196] A. J. Ferguson, N. Kopidakis, S. E. Shaheen, and G. Rumbles, *Dark Carriers, Trapping, and Activation Control of Carrier Recombination in Neat P3HT and P3HT:PCBM Blends*, *The Journal of Physical Chemistry C* **115** (Nov., 2011) 23134–23148.

[197] M. C. Heiber, T.-Q. Nguyen, and C. Deibel, *Charge carrier concentration dependence of encounter-limited bimolecular recombination in phase-separated organic semiconductor blends*, *Physical Review B* **93** (May, 2016) 205204.

[198] F. Deledalle, P. Shakya Tuladhar, J. Nelson, J. R. Durrant, and T. Kirchartz, *Understanding the Apparent Charge Density Dependence of Mobility and Lifetime in Organic Bulk Heterojunction Solar Cells*, *The Journal of Physical Chemistry C* **118** (May, 2014) 8837–8842.

[199] S. V. Kesava, Z. Fei, A. D. Rimshaw, C. Wang, A. Hexemer, J. B. Asbury, M. Heeney, and E. D. Gomez, *Domain Compositions and Fullerene Aggregation Govern Charge Photogeneration in Polymer/Fullerene Solar Cells*, *Advanced Energy Materials* **4** (Aug., 2014) n/a–n/a.

[200] B. P. Lyons, N. Clarke, and C. Groves, *The relative importance of domain size, domain purity and domain interfaces to the performance of bulk-heterojunction organic photovoltaics*, *Energy & Environmental Science* **5** (2012), no. 6 7657.

[201] S. Shoaee, S. Mehraeen, J. G. Labram, J.-L. Brédas, D. D. C. Bradley, V. Coropceanu, T. D. Anthopoulos, and J. R. Durrant, *Correlating Non-Geminate Recombination with Film Structure: A Comparison of Polythiophene: Fullerene Bilayer and Blend Films*, *The Journal of Physical Chemistry Letters* **5** (Nov., 2014) 3669–3676.

[202] C. Schwarz, H. Bässler, I. Bauer, J.-M. Koenen, E. Preis, U. Scherf, and A. Köhler, *Does Conjugation Help Exciton Dissociation? A Study on Poly(p-phenylene)s in Planar Heterojunctions with C60 or TNF*, *Advanced Materials* **24** (Feb., 2012) 922–925.

[203] C. Deibel, T. Strobel, and V. Dyakonov, *Origin of the Efficient Polaron-Pair Dissociation in Polymer-Fullerene Blends*, *Physical Review Letters* **103** (July, 2009) 036402.

[204] G. D'Avino, L. Muccioli, Y. Olivier, and D. Beljonne, *Charge Separation and Recombination at Polymer–Fullerene Heterojunctions: Delocalization and Hybridization Effects*, *The Journal of Physical Chemistry Letters* **7** (Feb., 2016) 536–540.

[205] A. C. Jakowetz, M. L. Böhm, J. Zhang, A. Sadhanala, S. Huettner, A. A. Bakulin, A. Rao, and R. H. Friend, *What Controls the Rate of Ultrafast Charge Transfer and Charge Separation Efficiency in Organic Photovoltaic Blends*, *Journal of the American Chemical Society* **138** (Sept., 2016) 11672–11679.

[206] H. Tamura and I. Burghardt, *Ultrafast Charge Separation in Organic Photovoltaics Enhanced by Charge Delocalization and Vibronically Hot Exciton Dissociation*, *Journal of the American Chemical Society* **135** (Nov., 2013) 16364–16367.

[207] Y. Huang, W. Wen, S. Mukherjee, H. Ade, E. J. Kramer, and G. C. Bazan, *High-Molecular-Weight Insulating Polymers Can Improve the Performance of Molecular Solar Cells*, *Advanced Materials* **26** (June, 2014) 4168–4172.

[208] N. Bansal, L. X. Reynolds, A. MacLachlan, T. Lutz, R. S. Ashraf, W. Zhang, C. B. Nielsen, I. McCulloch, D. G. Rebois, T. Kirchartz, M. S. Hill, K. C. Molloy, J. Nelson, and S. A. Haque, *Influence of Crystallinity and Energetics on Charge Separation in Polymer–Inorganic Nanocomposite Films for Solar Cells*, *Scientific Reports* **3** (Mar., 2013).

[209] J. C. Aguirre, S. A. Hawks, A. S. Ferreira, P. Yee, S. Subramaniyan, S. A. Jenekhe, S. H. Tolbert, and B. J. Schwartz, *Sequential Processing for Organic Photovoltaics: Design Rules for Morphology Control by Tailored Semi-Orthogonal Solvent Blends*, *Advanced Energy Materials* **5** (June, 2015) 1402020.

[210] Y. Sun, J. H. Seo, C. J. Takacs, J. Seifter, and A. J. Heeger, *Inverted Polymer Solar Cells Integrated with a Low-Temperature-Annealed Sol-Gel-Derived ZnO Film as an Electron Transport Layer*, *Advanced Materials* **23** (Apr., 2011) 1679–1683.

I don't know where I'm going from here, but I promise it won't be boring.
– David Bowie